Metallodrugs as protein modulators

Batista de Almeida, Andreia Filipa

Metallodrugs as Protein Modulators

Paranimfen:

Carian Boorsma
Viktoriia Starokoszkho

Cover design: Andreia de Almeida
Layout design: Andreia de Almeida
Printed by: IPSKAM Printing

ISBN printed version: 978-90-367-8745-1
ISBN electronic version: 978-90-367-8744-4

The research presented in this thesis was financially supported by Rosalind Franklin Fellowship Funds Programe and printing of the thesis was financially supported by the University of Groningen (RUG), Faculty of Mathematics and Natural Sciences (FMNS) and Univeristy Library.

university of groningen

Metallodrugs as Protein Modulators

PhD thesis

to obtain the degree of PhD at the
University of Groningen
on the authority of the
Rector Magnificus Prof. E. Sterken
and in accordance with
the decision by the College of Deans.

This thesis will be defended in public on

Friday 8 April 2016 at 16.15 hours

by

Andreia Filipa Batista de Almeida

born on 13 May 1986
in Trafaria, Almada, Portugal

Supervisors
Prof. G.M.M. Groothuis
Prof. A. Casini

Assessment Committee
Prof. W.J. Quax
Prof. R.K. Allemann
Prof. H.J. Haisma

ci·ên·ci·a

(latim *scientia*, *-ae*, conhecimento, saber, ciência)
substantivo feminino

1. Conjunto de conhecimentos fundados sobre princípios certos.

2. [Figurado] Saber, instrução, conhecimentos vastos.

General Introduction

1. Proteins as targets for metal compounds with pharmacological applications

This chapter is published:

Andreia de Almeida, Bruno Oliveira, João D.G. Correia, Graça Soveral and Angela Casini
Emerging Protein Targets for Metal–Based Pharmaceutical Agents: An Update
Coord.Chem.Rev. (2013) 257: 2689–2704
DOI: 10.1002/cmdc.201300107

1.1. Therapeutic and diagnostic metal compounds

Empirical evidence for the effectiveness of metal-based therapeutics has existed for centuries, and the use of metals and metal-containing compounds in medicine dates back millennia. Nowadays, the list of therapeutically prescribed metal-containing compounds includes platinum (anticancer), silver (antimicrobial), gold (antiarthritic), bismuth (antiulcer), antimony (antiprotozoal), vanadium (antidiabetic) and iron (anticancer and antimalarial) (Figure 1) [1-3]. Moreover, metal compounds as diagnostic tools have also been widely explored and are successfully applied in the clinical set for imaging of diseases [4-6]. For example, lanthanides occupy a relevant place as diagnostic agents, but also have many other medically important applications, as hypophosphatemic agents for kidney dialysis patients, as luminescent probes in cell studies, and for bone pain palliation [7]. In terms of purely therapeutic agents platinum coordination compounds, and one of them, cisplatin, recognized as anticancer drug in the late 1960s, have been intensely studied for several decades [8, 9]. Since then, strategies opening up new avenues are increasingly being sought using complexes of metals other than platinum such as ruthenium, gallium, iron, titanium and gold [10-17]. Thus, while non-classic platinum complexes are increasingly being developed because they do not mimic cisplatin in their modes of action, and are therefore explored to improve the pharmacological properties of the resulting compounds, metals other than platinum inherently have more or less proper preconditions for this purpose. Differences in coordination geometry, binding preferences according to the HSAB (hard and soft acids and bases) principle, important redox activity, kinetics of ligand exchange reactions, or even the simple capacity of replacement of essential metals form the chemical basis for a diversity of pharmacologically relevant interactions with biomolecules [18, 19].

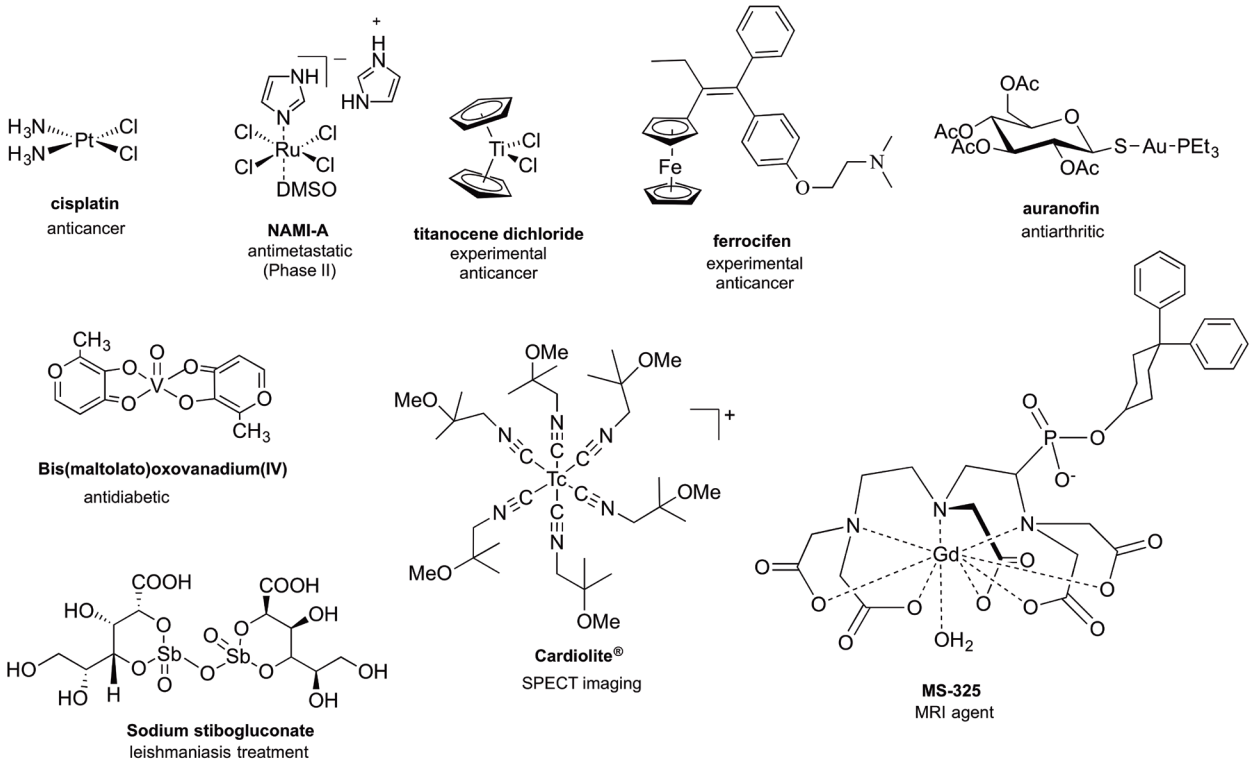

Figure 1. Metal-based pharmaceuticals with different therapeutic and imaging applications.

Concerning metal compounds as diagnostic agents, most of the research efforts expended in the past few years in the field of radiopharmaceutical sciences/nuclear medicine are aimed at the synthesis, characterization and biological evaluation of target-specific metal-based radioactive probes for nuclear imaging (Single Photon Emission Computed Tomography - SPECT and Positron Emission Tomography - PET) or internal radiotherapy. These complexes incorporate γ-emitting radiometals for use in SPECT (e.g. ^{99m}Tc and ^{111}In) or β^+-emitting radiometals for PET (e.g. ^{68}Ga and ^{64}Cu) [20-24]. Among the different metal complexes used for SPECT-imaging, it is worth mentioning sestamibi, marketed under the trademark Cardiolite®, which is a lipophilic cation of Tc(I) stabilized by six isonitrile ligands: $[^{99m}Tc(CNR)_6]^+$ (R = $CH_2C(CH_3)_2OCH_3$) (Figure 1). This cationic radiotracer was originally developed as a SPECT myocardial imaging agent, but currently is also used for both early cancer detection and non-invasive monitoring of the tumour Multidrug Resistance (MDR) transport function. This complex is considered the unique organometallic pharmaceutical used routinely in medicine and, together with cisplatin, is among the most successful synthetic complexes for medical application, from a scientific, commercial, and healthcare point of view [25, 26].

Besides the use of γ^- or β^+-emitting metal-based radiopharmaceuticals for diagnostic purposes, nuclear medicine takes also advantage of complexes containing β^--emitting radiometals for internal radiotherapy. That is the case of ^{153}Sm-EDTMP (Quadramet®, EDTMP = ethylenediamine tetra(methylene-phosphonic acid)) and ^{186}Re-HEDP (HEDP = hydroxyethylidenediphosphonate) for bone-pain palliation or ^{177}Lu-[DOTA^0,Tyr^3] octreotate, a ^{177}Lu-labelled somatostatine analogue, successfully used for therapy of neuroendocrine tumours [27-29]. Metal compounds are also used in molecular Magnetic Resonance Imaging (MRI) as contrast agents. In general, the latter are paramagnetic complexes (typically Gd^{3+}-based) (Figure 1) or super paramagnetic particles (typically iron oxides) that change the relaxation properties of water molecules that they encounter [30-32].

Recently, the major aim to study metal compounds for therapy and diagnosis stems from the wish to learn about their mechanisms of biological action in the expectation to improve selectivity, administration protocols and making new drugs. This work has been reviewed regularly, including by some of us [25, 33-41]. This part of the introduction is focused on the proteins/enzymes that have been more recently considered likely biological targets for metal compounds and studied at a molecular level, and the evidences of metal complexes-protein binding relevant to the drug/diagnostic agent's mechanisms of action will be explored.

1.2. Proteins as possible targets

The mechanisms of biological action of metal compounds for therapy and diagnosis have been widely investigated, although, in several cases still not fully elucidated. As an example, in the case of anticancer metallodrugs, DNA is not always the primary target as it appears for cisplatin [12, 42-44]. In fact, many of metal-containing chemotherapic agents actually show selectivity towards proteins with respect to nucleic acids, indicating that different modes of action occur depending on the specific type of metal complex. In recent years, the general consensus on the crucial role of the interactions of metallodrugs with proteins in determining the compounds' pharmacological action, uptake and biodistribution, as well as their overall toxicity profile, resulted in an exponential increase in the number of studies. Initially, these studies mostly concerned the two major serum

proteins, albumin and transferrin, involved in the transport of therapeutic metallodrugs, as well as metallothioneins, small, cysteine-rich intracellular proteins, primarily involved in storage and detoxification of soft metal ions [45, 46]. Nowadays, metal-based compounds are known to bind to several classes of proteins with different roles, including transporters, antioxidants, electron transfer proteins, DNA-repair proteins, as well as proteins/peptides simply used as model systems to characterize the reactivity of metallodrugs *in vitro*, but that are also present *in vivo* [44, 47-50].

Among the protein systems that have been most widely investigated as targets for metal therapeutic compounds it is worth mentioning the seleno-enzyme thioredoxin reductase (TrxR [51]), involved in the maintenance of the intracellular redox balance and overexpressed in certain cancer types, and reported to be inhibited mainly by gold compounds. In addition, several studies investigated protein kinases efficiently inhibited by ruthenium or iridium complexes [52, 53], various proteases inhibited by Pt(II), Ru(II), Re(IV), Cu(II) and Co(III) complexes [54-58], and histone deacethylase (HDAC) inhibition by Pt compounds [59]. Of note in the field, the group of Meggers has pioneered an approach in which metals can also be used as building blocks for well-defined, three-dimensional constructs, and used this principle in the development of organometallic complexes that mimic organic enzyme inhibitors [44]. Notably, other studies reported on the proteasome inhibition by anticancer gold(III) complexes, [60, 61] as well as by Ga(III), Zn(II) and Cu(II) compounds with asymmetric ligands [62]. Finally, reversible protein tyrosine phosphatase (PTP) inhibition by anti-diabetic vanadium complexes has been widely investigated [63].

Concerning macromolecular protein targets in nuclear molecular imaging, whose expression pattern and density are linked to a certain disease, cell surface receptors (e.g. G-protein coupled receptors), transporters (e.g. glucose transport protein GLUT1) and various enzymes [22, 23, 36] were among the most explored. Moreover, the folate receptor (FR), a cell surface protein, has been considered a promising target for diagnosis or therapy of cancer. The FR facilitates the uptake of folic acid (FA) a vitamin (B9) that is necessary for cell growth and proliferation. The FR is overexpressed in a variety of cancer types, with highest frequency observed in ovarian and endometrial carcinomas. Interestingly, besides being overexpressed in tumour, it is down-regulated in healthy adult cells. Therefore, the FR is an ideal structure for nuclear imaging using FR-targeted radiopharmaceuticals, and it has been extensively explored for diagnostic applications, namely using various radiometal complexes as recently reviewed by Müller and Schibli [64, 65]. Finally, the use of radioactive metal-based probes for targeting membrane receptors with receptor-specific peptides or for *in vivo* monitoring of tumour multidrug resistance (MDR) associated to membrane transporters has been also developed, but it will not be discussed herein as it has been already comprehensively reviewed [25, 36, 39].

Below, is presented in detail selected proteins/enzymes that have been recently studied and characterized for their interactions with therapeutic and diagnostic metal complexes, and that, most importantly, are likely targets for these metal compounds, including zinc-finger proteins, nitric oxide synthase, the zinc enzymes carbonic anhydrases, and thymidine kinases. Another protein target, aquaporins, will be further discussed in more detail in **Section 2** of this introductory chapter. The last part of this section will be focused on studies of metal compounds targeting parasitic enzymes for application in the treatment of infectious diseases. Particular attention will be paid to reviewing the studies on the characterization of the metal-protein target interactions at a molecular level, using different biophysical and analytical methods.

1.2.1. Zinc-finger proteins

Zinc is an essential metal in biology, being essential for growth and development. In fact 10% of the human genome encodes zinc proteins, representing ca. 3000 proteins of which 427 are zinc-finger (ZF) proteins. Zinc can bind in different ways in protein structures and so be classified into two main categories: (i) *catalytic zinc* in enzymes, where the binding site has a readily exchangeable water ligand coordinated and there can be up to three ions available for catalysis, and (ii) *structural zinc* with only protein residues in the coordination sphere, with general coordination of the type S_4, S_3N or S_2N_2 [66, 67]. In this latter case, zinc is not a direct participant in the conveyed interactions of the protein with other residues or molecules, but maintaining a tridimensional secondary/tertiary structure is essential for protein function. There are also intermediate cases such as the Ada protein, where the zinc is coordinated tetrahedrally only by amino acid residues (four cysteines) although one of the residues is a catalytic cysteine site [68]. This was the first observed case of a residue bounded to Zn^{2+} and acting as catalytic element, therefore not fitting this protein in either of the main categories.

Classically, zinc-finger (ZF) proteins belong to the structural zinc family where the zinc ion structurally organizes small peptidic domains (or bigger domains in case of multiple zinc ions) and different coordination, interactions and arrangements can contribute to the structural and functional variety of these proteins [68]. ZF proteins were shown to be intimately involved in a wide range of functions in DNA repairing, recognition, transcription, replication, apoptosis and metabolism. A remarkable example was the first described ZF motif in the transcription factor TFIIIA from the clawed toad *Xenopus laevis* [69], exhibiting a diverse array of structure and functions, the latter involving important cellular processes such as transcription, DNA repair, cellular signalling, metabolism and apoptosis. All of these processes are essential for cell growth and development, thus, having direct implications in health and disease, and so zinc-fingers are recognized more frequently as possible medicinal targets. In fact, these domains show a thermodynamic preference for Zn^{2+} to the detriment of other endogenous metal ions and, in case of metal substitution or coordination residue mutation, the protein function can be impaired or lost. Coordination compounds can affect ZF domain conformation either via zinc substitution or via oxidative damage and, therefore, may be important in the development of new therapeutic drugs [70].

Another important family of zinc-finger proteins includes the enzymes poly(adenosine diphosphate (ADP)-ribose) polymerase (PARPs), essential proteins involved in cancer resistance to chemotherapies. Moreover, PARPs play a key role in DNA repair by detecting DNA strand breaks and catalysing poly(ADP-ribosylation) [71] and, consequently, PARPs have been referred to as "the guardian angels" of DNA. Notably, PARP-1, the most studied member of the PARP family, is characterized by the presence of two long zinc-fingers (ZF-PARPs, also termed as nick-sensors), that are positioned upstream of the catalytic domain [72], and mediate specific nicked DNA recognition [73]. PARP-1 also binds to platinum-modified DNA [74, 75], and a systematic *in vitro* study was recently conducted, in which the effect of PARP-1 inhibition on the ability of nuclear proteins to bind platinum-modified DNA was evaluated by photo- cross-linking experiments [76]. According to these results, the activity of PARP following exposure to platinated DNA, resulted in the dissociation of DNA-bound proteins. Moreover, PARP inhibitors were able to sensitize some, but not all, of the cell lines towards cisplatin. Other studies describe the binding of PARP-1 to platinum

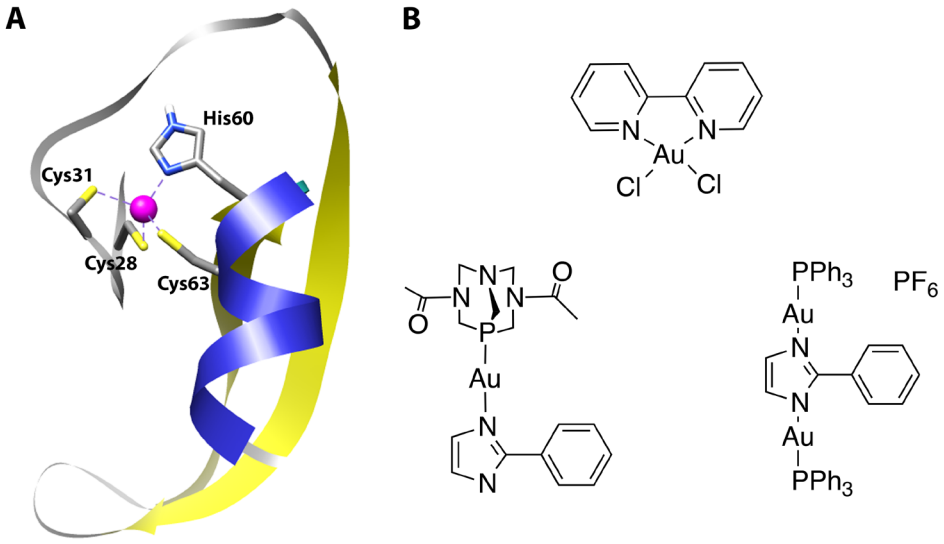

Figure 2. A: Ribbon representation of the NH2-terminal zinc finger of PARP-1, with the zinc binding motif shown as stick model. The Zn atom is depicted as a magenta sphere. This figure was generated using the pdb 2DMJ and Chimera software (http://www.cgl.ucsf.edu/chimera). The 106 amino acid sequence is as follows: GSSGSSGMAESSDKLYRVEYAKSGRASCKKCSESIPKDSLRMAIMVQSPMFDGKVPHWYHFSCFWKVGHSIRHPDVEVDG FSELRWDDQQKVKKTAEAGGSGPSSG (Zn-binding residues Cys28, Cys31, His60, and Cys63 in bold letters), **B:** Gold(III) and gold(I) complexes as PARP-1 inhibitors.

1,2-d(GpG) and 1,3-d(GpTpG) intrastrand cross-links on duplex DNA[77] and a more recent report demonstrated that PARP-1 differentiates between normal and platinum-damaged DNA, having higher binding affinity for the cisplatin 1,2-d(GpG) cross-links than for the unplatinated DNA or other types of cisplatin–DNA cross-links [74]. In this latter study it was also shown that PARP-1 may shield the DNA lesion from repair and triggers a cytotoxic response. Overall, in spite of these numerous studies, the activity of PARP upon cisplatin treatment remains controversial and not fully understood.

Within this framework, one of us recently described the ZF enzyme poly(adenosine diphosphate (ADP)-ribose) polymerase 1 (PARP-1) inhibition properties of different metal

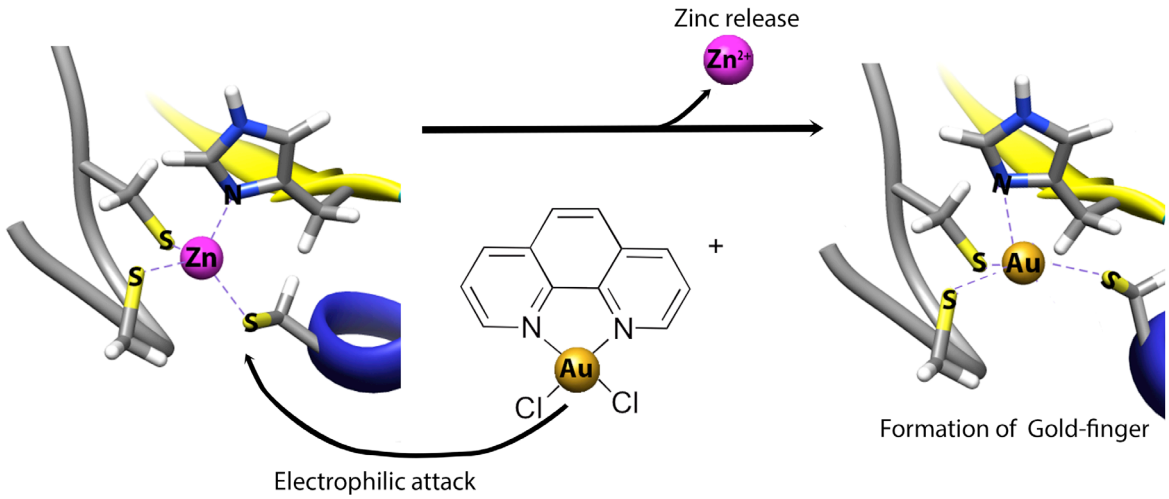

Figure 3. Model of the possible interaction between gold(III) complexes and PARP-1 N-terminal ZF domain.

compounds including cisplatin, and of a series of gold-based compounds with phosphine or bipyridyl ligands (Figure 2) [78, 79]. Interestingly, gold(III) complexes were among the most efficient in inhibiting purified PARP-1 followed by gold(I) compounds (IC_{50} in the nanoM range). Moreover, the gold complexes were able to efficiently inhibit PARP-1 in cancer cell extracts treated with the compounds, but only in certain human cancer cell lines.

Additional information on the reactivity of the metal complexes with PARP-1 N-terminal zinc-finger domain was obtained by high-resolution electrospray ionization Fourier-transform ion cyclotron mass spectrometry (ESI-FT-ICR MS) [78]. An excellent correlation between PARP-1 inhibition in protein extracts and the ability of the complexes to bind to the zinc-finger motif (in competition with zinc) was established. The results support a model whereby displacement of zinc from the PARP-1 zinc finger by other metal ions leads to decreased PARP-1 activity, and to formation of the so-called "gold-finger" (Figure 3).

Concerning ZF transcription factors, human DNA polymerase-α is inhibited by cisplatin via coordination with the cysteine residues on the protein's C4-ZF motif [80], causing tertiary structure distortion and displacing of the Zn ion. Ralph et al. have also shown by an ESI-MS approach that platinum compounds can interfere with binding of the transcription factor PU.1-DBD to a dsDNA molecule containing its consensus-binding site [81]. Moreover, cisplatin has also been recently reported to affect the conformation of the apo-form of the breast cancer susceptibility protein 1 (BRCA1) RING finger domain forming intra- and intermolecular Pt-BRCA1 adducts, where a preferential platinum-binding site was found at His117 [82]. The same authors investigated the functional consequences of the *in vitro* platination of the BRCA1 RING domain by cisplatin and analogues, which resulted in the inhibition of the ubiquitin ligase activity of BRCA1 [83].

Of note, platinum(II) complexes have been reported to interact with the C-terminal finger of the HIV nucleocapsid NCp7 zinc-finger leading to zinc ejection [84]. These latter studies show the opportunity of exploiting metal-based drugs as new classes of anti-HIV agents based on inhibition of HIV NCp7 function and targeting protein Cys residues [85]. Recently, the same authors showed that a platinated single-stranded oligonucleotide can alter the structure of a model ZF peptide and characterized this interaction at a molecular level by NMR spectroscopy [86]. The ZF conformation change results from the formation of an adduct between the platinated oligonucleotide and the peptide, stabilized by strong H-bonding interaction. Most importantly, these results have shown that the extent and rate of zinc displacement by inorganic compounds can be modulated by the nature (metal, ligands) of the reacting compound, and that DNA-tethered coordination complexes may be designed to target specific ZF motifs.

1.2.2. Nitric oxide synthase

Nitric Oxide Synthase (NOS) is the enzyme responsible for the catalytic oxidation of L-arginine (L-Arg) to L-citrulline and nitric oxide (NO), an endogenous free radical, which is a key signalling mammalian mediator in several physiological processes (e.g. vasodilation, neurotransmission, host-defence and platelet aggregation) [87]. NOS is a heme-containing enzyme that presents three structurally distinct isoforms. Two of them are constitutively expressed, being Ca^{2+}-dependent (nNOS [neuronal NOS, NOS1] and eNOS [endothelial NOS, NOS3]). The third isoform is Ca^{2+}-independent (iNOS, NOS2) and is inducible. The three isoforms differ in their tissue distribution and biological role [88]. The low levels of NO resulting from the activity of the constitutive isoforms

(eNOS and nNOS) regulate blood pressure, platelet aggregation and neurotransmission. The iNOS is expressed and induced at a transcriptional level by inflammatory stimuli (e.g. interferon, IFN-γ and bacterial lipopolysaccharide), and the relatively high levels of NO produced by this isoform contribute to the pathophysiology of several diseases, such as stroke, hypertension, cancer, ischemia, inflammation, colitis, and rheumatoid arthritis [89-91]. Therefore, the *in vivo* imaging of NO or NOS expression would allow earlier diagnosis, earlier treatment, better prognosis and individualized patient management of various diseases linked to NO/NOS deregulation [92, 93]. Taking into consideration the interest of one of us in the design of innovative radiometal-based complexes as probes for *in vivo* molecular imaging of NOS, a set of $M(CO)_3$-complexes (M = ^{99m}Tc, Re) containing pendant NOS-recognizing units have been designed [94-97].

At this stage it is worth mentioning that the development of novel ^{99m}Tc-based complexes for imaging applications implies always the use of a solution of sodium pertechnetate ($Na[^{99m}TcO_4]$) in saline as radioactive precursor. The dilute nature of this solution (10^{-8} M – 10^{-10} M) makes the structural characterization of the resulting ^{99m}Tc complexes impossible by the current analytical methods (e.g. elemental analysis, NMR and IR spectroscopy). One of the simplest ways to overcome this issue is to compare the chromatographic behaviour of the ^{99m}Tc complexes with that of the corresponding compounds prepared at the "macroscopic" scale with natural rhenium ("cold metal"). Indeed, technetium and rhenium, transition metals of group 7 of the periodic table, share similar coordination chemistry, and, consequently, rhenium complexes can be used as non-radioactive ("cold") surrogates of the respective ^{99m}Tc complexes.

Among the various $Re(CO)_3$-complexes mentioned above for NOS probing, prepared as "cold" surrogates of the analogue $^{99m}Tc(CO)_3$-complexes, those containing a pendant N^{ω}-NO_2-L-arginine moiety, an L-Arg derivative with known inhibitory ability towards NOS, displayed the most favourable targeting properties. In contrast, the complexes bearing a pendant L-Arg moiety, the natural substrate of NOS, lost completely the ability to recognize the enzyme. In the most promising complexes, the N^{ω}-NO_2-L-Arg pendant moiety is linked through its R-NH_2 or R-CO_2H group and an alkyl spacer of variable length to the $M(CO)_3$ core, which is stabilized by a tridentate bifunctional chelator of the pyrazolyl-diamine type (Pz). The complexes containing conjugates with a propyl *fac*-[$Re(CO)_3$(Pz-Prop-N^{ω}-NO_2-L-Arg)] or an hexyl spacer fac-[$Re(CO)_3$(Pz-Hex-N^{ω}-NO_2-L-Arg)], in which the R-NH_2 group of the inhibitor is involved in the conjugation to the metal centre, presented remarkable affinity for purified iNOS, being similar to that of the free non-conjugated inhibitor (K_i = 3-8 μM) in the case of the complex bearing the 6-carbon linker (K_i = 6 μM) (Figure 4).

Interestingly, the metal complexes presented higher inhibitory potency than the respective metal-free conjugates. Additionally, these complexes permeate also through RAW 264.7 macrophage cell membranes, interacting specifically with the target enzyme in the cytosol, as confirmed by the suppression of NO biosynthesis (30% - 50%) in LPS-treated macrophages. The respective $^{99m}Tc(CO)_3$-complexes also presented the ability to cross cell membranes, as demonstrated by internalization studies in the same cell model. Preliminary biodistribution studies in LPS-pretreated mature female C57BL6 mice, suggest that the complexes accumulate in tissues with iNOS upregulation.

Aiming to shed some light on the specific protein (iNOS)/ligand (rhenium complexes) interactions and to establish a preliminary structure-activity relationship, Oliveira et al. [98]

performed a molecular docking study to evaluate the binding modes of the N^{ω}-NO_2-L-arginine-containing conjugates and of the corresponding rhenium complexes. Molecular dynamics simulations were used to refine the conformations obtained by docking and to identify the most prevalent interactions between the Re complexes and the iNOS isoform, more specifically, between the "$Re(CO)_3$" metallic fragment and the active site of the enzyme. The higher inhibitory effect of the rhenium compound with the hexyl spacer (*fac*-[$Re(CO)_3$(Pz-Hex-N^{ω}-NO_2-L-Arg)]) arises from the stronger, unique, electrostatic interactions observed between the "$Re(CO)_3$" core and the residues Arg260 and Arg382 (Figure 5A). This interaction, is only possible due to the higher flexibility associated to the C6-carbon linker when compared to the C3 linker present in the other rhenium analogue. Moreover, the computational studies demonstrated that the metal centre plays a key role in the organization and orientation of the organic ligands, defining the overall shape of the inhibitors that fit better in the active pocket of iNOS (Figure 5B).

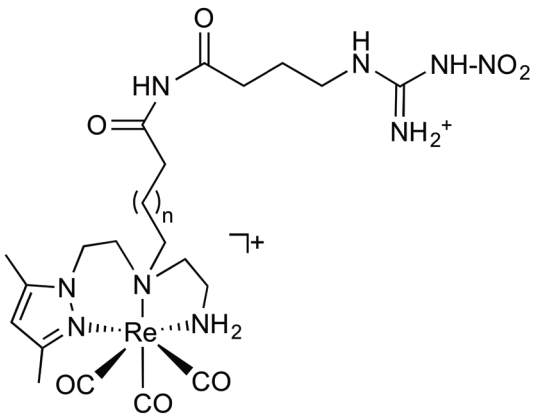

***fac*-[$Re(CO)_3$(Pz-Prop-N^{ω}-NO_2-L-Arg)]** (n = 1)
***fac*-[$Re(CO)_3$(Pz-Hex-N^{ω}-NO_2-L-Arg)]** (n = 4)

Figure 4. Rhenium tricarbonyl complexes with a pendant N^{ω}-NO_2-L-Arg moiety as inhibitors of nitric oxide synthase.

Brought together, computational methods may be useful for predicting the affinity of putative novel rhenium and technetium complexes. Such an approach may provide strategies for the design of novel metal-based substrates/inhibitors with unique shapes and higher structural diversity with the aim of targeting NOS *in vivo* more effectively.

1.2.3. Carbonic anhydrases

Mammalian carbonic anhydrases (CAs) are zinc metalloenzymes that comprise 16 different

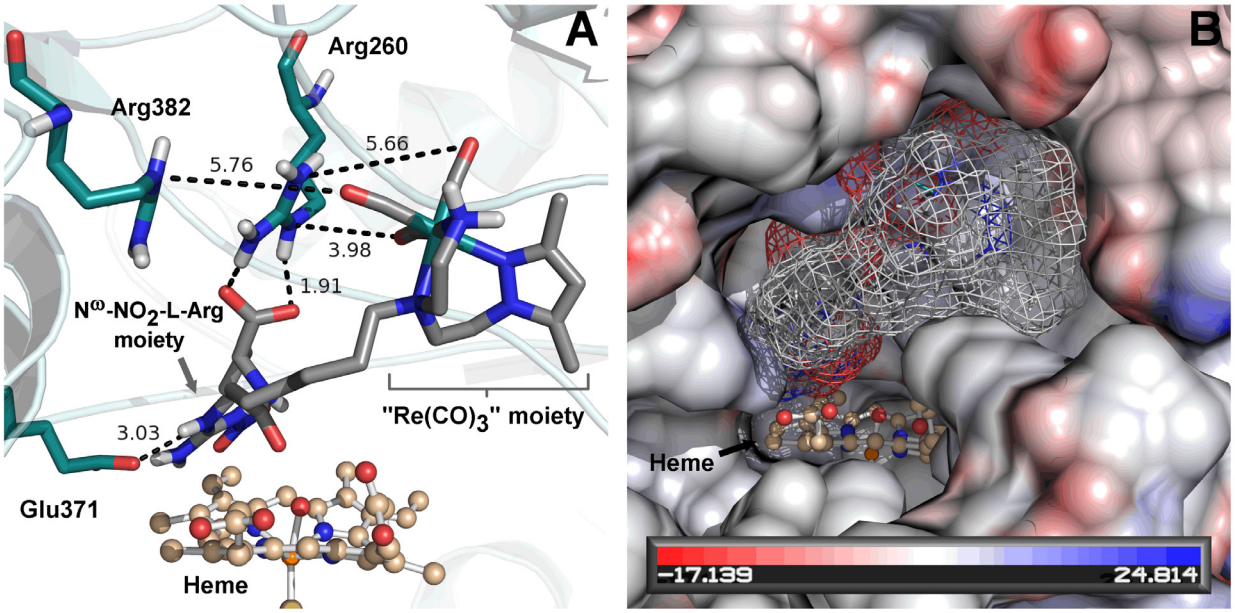

Figure 5. A: Proposed structure of fac-[$Re(CO)_3$(Pz-Hex-N^{ω}-NO_2-L-Arg)] in complex with iNOS obtained by MD simulation. The following color scheme is used: nitrogen in blue, oxygen in red, sulfur in yellow, iron in orange and rhenium in deep teal. All distances shown in Å. **B:** Molecular surface of the active site of the same system coloured according to electrostatic potential. The figure was generated using the VASCo PyMOL plug-in [99, 100].

isozymes, among which several cytosolic forms (CA I–III, CAVII), four membrane-bound isozymes (CA IV, CA IX, CA XII, and CA XIV), one mitochondrial form (CA V), as well as a secreted CA isozyme, CA VI. These enzymes catalyse a very simple physiological reaction, the interconversion between carbon dioxide and the bicarbonate ion, and are involved in crucial physiological processes connected with respiration and transport of CO_2/bicarbonate between metabolizing tissues and lungs, pH and CO_2 homeostasis, electrolyte secretion in a variety of tissues/organs, biosynthetic reactions (such as gluconeogenesis, lipogenesis and ureagenesis), bone resorption, calcification, tumorigenicity, and many other physiologic or pathologic processes. As will be discussed shortly, many of these isozymes are important targets for the design of inhibitors with clinical applications [101]. Among other biomedical applications (e.g. treatment of glaucoma by lowering of the intraocular pressure with CA inhibitors), CAs have been considered validated drug targets for cancer diagnosis and therapy since there is overexpression of specific isozymes in certain tumour types. Indeed, CA isozymes IX and XII are overexpressed in cancer cells of many hypoxic tumours, being involved in critical processes connected with cancer progression and response to therapy [101].

The Zn(II) ion of CAs is essential for catalysis. X-ray crystallographic data showed that the metal ion is situated at the bottom of a 15 Å deep active site cleft, being coordinated by three histidine residues (His94, His96, and His119) and a water molecule/ hydroxide ion (Figure 6A). The inhibition and activation of CAs are well understood processes, with most types of inhibitors binding to the metal centre, whereas the activators bind at the entrance of the active site cavity where they participate in the proton shuttling between the metal-coordinated water molecule and the environment [102]. Aromatic/heterocyclic sulfonamides and their derivatives, such as sulfamates and sulfamides, are the most investigated types of organic carbonic anhydrase inhibitors (CAI) [103, 104], having various biomedical applications as diuretics or as drugs for the treatment or prevention of a variety of disorders such as antiglaucoma drugs, anticonvulsants, antiobesity, anticancer, analgetic and antiinfective agents. Sulfonamides and their bioisosteres bind to the metal ion from the CA active site in deprotonated form, as anions, by replacing the metal-coordinated water molecule/hydroxide ion, which is necessary for catalysis, and thus exerting their inhibitory mechanism [105]. Recently, novel interesting chemotypes, in addition to the sulfonamides, were discovered, many of which are based on natural products, such as phenols/polyphenols, phenolic acids, and coumarins [106].

In this respect, metal-based compounds of various types were also studied for their CA inhibition properties. For example, metal complexes of heterocyclic sulfonamides (all clinically used CA inhibitors) have been reported to possess very efficient CA inhibitory properties, and their mechanisms of action have been explained as being due to both sulfonamidate anions, as well as metal ions (formed after dissociation of the complex in dilute solutions) which interact thereafter with different binding sites of the enzyme. Metal ions incorporated in such complexes mainly included transition metal ions such as Zn(II), Cu(II), Co(II) and Ni(II), as well as lanthanides(III) [107].

Most recently, more structurally elaborated complexes, were designed and tested as CAI. Among them, BR30 bears a benzenesulfonamide moiety and a cupric iminodiacetate (IDA-Cu^{2+}) unit (Figure 6B). Its rationale is to incorporate in the same molecule an aromatic sulfonamide fragment (that would coordinate to the zinc ion from the active site) and copper(II)-iminodiacetic

(IDA) moieties that may bind to His64 on the rim of the active sites of the various isoforms [108]. The crystal structures of human carbonic anhydrases I and II complexed with BR30 and other inhibitors of the same family have been determined. The ionized NH- group of each benzenesulfonamide coordinates to the active site Zn^{2+} ion and, in the case of BR30, the IDA-Cu^{2+} unit binds to His64 of CAII and His200 of CAI [109]. However, recent studies with 1,2-dithienylethene-based compounds incorporating benzenesulfonamide and Cu(II)-IDA-, bis-benzenesulfonamide-, bis-Cu(II)-IDA-, and bis-ethyleneglycol-methyl ether moieties, showed not equally promising results in terms of inhibitor selectivity for various isoforms [110].

Other copper(II) complexes of DTPA-, DOTA-, and TETA-tailed sulfonamides targeting the tumor-associated transmembrane isoform CA IX were also recently reported (Figure 6B) [111]. The new compounds were designed in such a way as to possess high affinity for Cu(II) ions, exploiting four pendant carboxylate moieties in the DTPA derivatives, as well as the cyclen/cyclam macrocyles and three pendant acetate moieties in the DOTA and TETA derivatives. Most importantly, copper complexes presented higher inhibitory potency than the corresponding sulfonamide ligands, and showed membrane impermeability, thus having the possibility to specifically target the transmembrane CA IX, which has an extracellular active site. Incorporation of radioactive copper isotopes in this type of CA inhibitor may lead to interesting diagnostic/therapeutic applications for such compounds, provided their stability in physiological conditions.

The X-ray crystal structures of four metallocene-based CA inhibitors containing triazole-ferrocene or triazole-ruthenocene fragments and a sulfonamide group in complex with CAII have also been recently reported by Salmon et al. [112]. In this study, the authors have concluded that the barrel-shaped hydrophobic ferrocene and ruthenocene moieties provide a structure-based avenue to better occupy the hydrophobic binding patch within the enzyme active site, and consequently allows the design of more efficient metallocene-based human CA inhibitors. Based on the knowledge of the structural parameters involved in the interaction enzyme-metallocene, the same authors have prepared a new series of derivatives of the same type with moderate to good inhibitory potency, with various metallocenes displaying significant selectivity for CA IX and CA XII. Indeed, the most potent compound is a ferrocene-based inhibitor that had a K_i of 5.9 nM and 6.8 nM at CA IX and XII, respectively. It is worth mentioning that the activity of one regioisomer of this potent compound towards the same isozymes is significantly lower. Additionally, the *in vitro* ADME properties (e.g. LogP, LogD, solubility, etc.) of representative metallocenes have been also determined. Brought together, the results confirmed that the barrel-shaped metallocene moiety provides a means of discriminating the CA isozymes active site when compared to the corresponding non-metallated phenyl analogues, while biopharmaceutical properties were unchanged [112, 113].

There are also a few examples of organometallic piano-stool complexes bound to CA II (Figure 8B). Monnard et al. have reported a series of d6-piano-stool Ru complexes bearing an arylsulfonamide anchor with only sub-micromolar affinity towards hCA II. The X-ray crystal structure of one of the complexes ($[(\eta^6\text{-}C_6Me_6)Ru(bispy_3)Cl]^+$) with hCA II have been determined, highlighting the nature of the host-guest interactions [114] .

Aimed at selective targeting of CA IX, *in vivo,* for diagnostic and/or treatment purposes, Alberto and co-workers have synthesized, following the so-called extended 3D space population concept, four arylsulfonamide, -sulfamide, and -sulfamate based CAIs with the organometallic motif $[(Cp\text{-}R)M(CO)_3]$ (M= Re or ^{99m}Tc) (Figure 6), and evaluated their affinity to CA isoforms

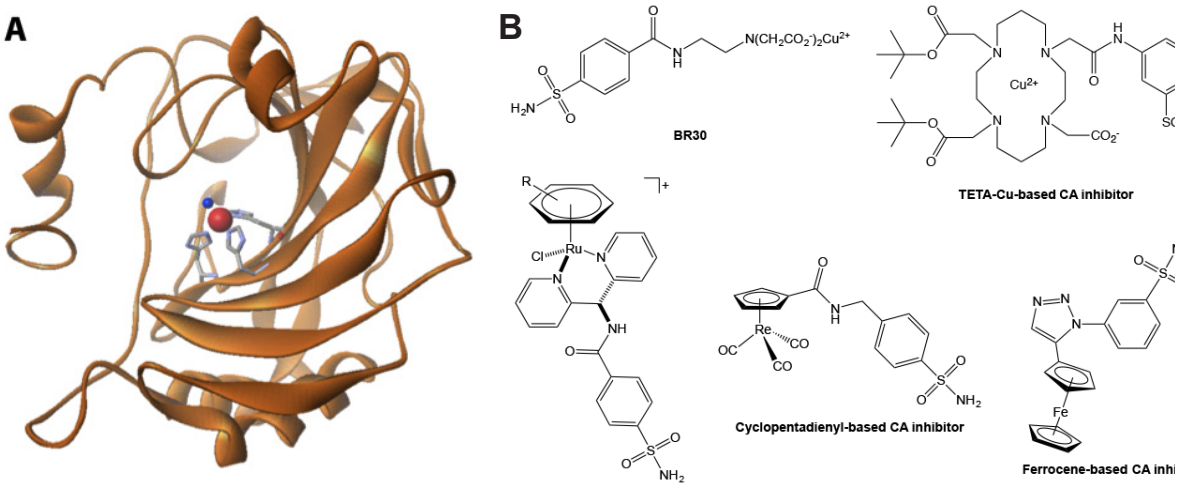

Figure 6. A: Carbonic anhydrase II structure. The Zn atom is depicted as a red sphere, the oxygen of the OH^- as a blue sphere, the three catalytic His residues as grey sticks. This figure was generated using the pdb 1CA2 and Chimera software (http://www.cgl.ucsf.edu/chimera), **B:** Sulfonamide-containing metal-based inhibitors of carbonic anhydrase.

[115]. The enzymatic assays with purified 12 CA isozymes have shown that the compounds presented inhibition constants in the low nanomolar range for some of the isoforms. The values obtained are in the same range as those found for organic inhibitors. One of the compounds displayed superior selectivity for hCA II, IX and XIV, which contrasts with the acetazolamide standard that does not show any distinct preference pattern for any of the isoforms. The binding mode of the aforementioned Re(I) complexes with CA was assessed by X-ray crystallography. The crystal structure of human CA II complexed with one of the compounds is presented in Figure 7A.

Recently, one of us reported on the moderate inhibition of human CA II by the antimetastatic Ru complex [tetrachloro(DMSO)(imidazole)-ruthenate(III)], NAMI-A [116]. The X-ray structure of the adduct formed between NAMI-A and hCAII could be solved at 1.8 Å resolution showing that Ru selectively binds His64, providing conclusive evidence that none of the original ligands of ruthenium in NAMI-A are conserved upon protein binding and supporting the view that the

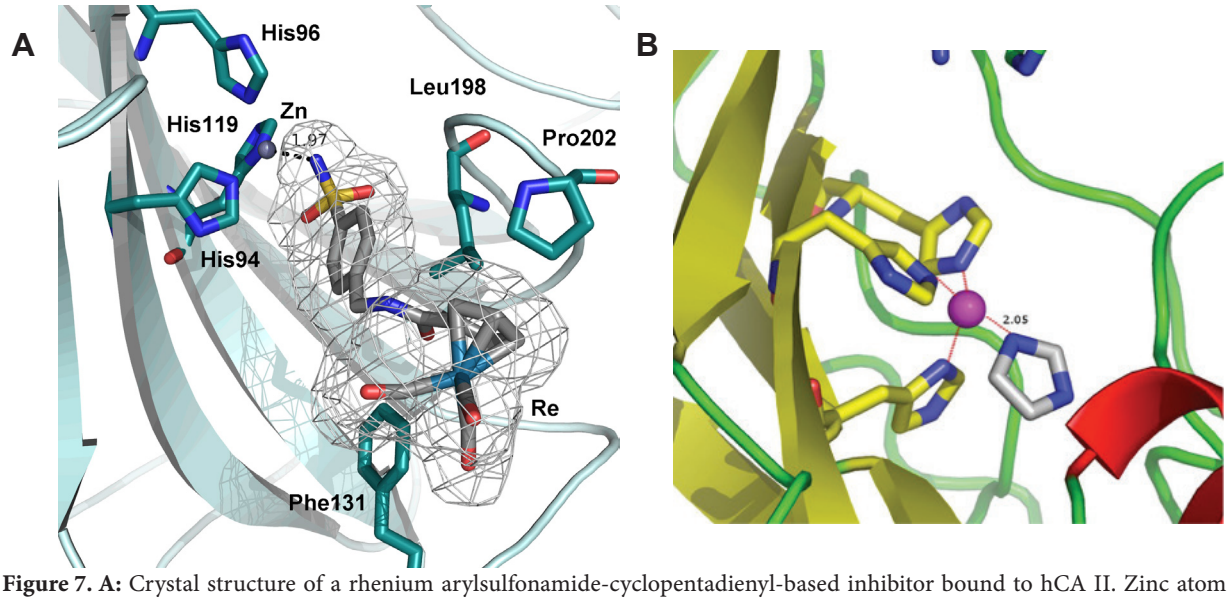

Figure 7. A: Crystal structure of a rhenium arylsulfonamide-cyclopentadienyl-based inhibitor bound to hCA II. Zinc atom is shown in grey sphere. The figure was generated using the pdb id 3RJ7 and PyMOL [100]. **B:** Detail of the active site of hCAII adduct with NAMI-A highlighting the imidazole from the compound directly coordinated to Zn^{2+} at a distance of 2.05 Å. The residues His94, His96, His119 are shown as yellow sticks; the Zn atom is depicted as a magenta sphere, and the imidazole ring as white sticks. This figure was generated using the pdb 3M1J and COOT [120].

compound can behave as an "extreme" prodrug. Interestingly, His64 plays an important role in hCA II catalysis, being situated in the middle of the active site cavity and acting as a proton shuttling residue between the zinc-bound water and the reaction medium, for the generation of the nucleophilic active form of the enzyme. Notably, examination of the electron-density map showed the presence of an imidazole ligand (not bound to Ru) in the active site region, anchored to the Zn(II) ion of the hCA II active site within almost regular tetrahedral coordination geometry (see Figure 7B). A similar binding mode to the zinc ion of hCA II has been previously reported for the competitive inhibitor 1,2,4-triazole,[117] polyamines,[118] as well as sulfocumarins,[119] and it is another interesting aspect of the observed reactivity that would deserve further exploration to exploit other strategies to CA inhibition.

Overall, the above-mentioned studies demonstrate that CA inhibition by metal compounds is worth attempting for various therapeutic applications. The development of diagnostic tools based on metal-based CAI is also an attractive future research direction.

1.2.4. Thymidine kinases

Thymidine kinases, namely human cytosolic thymidine kinase (hTK1) and herpes simplex virus thymidine kinase type 1 (HSV1-TK) are key enzymes for metabolisms of viruses and mammals, and have been proposed as suitable targets for non-invasive imaging of gene therapy and cancer [121-124]. Human thymidine kinase is a cytosolic enzyme that catalyses the γ-phosphate transfer from ATP to the 5′-hydroxyl groups of thymidine (dT) and 2′-deoxyuridine (dUrd). Different series of ^{99m}Tc(I)/Re(I) complexes for specific targeting of human thymidine kinase 1 (hTK1) have been proposed to detect/visualize increased hTK1 activity associated to proliferating cancer cells. In this context, the Re(I) complexes are considered "cold" surrogates of the respective ^{99m}Tc(I)-complexes.

Schibli et al. have introduced the first organometallic inhibitors of hTK1, namely a set of anionic Re(I) tricarbonyl complexes, which, besides the organometallic core stabilized by a tridentate imino-diacetic acid-based chelator, contain pendant 5′-aminothymidine analogues and alkyl chains of various lengths (Figure 8). The inhibitory potency of the complexes was tested towards hTK1 and also HSV1-TK, and it has been observed that in the case of hTK1 the inhibition capacity of the complexes improved with increasing spacer length. On the other hand, the complexes showed none or only slight inhibition of the HSV1-TK [125]. Based on the assumption that the lack of activity against HSV1-TK was the result of steric clashes with the enzyme's ternary structure due to inappropriate lengths of the spacers between the metal core and the thymidine moiety, the same group has prepared a new family of thymidine derivatives with either significantly shorter or longer alkyl spacers to avoid potential interferences between the metal core and the protein. The effect of the overall charge of the complex in its inhibitory capacity was also investigated [126]. Brought together, the enzymatic assays revealed mixed inhibition of hTK1 for all thymidine complexes independent of the spacer length. Moderate competitive inhibition of HSV1-TK was only achieved when the pendant thymidine fragment and the metal core were separated by a spacer of ca. 30 Å length. These findings were also supported by *in silico* molecular docking and molecular dynamic experiments. Further studies by the same group has shown that selective inhibition of HSV1-TK was only achieved with a new anionic rhenium organometallic complex bearing a pendant 5'-carboxamide 5-ethyl-2'-deoxyuridine derivative [127] (Figure 8). Indeed, inhibition of the hTK1

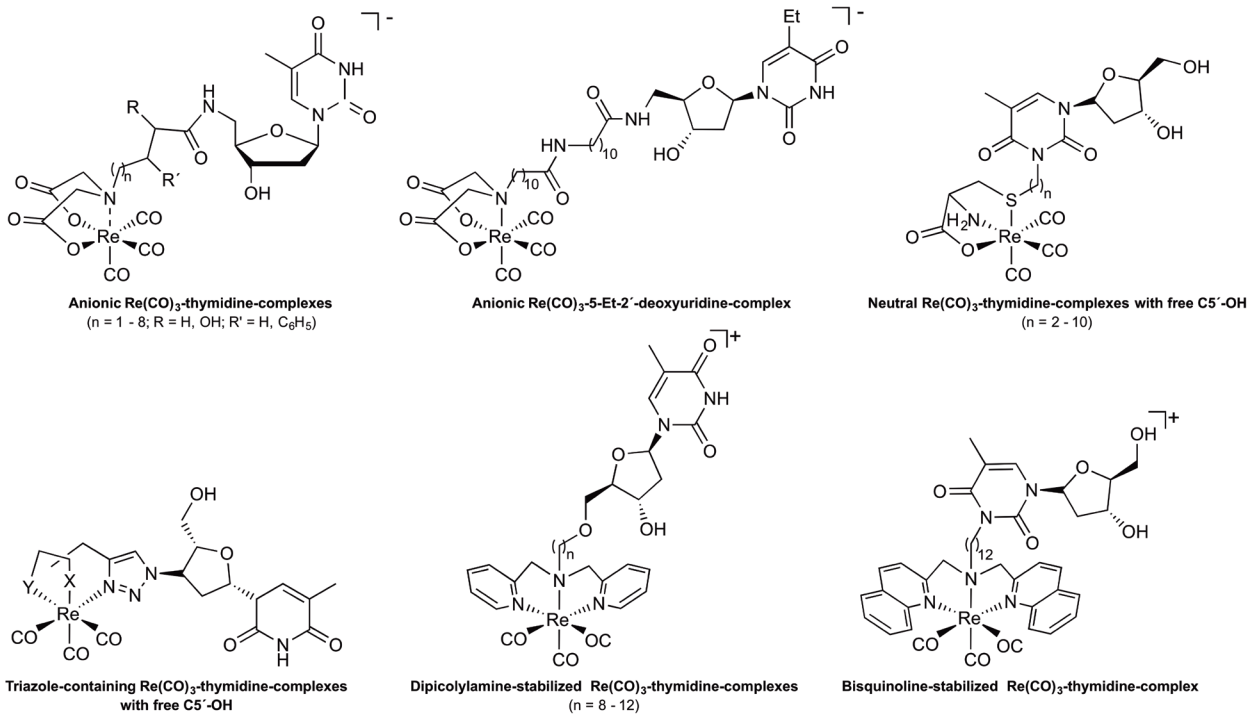

Figure 8. $Re(CO)_3$-complexes containing pendant thymidine and uridine moieties for targeting hTK1 or HSV1-TK.

previously reported for Re(I) analogue complexes of the 5'-carboxamide thymidine derivative described above was not observed [127].

The functionalization at position C5' in all the previously described M(I) compounds (M = Re, ^{99m}Tc) prevents phosphorylation and, consequently, such complexes were considered unattractive as potential radiotracers for non-invasive imaging of tumour progression as the mechanism by which they would be trapped inside cancer cells relies on phosphorylation of the complex. Therefore, new M(I) complexes (M = Re, ^{99m}Tc) containing thymidine derivatives with free C5'-hydroxyl group which are still recognized as substrates by hTK1 have been proposed. Schibli and co-workers synthesized and characterized a set of N3-functionalized Re and ^{99m}Tc organometallic thymidine analogues with neutral, cationic or anionic overall charge and spacers of various lengths between the organometallic core and the thymine base [128]. The phosphorylation of the metal complexes in the presence of hTK1 and ATP was assessed quantitatively relative to thymidine. Despite being all substrates of recombinant hTK1, it has been concluded that the neutral complexes were phosphorylated to a greater extent than the charged complexes and that the extent of phosphorylation was further improved by increasing the spacer length (Figure 9). A molecular dynamics simulation study performed with a modified hTK1 structure supported the experimental findings. Additionally, *in vitro* cell internalization experiments performed in a human neuroblastoma cell line (SKNMC) showed significant uptake for the neutral, lipophilic complexes. Further work by the same group has shown that neutral $[Re(CO)_2(NO)]_2^+$-labelled thymidine derivatives presented substrate activity towards hTK1 comparable to that of the structurally analogous anionic $[Re(CO)_3]^+$-labeled thymidine derivatives [129]. It is also worth mentioning that Struthers et al. have introduced an elegant strategy based on "click chemistry" for the preparation of neutral and cationic Re/^{99m}Tc organometallic complexes containing thymidine derivatives with free C5´hydroxyl group [130]. Most recently, using this synthetic strategy, the same authors introduced Re/^{99m}Tc tricarbonyl complexes with different structures and overall charges from a

common precursor, and the first organometallic hTK1 substrates in which thymidine is modified at the C3´ position were identified (Figure 8). Evaluation of substrate activity toward this enzyme has shown that the influence of the overall charge of the derivatives is dependent on the position of functionalization. In the case of the C3´-functionalized derivatives, neutral and anionic substrates were most readily phosphorylated, whereas for the N3-functionalized derivatives, cationic and neutral complexes were apparently better substrates for the enzyme than anionic derivatives [131].

With the aim of introducing rhenium tricarbonyl complexes bearing nucleosides for chemo- and/or radiotherapy, profiting from both the potential antiproliferative properties of Re(I) complexes and/or β^--emission of the radioisotopes ^{186}Re and ^{188}Re, Zubieta and co-workers have introduced a set of $Re(CO)_3$ complexes stabilized by various neutral tridentate chelators (e.g. dipicolylamine or bisquinoline type) with spacers of different lengths attached to pendant thymidine or uridine moieties at different positions (Figure 8). Among the cationic dipicolylamine-containing complexes, the one with a dodecylene spacer at C5' exhibited the highest toxicity against the A549 lung carcinoma cell line [132, 133]. However, despite this result, the toxicity of this complex could not be assigned solely and directly to the inhibition of hTK-1. Most recently, the same group reported a series of N3-conjugated $Re(CO)_3$-thymidine complexes stabilized by a bisquinoline bifunctional chelator. The complex carrying a dodecylene spacer presented again the highest cytotoxicity against A549 lung carcinoma cell line. Cellular uptake studies with the same compound have been performed by fluorescence microscopy, showing that it was clearly internalized into A549 cells. However, also in this family of compounds, the cytotoxic effect could not be correlated with the inhibitory ability of the complexes towards hTK-1 [134].

1.2.5. Parasite enzymes as targets

Malaria, trypanosomiasis and leishmaniasis are tropical diseases caused by parasitic protozoans. The malaria causative agent, transmitted by the mosquito vector (female mosquito of the Anopheles genus), is a unicellular eukaryote belonging to the *Apicomplexa* phylum and named *Plasmodium spp*. The protozoan parasites *Trypanosoma cruzi* and *Trypanosoma brucei* are the etiologic agents of american trypanosomiasis (Chagas disease) and human african trypanosomiasis (sleeping sickness), respectively. Both are transmitted to the mammalian host by insects: *T. brucei* by the tsetse fly through saliva, and *T. cruzi* by hematophagus triatomine bugs through the insect faeces near the site of the bite wound. Leishmaniasis is a disease with extensive morbidity and mortality with various forms that are caused by protozoa of the genus *Leishmania*.

Metal compounds have already found extensive application in the treatment of parasitic diseases in the pioneering times of modern pharmacology, mostly based on an empirical use [135, 136]. Various inorganic salts were thus administered against the major tropical diseases, sometimes with very good results. Notably, as a consequence of those ancient observations, a few antimony compounds (see Figure 1) still constitute the treatment of choice for some forms of leishmaniasis [136]. Bismuth is still used sporadically in the prophylaxis of malaria. Conversely, arsenicals, although effective, were withdrawn completely because of their recognized toxicity. However, no detailed structure/function studies were ever performed on antiparasitic metal-based compounds.

In recent years, the potential use of inorganic and/or organometallic compounds for treating parasitic illnesses, considering different types of drug targets, and having different mechanisms of actions, has been the subject of various articles [137-140]. Remarkably, the knowledge of the

biology of these parasites in our *postgenomic* era has greatly increased, and several protein targets have been identified against which novel metal compounds might be specifically developed and tested. Herein, we will briefly address the most interesting results and the most potent compounds when protein targets, mainly enzymes, are considered.

As far as it concerns malaria treatment, metal complexation (e.g. Ru, Au, Ir or Fe) of existing antimalarial drugs (e.g. chloroquine) has been proposed as an effective option for drug improvement, namely towards higher activities against resistant parasites [138]. Recently, selected metallodrugs such as auranofin, aurothiomalate, triethylphosphine gold(I) chloride, cisplatin, the ruthenium(III) complex NAMI-A, mononuclear and dinuclear gold(III) complexes, as well as bismuth and antimony compounds were evaluated for their antiplasmodial properties [141, 142]. All tested metal compounds, although with different potencies, effectively reduced *P. falciparum* growth *in vitro*, implying high and broad parasite sensitivity to these metals. Good candidate molecular targets for these metal compounds are parasite biomolecules containing functionally relevant thiol and selenol groups such as the previously mentioned thioredoxin reductase, an ubiquitous protein involved in intracellular redox balance, and falcipain, a cysteine protease typical of *P. falciparum*.

Indeed, since cysteine proteases play key roles in parasitic life cycles including *Schistosoma*, *Plasmodium*, *T. brucei*, *T. cruzi*, and *Leishmania*, they have also been considered promising parasite targets for drug development. Colotti et al. recently reported the crystal structure for Leishmania trypanothione reductase disclosing the actual mechanism of enzyme inhibition by antimonials [143]. It was shown that trivalent antimony binds to the protein active site with high affinity, strongly inhibiting enzyme activity. The metal binds directly to Cys52, Cys57, Thr335 and His461, thereby blocking hydride transfer and trypanothione reduction. Details of the structure are shown in Figure 9.

Following a strategy similar to that established for anti-malarial agents, one of the approaches that is being explored for treating trypanosomiasis is the use of metallated anti-trypanosomal compounds. The most successful metal-complexes proposed were $[Au_2(mpo\text{-}H)_2(PPh_3)_2]$, $[Pt(mpo\text{-}H)_2]$, $[Pd(mpo\text{-}H)_2]$ and $[VO(mpo\text{-}H)_2]$, which bear 2-mercapto-pyridine *N*-oxide (mpo), a strong and selective inhibitor of NADH–fumarate reductase [144]. The complexes showed significantly increased activities compared to mpo on epimastigotes of different *T. cruzi* strains. A direct correlation between parasite inhibition and NADH-fumarate reductase inhibition was found, highlighting this enzyme as the most likely target [145].

The validation of parasite cysteine proteases as relevant drug targets, as mentioned before, stimulated the assessment of the inhibitory activity of a series of mixed-ligand oxorhenium(V) complexes of the so-called [3+1] type, and cyclometallated organo Au(III) and Pd(II) complexes against parasite cysteine proteases cruzain from *T. cruzi* and cathepsin B-like cysteine protease (cpB) from *Leishmania major* [139]. Additionally, the inhibitory effectiveness of some of the complexes against *in vitro* models of parasite growth and infectivity was also examined (*T. cruzi*, *L. major, L. mexicana* and *L. donovani*) [139]. The enzymatic assays revealed that the inhibitory potency of some of the complexes is comparable to that of mammalian cathepsin B, also determined in a parallel experiment. The cell studies have shown that the only gold complex tested was both inactive and non-toxic, whereas the only palladium compound assayed, despite being toxic at the highest concentration, extended the life cycle of *T. cruzi* amastigotes in J774 macrophages at lower

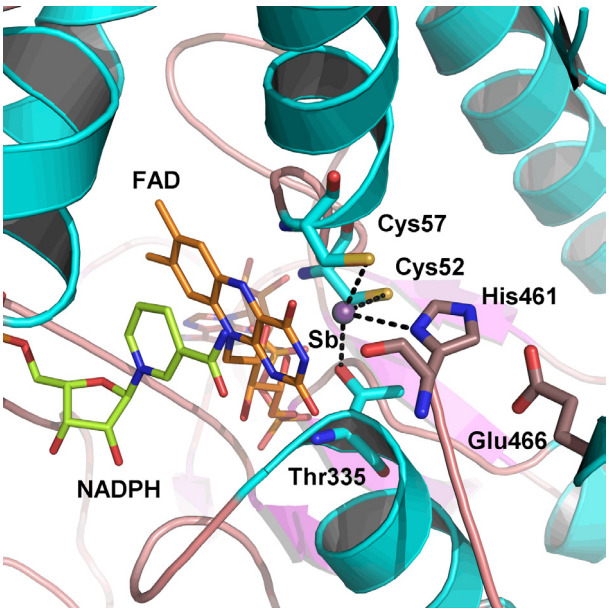

Figure 9. Figure 10: X-ray structure of the Sb(III) binding site of trypanothione reductase. Antimonial atom is shown in violet. The Sb(III) coordinating residues (Cys52, Cys57, His461 of chain B, and Thr335) are indicated as sticks. NADPH and FAD are colored light green and orange, respectively. The Glu466 of chain B, which is involved in trypanothione reduction, is depicted in pink sticks. This figure was generated using the pdb ID 2W0H and PyMOL [100].

concentrations. In the case of the rhenium compounds, the one with the highest inhibitory potency towards purified cruzain was inactive against *T. cruzi*. Conversely, the complex with the lowest inhibitory potency, was active against the parasite. These results could be ascribed to the different abilities of the compounds to cross the cell membrane.

Nitrogen-containing bisphosphonates (N-BPs) are a class of drugs used in the treatment of bone-related diseases, namely osteoporosis, Paget´s disease and tumour bone metastasis, among others. The clinical success of BP's is also associated with their use in radiopharmaceuticals for bone imaging (^{99m}Tc-labeled BPs) or for bone-pain palliation (e.g. ^{153}Sm- or $^{186/188}$Re-labeled BPs)[27]. N-BPs decrease bone resorption by inhibiting farnesyl pyrophosphate synthase (FPPS), a key regulatory enzyme in the mevalonate pathway, and thereby preventing the prenylation of small GTPases, which are essential for osteoclast function. Interestingly, besides mammals, FPPS exists also in parasites such as *T. cruzi*, and various organic bisphosphonates were found to inhibit the proliferation of *T. cruzi* both *in vitro* and *in vivo* without toxicity for the host cells [146]. In spite of the promising results, bisphosphonates in general are known to present a poor oral bioavailability, mainly due to the high ionization of phosphonate groups at physiological pH. With the aim of overcoming this issue, bisphosphonate-metal complexes have been proposed to improve the pharmacological properties of the bisphosphonates and improve their anti-parasitic action. For example, Demoro et al. have studied a series of complexes of anti-resorptive drugs in clinical use such as alendronate (Ale), pamidronate (Pam) and risedronate (Ris) with Cu, Co, Mn and Ni [140, 147]. Some of the complexes presented an improved antiproliferative effect against *T. cruzi* compared to the free non-coordinated bisphosphonate. In most cases the anti-*T. cruzi* activity could be correlated with the inhibition of parasitic farnesyl diphosphate synthase (TcFPPS) *in vitro*. It is also worth mentioning that all metal-bisphosphonate complexes are selective inhibitors of TcFPPS, showing no or little inhibition of human FPPS.

With respect to the use of metal compounds for treating parasitic diseases through inhibition of parasite enzymes, namely cysteine proteases or farnesyl diphosphate synthase, special attention should be given to selectivity issues. Indeed, the compounds should not be recognized by the respective mammalian enzymes in order to avoid toxicity and unwanted side effects. Although challenging, this goal can be attainable in the near future by structural studies combining X-ray crystallography, computational chemistry and modern analytic techniques based on NMR or mass spectrometry (MS). Moreover, based on proteomic techniques, novel specific targets in parasites should be identified and validated as relevant drug targets for metal complexes.

References

[1] K.H. Thompson, C. Orvig, Science, 300 (2003) 936-939.
[2] D. Gaynor, D.M. Griffith, Dalton Trans, 41 (2012) 13239-13257.
[3] A. Levina, P.A. Lay, Dalton Trans., 40 (2011) 11675-11686.
[4] M.A. Pysz, S.S. Gambhir, J.K. Willmann, Clin Radiol, 65 (2010) 500-516.
[5] H.J. Wester, Clin Cancer Res, 13 (2007) 3470-3481.
[6] R. Weissleder, M.J. Pittet, Nature, 452 (2008) 580-589.
[7] S.P. Fricker, Chem. Soc. Rev., 35 (2006) 524-533.
[8] B. Rosenberg, L. Vancamp, T. Krigas, Nature, 205 (1965) 698.
[9] K.R. Barnes, S.J. Lippard, Metal Ions in Biolgical Systems, Vol 42: Metal Complexes in Tumor Diagnosis and as Anticancer Agents, 42 (2004) 143-177.
[10] M.A. Jakupec, M. Galanski, V.B. Arion, C.G. Hartinger, B.K. Keppler, Dalton Trans., (2008) 183-194.
[11] L. Ronconi, D. Fregona, Dalton Trans., (2009) 10670-10680.
[12] W.H. Ang, A. Casini, G. Sava, P.J. Dyson, J. Organomet. Chem., 696 (2011) 989-998.
[13] A. Casini, L. Messori, Curr Top Med Chem, 11 (2011) 2647-2660.
[14] S. Komeda, A. Casini, Curr Top Med Chem, 12 (2012) 219-235.
[15] M. Jakupec, Keppler, B.K., Gallium and other main group metal compounds as antitumor agents, in: A. Sigel, Sigel, H. (Ed.) Metal Ions in Biological Systems, Marcel Dekker Inc., 2004.
[16] G. Gasser, I. Ott, N. Metzler-Nolte, J. Med. Chem., 54 (2011) 3-25.
[17] A. Vessieres, S. Top, W. Beck, E. Hillard, G. Jaouen, Dalton Trans., (2006) 529-541.
[18] J. Reedijk, Plat. Metals Rev., 52 (2008) 2-11.
[19] U. Jungwirth, C.R. Kowol, B.K. Keppler, C.G. Hartinger, W. Berger, P. Heffeter, Antioxid Redox Sign, 15 (2011) 1085-1127.
[20] S.L. Pimlott, A. Sutherland, Chem Soc Rev, 40 (2011) 149-162.
[21] T.J. Wadas, E.H. Wong, G.R. Weisman, C.J. Anderson, Chem Rev, 110 (2010) 2858-2902.
[22] S. Vallabhajosula, L. Solnes, B. Vallabhajosula, Semin Nucl Med, 41 (2011) 246-264.
[23] M.D. Bartholoma, A.S. Louie, J.F. Valliant, J. Zubieta, Chem Rev, 110 (2010) 2903-2920.
[24] I. Velikyan, Med Chem, 7 (2011) 345-379.
[25] F. Mendes, A. Paulo, I. Santos, Dalton Trans., 40 (2011) 5377-5393.
[26] G.R. Morais, A. Paulo, I. Santos, Organometallics, 31 (2012) 5693-5714.
[27] E. Palma, J.D.G. Correia, M.P.C. Campello, I. Santos, Mol Biosyst, 7 (2011) 2950-2966.
[28] B.L.R. Kam, J.J.M. Teunissen, E.P. Krenning, W.W. de Herder, S. Khan, E.I. van Vliet, D.J. Kwekkeboom, Eur J Nucl Med Mol I, 39 (2012) 103-112.
[29] T. Stigbrand, J. Carlsson, G.P. Adams, in, Springer, 2008.
[30] P. Caravan, R.B. Lauffer, Contrast Agents: Basic principles, in: R.R. Edelman, J.R. Hesselink, Z.M. B., C.J. V. (Eds.) Clinical Magnetic Resonance Imaging, Saunders, Philadelphia, 2005, pp. 357-375.
[31] P. Caravan, J.J. Ellison, T.J. McMurry, R.B. Lauffer, Chem. Rev., 99 (1999) 2293-2352.
[32] E. Terreno, W. Dastru, D.D. Castelli, E. Gianolio, S.G. Crich, D. Longo, S. Aime, Curr Med Chem, 17 (2010) 3684-3700.
[33] A. Casini, J Inorg Biochem, 109 (2012) 97-106.
[34] J. Reedijk, Eur.J. Inorg.Chem., (2009) 1303-1312.
[35] Z.D. Bugarcic, J. Bogojeski, B. Petrovic, S. Hochreuther, R. van Eldik, Dalton Trans., 41 (2012) 12329-12345.
[36] J.D.G. Correia, A. Paulo, P.D. Raposinho, I. Santos, Dalton Trans., 40 (2011) 6144-6167.
[37] M. Morais, P.D. Raposinho, M.C. Oliveira, D. Pantoja-Uceda, M.A. Jimenez, I. Santos, J.D.G. Correia, Organometallics, 31 (2012) 5929-5939.
[38] P. Laverman, J.K. Sosabowski, O.C. Boerman, W.J.G. Oyen, Eur J Nucl Med Mol I, 39 (2012) 78-92.
[39] M. Fani, H.R. Maecke, Eur J Nucl Med Mol I, 39 (2012) 11-30.
[40] P.C.A. Bruijnincx, P.J. Sadler, Curr. Opin. Chem. Biol., 12 (2008) 197-206.
[41] D. Gibson, Dalton Trans., (2009) 10681-10689.
[42] A. Casini, A. Guerri, C. Gabbiani, L. Messori, J. Inorg. Biochem., 102 (2008) 995-1006.
[43] G. Sava, A. Bergamo, P.J. Dyson, Dalton Trans., 40 (2011) 9069-9075.
[44] E. Meggers, Chem. Comm., (2009) 1001-1010.
[45] A.R. Timerbaev, C.G. Hartinger, S.S. Aleksenko, B.K. Keppler, Chem. Rev., 106 (2006) 2224-2248.
[46] M. Knipp, Curr Med Chem, 16 (2009) 522-537.
[47] D. Griffith, J.P. Parker, C.J. Marmion, Anti-Cancer Agent Me, 10 (2010) 354-370.
[48] C.M. Che, F.M. Siu, Curr. Opin. Chem. Biol., 14 (2010) 255-261.
[49] A. Casini, J. Reedijk, Chemical Science, 3 (2012) 3135-3144.
[50] K.P. Bhabak, B.J. Bhuyan, G. Mugesh, Dalton Trans., 40 (2011) 2099-2111.
[51] A. Bindoli, M.P. Rigobello, G. Scutari, C. Gabbiani, A. Casini, L. Messori, Coord. Chem. Rev., 253 (2009) 1692-1707.
[52] E. Meggers, Angew. Chem.-Int. Edit., 50 (2011) 2442-2448.
[53] L. Feng, Y. Geisselbrecht, S. Blanck, A. Wilbuer, G.E. Atilla-Gokcumen, P. Filippakopoulos, K. Kraling, M.A. Celik, K. Harms, J. Maksimoska, R. Marmorstein, G. Frenking, S. Knapp, L.O. Essen, E. Meggers, J. Am. Chem. Soc., 133 (2011) 5976-5986.
[54] S.P. Fricker, Metallomics, 2 (2010) 366-377.
[55] A. Casini, C. Gabbiani, F. Sorrentino, M.P. Rigobello, A. Bindoli, T.J. Geldbach, A. Marrone, N. Re, C.G. Hartinger, P.J. Dyson, L. Messori, J. Med. Chem., 51 (2008) 6773-6781.
[56] R. Sasanelli, A. Boccarelli, D. Giordano, M. Laforgia, F. Arnesano, G. Natile, C. Cardellicchio, M.A.M. Capozzi, M. Coluccia, J. Med. Chem., 50 (2007) 3434-3441.
[57] T.W. Failes, C. Cullinane, C.I. Diakos, N. Yamamoto, J.G. Lyons, T.W. Hambley, Chem.-Eur. J., 13 (2007) 2974-2982.

[58] A. Casini, F. Edafe, M. Erlandsson, L. Gonsalvi, A. Ciancetta, N. Re, A. Ienco, L. Messori, M. Peruzzini, P.J. Dyson, Dalton Trans., 39 (2010) 5556-5563.
[59] D. Griffith, M.P. Morgan, C.J. Marmion, Chem. Comm., (2009) 6735-6737.
[60] X. Zhang, M. Frezza, V. Milacic, L. Ronconi, Y.H. Fan, C.F. Bi, D. Fregona, Q.P. Dou, Journal of Cellular Biochemistry, 109 (2010) 162-172.
[61] L. Dalla Via, C. Nardon, D. Fregona, Future Med Chem, 4 (2012) 525-543.
[62] C.N. Verani, J. Inorg. Biochem., 106 (2012) 59-67.
[63] K.H. Thompson, J. Lichter, C. Lebel, M.C. Scaife, J.H. McNeill, C. Orvig, J. Inorg. Biochem., 103 (2009) 554-558.
[64] C. Muller, Curr Pharm Design, 18 (2012) 1058-1083.
[65] C. Muller, R. Schibli, J Nucl Med, 52 (2011) 1-4.
[66] A.I. Anzellotti, N.P. Farrell, Chem. Soc. Rev., 37 (2008) 1629-1651.
[67] W. Maret, Y. Li, Chemical reviews, 109 (2009) 4682-4707.
[68] J.a. Tainer, M.M. Thayer, R.P. Cunningham, Current opinion in structural biology, 5 (1995) 20-26.
[69] J. Miller, A.D. Mclachlan, A. Klug, Embo J, 4 (1985) 1609-1614.
[70] A. Witkiewicz-Kucharczyk, W. Bal, Toxicol Lett, 162 (2006) 29-42.
[71] V. Schreiber, F. Dantzer, J.C. Ame, G. de Murcia, Nat Rev Mol Cell Bio, 7 (2006) 517-528.
[72] P.A. Nguewa, M.A. Fuertes, B. Valladares, C. Alonso, J.M. Perez, Progress in Biophysics & Molecular Biology, 88 (2005) 143-172.
[73] G. Demurcia, J. Menissier, Trends in Biochemical Sciences, 19 (1994) 250-250.
[74] G.Y. Zhu, S.J. Lippard, Biochem., 48 (2009) 4916-4925.
[75] E.R. Guggenheim, D. Xu, C.X. Zhang, P.V. Chang, S.J. Lippard, ChemBioChem, 10 (2009) 141-157.
[76] E.R. Guggenheim, A.E. Ondrus, M. Movassaghi, S.J. Lippard, Bioorgan Med Chem, 16 (2008) 10121-10128.
[77] C.X. Zhang, P.V. Chang, S.J. Lippard, J. Am. Chem. Soc., 126 (2004) 6536-6537.
[78] F. Mendes, M. Groessl, A.A. Nazarov, Y.O. Tsybin, G. Sava, I. Santos, P.J. Dyson, A. Casini, J. Med. Chem., 54 (2011) 2196-2206.
[79] M. Serratrice, F. Edafe, F. Mendes, R. Scopelliti, S.M. Zakeeruddin, M. Gratzel, I. Santos, M.A. Cinellu, A. Casini, Dalton Trans., 41 (2012) 3287-3293.
[80] R.N. Bose, W.W. Yang, F. Evanics, Inorg. Chim. Acta, 358 (2005) 2844-2854.
[81] J. Talib, J.L. Beck, T. Urathamakul, C.D. Nguyen, J.R. Aldrich-Wright, J.P. Mackay, S.F. Ralph, Chem. Comm., (2009) 5546-5548.
[82] A. Atipairin, B. Canyuk, A. Ratanaphan, Chem Biodivers, 7 (2010) 1949-1967.
[83] A. Atipairin, B. Canyuk, A. Ratanaphan, Breast Cancer Res Tr, 126 (2011) 203-209.
[84] Q.A. de Paula, J.B. Mangrum, N.P. Farrell, J. Inorg. Biochem., 103 (2009) 1347-1354.
[85] A. Scozzafava, A. Casini, C.T. Supuran, Curr Med Chem, 9 (2002) 1167-1185.
[86] S. Quintal, A. Viegas, S. Erhardt, E.J. Cabrita, N.P. Farrell, Biochem., 51 (2012) 1752-1761.
[87] J.F. Kerwin, J.R. Lancaster, P.L. Feldman, J. Med. Chem., 38 (1995) 4343-4362.
[88] S. Moncada, R.M.J. Palmer, E.A. Higgs, Pharmacol Rev, 43 (1991) 109-142.
[89] R. Korhonen, A. Lahti, H. Kankaanranta, E. Moilanen, Curr Drug Targets Inflamm Allergy, 4 (2005) 471-479.
[90] D. Fukumura, S. Kashiwagi, R.K. Jain, Nat Rev Cancer, 6 (2006) 521-534.
[91] A.J. Duncan, S.J. Heales, Mol Aspects Med, 26 (2005) 67-96.
[92] T. Nagano, T. Yoshimura, Chem Rev, 102 (2002) 1235-1270.
[93] H. Hong, J. Sun, W. Cai, Free Radic Biol Med, 47 (2009) 684-698.
[94] B.L. Oliveira, J.D.G. Correia, P.D. Raposinho, I. Santos, A. Ferreira, C. Cordeiro, A.P. Freire, Dalton Trans., (2009) 152-162.
[95] B.L. Oliveira, P.D. Raposinho, F. Mendes, F. Figueira, I. Santos, A. Ferreira, C. Cordeiro, A.P. Freire, J.D.G. Correia, Bioconjugate Chem, 21 (2010) 2168-2172.
[96] B.L. Oliveira, P.D. Raposinho, F. Mendes, I.C. Santos, I. Santos, A. Ferreira, C. Cordeiro, A.P. Freire, J.D.G. Correia, J. Organomet. Chem., 696 (2011) 1057-1065.
[97] B.L. Oliveira, I.S. Moreira, P.A. Fernandes, M.J. Ramos, I. Santos, J.D. Correia, J Mol Model, 19 (2013) 1537-1551.
[99] G. Steinkellner, R. Rader, G.G. Thallinger, C. Kratky, K. Gruber, Bmc Bioinformatics, 10 (2009).
[100] W.L. DeLano, in, DeLano Scientific, San Carlos, CA, USA., 2002.
[101] C.T. Supuran, Nat Rev Drug Discov, 7 (2008) 168-181.
[102] C.T. Supuran, Future Med Chem, 3 (2011) 1165-1180.
[103] C.T. Supuran, A. Scozzafava, A. Casini, Med Res Rev, 23 (2003) 146-189.
[104] A. Casini, J.Y. Winum, J.L. Montero, A. Scozzafava, C.T. Supuran, Bioorg Med Chem Lett, 13 (2003) 837-840.
[105] F. Abbate, A. Casini, A. Scozzafava, C.T. Supuran, Bioorg Med Chem Lett, 14 (2004) 2357-2361.
[106] C.T. Supuran, Mol Divers, 15 (2011) 305-316.
[107] J. Borras, G. Alzuet, S. Ferrer, C.T. Supuran, Metal complexes of heterocyclic sulfonamides as carbonic anhydrases inhibitors, CRC Press, Boca Raton (FL), 2004.
[108] A.L. Banerjee, D. Eiler, B.C. Roy, X. Jia, M.K. Haldar, S. Mallik, D.K. Srivastava, Biochem., 44 (2005) 3211-3224.
[109] K.M. Jude, A.L. Banerjee, M.K. Haldar, S. Manokaran, B. Roy, S. Mallik, D.K. Srivastava, D.W. Christianson, J. Am. Chem. Soc., 128 (2006) 3011-3018.
[110] D. Vomasta, A. Innocenti, B. Konig, C.T. Supuran, Bioorg Med Chem Lett, 19 (2009) 1283-1286.
[111] M. Rami, A. Cecch, J.L. Montero, A. Innocenti, D. Vullo, A. Scozzafava, J.Y. Winum, C.T. Supuran, ChemMedChem, 3 (2008) 1780-1788.
[112] A.J. Salmon, M.L. Wiliams, Q.K. Wu, J. Morizzi, D. Gregg, S.A. Charman, D. Vullo, C.T. Supuran, S.A. Poulsen, J. Med. Chem., 55 (2012) 5506-5517.
[113] A.J. Salmon, M.L. Williams, A. Hofmann, S.A. Poulsen, Chem. Comm., 48 (2012) 2328-2330.
[114] F.W. Monnard, T. Heinisch, E.S. Nogueira, T. Schirmer, T.R. Ward, Chem. Comm., 47 (2011) 8238-8240.
[115] D. Can, B. Spingler, P. Schmutz, F. Mendes, P. Raposinho, C. Fernandes, F. Carta, A. Innocenti, I. Santos, C.T. Supuran, R.

Alberto, Angew. Chem.-Int. Edit., 51 (2012) 3354-3357.
[116] A. Casini, C. Temperini, C. Gabbiani, C.T. Supuran, L. Messori, ChemMedChem, 5 (2010) 1989-1994.
[117] S. Mangani, A. Liljas, Journal of Molecular Biology, 232 (1993) 9-14.
[118] F. Carta, C. Temperini, A. Innocenti, A. Scozzafava, K. Kaila, C.T. Supuran, J. Med. Chem., 53 (2010) 5511-5522.
[119] K. Tars, D. Vullo, A. Kazaks, J. Leitans, A. Lends, A. Grandane, R. Zalubovskis, A. Scozzafava, C.T. Supuran, J. Med. Chem., 56 (2012) 293-300.
[120] P. Emsley, K. Cowtan, Acta Crystallographica Section D-Biological Crystallography, 60 (2004) 2126-2132.
[121] L.H. Naylor, Biochem. Pharmacol., 58 (1999) 749-757.
[122] J.H. Kang, J.K. Chung, J Nucl Med, 49 (2008) 164s-179s.
[123] M. Hengstschlager, M. Knofler, E.W. Mullner, E. Ogris, E. Wintersberger, E. Wawra, J. Biol. Chem., 269 (1994) 13836-13842.
[124] M. Hengstschlager, O. Pusch, E. HengstschlagerOttnad, P.F. Ambros, G. Bernaschek, E. Wawra, DNA Cell Biol, 15 (1996) 41-51.
[125] R. Schibli, M. Netter, L. Scapozza, M. Birringer, P. Schelling, C. Dumas, J. Schoch, P.A. Schubiger, J. Organomet. Chem., 668 (2003) 67-74.
[126] M. Stichelberger, D. Desbouis, V. Spiwok, L. Scapozza, P.A. Schubiger, R. Schibli, J. Organomet. Chem., 692 (2007) 1255-1264.
[127] D. Desbouis, P.A. Schubiger, R. Schibli, J. Organomet. Chem., 692 (2007) 1340-1347.
[128] D. Desbouis, H. Struthers, V. Spiwok, T. Kuster, R. Schibli, J. Med. Chem., 51 (2008) 6689-6698.
[129] H. Struthers, A. Hagenbach, U. Abram, R. Schibli, Inorg. Chem., 48 (2009) 5154-5163.
[130] H. Struthers, B. Spingler, T.L. Mindt, R. Schibli, Chem.-Eur. J., 14 (2008) 6173-6183.
[131] H. Struthers, D. Viertl, M. Kosinski, B. Spingler, F. Buchegger, R. Schibli, Bioconjugate Chem, 21 (2010) 622-634.
[132] M.D. Bartholoma, A.R. Vortherms, S. Hillier, B. Ploier, J. Joyal, J. Babich, R.P. Doyle, J. Zubieta, ChemMedChem, 5 (2010) 1513-1529.
[133] L. Wei, J. Babich, W.C. Eckelman, J. Zubieta, Inorg Chem, 44 (2005) 2198-2209.
[134] M.D. Bartholoma, A.R. Vortherms, S. Hillier, J. Joyal, J. Babich, R.P. Doyle, J. Zubieta, Dalton Trans, 40 (2011) 6216-6225.
[135] R.A. Sanchez-Delgado, A. Anzellotti, Mini-Rev Med Chem, 4 (2004) 23-30.
[136] M. Navarro, C. Gabbiani, L. Messori, D. Gambino, Drug Discovery Today, 15 (2010) 1070-1078.
[137] D. Gambino, Coord. Chem. Rev., 255 (2011) 2193-2203.
[138] C. Biot, W. Castro, C.Y. Botte, M. Navarro, Dalton Trans., 41 (2012) 6335-6349.
[139] S.P. Fricker, R.M. Mosi, B.R. Cameron, I. Baird, Y.B. Zhu, V. Anastassov, J. Cox, P.S. Doyle, E. Hansell, G. Lau, J. Langille, M. Olsen, L. Qin, R. Skerlj, R.S.Y. Wong, Z. Santucci, J.H. McKerrow, J. Inorg. Biochem., 102 (2008) 1839-1845.
[140] B. Demoro, F. Caruso, M. Rossi, D. Benitez, M. Gonzalez, H. Cerecetto, M. Galizzi, L. Malayil, R. Docampo, R. Faccio, A.W. Mombru, D. Gambino, L. Otero, Dalton Trans., 41 (2012) 6468-6476.
[141] A.R. Sannella, A. Casini, C. Gabbiani, L. Messori, A.R. Bilia, F.F. Vincieri, G. Majori, C. Severini, Febs Lett, 582 (2008) 844-847.
[142] C. Gabbiani, L. Messori, M.A. Cinellu, A. Casini, P. Mura, A.R. Sannella, C. Severini, G. Majori, A.R. Bilia, F.F. Vincieri, J. Inorg. Biochem., 103 (2009) 310-312.
[143] P. Baiocco, G. Colotti, S. Franceschini, A. Ilari, J. Med. Chem., 52 (2009) 2603-2612.
[144] M. Vieites, P. Smircich, B. Parajon-Costa, J. Rodriguez, V. Galaz, C. Olea-Azar, L. Otero, G. Aguirre, H. Cerecetto, M. Gonzalez, A. Gomez-Barrio, B. Garat, D. Gambino, J. Biol. Inorg. Chem., 13 (2008) 723-735.
[145] M. Vieites, P. Smircich, L. Guggeri, E. Marchan, A. Gomez-Barrio, M. Navarro, B. Garat, D. Gambino, J. Inorg. Biochem., 103 (2009) 1300-1306.
[146] S.L. Croft, M.P. Barrett, J.A. Urbina, Trends Parasitol, 21 (2005) 508-512.
[147] B. Demoro, F. Caruso, M. Rossi, D. Benitez, M. Gonzalez, H. Cerecetto, B. Parajon-Costa, J. Castiglioni, M. Galizzi, R. Docampo, L. Otero, D. Gambino, J. Inorg. Biochem., 104 (2010) 1252-1258.

2. Aquaporins in Health and Disease

This chapter is based on two publications:

Andreia de Almeida, Graça Soveral and Angela Casini
Gold compounds as aquaporin inhibitors: new opportunities for therapy and imaging
Med.Chem.Comm. (2014) 5: 1444–1453

Angela Casini and Andreia de Almeida
Aquaporins in health and disease: New molecular targets for drug discovery
Chapter: Inorganic compounds as aquaporins substrates or as potent inhibitors: a coordination chemistry point of view
CRC Press/Taylor & Francis Group (in press)

Med.Chem.Comm.

CRC Press/Taylor & Francis Group

Aquaporins represent a family of transmembrane water channel proteins widely distributed in various tissues throughout the body that play a major role in transcellular and transepithelial water movement [1, 2]. Among the 13 mammalian AQPs described so far, two sub-groups are now classified mainly accordingly to their transport capabilities: i) *orthodox or classical aquaporins* (AQP0, AQP1, AQP2, AQP4, AQP5, AQP6 and AQP8), which are primarily water selective and facilitate water movement across cell membranes in response to osmotic gradients, and ii) *aquaglyceroporins* (AQP3, AQP7, AQP9 and AQP10) which facilitate the transport of small uncharged solutes such as glycerol and urea in addition to water [3]. Although AQP6 has been proved to be a pH-sensitive chloride channel or possibly a nitrate channel and AQP8 has been found permeable to urea, they are both classified under the classical AQP group. A third sub-group named superaquaporin (S-aquaporins) (AQP11 and AQP12)[4] was defined based on their primarily subcellular location and lower sequence similarity to the other mammalian AQPs; although their permeability specificity has been difficult to establish, AQP11 was recently reported to transport both water and glycerol [5]. There is also controversial evidence that some AQPs may transport gases and ions across membranes [6]. The mammalian AQPs are expressed in various epithelia and endothelia involved in fluid transport, such as kidney tubules and glandular epithelia, as well as in other cell types such as brain glial cells, epidermis and adipocytes.

2.1. Aquaporin structure and function

A functional AQP consists of four monomers super-assembled in membranes as tetramers (Figure 1 A-B). There is a considerable body of information about AQP structure from electron and X-ray crystallography [2], in several organisms, showing AQP monomers (~30 kDa) containing six membrane-spanning helical domains surrounding a narrow aqueous pore (Figure 1 C-D).

The most remarkable feature of the aquaporin channels is their high selectivity and efficiency for water or glycerol permeation; in fact, AQPs allow water/glycerol to move freely and bidirectionally across the cell membrane, but exclude all ions such as hydroxide and hydronium ions [7], the latter being essential to preserve the electrochemical potential across the membrane. Although classical aquaporins are still considered mostly specific for water, AQP1-mediated permeation by small polar solutes has been recently proposed, while an inverse correlation between permeability and solute hydrophobicity was found [8]. In the pore region, the water specificity is achieved by the presence of specific amino acid residues conferring size constrictions and/or charge characteristics that enable water molecules to pass through, while preventing permeation to protons or any solutes above 2.8 Å.

AQPs share a common protein fold, with the typical six membrane-spanning helices surrounding the 20-Å-long and 3-4-Å-wide amphipathic channel (Figure 1).

Two constriction sites with distinguishing features that identify the protein subfamilies compose the AQP channel. A first selectivity filter (SF), so called aromatic/Arginine SF (ar/R SF), is a constricted region formed by three (in aquaglyceroporins) or four (in orthodox aquaporins) residues near the periplasmic/extracellular entrance (Figure 1E), determining the size of molecules allowed to pass through and providing distinguishing features that identify the subfamilies [9].

One ar/R residue that is conserved in all isoforms is an arginine, which gives the name to this region. The positive charge of this sidechain, at neutral pH, is the first electrostatic barrier to

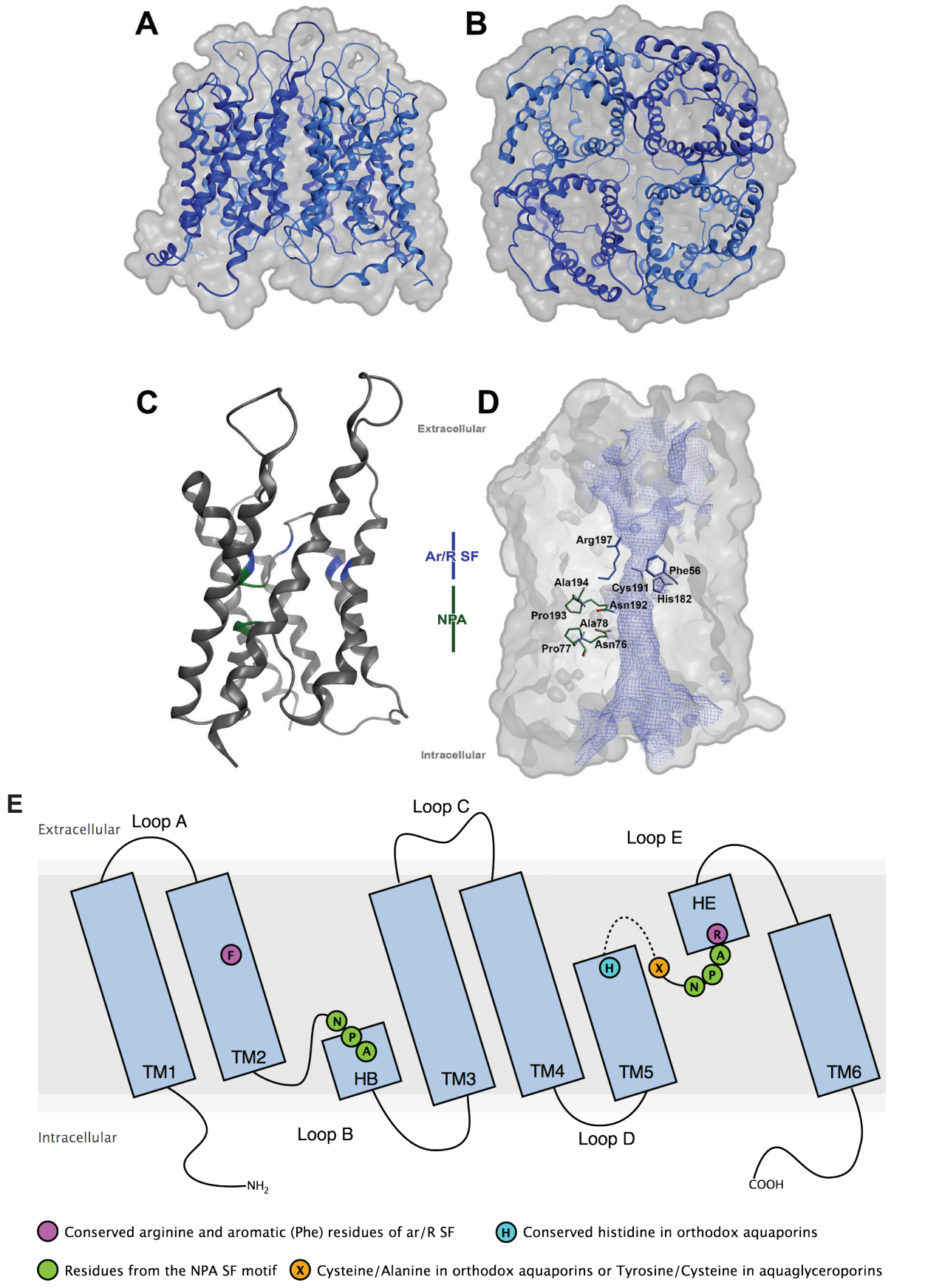

Figure 1. Structure of AQP1 water channel (pdb code 1H6I). Top panels represent the functional membrane-embedded tetramer, both in ribbon and surface representation, in lateral (A) and extracellular top (B) views. Panels C and D display the monomeric form of the channel, displayed in ribbon (C) and surface (D), with the channel surface represented as blue mesh. The main protein regions are identified: ar/R SF filter residues and identified cysteine are coloured in blue (sulphur atom in yellow), NPA residues in green. The figures were generated with MOE software. E: Schematic representation of the helical structure of an AQP. (TM: Transmembrane helix; H: Half Helix).

the passage of charged species. The second residue to name this filter is an aromatic side-chain, which is, in most cases, a phenylalanine, located at the second transmembrane helix (TM2). In classical aquaporins, the other two residues are most commonly histidine and cysteine, located in TM5 and loop E, respectively. A more neutral residue, in some cases, may substitute the cysteine. In aquaglyceroporins, the third residue is usually also an aromatic one, such as tyrosine, located in loop E, in the same position as the cysteines in orthodox aquaporins. Interestingly, in microorganisms, the position of the phenylalanine in the sequence appears to be switched with the third residue as, in the bacterial glycerol facilitator (bGlpF), *Plasmodium falciparum* aquaporin (PfAQP) or *Leishmania* AQP1 (LAQP1, a tryptophan is located in TM2 and the phenylalanine is located in loop E instead.

The second selectivity filter, generating an electrostatic barrier essential for proton exclusion, is composed by two conserved asparagine-proline-alanine (NPA) sequence motifs, located at the N-terminal ends of the two half-helices, at the centre of the channel (Figure 1C-E), HB and HE. The localization of these sequences of residues appears to be important also for the maintenance of the channel's structure, as the motifs meet in the centre of the channel, forming important hydrogen bonds (Figure 1C). The asparagine residues, in particular, seem to be conserved in all isoforms and in all organisms. The sidechains of the asparagine residues are located inside the channel and form an electrostatic barrier that has been shown to flip water molecules, preventing them to go back in direction (Figure 2B) [10, 11]. As this is not the narrowest part of the channel, this selectivity filter acts mostly by selecting residues based on affinity, rather than size. It has been shown that the OH groups of glycerol molecules form several H-bonds in the NPA region.

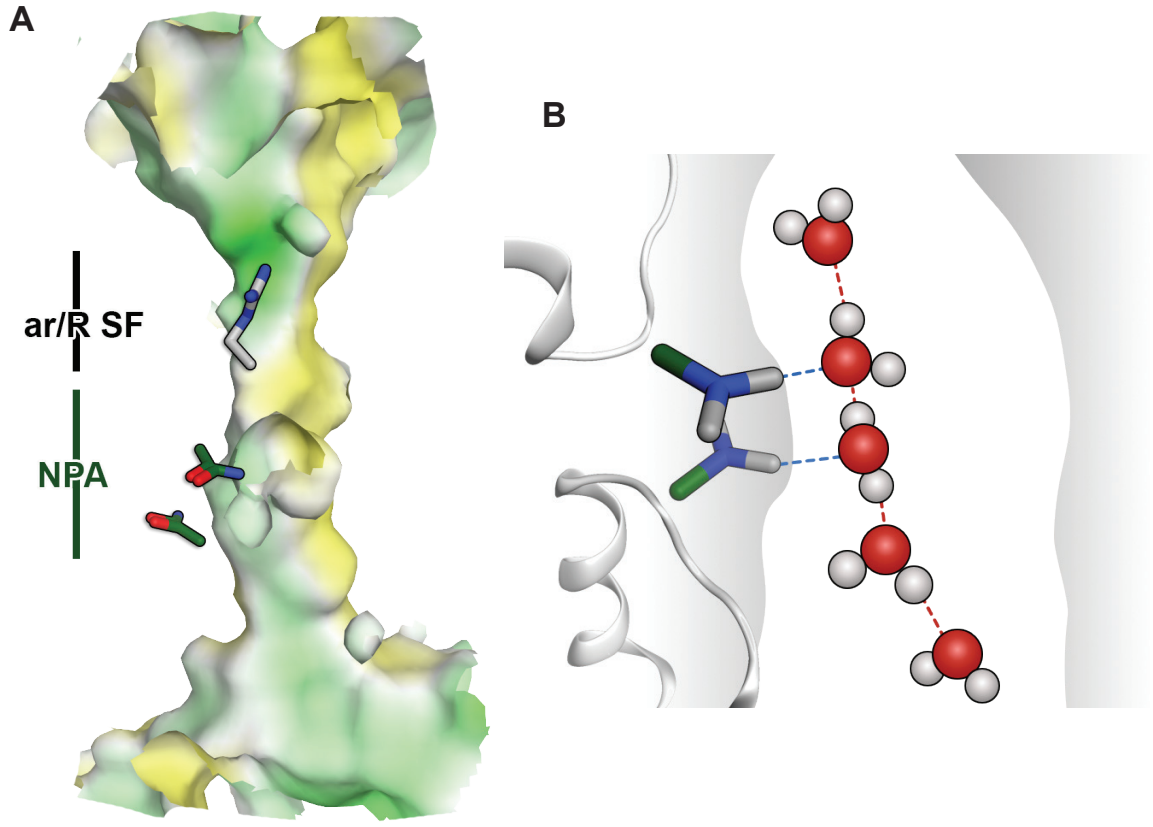

Figure 2. (A) Molecular representation of the channel lining of hAQP7 with hydrophobic and hydrophilic aminoacids are represented in green and yellow, respectively). Arg229, Asn94 and Asn226 represent the two selectivity filters. The figure was generated with MOE software. (B) Schematic representation of the phenomenon of water flipping, after crossing the NPA filter. Dashed lines represent H-bonds between atoms. Adapted from data presented in chapter 2.3.

Table 1. Comparison of the sequences (% of identity) of all human aquaporins. Sequence alignments were performed using Uniprot database. Isoforms highlighted in bold are aquaglyceroporins and * refers to the subclass S-Aquaporins.

	AQP0	AQP1	AQP2	AQP3	AQP4	AQP5	AQP6	AQP7	AQP8	AQP9	AQP10	AQP11*	AQP12*
AQP0		43.2	59.4	23.2	35.0	51.7	45.8	23.3	24.6	21.6	21.7	13.6	16.2
AQP1	43.2		40.7	20.5	35.3	43.4	37.8	19.0	21.1	21.3	19.9	14.5	18.1
AQP2	59.4	40.7		23.7	37.0	62.4	51.2	24.7	25.2	21.9	21.0	13.4	15.7
AQP3	23.2	20.5	23.7		20.6	24.3	21.3	38.0	22.7	46.4	45.1	15.2	15.7
AQP4	35.0	35.3	37.0	20.6		39.8	33.3	20.5	21.3	21.0	17.7	12.3	16.3
AQP5	51.7	43.4	62.4	24.3	39.8		49.8	20.6	26.9	24.0	20.9	14.9	19.1
AQP6	45.8	37.8	51.2	21.3	33.3	49.8		22.2	23.5	23.6	19.9	16.2	20.8
AQP7	23.3	19.0	24.7	38.0	20.5	20.6	22.2		20.0	33.8	33.9	13.2	13.2
AQP8	24.6	21.1	25.2	22.7	21.3	26.9	23.5	20.0		23.6	18.2	14.0	17.8
AQP9	21.6	21.3	21.9	46.4	21.0	24.0	23.6	33.8	23.6		46.5	15.5	15.1
AQP10	21.7	19.9	21.0	45.1	17.7	20.9	19.9	33.9	18.2	46.5		14.1	16.4
AQP11*	13.6	14.5	13.4	15.2	12.3	14.9	16.2	13.2	14.0	15.5	14.1		20.6
AQP12*	16.2	18.1	15.7	15.7	16.3	19.1	20.8	13.2	17.8	15.1	16.4	20.6	

Another interesting feature of aquaporins is the composition of the channel lining, half hydrophilic and half hydrophobic (Figure 2A). This helps orienting the substrate molecules, allowing important hydrogen bonds to be formed, in order to guide the substrate through the channel, while preventing that hydrogen bonds are formed on the opposite side. In fact, the latter would otherwise make the passage slower. As an example, as described later in Chapter 2.2, we can observe glycerol molecules oriented with the OH groups to form H-bonds with the sidechains of the asparagine residues of the NPA SF, while the carbon atoms are oriented to the hydrophobic side of the channel.

In spite of the fact that all aquaporins share a common tridimensional structure, their aminoacid composition is considerably different. For example, the sequence identity between human aquaporins can vary from 62.4% (AQP5-AQP2) to 12.3% (AQP4-AQP11) (Table 1). These differences are key to each isoform's selectivity. Thus, it is not surprising that aquaporins of the same type share a higher sequence identity, e.g., aquaglyceroporins have a higher sequence identity with others of the same group and lower with orthodox aquaporins. As explained in detail above, the selectivity filters of aquaporins are variable, according to the permeated solutes and to the protein isoform. Also the channel lining composition changes significantly between isoforms, even though the type of aminoacids in a certain position is commonly the same. As the side-chains of aminoacids can have different sizes, even for aminoacids of the same type, the sequence of each isoform determines also the size of the pore and, consequently, the size of the molecules permeated. This feature is not only important for solute selectivity, but also a key feature for selective drug targeting to different aquaporin isoforms, as discussed in detail in Chapters 2.1-3.

As can be seen in Table 1, the sequence identity of AQP8 with other isoforms is around 23%, appearing not to be fitting in any of the two main aquaporin subfamilies. Moreover, AQP8 does not have a common ar/R SF: even though it has the conserved arginine, the phenylalanine is substituted by a histidine and the other residues by glycine and isoleucine residues. This change in the selectivity filter directly affects the size of the pore, as glycine and isoleucine are much smaller than the tyrosine in one of the positions. In fact, AQP8 has been shown to permeate ammonia and to belong to the so-called aquaammoniaporin family [12].

Another special case is constituted by AQP11 and AQP12. These aquaporins belong to the S-aquaporin subfamily, as they are very different from the other human isoforms (Table 1). In fact, this subfamily has only been identified in humans and a nematode, *C. elegans*, and, in all cases, its expression is exclusively intracellular [13, 14]. The role of these two human isoforms is still unclear and the intracellular distribution makes it difficult to study their function and permeability, even if transfected in a simple model, as oocytes. Despite this, AQP11 has been shown to permeate both water and glycerol [15, 16] and, despite no human diseases have been linked to the superaquaporin family, knockout studies in mice reveal a crucial role of this isoform in kidney development [17]. One of the special characteristics of these aquaporins is the lack of the conserved arginine, substituted by a leucine, in both cases, and different NPA motifs (NPC/NPA in AQP11 and NPT/NPA in AQP12). The substitution of the conserved arginine by a smaller, uncharged and hydrophobic residue may account for different selectivity and pore size. Moreover, while changes in the NPA motif seem to affect water permeability, they do not appear to have a clear role in channel structure and cellular localization [18]. Thus, the role of AQP11 and AQP12 in human health and pathology, as well as their structure and function, still remains to be disclosed.

2.2. Aquaporins in disease

Much of our understanding of AQP functions in mammalian physiology has come from relatively recent phenotype analysis of mice lacking one of the AQPs [19]. These studies have confirmed the anticipated involvement of AQPs in the mechanism of urine concentration and glandular fluid secretion, and led to the discovery of unanticipated roles of AQPs in brain water balance, cell migration (angiogenesis, wound healing), cell proliferation, neural function (sensory signaling, seizures), epidermal hydration and ocular function. Specifically, the aquaglyceroporins, regulate glycerol content in epidermal, fat and other tissues, and are involved in skin hydration, cell proliferation, carcinogenesis and fat metabolism. In cancer, AQPs have proved to be highly expressed in different tumor types, where they are involved in tumor invasion, metastasis and growth [20]. Below are summarized the main features of the human aquaglyceroporins characterized so far and the evidences of their possible roles in human diseases.

2.2.1. Aquaglyceroporins

The subclass of water channels termed aquaglyceroporins includes isoforms (AQP3, AQP7, AQP9 and AQP10), which are also able to transport glycerol and possibly urea as well as other small non-charged solutes. Their physiological roles have been more difficult to ascertain, in part because the understanding of the role of glycerol in mammals is incomplete. There is now compelling evidence for the involvement of aquaglyceroporin-mediated glycerol transport in cell proliferation, adipocyte metabolism and epidermal water retention, and their dysfunction or aberrant expression has been correlated with several pathophysiological conditions.

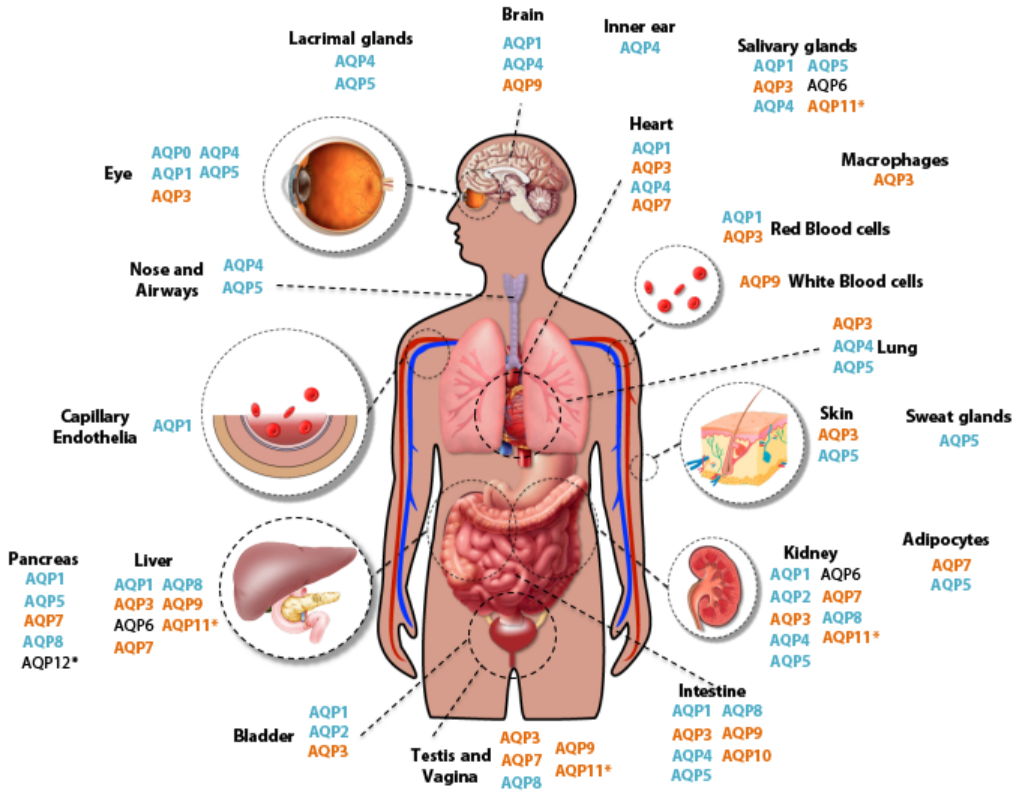

Figure 3. Schematic representation of the expression of aquaporins in the human body. In blue are represented the water channels, in orange the aquaglyceroporins and in black the isoforms whose permeability is still unclear. * represents the superaquaporin subfamily.

AQP3 is expressed in a wide variety of organs such as the kidney and urinary tract, digestive tract, respiratory tract, skin, and eye [21] (Figure 3). Phenotype analysis of AQP3-null mice revealed an important role of AQP3 in kidney and in epidermal physiology, leading to defects in urine-concentrating function [22], reduced skin hydration and elasticity and impaired skin wound healing [21]. Interestingly, AQP3 is highly expressed in skin tumors and AQP3 deficiency or blockage inhibits cell proliferation and reduces tumor growth in mice, which may result from impaired glycerol uptake by tumor cells [23]. AQP3 was also found to have high expression levels in tumors from different origin, such esophageal and oral squamous cell carcinoma [24], ovarian [25] and cervical [26] cancer. Liu et al investigated AQP3 expression in normal and neoplastic lung tissues and found AQP3 expression was related to tumor differentiation and clinical stage in lung adenocarcinomas [27], pointing to a novel function for AQP3 expression in high-grade tumors. The involvement of AQP3 expression and functional activity in cell proliferation was further demonstrated using a human epidermoid carcinoma cell line [28, 29], suggesting that the modulation of AQP3 expression or function could be explored for cancer therapeutics.

AQP7 is widely expressed in testis [30], kidney, pancreas and adipose tissue [31] (Figure 3), where its role in glycerol release/uptake in adipocytes has been correlated with obesity onset [32]. In adipocytes, triglycerides are hydrolyzed to glycerol and free fatty acids, which are released into the circulation. Thus, glycerol is taken up by the liver for hepatic glucose synthesis. While for sometime controversy on the precise cellular localization of AQP7 existed [31], its simultaneous expression in adipocytes and in the capillary endothelia of mice adipose tissue was detected and its role as a water and glycerol channel was correlated with adipocyte lipid accumulation [33]. AQP7 has also been investigated in human subjects and studies revealed a correlation of AQP7 down-regulation with obesity [34] or with reduced plasma glycerol during exercise [35]. Additional investigations in mice and human-AQP7 are needed to better define AQP7 role on obesity and diabetes.

AQP9 is expressed in various organs (Figure 3), including testis, brain, leukocytes, epididymis, spleen and liver [36] where it was proposed to play a role in glycerol uptake for gluconeogenesis during fasting [37, 38]. In hepatocytes it is expressed in the sinusoidal (basolateral) plasma membrane. Because AQP9 is also highly permeable to glycerol and urea, it may provide an entry route for glycerol and an exit route for urea and a number of other solutes produced within hepatocytes [39]. Indeed, *in vivo* studies have demonstrated that in rats fasted for 96 hours, expression of AQP9 in the liver increases 20-fold, suggesting that during starvation, the liver takes up glycerol for gluconeogenesis and does it with the involvement of AQP9 [38]. In addition, studies in AQP9-null mice suggested an impairment of liver glycerol uptake, which may result in an improvement of the diabetic state [31, 40], but further studies are necessary to determine the exact contribution of AQP9 in metabolic disorders such as diabetes and obesity.

Human AQP10 is found mainly in the gastrointestinal tract, but was also detected in teeth, muscle and gingiva [31] (Figure 3). Recently, *in vivo* studies on healthy volunteers have demonstrated the presence of AQP10 (together with AQP3) in the stratum corneum [41]. Interestingly, AQP10 was reported to be a pseudogene in mice [42], rendering impossible the generation of AQP10-null mice for the identification of disease phenotypes. Thus, the functional significance of this aquaglyceroporin is still obscure.

In addition to mammalian pathophysiology, some aquaglyceroporins seem to be relevant in non-mammalian cell survival. This is the case of AQP3 and AQP9 expressed in human and mice red

blood cells respectively, facilitating glycerol delivery to the cells infected with the malaria parasite *Plasmodium falciparum*. Since glycerol can be used by the malaria parasite for lipid biogenesis and as an energy source, inhibition of AQP3 and AQP9 may be exploited in the search for antimalarial agents [43]. In addition, *P. falciparum* has its own aquaglyceroproin (PfAQP) whose X-ray structure has been reported and which contains NLA and NPS residue patterns instead of the NPA motifs of other AQPs [44].

Interestingly, a number of aquaglyceroporins were identified in parasitic protozoa (*Plasmodium*, *Trypanosoma brucei*, *Leishmania*, *Toxoplasma* and *Cryptosporifium*) and are known to permeate water, glycerol, urea and several other polyols [45]. Parasitic AQPs are important for glycerol recruitment during the organism's reproductive blood stage and, thus, modulation of those AQPs involved in parasite life-cycle regulation or reproduction may represent a strategy for novel therapeutics. Moreover, parasitic AQPs appear to be the major entry routes of uptake of cytotoxic compounds (hydroxyurea, dihydroxyacetone, and the hydroxide of trivalent metalloids arsenic and antimony) able to kill protozoan parasites, and AQP deletion renders the parasites more resistant to treatments [46]. Thus, the use of parasitic AQPs as a vehicle for toxic substances may also be a further pathway for research. Interestingly, since aquaporins are able to transport solutes bilaterally across the cellular membranes they can not only import glycerol for metabolism, but, due to their ability to transport other solutes, such as urea and ammonia, may also be important to export small-molecule toxins, important for pathogenicity [45].

2.3. Aquaglyceroporins as metalloids transporters

2.3.1 Arsenic compounds transport through aquaglyceroporins

Arsenic has been used in several forms, including in industrial components, medicines, embalming, manufacture of cosmetics, rodenticides and pesticides, pigments, food and wood preservatives. It is the most ubiquitous environmental toxin and carcinogen, labelled as Group 1 human carcinogen and, even though arsenic embalming and pigments are no longer available, arsenic is still present in several building structures as lead alloys as well as component of batteries, lasers, diodes and transistors. Water contamination with arsenic is a major problem in several countries and chronic exposure may cause different types of cancer, including skin, bladder and lung cancers [47]. Thus, exposure to this element is still one of the biggest issues in world-health.

Arsenic is bioavailable in three oxidation states, As(V) (arsenate), As(III) (arsenite) and As(0) (elemental). As(III), when dissolved in water at pH 7.0 forms arsenous acid, $As(OH)_3$ (Figure 4) and this species is neutral at physiological pH (pK_{a1} = 9.3, pK_{a2} = 13.5 and pK_{a3} = 14.0) [48]. The aqueous form of arsenic(V) oxide is arsenic acid, H_3AsO_4 (Figure 4), and in physiological conditions, it exists as hydrogen arsenate and dihydrogen arsenate (pK_{a1} = 2.19, pK_{a2} = 6.94 and pK_{a3} = 11.5). Exposure to trivalent arsenic is more toxic than exposure to its pentavalent form, most likely due to the increased affinity of As(III) for sulphur ligands [49]. Interestingly, while pentavalent arsenic is transported into cells via phosphate transport systems in both prokaryotes and eukaryotes, initial studies using *Escherichia coli* showed that As(III) accumulation goes via the glycerol facilitator protein (GlpF), which belongs to the aquaglyceroporin family [50]. Moreover, it appears that trivalent arsenic is transported as the neutral form of arsenous acid. In fact, X-ray

absorption spectroscopy (XAS) was used to determine the nearest neighbour coordination environment of As(III) under a variety of solution conditions [51]. Extended X-ray Absorption Fine Structure (EXAFS) analysis demonstrated three oxygen ligands at 1.78 Å from the arsenic atom, showing that the major species in solution is $As(OH)_3$, an inorganic molecular mimic of glycerol (Figure 4).

In humans, two aquaglyceroporins have been identified as arsenic transporters, namely AQP7 and AQP9, with the latter being the most effective arsenous acid transporter, four-fold higher than AQP7. Conversely, the other human aquaglyceroporins AQP3 and AQP10 show little arsenic transport. These results were obtained in *Xenopus* oocytes engineered to overexpress the four human glycerol channels [52]. Subsequent studies suggested that $As(OH)_3$ and glycerol use the same translocation pathway, as mutations in selectivity filter residues of AQPs affected the transport of both solutes to the same extent [52]. Interestingly, AQP9 is also abundantly expressed in leukocytes; however, in this cell type no glycerol permeability via this isoform could be observed, leaving the possible role for AQP9 uptake of $As(OH)_3$ in leukocytes still to be disclosed [53].

Human AQP9 is highly expressed in the liver, where it is responsible for fluxes of glycerol, for processes like glycolysis and gluconeogenesis, and urea, having an interplay with human AQP7 in adipose tissue [54]. Liver is responsible for metabolizing most drugs and excreting their metabolic products and, in mammalian cells, the metabolism of arsenic involves detoxification of the arsenic species in the liver. Notably, ca. 70% of arsenic is excreted and hAQP9, as efficient arsenic transporter, may be responsible for excretion of arsenic from the liver into the bloodstream. Metabolic processing of inorganic As(III) is carried out by a series of methylation reactions. These reactions involve the interaction of arsenous acid with arsenic(III) methyltransferase (AS3MT). This protein catalyses the methylation of both arsenous acid and methylarsonous acid (MAs(III)) in the presence of adequate reduction and methyl equivalents. Thus, inorganic arsenic (As(III)) can also be metabolized via methylation to methylarsonic acid (MAs(V)) and dimethylarsinic acid (DMAs(V)) (Figure 4). The liver is considered a major site of arsenic methylation to MAs(III) [55-57]. Therefore, hAQP9 ability to transport arsenic in its methylated form was evaluated using a *Sacharomyces cerevisiae* strain HD9 (*acr3Δ ycf1Δ fps1Δ*), resistant to As(III). Usually, these cells exhibit little permeability to As(III) and MAs(III), but when AQP9 expression was induced in HD9 cells, cells became sensitive to both As-containing species [58, 59]. Interestingly, AQP9 appears to be three-fold more permeable to MAs(III) than to $As(OH)_3$. Since the final fate of the monomethylated form of arsenic is excretion, the proposed mechanism of transport of arsenical species in the liver involves uptake of As(III), likely as $As(OH)_3$, and excretion into the bloodstream of MAs(III) through AQP9 [58]. The methylated arsenicals are released from the liver into the bloodstream and end up in urine, skin, hair, and other tissues.

In spite of its known toxic effects, the use of arsenic in medicine is an ancient practice [60]. Thus, Hippocrates (460-377 B.C.) recommended a paste of realgar, a mineral form of arsenic, as treatment for ulcers and used arsenic as an escharіotic to treat skin and breast cancer. Interestingly, in the 19th century, arsenic was a major component of *Materia Medica*, and was used to treat a variety of diseases, from skin problems, to ulcers and cancer. In 1910, Noble laureate Paul Ehrlich developed Salvarsan (dihydroxy-diamino-arsenobenzene-dihydrochloride), an organic arsenical for the treatment of syphilis [60]. Due to its severe toxicity, fatal arsenic poisoning from medical treatments was very common in the past. Nowadays, a few arsenic drugs are still in use. The greatest

clinical success has been the use of arsenic trioxide (As_2O_3, Trisenox®) (Figure 4) in the treatment of haematological cancers, most notably in acute promyelocytic leukaemia (APL), which is a subtype of acute myeloid leukaemia (AML) [61]. An established major determinant of the action of arsenical-containing drugs is the pathway of metallodrug uptake in cancer cells, and, therefore, understanding the factors that modulate the cellular accumulation of arsenic is important to improve the effects of chemotherapy. Arsenic trioxide almost certainly dissolves to form inorganic $As(OH)_3$, the species that moves through aquaglyceroporin channels. Overexpression of AQP9, AQP7 or AQP3 renders human leukaemia cells hypersensitive to the drug as a result of higher steady-state levels of accumulation [62]. In particular, sensitivity to arsenic trioxide is directly proportional to AQP9 expression in leukaemia cells of different lineages [63]. For example, the APL cell line NB4 showed the highest expression level of AQP9 and is the most sensitive to the drug. Conversely, the chronic myeloid leukemia cell line K562 shows low endogenous AQP9 expression, and it is insensitive to As_2O_3. When human AQP9 was overexpressed either in K562 or in the promyelocytic leukemia cell line HL60, both became hypersensitive to As(III) due to higher intracellular accumulation of the metalloid [63].

Since, according to these studies, responsiveness to drug therapy is correlated with increased expression of the drug uptake system, the possibility of using pharmacological agents to increase aquaglyceroporin expression delivers the promise of therapies for the treatment of leukaemia in combination with Trisenox.

Among the successful organoarsenical drugs, melarsoprol (2-[4-[(4,6-diamino-1,3,5-triazin-2-yl) amino]phenyl]-1,3,2-dithiarsolane-4-methanol) (Figure 4) is a prodrug currently used as treatment for late-stage east *African trypanosomiasis*, commonly known as sleeping sickness [64]. Melarsoprol is metabolized into the highly reactive melarsen oxide, which irreversibly binds to vicinal sulfhydryl groups causing the inactivation of various enzymes. Even though melarsoprol is highly toxic, with severe side effects similar to those of arsenic poisoning, and causes fatal reactive encephalopathy in ca. 5% of the patients, this is the only effective chemotherapeutic in both strains of *Trypanosoma brucei* and in late-stages of trypanosomiasis [64, 65]. In spite of the efficacy of melarsoprol, one recurrent problem of the treatment with arsenic compounds is the development of parasite resistance.

T. brucei parasites contain three aquaglyceroporins, TbAQP1-3, which are thought to be involved in osmoregulation and glycerol transport [66]. Interestingly, *T. brucei*'s aquaglyceroporins were shown to be involved in merlasoprol/pentamidine cross-resistance (MPXR), when deletion of both TbAQP2 and TbAQP3 showed a 2-fold increase of IC_{50} of the arsenic drug and 15-fold increase in pentamidine, compared to the wild-type strain [67]. Later, it was confirmed that only TbAQP2 was involved in resistance, as knockout strains for TbAQP3 did not show any difference in melarsoprol/pentamidine toxicity, when compared to the wild-type strain [68]. Reintroducing an inducible copy of TbAQP2 into *aqp2/aqp3*-null cells, which restored MPXR, validated these results. Interestingly, the induction of TbAQP2 expression restored cell sensitivity to treatment, even in the absence of TbAQP3, while induction of TbAQP3 did not have an effect in MPXR [68]. These studies reinforce the crucial role of TbAQP2 in drug uptake and support the central role of this aquaporin isoform in MPXR. Although TbAQP2 and TbAQP3 are closely related, TbAQP2 lacks the usual motifs of the selectivity filter. Indeed, while TbAQP1 and TbAQP3 harbour the conventional 'NPA/NPA' motifs, TbAQP2 is the only *T. brucei* isoform with NSA/NPS and to

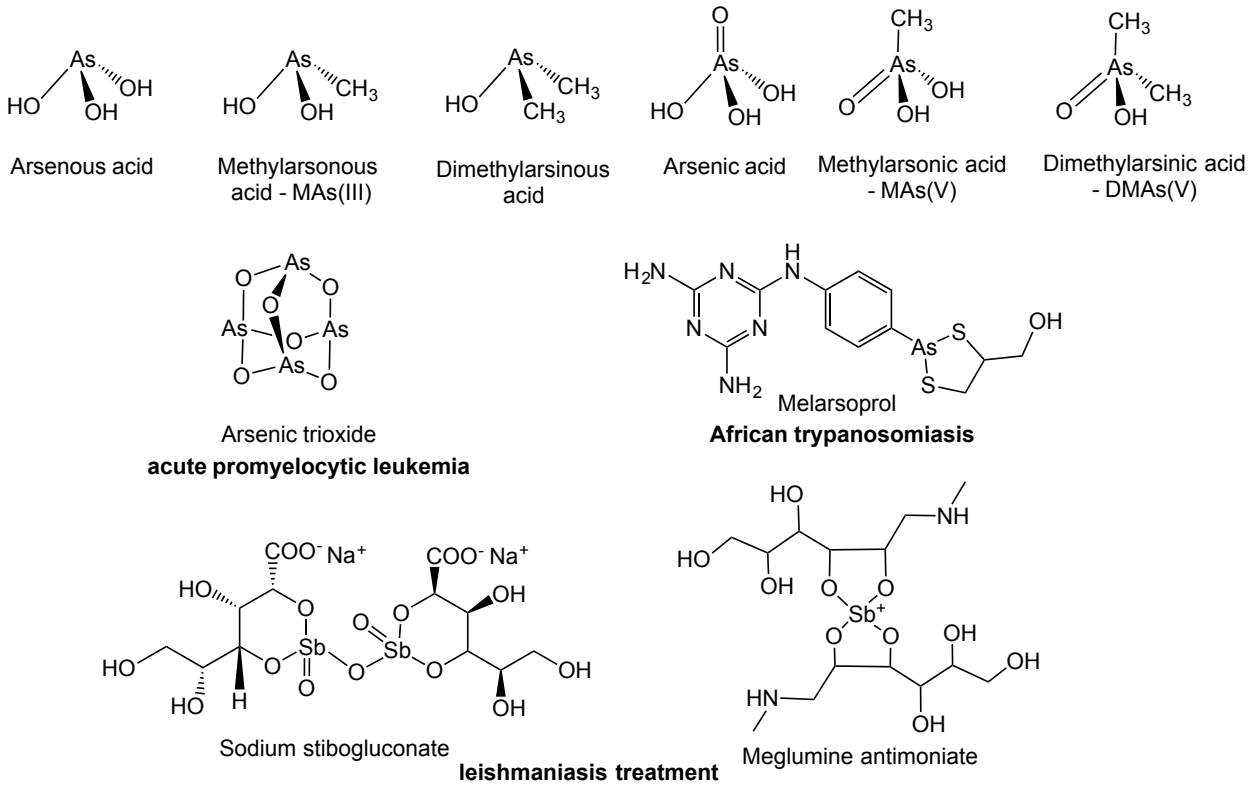

Figure 4. Structure of metal-based compounds as aquaporins inhibitors.

lack the conserved arginine in the ar/R selectivity filter, and this difference may account for the selectivity towards metalloid transport.

Following promising results with arsenic trioxide, melarsoprol was also tested *in vitro* and entered clinical trials as a treatment for acute promeylocytic leukemia [69, 70]. However, Due to its severe neurotoxicity, in the same dosage and treatment scheme used for the treatment of trypanosomiasis, clinical trials for the treatment of APL with melarsoprol were abandoned [69].

2.3.2. Antimonial compounds transport through aquaglyceroporins

Antimony compounds are used in the semiconductor industry, ceramics and plastics, flame-retardant applications, and are often alloyed with other metals to increase their strength and hardness. Exposure to antimony can occur from natural sources and also from industrial activities. The primary effects from chronic exposure to antimony in humans are respiratory problems, lung damage, cardiovascular effects, gastrointestinal disorders, and adverse reproductive outcome.

Nowadays, antimony-based drugs found applications in the treatment of protozoal diseases. Specifically, pentavalent antimony-containing drugs with of Sb(V) with N-methyl-D-glucamine such as Pentostam® (sodium stibogluconate) and Glucantime® (meglumine antimoniate) (Figure 4) are the treatment of choice for *Leishmania* infections (leishmaniasis). Leishmaniasis is a disease caused by the protozoan parasite *Leishmania*, from the same family as *Trypanosoma*. The disease, endemic in 88 countries, with 400,000 cases per year, is transmitted by a type of sandfly and can manifest in three main forms: cutaneous, mucocutaneous, or visceral [71, 72]. While anti-leishmania vaccines are still under development or undergoing clinical trials [73], antimony [Sb(V)]-based compounds have been used for treatment of all forms of the disease for more than 60 years [74]. However, as for arsenic drugs, a large increase in cases of resistance to treatment with

antimonials has been reported; for example, in India, 65% of previously untreated patients fail to respond promptly or relapse after therapy with antimonials [75]. Thus, it is extremely important to understand the mechanisms of action and resistance of pentavalent antimonial drugs in order to develop better therapeutic agents.

According to one of the most accredited mechanisms of activity, pentavalent antimony (Sb(V)) behaves as a prodrug, which undergoes biological reduction to much more active/toxic trivalent form of antimony Sb(III), that exhibits antileishmanial activity. [76] However, the site (amastigote or host macrophage) and mechanism of reduction (enzymatic or nonenzymatic) remain controversial. Furthermore, the ability of Leishmania parasites to reduce Sb(V) to Sb(III) is stage-specific. The first transport studies of antimony in *Leishmania* parasites were performed using a pentavalent Sb(V) compound (^{125}Sb), sodium stibogluconate (commercialized as Pentostam) (Figure 4) [77]. Moreover, mass spectroscopic approaches revealed the accumulation of two forms of antimony (Sb(V) and Sb(III)) in both stages of the parasite [78]. Thus, the possibility of *in vivo* metabolic conversion of pentavalent Sb(V) to trivalent Sb(III) antimonials was suggested, followed by uptake into the parasite.

Although antimony is less abundant than arsenic, their chemical properties are very similar. In fact, in solution, arsenic and antimony are mainly present as their trivalent species, as $As(OH)_3$ and $Sb(OH)_3$, respectively, both sharing some similarity to glycerol. In fact, as for As(III), it has been shown that Sb(III) can be transported in *E. coli*, by the glycerol facilitator (GlpF) [50]. In *E. coli*, disruption of GlpF leads to a resistant phenotype and reduced levels of uptake of Sb(III) (and As(III)), confirming that aquaglyceroporins are an important route for antimony uptake [79]. Indeed, structural, thermodynamic, and electrostatic comparison of As(III) and Sb(III) species at physiological pH showed that they exhibit similar conformation and charge distribution and a slightly smaller volume than glycerol, which may aid in their passage through the narrowest region of the GlpF channel [80]. However, the metalloid hydroxyl groups lack the flexibility of glycerol, which probably helps the latter to adapt its conformation to the topology of the GlpF channel.

Interestingly, in *Leishmania* cells, the accumulation of Sb(III) is competitively inhibited by the related metal As(III), suggesting that Sb(III) and As(III) enter the parasite cell via the same route [78]. Notably, *Leishmania* parasites express one aquaglyceroporin, LAQP1, which has been demonstrated to mediate Sb(III) uptake, and whose overexpression restores Sb(III)-sensitivity to three resistant phenotypes [81]. Studies by Kumar et al. showed that LAQP1 can be used as a biomarker for Sb(III)-resistance, as LAQP1 downregulation in resistant parasites is strongly correlated to reduction of compound's efficacy on parasite viability [82]. In spite of these results, the exact mechanism of transport and resistance to Sb(III) in *Leishmania* is still not fully understood [83].

As the *Leishmania* parasite develops inside human macrophages, it is crucial, for the therapeutic effects of metalloids, to understand their mechanism of uptake into these human cells. Macrophages express AQP3 in their membrane and this protein is essential for macrophage development and motility [84]. This channel isoform does not appear to be very efficient in As(III) transport, but overexpression of AQP3 in human embryonic kidney cells (HEK-293T) led to an increase of As(III) accumulation and cells' sensitivity to the drug [85]. Considering that As(III) and Sb(III) most likely share routes of uptake, AQP3 is also a likely candidate for Sb(III) transport into macrophages.

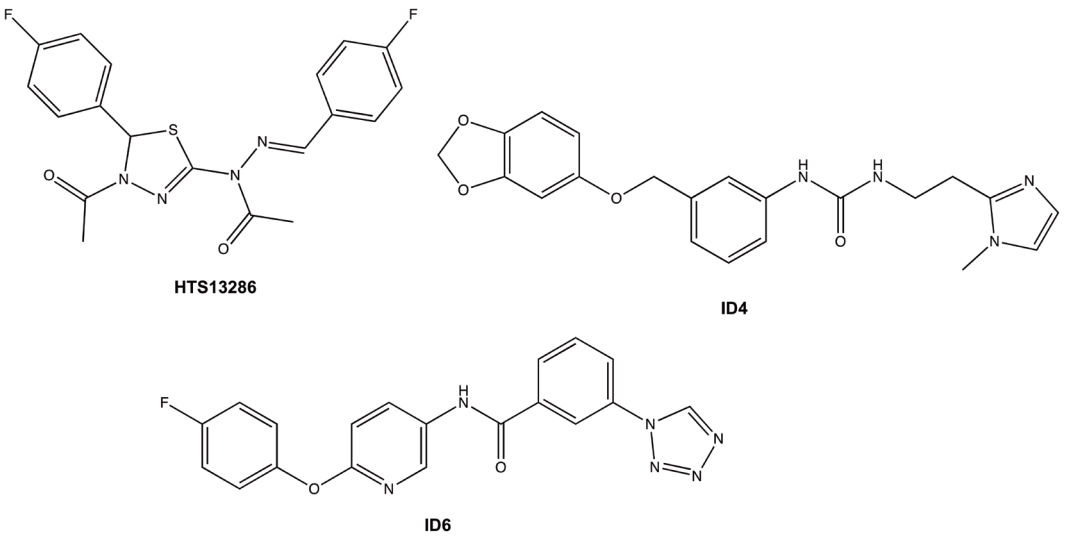

Figure 5. Small-molecule inhibitors of AQP9.

2.4. AQP modulators (inhibitors)

As important players in several physiological roles, as well as in many diseases, aquaporins have been identified as important drug targets [86]. However, the identification of AQP modulators has turned out to be unexpectedly challenging. Three classes of AQP-targeted small molecules have been described so far: i) small-molecule organic inhibitors; ii) small-molecule organic modulators targeting the interaction between AQP4 and the neuromyelitis optica (NMO) autoantibody; iii) inorganic inhibitors [87].

Following this categorization, the chemical compounds that modulate (inhibitors/regulators) AQP mediated water flux include heavy metals (e.g. $HgCl_2$, silver sulfadiazine) [88-91], and inorganic salts (e.g. $ZnCl_2$, $NiCl_2$) [92], quaternary ammonium salts [93-95], as well as sulfonamides, all acting as inhibitors of orthodox water channels [96]. Unfortunately, all these compounds are not suitable for therapeutic applications or to study AQP function in biological systems mostly due to their toxic side effects and lack of selectivity.

Concerning aquaglyceroporin modulators, only a few small molecule inhibitors of AQP9 water permeability were identified (Figure 5), although it must be noted that effects on glycerol transport have not been evaluated for most of these compounds, made exception for HTS13286, which was shown to effectively inhibit this isoform [97, 98]. Moreover, as the compounds' solubility in aqueous solution is very limited, they are currently not suitable for *in vivo* experiments. Overall, independent verification of AQP inhibition by these compounds is still awaited.

2.4.1. Small-molecule organic inhibitors

The library of small-molecule AQP inhibitors is still limited in number. Nonetheless, a few different classes of compounds are known (Figure 6).

Aquaporins and ion channels are evolutionary different but share a number of common features. Due to these common features, several authors investigated the possible inhibitory properties of the tetraalkylammonium ion channel blockers [92, 98]. Two of these quaternary ammonium compounds, **tetraethylammonium** (TEA) and **tetrapropylammonium** (TPrA), have been found to be inhibitors of AQP1 and, later, AQP2 and AQP4. While TPrA showed AQP1

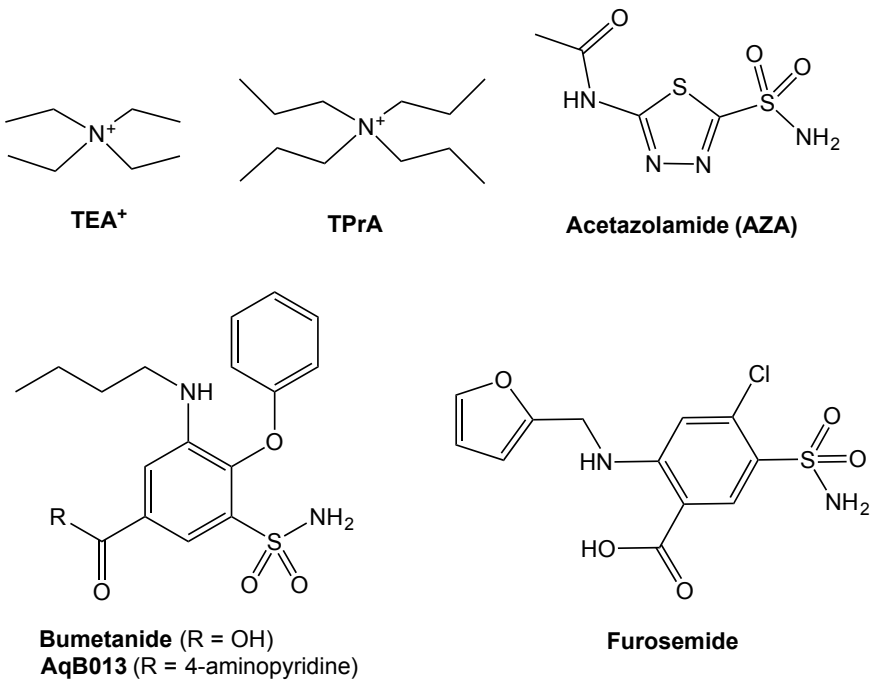

Figure 6. Small-molecule organic inhibitors of aquaporins.

inhibition at 100 μM, TEA showed stronger inhibition of three water channel isoforms, with IC_{50} of about 1.4, 6.2 and 9.8 μM for AQP1, AQP2 and AQP4, respectively, and no inhibition of two other isoforms, AQP5, a water channel, and AQP3, an aquaglyceroporin [92, 98]. Site-directed mutagenesis indicated that TEA may have a binding site in loop E, particularly involving Tyr186, a residue close to the ar/R SF of AQP1, as mutation of this tyrosine considerably reduces inhibition [92]. Interestingly, this tyrosine is conserved in AQP1, 2 and 4 but is not present in the isoforms that show no inhibition by TEA. Further studies revealed that, at a TEA concentration of 100 μM, the three water channel isoforms containing a mutated tyrosine to phenylalanine showed no significant decrease in water permeability, supporting the role of this residue in the binding of this drug [98]. The same authors performed molecular dynamics simulations of the interaction of TEA with AQP1 and revealed that, even though Tyr186 appears to be crucial for inhibition, it is still unclear if this is by direct or indirect interaction. The simulations demonstrate that the binding site may be formed by residues in loop A, C and E and loop A may be of particular importance, by acting as a cap and preventing TEA to leave the binding site. Despite these promising results, the inhibition of aquaporins by TEA could not be confirmed using other methodologies [99].

Blockers for Na^+-K^+-$2Cl^-$ (NKCC1) co-transporter, were also identified to inhibit AQP1 and AQP4 isoforms. One of these inhibitors, **bumetanide**, was identified to have several positive physiological effects in *in vivo* models, such as reduction of edema after an ischemic-induced event [100, 101], inhibiting seizure episodes both in animal models [102-104] and infants [105]. Interestingly, all these effects were initially attributed to inhibition of NKCC1 [106] but it was later discovered that, instead of NKCC1, the effect on brain swelling reduction after ischemia was due to AQP4 inhibition [107]. Research with *Xenopus* oocytes revealed that the inhibition of AQP4 by bumetanide was low when oocytes where incubated with bumetanide-contaning solution, but increased when the oocytes were injected with the drug, suggesting that the compound may bind to AQP4 in the intracellular side of the channel [107, 108]. In a similar fashion, **Furosemide**, another NKCC1 inhibitor, is active against both AQP1 and AQP4 only when administered internally to the

oocytes, by injection [108]. Remarkably, a new bumetanide-related compound without inhibitory properties against NKCC1, **AqB013**, shows strong inhibition of both aquaporin isoforms when administered externally in the medium ($IC_{50} \approx 20$ μM) [108].

Even though inhibitors of other channels may seem promising, other drugs showed potency towards aquaporins, namely **acetazolamide** (AZA). This compound is a carbonic anhydrase inhibitor used for the treatment of epileptic seizures, glaucoma and idiopathic intracranial hypertension, among others. The inhibition of AQP1-mediated water transport by AZA was evaluated in *Xenopus* oocytes [109] and HEK cells [110], the later using a fluorescence intensity assay, together with a surface Plasmon resonance assay, to determine binding. In both systems AZA was found to inhibit AQP1. In oocytes, AZA appeared to potently inhibit water transport, in micromolar range, and similar to HEK cells, with a determined K_D of 174 μM. Even though, just as TEA, these results could not be confirmed by further studies [99], AZA was tested in a *Xenopus* oocyte system expressing hAQP4-M23, an aquaporin 4 isoform. Results showed a dose-dependent inhibition of water permeability, with a very low IC_{50} of 0.9 μM and a maximum of inhibition of 85% [111]. Again, these results are quite controversial, as later research performed using human erythrocytes and epithelial cells failed to show any inhibition of AQP4 by AZA, up to concentrations of 10 mM [112].

Recently, ca. 1,000,000 compounds were screened on AQP9 by virtual screening revealed an intracellular binding site for inhibitors. The best compounds from the initial virtual screening were tested in AQP9-expressing Chinese hamster ovarian cells (CHO) using a fluorescent calcein assay [97]. From the whole library, 6 compounds (**ID1-6**), two of them showed in Figure 5, arose as AQP9 inhibitors, with IC_{50} between 4 and 10 μM. Several computational studies were performed to evaluate the possible binding mode of these compounds but these studies did not evidence the same affinities found *in vitro*.

Several attempts have been made to design compounds with the purpose of targeting aquaglyceroporins, mainly by designing compounds based on the natural substrate of the channel, glycerol [113]. In one study, various derivatives were designed to target a parasite isoform pfAQP, from *P. falciparum*. In order to evaluate inhibition, the authors performed both *in vitro* growth inhibition and toxicity assays, using two different parasite strains, as well as functional assays, using pfAQP-expressing yeast. Despite the fact that growth and toxicity inhibition results revealed that some of the tested drugs had a very potent effect, with IC_{50} as low as 1.4 μM, these did not show any inhibition of pfAQP in the yeast functional assays. This shows that even rational ab initio design of AQP inhibitors is a very challenging task and more functional models and methodologies need to be developed/improved.

2.4.2. AQP4-targeted NMO therapeutics

Aquaporin-4 is an isoform present in several tissues and cell types in the human body and involved in many pathological conditions. One of these states is neuromyelitis optica (NMO), an inflammatory demyelinating disease of spinal cord and optic nerve caused by pathogenic autoantibodies (NMO-IgG) against AQP4 in astrocytes [114]. A study on astrocytes revealed that the binding of NMO-IgG to AQP4 directly impairs water flux, which may lead to some of the symptoms observed for NMO, such as edema, inflammation and demyelination [115]. This

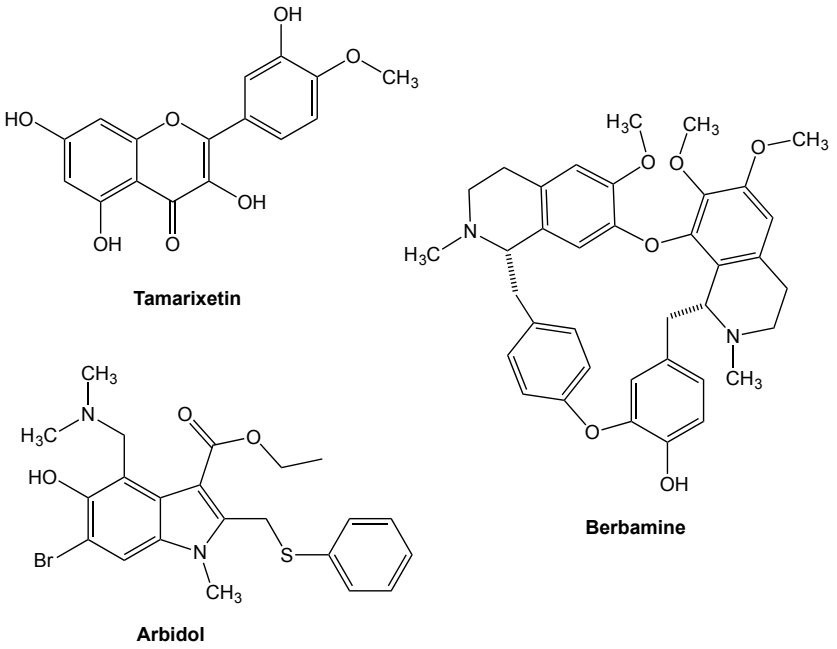

Figure 7. AQP4-targeted NMO therapeutics.

revealed a new possible approach for modulators as, in this case, an inhibition of AQP4 would lead to unwanted outcomes. A high-throughput screening of ca. 60,000 compounds, using a human recombinant monoclonal NMO-IgG and transfected Fisher rat thyroid cells stably expressing human M23-AQP4, revealed three classes of possible inhibitors: i) **arbidol**, an antiviral drug; ii) **tamarixetin**, a flavonoid and iii) **berbamine**, and other alkaloid derivatives (Figure 7) [116]. Remarkably, these drugs were able to block the binding of NMO-IgG to AQP4 without inhibiting water transport. Moreover, the blockage of NMO-IgG-AQP4 interaction led to a decrease in drug toxicity, consistent with a more functional water channel. Even though further studies are required in order to be able to translate these studies into clinical therapies, this show potential for modulators of aquaporins, other than inhibitors.

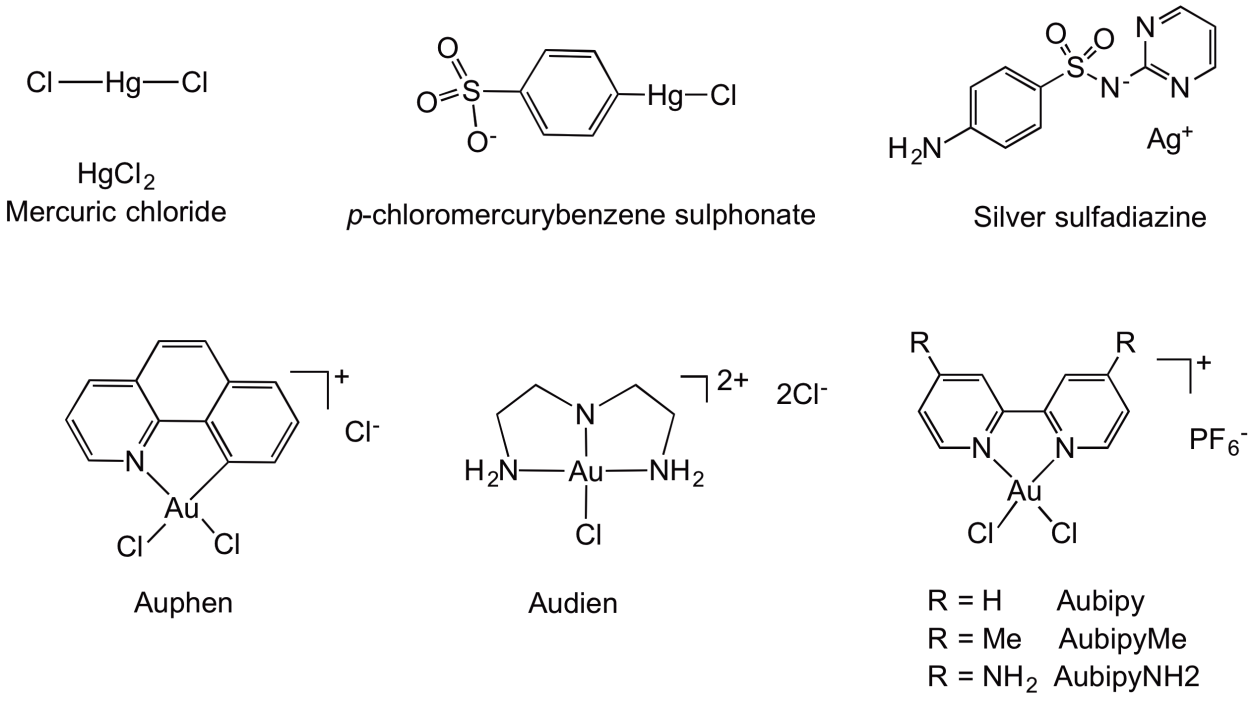

Figure 8. Inorganic inhibitors of aquaporins

2.4.3. Inorganic inhibitors

As metals play important roles in biological systems and the interaction of metal drugs and salts, such as mercurials, with biomolecules is well described, it is also interesting to develop and/or test inorganic aquaporin inhibitors.

Several antibacterials contain metals, in particular silver-containing molecules, such as **silver sulfadiazine**. Peribacteroid membrane (PBM) of soybean nodules contains a high density of Noduline 26 (NOD26), an aquaglyceroporin, which makes these membranes a good system for evaluation of the function of this AQP isoform [117, 118]. One study used this system to investigate the effects of silver sulfadiazine and silver nitrate ($AgNO_3$) in comparison to other transition metals (including gold, which will be discussed further on), using dynamic light scattering (DLS) [119]. Interestingly, the silver compounds showed a more potent inhibition of NOD26-mediated water transport, with IC_{50} one order of magnitude lower than $HgCl_2$. The same study used also human red blood cells (hRBC) to test inhibition of water transport, mainly via AQP1, by the silver drugs. The inhibition showed to be of the same potency of the one found in PBM vesicles, with IC_{50} of 3.90 and 1.24 μM for $AgNO_3$ and silver sulfadiazine, respectively [119].

The development of new drugs as AQP inhibitors has revealed to be quite challenging, but also the development of new high-throughput methodologies for aquaporin screening has demonstrated to not be so trivial either. Nonetheless, Mola et al. have developed a methodology to assess AQP function, based on calcein fluorescence [120]. This assay allowed the screening of 3,575 small molecules, 418 of which are US Food and Drug Administration (FDA)-approved. The compounds were screened on mouse astrocytes, with endogenous expression of AQP4, mouse fibroblasts, which express also AQP1, and AQP-deficient astrocytoma cells (TNC1 cells), transfected with AQP4. The best drugs were further tested using stopped-flow and six compounds were found to be inhibitors of water transport, among them **NSC168597** and **NSC164914**, containing lead and antimony, respectively. These drugs were further tested on erythrocytes, using a stopped-flow method, again for inhibition of AQP1, widely expressed in this cell type. These two compounds showed to be inhibitors of water transport via both AQP4, in different cell types, and AQP1 in erythrocytes [120].

2.4.3.1. Mercurial compounds as aquaporins inhibitors

Concerning mercurial compounds, it has always been postulated that aquaporins are inhibited by Hg^{2+} ions via covalent modification of cysteine residues based on the classical Hard Soft Acid Base (HSAB) theory. In order to confirm such mechanism and to assess the importance of cysteine residues for mercury inhibition, several studies were performed on Cys-mutated isoforms of human AQP1. For example, *Xenopus* oocytes were transfected with each Cys-mutated AQP1 isoform and the effects of mercury inhibition were evaluated [121, 122]. From all cysteine residues in AQP1, only one was shown to be responsible for sensitivity to the mercurial salt $HgCl_2$, namely Cys189. When this cysteine is mutated to either serine or glycine, water permeability of the oocytes was slightly decreased, indicating that this residue may be of importance for water transport. Moreover, cells expressing the Cys189Ser mutant lost sensitivity to $HgCl_2$, and didn't show significant inhibition by $HgCl_2$ up to a concentration of 3 mM. Later on, as the atomic-resolution structure of human AQP1 was solved, Cys189 was shown to be positioned inside the channel, just above the ar/R SF [123].

Therefore, it was hypothesized that Hg^{2+} binding to this site was likely to prevent passage of water molecules via steric effects.

The current literature provides two mechanisms of inhibition of AQPs by mercury: the first is simple occlusion of the water pore by the mercury atoms/ions found in the vicinity of the cysteine residues lining the water channel wall; the second is conformational change (collapse of the water pore) at the selectivity filter (SF) (namely, the aromatic/ arginine (ar/R) constriction) region, induced by mercury bonded to a cysteine residue nearby. In an effort to better understand the influence of cysteines and their location on the inhibition of hAQP1 by mercury, Savage et al. studied the bacterial homolog of hAQP1, AqpZ [124]. This bacterial isoform has been previously described as a water channel [125] and it is structurally very similar to hAQP1, containing the same ar/R SF residues, but it is not sensitive to mercury since it lacks Cys189 crucial for Hg^{2+} inhibition in hAQP1. In this position, AqpZ has a threonine residue, Thr183. Thus, by site-directed mutagenesis a model AqpZ was obtained lacking all endogenous cysteins and with a mutation Thr183Cys, in order to evaluate the role of this specific residue [124]. The crystal structure of this mutant, co-crystalized with $HgCl_2$, showed no significant conformational changes between the apo- and metal bound forms, suggesting that inhibition by mercury is not due to major changes in the tridimensional structure of AqpZ both at the level of the monomer folding and of the tetrameric axes. Instead, as seen in Figure 9, a Hg^{2+} ion (Hg-1) appears to be positioned inside the channel, just bellow the ar/R SF, suggesting a steric blockage of the channel upon metal binding [124]. Notably, the distance between the Hg^{2+} atom and Thr183Cys is not ideal to demonstrate binding to the thiol residue (ca. 5.6 Å). In this structure, another Hg^{2+} atom (Hg-2) is outside the pore (Figure 9), pointing towards Cys183 (distance of ca. 4.0 Å) and residing in a hydrophilic pocket

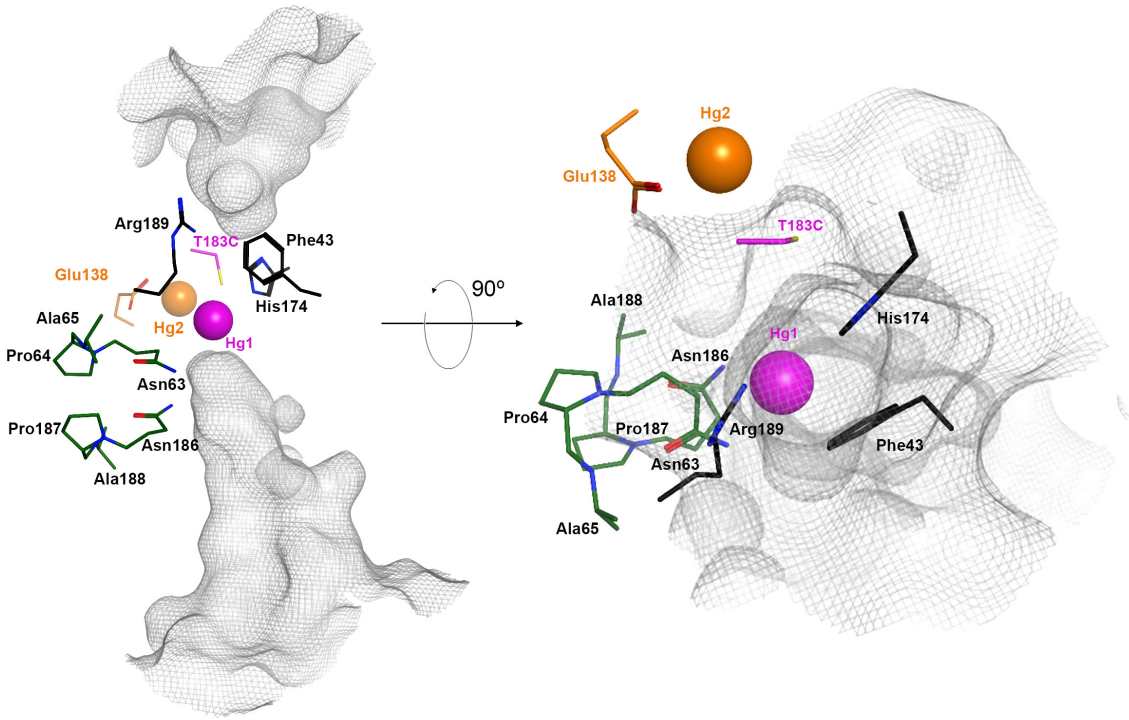

Figure 9. Structure of the mercury-blocked AqpZ Tyr183Cys mutant. Molecular surface of residues lining the pore is shown as grey mesh. Selectivity filter residues are shown in black, while NPA motifs are represented in green. Two mercury atoms are located inside or close to the channel and are shown in space-filling representation, in magenta (Hg-1) and orange (Hg-2), respectively. The same colour code is used to represent the amino acid residue that is located closer to each of the mercury atoms, in magenta and orange. Adapted from reference [124].

formed by conserved Glu138 and Ser177 where it makes favourable electrostatic interactions at 2.6 Å and 3.1 Å distance, respectively. Interestingly, Glu138 appears to be important for maintaining the orientation of the backbone carbonyl oxygen of Gly190, Cys191, and Gly192. This may imply that a conformational change can also occur in Thr183Cys-AQPZ bound to mercury, although this mechanism has still to be confirmed. In order to validate steric blockage by mercury, the authors produced another mutant, Leu170Cys, with the cysteine located in between the ar/R SF and the NPA motifs. This mutant was proven to be even more sensitive to $HgCl_2$ and the resulting X-ray structure revealed four Hg^{2+} atoms inside the channel, one covalently bound to the thiol group of Leu140Cys. Overall, authors conclude that their results indicate that binding of Hg^{2+} to thiol residue of Cys side-chain inside the channel is ideal for AQPs inhibition of solute transport, most likely due to steric blockage [124]. However, since a real coordination bond could not be assessed between Hg^{2+} and the thiol residue of Cys183, further structural information should be provided to validate the proposed mechanism.

The second mechanism of AQP inhibition by mercurial compounds was proposed in an i*n silico* study on the basis of molecular dynamics (MD) simulations of the bovine aquaporin AQP1 (bAQP1) [126]. As hAQP1, also bAQP1 has cysteine residue, Cys191, at the ar/R region, located 8 Å above the NPA region, which may bound Hg. According to the MD simulations of both free AQP1 and Hg-bound AQP1, the energy barrier for Hg-AQP1 is much higher than that of free AQP1 at the ar/R region. Moreover, calculations show that mercury binding induces a collapse of the orientation of amino acid residues at the ar/R region and the constriction of the space between Arg197 and His182.

A third mechanism of mercury inhibition has been proposed on the basis of MD simulations by Zhang et al. according to which the mercury ion, covalently bound to the cysteine residue (Cys170) in the Leu170Cys mutant of AQPZ, causes water molecules to clog the water channel [127]. The obtained *in silico* results unravelled the interactions between the mercury ion and the waters in its vicinity and found that five to six waters are strongly attracted by the mercury ion, occluding the space of the water channel. However, it should be noted that binding of water molecules to Hg ions is highly reversible and the predicted mechanism may not be relevant in physiological environment.

Other transition metal compounds have been investigated, as inhibitors, with respect to water permeation through aquaporins (e.g. human AQP1). Thus, for example $AgNO_3$ and $HAuCl_4$ were among the most effective in inhibiting water transport. In the case of mercury, the mechanism of silver and gold inhibition is most likely due to their ability to interact with sulfhydryl groups of proteins. Interestingly, silver resulted to be more efficient in inhibiting water transport than $HgCl_2$. For example, silver as $AgNO_3$ or silver sulfadiazine (Figure 8) inhibited with high potency (EC_{50} 1-10 μM) the water permeability of the peribacteroid membrane from soybean (containing Nodulin 26 aquaporin NOD26), the water permeability of the plasma membrane from roots (containing plasma membrane integral proteins), and the water permeability of human red blood cells (containing AQP1) [119]. However, it should be noted that more recent results by Casini et al. showed that silver sulfadiazine is actually not inhibiting water transport via AQP1 in human red blood cells even at 100 μM concentration [128].

2.4.3.2. Inhibition of human AQP3 by gold(III) complexes

The limited number of AQP modulators available in the literature, prompted us to explore the properties of coordination metal complexes as possible inhibitors. Thus, we reported on the potent and selective inhibition of AQP3 by a water-soluble gold(III) coordination compound, [Au(phen) Cl_2]Cl (phen = 1,10-phenatroline, Auphen) (Figure 8). Notably, Auphen inhibited glycerol transport in human red blood cells (hRBC), with an IC_{50} = 0.8 ± 0.08 μM, while having only a modest inhibitory effect on water permeability [129]. hRBC are know to express large amount of AQP1 and AQP3 accountable for membrane permeability to water and glycerol, respectively [130]. The selectivity of the compound towards AQP3 was confirmed in transfected PC12 cell lines with overexpression of either AQP1 or AQP3. Later, we have shown that Auphen also potently inhibits human AQP7 in adipocytes. The data available on this topic will be further discussed in Chapter 2.2.

Among all the identified aquaporin inhibitors, gold(III) compounds shows a big advantage as a possible therapeutic agent: selectivity. Most of the described inhibitors were tested on only one AQP isoform or lack any selectivity for different aquaporins. TEA is the only inhibitor that showed to be selective towards certain orthodox aquaporins (AQP1, AQP2 and AQP4). Unfortunately, due to the broad spectrum of targets and the severe, and even fatal, side effects in patients, this drug is not a suitable candidate for therapeutic applications [131]. On the other hand, inorganic drugs containing gold, such as auranofin, are already currently in the market and have been shown to have many properties, including as anti-cancer agents [132]. As gold(III) drugs, as Auphen, show selectivity towards aquaglyceroporin isoforms (AQP3 and AQP7) and no activity towards orthodox aquaporins (AQP1), they are advantageous when compared to other compounds, as potential therapeutical drugs.

Effects of gold compounds on cell proliferation

Concerning the possible roles of aquaglyceroporins, specifically AQP3, in cancer progressions, we also recently analysed in depth Auphen's capacity of inhibiting cell proliferation in different cell lines (cancerous and non-cancerous), with different levels of AQP3 expression, and also investigated the possible correlation of the observed antiproliferative activities with the AQP3 inhibition properties of Auphen in the selected cells [27].

To this end, various mammalian cell lines differing in AQP3 expression level were used: no expression (PC12), moderate (NIH/3T3) or high (A431, epidermoid carcinoma) endogenous expression, cells stably expressing AQP3 (PC12-AQP3), and HEK293T cells transiently transfected (HEK-AQP3) for AQP3 expression. Auphen reduced approximately 50% the proliferation of A431 and PC12-AQP3 cells, 15% in HEK-AQP3 and had no effect in wt-PC12 and NIH/3T3. Dose response curves with the A431 tumoral cell line showed an EC_{50} of 1.99 ± 0.47 μM. Silencing AQP3 expression in the same A431 cell line alleviated Auphen effect on cell proliferation with a subsequent increase in the EC_{50}. The effect on cell proliferation was confirmed by detecting a strong arrest in the S-G2/M phases of the cell cycle of cells treated with Auphen.

Additionally, functional studies allowed correlating the inhibition of cell proliferation with the impairment of AQP3 activity. In fact, evaluation of glycerol permeability of cells differing in AQP3 expression showed 50% inhibition of glycerol uptake in A431 treated cells, demonstrating

that the anti-proliferative effect of Auphen correlates with its ability to block the AQP3 channel. Overall, these results anticipate a targeted therapeutic effect on carcinomas and other cancer types with large AQP3 expression and provide a rational for the use of gold compounds as anticancer agents.

2.4.3.3. Inhibition of aquaporins by other transition metal ions

Interestingly, ionic metal compounds have also been shown to modulate the function of AQPs. For example, among the endogenous transition metal ions, Ni^{2+} ions in the form of $NiCl_2$ has been demonstrated to cause water permeability (P_f) decrease in cells expressing human AQP3-GFP in a dose-dependent manner and the effect was rapid and reversible [133]. Moreover, the effect of Ni^{2+} was pH-dependent: at neutral and acidic pH, the AQP3-mediated water permeability was completely inhibited by 1 mM $NiCl_2$. At pH 7.4 and 8.0, the P_f in transfected cells was decreased by Ni^{2+}, but remained significantly higher than that in non-transfected cells. Conversely, treatment of cells with 1 mM $ZnCl_2$ or $CdCl_2$ did not produce any effect on AQP3 water permeability. Site-directed mutagenesis studies identified three residues, Trp128 and Ser152 in the second extracellular loop and His241 in the third extracellular loop of AQP3, as determinants of Ni^{2+} sensitivity [133]. Interestingly, Ser152 was identified as a common determinant of both Ni^{2+} and pH sensitivity. In the same study, the water permeability of neither AQP4 nor of AQP5 transfected cells was Ni^{2+}or pH-sensitive [133]. Alignment of the protein structures showed that all amino acid residues involved in the regulation of AQP3 by Ni^{2+} or pH are absent in AQP4 and AQP5.

In a subsequent study, the same three extracellular amino acidic residues in AQP3 were found to be essential for the inhibition of both water and glycerol AQP3 permeability by $CuSO_4$ in human epithelial cell line BEAS-2b that was transiently transfected with human AQP3 [134]. However, in the same study, neither Cu^{2+} nor Ni^{2+} ions influenced the permeability of AQP7-overexpressing cells.

In contrast to Hg^{2+}, divalent copper and nickel ions form coordination bonds with amino acids that are to a large extent reversible by simple washout of the metal ions (the effect of mercury is only reversible upon treatment of the cells with a reducing agent, such as β-mercaptoethanol). The speed and reversibility of the inhibition effects of these transition metal ions may be convenient to use them as test tools in AQP3 functional studies. Moreover, the results of these studies provide also a better understanding of the gating mechanisms of AQPs, and of processes that may occur in severe copper metabolism defects and nickel/copper poisoning.

References

[1] L.S. King, D. Kozono, P. Agre, Nat Rev Mol Cell Bio, 5 (2004) 687-698.
[2] Y. Fujiyoshi, K. Mitsuoka, B.L. de Groot, A. Philippsen, H. Grubmuller, P. Agre, A. Engel, Curr Opin Struct Biol, 12 (2002) 509-515.
[3] G. Benga, Mol Asp of Med, 33 (2012) 514-517.
[4] K. Ishibashi, Cell Mol Biol, 52 (2006) 20-27.
[5] A. Madeira, S. Fernández-Veledo, M. Camps, A. Zorzano, T.F. Moura, V. Ceperuelo-Mallafré, J. Vendrell, G. Soveral, Obesity, (2014) 22(9):2010-7
[6] B. Wu, E. Beitz, Cell Mol Life Sci, 64 (2007) 2413-2421.
[7] K. Murata, K. Mitsuoka, T. Hirai, T. Walz, P. Agre, J.B. Heymann, A. Engel, Y. Fujiyoshi, Nature, 407 (2000) 599-605.
[8] J.S. Hub, B.L. De Groot, Proc. Natl. Acad. Sci. U. S. A., 105 (2008) 1198-1203.
[9] D.F. Savage, J.D. O'Connell, 3rd, L.J. Miercke, J. Finer-Moore, R.M. Stroud, Proc Natl Acad Sci U S A, 107 (2010) 17164-17169.
[10] N. Smolin, B. Li, D.A. Beck, V. Daggett, Biophys J, 95 (2008) 1089-1098.
[11] T.P. Jahn, A.L. Moller, T. Zeuthen, L.M. Holm, D.A. Klaerke, B. Mohsin, W. Kuhlbrandt, J.K. Schjoerring, FEBS letters, 574

(2004) 31-36.
[12] D.a. Gorelick, J. Praetorius, T. Tsunenari, S. Nielsen, P. Agre, BMC biochemistry, 7 (2006) 14.
[13] Y. Morishita, Y. Sakube, S. Sasaki, K. Ishibashi, J Pharmacol Sci, 96 (2004) 276-279.
[14] K. Yakata, Y. Hiroaki, K. Ishibashi, E. Sohara, S. Sasaki, K. Mitsuoka, Y. Fujiyoshi, Biochim Biophys Acta, 1768 (2007) 688-693.
[15] A. Madeira, S. Fernández-Veledo, M. Camps, A. Zorzano, T.F. Moura, V. Ceperuelo-Mallafré, J. Vendrell, G. Soveral, Obesity, 00 (2014) 1-8.
[16] E.E. Tchekneva, Z. Khuchua, L.S. Davis, V. Kadkina, S.R. Dunn, S. Bachman, K. Ishibashi, E.M. Rinchik, R.C. Harris, M.M. Dikov, M.D. Breyer, J Am Soc Nephrol : JASN, 19 (2008) 1955-1964.
[17] M. Ikeda, A. Andoo, M. Shimono, N. Takamatsu, A. Taki, K. Muta, W. Matsushita, T. Uechi, T. Matsuzaki, N. Kenmochi, K. Takata, S. Sasaki, K. Ito, K. Ishibashi, J Biol Chem, 286 (2011) 3342-3350.
[18] A.S. Verkman, B.X. Yang, Y.L. Song, G.T. Manley, T.H. Ma, Exp Physiol, 85 (2000) 233S-241S.
[19] D. Ribatti, G. Ranieri, T. Annese, B. Nico, Bba-Gen Subjects, 1840 (2014) 1550-1553.
[20] M. Hara-Chikuma, A.S. Verkman, J Mol Med (Berl), 86 (2008) 221-231.
[21] T.H. Ma, Y.L. Song, B.X. Yang, A. Gillespie, E.J. Carlson, C.J. Epstein, A.S. Verkman, Proc. Natl. Acad. Sci. U. S. A., 97 (2000) 4386-4391.
[22] M. Hara-Chikuma, A.S. Verkman, Mol Cell Biol, 28 (2008) 326-332.
[23] M. Kusayama, K. Wada, M. Nagata, S. Ishimoto, H. Takahashi, M. Yoneda, A. Nakajima, M. Okura, M. Kogo, Y. Kamisaki, Cancer science, 102 (2011) 1128-1136.
[24] C. Ji, C. Cao, S. Lu, R. Kivlin, A. Amaral, N. Kouttab, H. Yang, W.M. Chu, Z.G. Bi, W. Di, Y.S. Wan, Cancer Chemother. Pharmacol., 62 (2008) 857-865.
[25] R. Chen, Y. Shi, R. Amiduo, T. Tuokan, L. Suzuk, PloS one, 9 (2014) e98576.
[26] Y.L. Liu, T. Matsuzaki, T. Nakazawa, S.I. Murata, N. Nakamura, T. Kondo, M. Iwashina, K. Mochizuki, T. Yamane, K. Takata, R. Katoh, Hum Pathol, 38 (2007) 171-178.
[27] A. Serna, A. Galán-Cobo, C. Rodrigues, I. Sánchez-Gomar, J.J. Toledo-Aral, T.F. Moura, A. Casini, G. Soveral, M. Echevarría, J Cell Physiol, (2014) 10.1002/jcp.24632.
[29] K. Ishibashi, M. Kuwahara, Y. Gu, Y. Kageyama, A. Tohsaka, F. Suzuki, F. Marumo, S. Sasaki, J. Biol. Chem., 272 (1997) 20782-20786.
[30] A. Rojek, J. Praetorius, J. Frøkiaer, S. Nielsen, R.A. Fenton, Annual Review of Physiology, 70 (2008) 301-327.
[31] M. Hara-Chikuma, E. Sohara, T. Rai, M. Ikawa, M. Okabe, S. Sasaki, S. Uchida, A.S. Verkman, J. Biol. Chem., 280 (2005) 15493-15496.
[32] A. Madeira, M. Camps, A. Zorzano, T.F. Moura, G. Soveral, Plos One, 8 (2013) e83442.
[33] M.P. Marrades, F.I. Milagro, J.A. Martinez, M.J. Moreno-Aliaga, Biochem Bioph Res Co, 339 (2006) 785-789.
[34] H. Kondo, I. Shimomura, K. Kishida, H. Kuriyama, Y. Makino, H. Nishizawa, M. Matsuda, N. Maeda, H. Nagaretani, S. Kihara, Y. Kurachi, T. Nakamura, T. Funahashi, Y. Matsuzawa, Eur. J. Biochem., 269 (2002) 1814-1826.
[35] M.L. Elkjaer, Z. Vajda, L.N. Nejsum, T.H. Kwon, U.B. Jensen, M. Amiry-Moghaddam, J. Frokiaer, S. Nielsen, Biochem Bioph Res Co, 276 (2000) 1118-1128.
[36] S. Jelen, S. Wacker, C. Aponte-Santamaria, M. Skott, A. Rojek, U. Johanson, P. Kjellbom, S. Nielsen, B.L. de Groot, M. Rutzler, J Biol Chem, 286 (2011) 44319-44325.
[37] J.M. Carbrey, D.A. Gorelick-Feldman, D. Kozono, J. Praetorius, S. Nielsen, P. Agre, Proc. Natl. Acad. Sci. U. S. A., 100 (2003) 2945-2950.
[38] H. Kuriyama, I. Shimomura, K. Kishida, H. Kondo, N. Furuyama, H. Nishizawa, N. Maeda, M. Matsuda, H. Nagaretani, S. Kihara, T. Nakamura, Y. Tochino, T. Funahashi, Y. Matsuzawa, Diabetes, 51 (2002) 2915-2921.
[39] N. Maeda, T. Hibuse, T. Funahashi, Handbook of experimental pharmacology, (2009) 233-249.
[40] J. Jungersted, J. Bomholt, N. Bajraktari, J. Hansen, D. Klærke, P. Pedersen, K. Hedfalk, K. Nielsen, T. Agner, C. Hélix-Nielsen, Arch Dermatol Res, 305 (2013) 699-704.
[41] T. Morinaga, M. Nakakoshi, A. Hirao, M. Imai, K. Ishibashi, Biochem Bioph Res Co, 294 (2002) 630-634.
[42] Y. Liu, D. Promeneur, A. Rojek, N. Kumar, J. Frokiaer, S. Nielsen, L.S. King, P. Agre, J.M. Carbrey, Proc Natl Acad Sci U S A, 104 (2007) 12560-12564.
[43] Z.E. Newby, J. O'Connell, 3rd, Y. Robles-Colmenares, S. Khademi, L.J. Miercke, R.M. Stroud, Nature Struct Mol Biol, 15 (2008) 619-625.
[44] M. Hansen, J.F.J. Kun, J.E. Schultz, E. Beitz, J. Biol. Chem., 277 (2002) 4874-4882.
[45] R. Mukhopadhyay, H. Bhattacharjee, B.P. Rosen, Bba-Gen Subjects, 1840 (2014) 1583-1591.
[46] S.M. Cohen, L.L. Arnold, B.D. Beck, A.S. Lewis, M. Eldan, Crc Cr Rev Toxicol, 43 (2013) 711-752.
[47] O. Ni Dhubhghaill, P. Sadler, The structure and reactivity of arsenic compounds: Biological activity and drug design, in: Bioinorganic Chemistry, Springer Berlin Heidelberg, 1991, pp. 129-190.
[48] S. Hirano, X. Cui, S. Li, S. Kanno, Y. Kobayashi, T. Hayakawa, A. Shraim, Arch Toxicol, 77 (2003) 305-312.
[49] Y.-L. Meng, Z. Liu, B.P. Rosen, J Biol Chem, 279 (2004) 18334-18341.
[50] A. Ramírez-Solís, R. Mukopadhyay, B.P. Rosen, T.L. Stemmler, Inorg Chem, 43 (2004) 2954-2959.
[51] Z. Liu, J.M. Carbrey, P. Agre, B.P. Rosen, Biochem Biophys Res Comm, 316 (2004) 1178-1185.
[52] K. Ishibashi, M. Kuwahara, Y. Gu, Y. Tanaka, F. Marumo, S. Sasaki, Biochem Biophys Res Comm, 244 (1998) 268-274.
[53] N. Maeda, T. Funahashi, I. Shimomura, Nature clinical practice. Endocrinol Metab, 4 (2008) 627-634.
[54] D.J. Thomas, S.B. Waters, M. Styblo, Toxicol App Pharm, 198 (2004) 319-326.
[55] M. Vahter, Science progress, 82 (Pt 1) (1999) 69-88.
[56] M. Vahter, Toxicology, 181-182 (2002) 211-217.
[57] Z. Liu, M. Styblo, B.P. Rosen, Environ Health Persp, 114 (2006) 527-531.
[58] Z. Liu, J. Shen, J.M. Carbrey, R. Mukhopadhyay, P. Agre, B.P. Rosen, P Natl A Sci USA, 99 (2002) 6053-6058.
[59] E.P. Swindell, P.L. Hankins, H. Chen, D.U. Miodragovic, T.V. O'Halloran, Inorg Chem, 52 (2013) 12292-12304.

[60] H.J. Iland, J.F. Seymour, Current treatment options in oncology, 14 (2013) 170-184.
[61] H. Bhattacharjee, J. Carbrey, B.P. Rosen, R. Mukhopadhyay, Biochem Biophys Res Comm, 322 (2004) 836-841.
[62] J. Leung, A. Pang, W.H. Yuen, Y.L. Kwong, E.W. Tse, Blood, 109 (2007) 740-746.
[63] N. Baker, H.P. de Koning, P. Maser, D. Horn, Trends in Parasit, 29 (2013) 110-118.
[64] D. Steverding, Parasit Vectors, 3 (2010) 15.
[65] N.L. Uzcategui, A. Szallies, S. Pavlovic-Djuranovic, M. Palmada, K. Figarella, C. Boehmer, F. Lang, E. Beitz, M. Duszenko, J Biol Chem, 279 (2004) 42669-42676.
[66] S. Alsford, S. Eckert, N. Baker, L. Glover, A. Sanchez-Flores, K.F. Leung, D.J. Turner, M.C. Field, M. Berriman, D. Horn, Nature, 482 (2012) 232-236.
[67] N. Baker, L. Glover, J.C. Munday, D. Aguinaga Andrés, M.P. Barrett, H.P. de Koning, D. Horn, P Natl A Sci, 109 (2012) 10996-11001.
[68] S.L. Soignet, W.P. Tong, S. Hirschfeld, R.P. Warrell, Jr., Cancer Chemoth Pharm, 44 (1999) 417-421.
[69] A. Konig, L. Wrazel, R.P. Warrell, Jr., R. Rivi, P.P. Pandolfi, A. Jakubowski, J.L. Gabrilove, Blood, 90 (1997) 562-570.
[70] R.W. Ashford, K.A. Kohestany, M.A. Karimzad, Ann Trop Med Parasit, 86 (1992) 361-371.
[71] R.W. Ashford, J. Seaman, J. Schorscher, F. Pratlong, T Roy Soc Trop Med H, 86 (1992) 379-380.
[72] L. Kedzierski, J Golb Infect Dis, 2 (2010) 177-185.
[73] B.L. Herwaldt, The Lancet, 354 (1999) 1191-1199.
[74] S. Sundar, Tropical Med Int Health : TM & IH, 6 (2001) 849-854.
[75] A.K. Haldar, P. Sen, S. Roy, Mol Biol Int, 2011 (2011) 23.
[76] J.D. Berman, J.V. Gallalee, B.D. Hansen, Exp Parasit, 64 (1987) 127-131.
[77] C. Brochu, J. Wang, G. Roy, N. Messier, X.Y. Wang, N.G. Saravia, M. Ouellette, Antimicrob Agents Ch, 47 (2003) 3073-3079.
[78] O.I. Sanders, C. Rensing, M. Kuroda, B. Mitra, B.P. Rosen, J Bacteriol, 179 (1997) 3365-3367.
[79] A. Porquet, M. Filella, Chem Res Toxicol, 20 (2007) 1269-1276.
[80] B. Gourbal, N. Sonuc, H. Bhattacharjee, D. Legare, S. Sundar, M. Ouellette, B.P. Rosen, R. Mukhopadhyay, J Biol Chem, 279 (2004) 31010-31017.
[81] D. Kumar, R. Singh, V. Bhandari, A. Kulshrestha, N.S. Negi, P. Salotra, Parasitol Res, 111 (2012) 223-230.
[82] Ashutosh, S. Sundar, N. Goyal, J Med Microbiol, 56 (2007) 143-153.
[83] N. Zhu, X. Feng, C. He, H. Gao, L. Yang, Q. Ma, L. Guo, Y. Qiao, H. Yang, T. Ma, FASEB J, 25 (2011) 4233-4239.
[84] T.C. Lee, I.C. Ho, W.J. Lu, J.D. Huang, J Biol Chem, 281 (2006) 18401-18407.
[85] A.S. Verkman, M.O. Anderson, M.C. Papadopoulos, Nat Rev Drug Discov, 13 (2014) 259-277.
[86] A.S. Verkman, M.O. Anderson, M.C. Papadopoulos, Nat Rev Drug Discov, (2014).
[87] G.M. Preston, T.P. Carroll, W.B. Guggino, P. Agre, Science, 256 (1992) 385-387.
[88] G.M. Preston, J.S. Jung, W.B. Guggino, P. Agre, J. Biol. Chem., 268 (1993) 17-20.
[89] Y. Yukutake, S. Tsuji, Y. Hirano, T. Adachi, T. Takahashi, K. Fujihara, P. Agre, M. Yasui, M. Suematsu, Biology of the Cell, 100 (2008) 355-363.
[90] M. Zelenina, S. Tritto, A.A. Bondar, S. Zelenin, A. Aperia, J. Biol. Chem., 279 (2004) 51939-51943.
[91] Y. Yukutake, Y. Hirano, M. Suematsu, M. Yasui, Biochemistry, 48 (2009) 12059-12061.
[92] H.L. Brooks, J.W. Regan, A.J. Yool, Mol Pharmacol, 57 (2000) 1021-1026.
[93] A.J. Yool, A.M. Weinstein, News Physiol Sci, 17 (2002) 68-72.
[94] F.J.M. Detmers, B.L. De Groot, E.M. Muller, A. Hinton, I.B.M. Konings, M. Sze, S.L. Flitsch, H. Grubmuller, P.M.T. Deen, J. Biol. Chem., 281 (2006) 14207-14214.
[95] V.J. Huber, M. Tsujita, T. Nakada, Mol Aspof Med, 33 (2012) 691-703.
[96] S. Jelen, S. Wacker, C. Aponte-Santamaria, M. Skott, A. Rojek, U. Johanson, P. Kjellbom, S. Nielsen, B. de Groot, M. Rutzler, J Biol Chem, (2011).
[97] S.J. Wacker, C. Aponte-Santamaria, P. Kjellbom, S. Nielsen, B.L. de Groot, M. Rutzler, Mol Memb Biol, 30 (2013) 246-260.
[98] F.J. Detmers, B.L. de Groot, E.M. Muller, A. Hinton, I.B. Konings, M. Sze, S.L. Flitsch, H. Grubmuller, P.M. Deen, J Biol Chem, 281 (2006) 14207-14214.
[99] B. Yang, J.K. Kim, A.S. Verkman, FEBS letters, 580 6679-6684.
[100] Y. Yan, R.J. Dempsey, D. Sun, J Cereb Blood Flow Metab, 21 (2001) 711-721.
[101] Y. Yan, R.J. Dempsey, A. Flemmer, B. Forbush, D. Sun, Brain Res, 961 (2003) 22-31.
[102] K.H. Reid, S.Z. Guo, V.G. Iyer, Brain Research, 864 (2000) 134-137.
[103] V.I. Dzhala, D.M. Talos, D.A. Sdrulla, A.C. Brumback, G.C. Mathews, T.A. Benke, E. Delpire, F.E. Jensen, K.J. Staley, Nat Med, 11 (2005) 1205-1213.
[104] A. Mazarati, D. Shin, R. Sankar, Epilepsia, 50 (2009) 2117-2122.
[105] K.T. Kahle, S.M. Barnett, K.C. Sassower, K.J. Staley, J Child Neur, 24 (2009) 572-576.
[106] K.T. Kahle, K.J. Staley, Neurosurgical focus, 25 (2008) E22.
[107] E. Migliati, M. Amiry-Moghaddam, S. Froehner, M. Adams, O. Ottersen, A. Bhardwaj, Neurocrit Care, 13 (2010) 123-131.
[108] E. Migliati, N. Meurice, P. DuBois, J.S. Fang, S. Somasekharan, E. Beckett, G. Flynn, A.J. Yool, Mol Pharmacol, 76 (2009) 105-112.
[109] B. Ma, Y. Xiang, S.M. Mu, T. Li, H.M. Yu, X.J. Li, Acta Pharm Sinic, 25 (2004) 90-97.
[110] J. Gao, X. Wang, Y. Chang, J. Zhang, Q. Song, H. Yu, X. Li, Anal Biochem, 350 (2006) 165-170.
[111] Y. Tanimura, Y. Hiroaki, Y. Fujiyoshi, J Struct Biol, 166 (2009) 16-21.
[112] B. Yang, H. Zhang, A.S. Verkman, Bioorgan Med Chem, 16 (2008) 7489-7493.
[113] A. Robin, F. Brown, N. Bahamontes-Rosa, B. Wu, E. Beitz, J.F. Kun, S.L. Flitsch, J Med Chem, 50 (2007) 4243-4249.
[114] M.C. Papadopoulos, A.S. Verkman, The Lancet. Neurology, 11 (2012) 535-544.
[115] S.R. Hinson, M.F. Romero, B.F.G. Popescu, C.F. Lucchinetti, J.P. Fryer, H. Wolburg, P. Fallier-Becker, S. Noell, V.A. Lennon, P Natl Acad Sci USA, 109 (2012) 1245-1250.

[116] L. Tradtrantip, H. Zhang, M.O. Anderson, S. Saadoun, P.W. Phuan, M.C. Papadopoulos, J.L. Bennett, A.S. Verkman, FASEB J, 26 (2012) 2197-2208.
[117] R.M. Dean, R.L. Rivers, M.L. Zeidel, D.M. Roberts, Biochemistry, 38 (1999) 347-353.
[118] M.G. Fortin, N.A. Morrison, D.P. Verma, Nucleic Acids Res, 15 (1987) 813-824.
[119] C.M. Niemietz, S.D. Tyerman, FEBS letters, 531 (2002) 443-447.
[120] M.G. Mola, G.P. Nicchia, M. Svelto, D.C. Spray, A. Frigeri, Anal Chem, 81 (2009) 8219-8229.
[121] R. Zhang, A.N. van Hoek, J. Biwersi, A.S. Verkman, Biochemistry, 32 (1993) 2938-2941.
[122] G.M. Preston, J.S. Jung, W.B. Guggino, P. Agre, J Biol Chem, 268 (1993) 17-20.
[123] H. Sui, B.G. Han, J.K. Lee, P. Walian, B.K. Jap, Nature, 414 (2001) 872-878.
[124] D.F. Savage, R.M. Stroud, J Mol Biol 368 (2007) 607-617.
[125] M.J. Borgnia, D. Kozono, G. Calamita, P.C. Maloney, P. Agre, J Mol Biol, 291 (1999) 1169-1179.
[126] Y. Hirano, N. Okimoto, I. Kadohira, M. Suematsu, K. Yasuoka, M. Yasui, Biophys J, 98 (2010) 1512-1519.
[127] Y. Zhang, Y. Cui, L.Y. Chen, Biophys Chem, 160 (2012) 69-74.
[128] A.P. Martins, A. Marrone, A. Ciancetta, A. Galán Cobo, M. Echevarría, T.F. Moura, N. Re, A. Casini, G. Soveral, PloS one, 7 (2012) e37435.
[129] A.P. Martins, A. Marrone, A. Ciancetta, A.G. Cobo, M. Echevarria, T.F. Moura, N. Re, A. Casini, G. Soveral, Plos One, 7 (2012).
[130] E. Campos, T.F. Moura, A. Oliva, P. Leandro, G. Soveral, Biochem Biophys Res Commun, 408 (2011) 477-481.
[131] A.J. Graham, British Med Jl, 2 (1950) 321-322.
[132] M.E. Suarez-Almazor, C.H. Spooner, E. Belseck, B. Shea, The Cochrane database of systematic reviews, (2000) Cd002048.
[133] M. Zelenina, A.a. Bondar, S. Zelenin, A. Aperia, J Biol Chem, 278 (2003) 30037-30043.
[134] M. Zelenina, S. Tritto, A.a. Bondar, S. Zelenin, A. Aperia, J Biol Chem, 279 (2004) 51939-51943.

3. Aim and Outline

Incorporation of metals into drug scaffolds offers a vast potential for creating promising metal-based drug candidates with unique chemistry and biological activity of clinical significance. As demonstrated by the numerous examples of metal-based complexes with enzyme inhibitory activity (or more in general able to modulate protein activities) cited in the literature, research in medicinal inorganic chemistry, as well as in the investigation of metal compound-protein interactions, has great potential for drug design. As an example, the possibility for metal compounds to alter zinc-finger domains is very attractive in the development of novel anticancer compounds.

In this context, protein modulation (inhibition or activation) by metal compounds for different therapeutic and/or imaging purposes is an intriguing research topic. The integration of chemistry and molecular biology with imaging techniques is providing exciting opportunities in the early detection and treatment of different pathologies. Indeed, the design of ***theranostic*** compounds, where diagnosis is combined with therapy, is highly valuable, for example, to address a disease as complex as cancer.

The interplay between metal/metalloid compounds and aquaporins (AQPs), possible biological targets for metal compounds, has been shown to be very important from different points of view. For example, the uptake of certain inorganic compounds by aquaglyceroporins may have physiological significance, which has not been fully investigated yet. Potential consequences include efficacy of metallodrugs and sensitivity to environmental metals/metalloids, as in the case of arsenic leading to toxic effects. Similarly, the effectiveness of inorganic compounds as drugs may depend on the level of expression of specific AQPs isoforms that may facilitate transport into the cells, which may differ from one cell/tissue type to another.

In addition, the intriguing properties of metal complexes as inhibitors of AQPs are worth exploring to develop novel possible therapeutic agents and/or chemical probes to study AQPs functions in cells. Thus, the use of coordination and organometallic gold compounds as aquaglyceroporins inhibitors holds great potential to reduce cell proliferation in cancer cells, as well as to understand the roles of AQPs in cancer development. However, more research efforts are necessary to elucidate the mechanisms of interactions of inorganic compounds with AQPs at a molecular level, which should be conducted via various methods in the frame of a highly interdisciplinary approach.

In this context, knowledge of inorganic chemistry is essential to explain the chemical speciation of metallodrugs and metal ions in a physiological environment, as well as their reactivity with biomolecules, to elucidate the mechanism of transport of inorganic compounds, as well as their inhibition properties of different protein isoforms.

Overall, from the point of view of Medicinal Chemistry, the exploration of the periodic table presents exciting challenges, where inorganic compounds, and metal complexes in particular, exert drug-like actions by mechanisms that can be quite distinct from those of organic drugs. In fact, metallodrugs show unique modes of activity based on the choice of the metal, its oxidation state, the types and number of coordinated ligands and the coordination geometry.

Outline of the thesis

Based on the above mentioned considerations, **the main aim** of the work described in this thesis was:

• To investigate the properties of **metal-based compounds** as possible **anticancer agents** or as **chemical probes** to study protein functions in biological systems.

In fact, the understanding of the biological effects induced by different families of inorganic compounds, and achieving structure-activity relationships, are crucial for new drugs development. In addition, validating possible protein targets for metal compounds, will assist identifying their mechanism of pharmacological action and toxicity and, finally will help achieving selectivity via appropriate modifications of the chemical scaffolds.

Based on this primary aim, the work described in this thesis focuses on:

A) The study of gold complexes as aquaporin inhibitors.

B) The characterization of the properties of different families of gold compounds as anticancer agents *in vitro*.

Accordingly, the manuscript is divided into two main parts:

In **Part A**, the membrane water and glycerol channels aquaporins are studied as targets for metal compounds. Specifically, aquaglyceroporin isoforms are investigated. Thus, in **Chapter A1**, the inhibitory effects of several coordination gold(III) compounds, with N-donor ligands or organometallics, on human aquaglyceroporin-3 (AQP3) are characterized by stopped-flow methods in selected cellular models. In addition, several computational methodologies, such as non-covalent docking, QM/MM and DFT calculations, performed in collaboration with other groups, were applied to study the mechanisms of AQP3 inhibition by gold complexes at a molecular level.

This study revealed initial structure-activity relationship, crucial to improve design of more potent and selective inhibitors.

Following these interesting results on AQP3, human aquaglyceroporin-7 (AQP7) was studied, which is mainly expressed in adipocytes. Hence, in **Chapter A2** the inhibition of water and glycerol permeability of human AQP7 by the gold(III) complex $[Au(phen)Cl_2]Cl$ (phen=1,10-phenantroline; Auphen), transfected in a murine adipocyte model was studied. The mechanism of inhibition of hAQP7 by Auphen, was investigated using *in silico* methodologies, including homology modelling and non-covalent docking. The proposed mechanism of inhibition appears to be different from that observed in the case of hAQP3. This information is useful to improve inhibitor's design and isoform-selectivity.

As described in the introductory chapter, several aquaporin isoforms are known to be inhibited (unselectively) by mercury ions. Several authors studied the inhibition of orthodox aquaporins by mercury using different techniques, such as X-ray crystallography and molecular dynamics (MD) simulations. In **Chapter A3**, for the first time, the mechanism of inhibition of an aquaglyceroporin, AQP3, by mercury is described, using MD. Interestingly, the reported results are

useful to understand the mechanism of inhibition of the gold compounds developed by us, since gold has a similar affinity to mercury for binding amino acids. From these studies it appeared that metal coordination to specific amino acid residues induces protein conformational changes which lead to channel blockage and inhibition of glycerol transport.

MD simulations also can provide insights into other mechanisms of inhibition of water and glycerol transport in AQPs, such as channel gating by different stimuli (e.g. pH). In fact, it has been previously described that AQP3 is gated by pH, however no clear insight into the mechanisms of pore closure at a molecular level have been provided so far. Therefore, **in Chapter A4**, the pH gating of human AQP3 in red blood cells, as well as the pH gating of rat AQP3, in a yeast cell model, respectively, was studied using stopped-flow spectroscopy. Moreover, the same phenomenon of pH gating was described for human AQP7, expressed in a yeast cell model. Thus, in this chapter, using computational tools, we propose an hypothesis for the different mechanisms of pH gating in AQP3 and AQP7.

Part B focuses on the study of metal compounds as anticancer agents. Selected results out of the screening of different families of coordination metal compounds performed in the last four years are presented. Specifically, in **Chapter B1** the synthesis and biological activity of a series of gold(I) organometallic compounds are reported. The synthesis and structural characterization of the compound was performed within our group by an other PhD candidate, while my work was focused on the biological characterization. The complexes under investigation are gold(I) *N*-heterocyclic-carbenes (NHC) with different ancillary ligands aimed at fine-tuning their hydrophilic/lipophilic character. All the complexes were tested for their antirpoliferative effects in several cancerous and non-cancerous cell lines. Additionally, the cellular uptake and distribution of the complexes with a fluorescent coumarine moiety was evaluated by fluorescence microscopy. Moreover, in order to get mechanistic insights on the activity of the gold(I) complexes, these were evaluated for their inhibition effects on different types of targets such as the zinc finger protein PARP-1 and enzymes involved in maintaining the intracellular redox balance such as thioredoxin reductase (TrxR), glutathione reductase (GR) and glutathione peroxidase (GP), in collaboration with the group of Prof. Maria Pia Rigobello (University of Padova, Italy)

In **Chapter B2** a series of luminescent polynuclear metal complexes with biological activity in cancer cells is reported. These metal-based compounds bear two different moieties: a ruthenium(II) centre with bipyridyl ligands, with luminescent properties that can be used to track the compound in cells, and a "therapeutic centre" consisting of Au(I), Ru(III) or Rh(III) ions. Moreover, a few of these complexes were conjugated with a thioglucose moiety, aimed at improving cellular uptake via active transport mediated by glucose transporters. The synthesis of these complexes was achieved in collaboration with the group of Prof. Pierre Le Gendre (University of Burgundy, France). In this chapter we describe the anticancer activity of the complexes in different cell lines, which allowed us to select the most promising compounds in our series, as well as the cellular distribution of representative compounds. Moreover, investigation of the possible uptake of the complexes by the glucose transporter GLUT-1 was conducted.

The contents of each chapter are summarized and discussed in the **Summary and Discussion Chapter** of this thesis, where general considerations on the different biological properties of the various investigated families of metal compounds are presented, as well as perspectives for future design of metal complexes for applications in chemical biology and medicine.

Part A

Aquaporins as Drug Targets

A1. Gold Compounds as Aquaglyceroporin-3 inhibitors

This chapter is based on two publications:

Ana Paula Martins, Antonella Ciancetta, Andreia de Almeida, Alessandro Marrone, Nazareno Re, Graça Soveral and Angela Casini
Aquaporin Inhibition by Gold(III) Compounds: New Insights
Chem.Med.Chem. (2013) 8: 1086-1092
Supplementary information available: DOI: 10.1002/cmdc.201300107

Andreia de Almeida, Andreia Mósca, Graça Soveral and Angela Casini
Insights on the Mechanism of Aquaporin Inhibition by Gold Compounds with N-donor Ligands
(submitted)

Chem.Med.Chem

Abstract

Aquaporins (AQPs) are membrane water/glycerol channels with essential roles in biological systems, as well as being promising targets for therapy and imaging. Using a stopped-flow method, a series of gold(III), platinum(II) and copper(II) complexes bearing nitrogen donor ligands, such as 1,10-phenatroline, 2,2'-bipyridine, 4,4'-dimethyl-2,2'-bipyridine, 4,4'-diamino-2,2'-bipyridine and 2,2';6',2"-terpyridine, were evaluated in human red blood cells expressing AQP1 and AQP3, responsible for water and glycerol movement, respectively. The results showed that the gold(III) complexes selectively modulate AQP3 over AQP1. Additionally, another series of gold(III) complexex was tested, namely with the dipyridin-2-ylamine (dipyam) ligand, two gold(III) complexes with 2-(2'-pyridyl)benzimidazole (PbImH) ligand, and an organometallic gold(III) compound with C^N cyclometallated 2-benzylpyridine (py^b-H).

Molecular modeling and density functional theory (DFT) calculations were subsequently performed to rationalize the observations and to investigate the possible molecular mechanism through which these gold compounds act on their putative target (AQP3). In the absence of any crystallographic data, a previously reported homology model was used for this purpose. Combined, the findings of this study show that potent and selective modulation of these solute channels is possible, however further investigation is required into the selectivity of this class of agents against all AQP isoforms and their potential therapeutic uses.

1.1. Introduction

Aquaporins (AQPs) belong to a highly conserved group of membrane proteins involved in the transport of water and small solutes and with a variety of important physiological roles. The 13 human AQP isoforms (AQP0-12) are differentially expressed in many types of cells and tissues in the body and can be divided into two major groups: those strictly selective for water (called orthodox aquaporins), and those that are also permeable to other small solutes including glycerol (called "aquaglyceroporins"). The latter include AQP3, AQP7, AQP9 and AQP10 isoforms [1]. Phenotype analysis of AQP-null mice, as well as pathophysiological studies, suggested AQPs as drug targets. Indeed, it has recently emerged that AQPs are implicated in various diseases such as polycystic kidney disease, cataract, brain oedema, gallstone disease and nephrogenic diabetes insipidus, as well as in the development of obesity and cancer [2]. Moreover, analysis of AQP involvement in the life-cycle of disease causing organisms suggests additional opportunities for pharmacological intervention in the treatment of human diseases [3].

In recent years, there were reports of chemical compounds that modulate AQP mediated water flux including heavy metals [4-7], quaternary ammonium salts [8-10], and inorganic salts [11]. Those compounds are valuable for gaining insight into the effect of AQP modulation at a cellular level; however, unfortunately, they are not suitable for therapeutic applications mostly due to their toxic side effects and lack of selectivity. In addition, recent reports have described a few small molecule, organic AQP modulators, mainly sulfonamides, that act as inhibitors of orthodox water channels [12], as well as some compounds containing carboxylic groups [13]. Only a few small molecule inhibitors of AQP9 glycerol permeability were identified; however, as their solubility in aqueous solution is very limited, these compounds are currently not suitable for *in vivo*

experiments [14].

Within this frame, our group recently reported on the potent and selective inhibition of AQP3 by a water-soluble gold(III) coordination compound, $[Au(phen)Cl_2]Cl$ (phen = 1,10-phenatroline, Auphen) (Figure 1). Notably, Auphen resulted to inhibit glycerol transport in human red blood cells (hRBC) with an $IC_{50} = 0.80 \pm 0.08$ μM, while having only a modest inhibitory effect on water permeability mediated by AQP1 [15]. Inspired by these initial promising results, we investigated other gold-based compounds as possible AQP3 inhibitors in order to achieve basic structure-activity relationships, fundamental for drug design. Thus, we selected a series of square planar gold(III) complexes containing functionalised bipyridine ligands of general formula $[Au(N^N)Cl_2][PF_6]$ [where N^N = 2,2'-bipyridine, 4,4'-dimethyl-2,2'-bipyridine, and 4,4'-diamino-2,2'-bipyridine, Aubipys], as well as the compound $[Au(terpy)Cl]Cl_2$ (terpy = terpyridine, Auterpy) containing the tetracoordinated gold(III) chromophore AuN_3Cl (Figure 1). Moreover, the 1,10-phenantroline derivatives of Pt(II) and Cu(II) were also included in our investigation to compare the effects of metal substitution on the AQP3 inhibition potency. Additionally, new series of Au(III) complexes with N-donor ligands of different types, as well as an organometallic Au(III) complex with a C^N cyclometallated ligand were also screened as possible selective AQP3 inhibitors to improve structure-activity relationships studies.

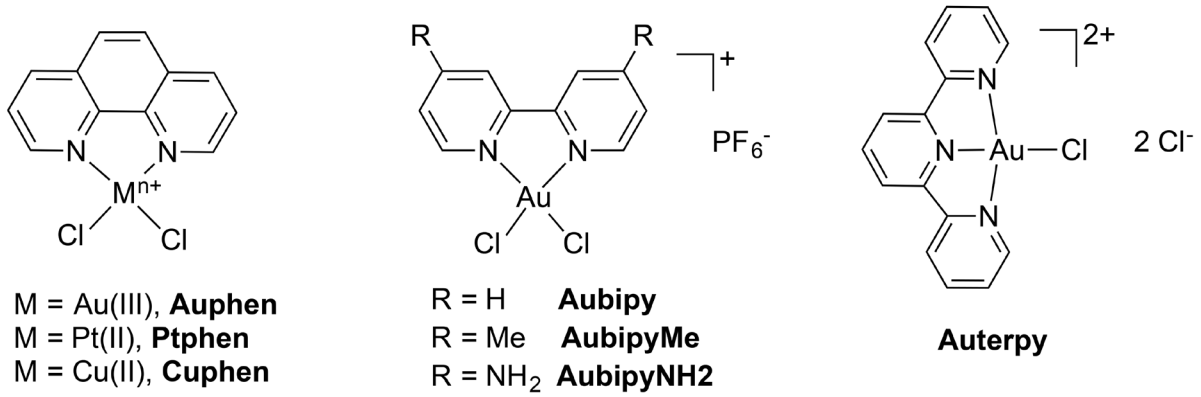

Figure 1. Structures of the gold(III) complexes reported in the first part of this study.

The effects of the compounds on both water and glycerol permeation were tested by stopped-flow spectroscopy on hRBC, which express AQP1 and AQP3 responsible for membrane permeability to water and glycerol, respectively [16]. Additionally, density functional theory (DFT) and molecular modelling studies allowed to further characterize the mechanisms of AQP3 inhibition by gold(III) coordination compounds.

1.2. Results and Discussion

1.2.1. Inhibition of hAQP3 by the Aubipy series

Figure 2 shows the effect induced by the metal complexes on AQP1 and AQP3 in hRBC in comparison to $HgCl_2$, the benchmark inhibitor of aquaporin activity [17]. The compounds were tested at different concentrations by incubating the samples for 30 min at room temperature (RT) until maximum of inhibition was reached (see Experimental Section for details) [15]. All the gold(III) compounds showed no or a modest effect on water permeability, while being able to drastically reduce glycerol transport. The obtained results demonstrate that all the gold(III)

complexes are the most effective inhibitors of glycerol permeability via AQP3, with IC_{50} in the low micromolar range (Table 1), and comparable in potency to Auphen. Within the metal-compounds series, the AQP3 inhibition potency decreased drastically in the order Auphen > Cuphen >> Ptphen (Figure 2, Table 1).

Table 1. IC_{50} (μM) values of metal complexes.

Compound	IC_{50}[a]	Hill Slope
Aubipy	2.3 ± 0.7	1.86 ± 0.4
AubipyMe	1.0 ± 0.4	1.76 ± 0.6
$AubipyNH_2$	2.9 ± 1.1	3.08 ± 0.8
Auterpy	1.0 ± 0.2	2.15 ± 0.3
Auphen	0.8 ± 0.1 [b]	3.9 ± 0.3
Cuphen	81.9 ± 4.1	2.0 ± 0.5
Ptphen	> 200	-

[a] Mean ± SE of at least three determinations. [b] from ref [15].

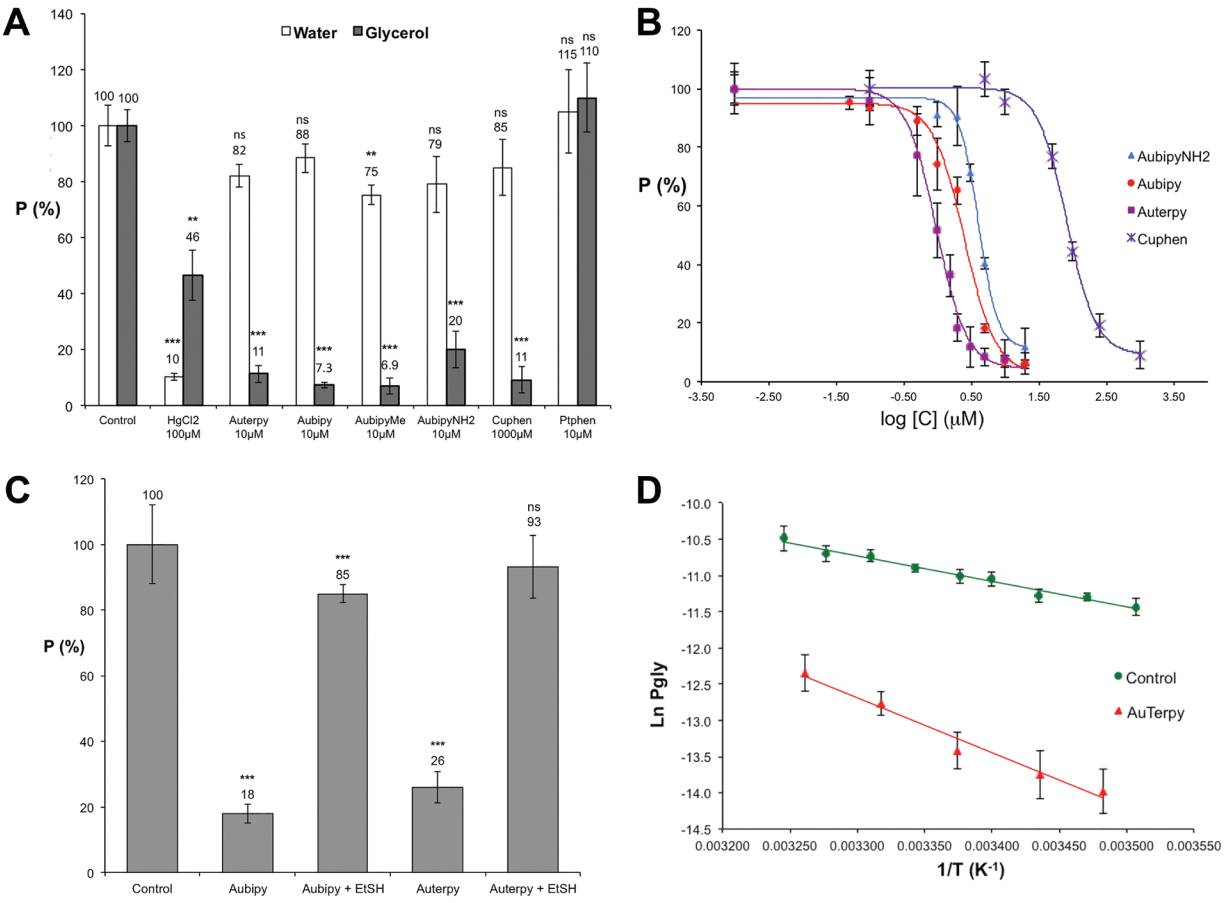

Figure 2. A: Inhibition of the osmotic water (AQP1) or glycerol (AQP3) permeability (P) in human RBC induced by different metal complexes after 30 min incubation at RT.; B: Concentration dependent inhibition of glycerol permeability (P) in hRBC by representative metal compounds; C: Inhibition of glycerol permeability (P, % of control) of hRBCs after Aubipy and Auterpy treatment (30 min at RT, 2 mM and 5 mM, respectively), and reversibility by incubation with 2-mercaptoethanol (1 mM for 30 min) (***p < 0.001). D: Arrhenius plot of hRBC glycerol permeability in the absence (control) or presence of 5 mM Auterpy (30 min incubation at RT previous to permeability measurements). Activation energy (E_a) values for glycerol permeation increased drastically when Auterpy was present (7.0 ± 0.06 to 15.2 ± 1.3 kcal mol^{-1}).

Moreover, all the Hill slope values are greater than 1 (Table 1), suggesting a possible cooperative binding effect. Actually, knowing that the aquaporin channels are tetrameric proteins in the membrane and each tetramer is formed by four identical monomers, the total of four Cys40 residues are available for binding. Thus, the Hill slope (H) value for Auphen (ca. 4. Table 1) points to a maximal cooperativity and correlates well with its high potency while for the other gold compounds, with the exception of AubipyNH_2 that showed a slightly higher H value, all the H values were close to 2 suggesting an intermediate cooperativity.

The activation energy (E_a) for water and glycerol transport, a valuable parameter indicating the contribution of protein channels to permeation, was also estimated from an Arrhenius plot. Representative results for Auterpy are shown in Figure 2D. The observed increase in E_a, similarly to what we previously observed for Auphen [15], is in accordance with a blockage of the AQP3 channel.

In order to obtain information on the possible binding sites of the gold complexes in AQP3, hRBCs pre-treated with compounds for 30 min at RT were subsequently washed with the reducing agent 2-mercaptoethanol (EtSH, 1 mM) according to established procedures [17]. As observed for Auphen [15], incubation of the treated hRBC sample with excess EtSH produced an almost complete recovery of glycerol permeability (ca. 90%), suggesting that EtSH effect on cysteine residues is competing with gold binding to the pore. Representative results for Auterpy and Aubipy are shown in Figure 2C. These results, as well as the known affinity of gold ions for binding to sulfhydryl groups of proteins, suggest that AQP3 inhibition by Au complexes may involve direct protein binding of the Au centre to Cys residues, as it has already been described for $HgCl_2$ [18].

1.2.2. Expanding the series of gold(III) compounds

Following the above mentioned promising results on Auphen and Aubipy derivatives and the knowledge that the gold centre plays a crucial role in AQP inhibition, it is important to deepen our understanding on the structure-activity relationships of gold-based complexes as AQPs inhibitors. For this purpose, four new gold(III) compounds (Figure 3) were tested on hRBC using stopped-flow spectroscopy. The new series included: a gold(III) complex with the dipyridin-2-ylamine (dipyam) ligand [Au(dipyam)Cl_2][PF_6] (AuDipyAm) [19], closely related to the above mentioned bipyridine series, two gold(III) complexes with 2-(2'-pyridyl)benzimidazole (PbImH) ligand, and an organometallic gold(III) compound with C^N cyclometallated 2-benzylpyridine (py^b-H) ((py^b-H)AuCl_2) [20].

As previously observed for Auphen and Aubipys, the a few of the new compounds act as inhibitors of glycerol transport via AQP3, but not of water transport via AQP1. The obtained results are summarized in Figure 3. One of the least active complexes of the series is the organometallic compound (py^b-H)AuCl_2, that did not show inhibition up to 50 μM. It should be noted that the organometallic bond renders the gold centre less reactive and the compound generally more stable, with respect to ligand exchange reactions, than a classical metal-ligand coordination bond. Thus, the observed scarce inhibition may be due to such reduced reactivity of this compound. Interestingly, the coordination compound Audipyam, although with a similar scaffold as the organometallic complex, shows low inhibition of glycerol permeation, but still with an IC_{50} value above 20 μM which is not ideal for a selective inhibitor. It is worth mentioning that, in addition to differences in ligand exchange reactivity, the two compounds may differ also in other chemicophysical properties,

such as for example the electrophilicity of the gold centre and the redox potential, which may account for the observed differences in AQP3 inhibition.

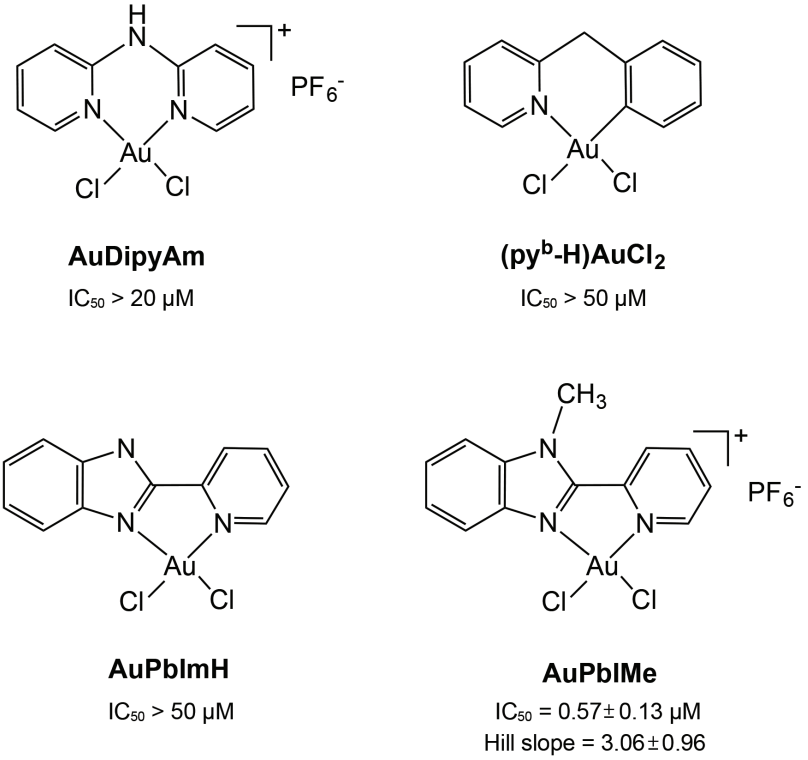

Figure 3. Structures of the gold(III) compounds studied as hAQP3 inhibitors in hRBC model, relative IC_{50} (μM) inhibition values and Hill slope (Mean ± SE of at least three determinations).

The other two tested coordination compounds are both gold(III) drugs based on N-donor pyridyl-benzimidazole ligand. The first, AuPbImH has been previously published as the lead compound in a series of Au(I) and Au(III) mono and binuclear derivatives with anticancer properties *in vitro* [20]. Interestingly, this compound showed to be active in two human ovarian carcinoma cell lines, A2780 and A2780cisR, with IC_{50} of 6.60 ± 4.01 μM and 5.31 ± 0.66 μM, respectively. The second cell line is resistant to cisplatin and the ratio between the two, close to 1, reveals that this drug does not appear to follow the same toxic route as cisplatin and is effective on both cell lines in a similar manner. As promising as this compound may appear as antiproliferative agent, in our hRBC model it was not one of the most active compounds inhibiting glycerol transport, with an IC_{50} greater than 50 μM (more than 10-fold difference with respect to the Aubipy series).

Notably, the AuPbImMe complex, containing the 1-methyl-2-(2'-pyridyl)benzoimidazole ligand, is the most potent of the four new tested compounds, with an IC_{50} of 0.57 ± 0.13 μM, even more effective than Auphen, and ca. two orders of magnitude more potent than the related AuPbImH complex. As shown in Figure 3, the only difference with AuPbImH is the addition of a CH_3 group to one of the nitrogen atoms in the benzoimidazole ring, conferring a positive charge to the resulting complex. In spite of the fact that this seems to be a small structural difference, this addition may influence the reactivity of the gold(III) centre as well as its chemicophysical properties (e.g. redox potential), and further studies are necessary to fully rationalize how such differences may affect the AQP3 inhibition of the two complexes so radically.

In order to study the reversibility of inhibition, hRBCs were pre-treated with the drugs for 30 min at RT and subsequently washed with the reducing agent 2-mercaptoethanol (EtSH, 1 mM), according to established procedures [17]. In Figure 4B it is clear the inhibition of glycerol

permeation by 1 μM AuPbImMe is not affected after washing cells with PBS buffer. Conversely, as observed for the previously studied gold compounds, washing with excess EtSH (Phosphate β-Mercaptoethanol, BME buffer) led to an almost complete recovery of glycerol permeability. Since EtSH is a very strong reducing agent, one cannot exclude that the inhibition by gold(III) compounds may be due to oxidation of the thiol group of Cys residues, which may be then reversed by EtSH addition. Therefore, in order to exclude possible oxidative effects by Au(III), we investigated the reversibility of inhibition by AuPbImMe by washing the hRBC with 1 mM of L-cysteine, which while maintaining its affinity to gold binding, is not a reducing agent. Interestingly, recovery after washing with L-Cys seems to similar to EtSH washing, suggesting that there is no oxidation of Cys, but that L-Cys may simply compete with Cys residues for binding to gold.

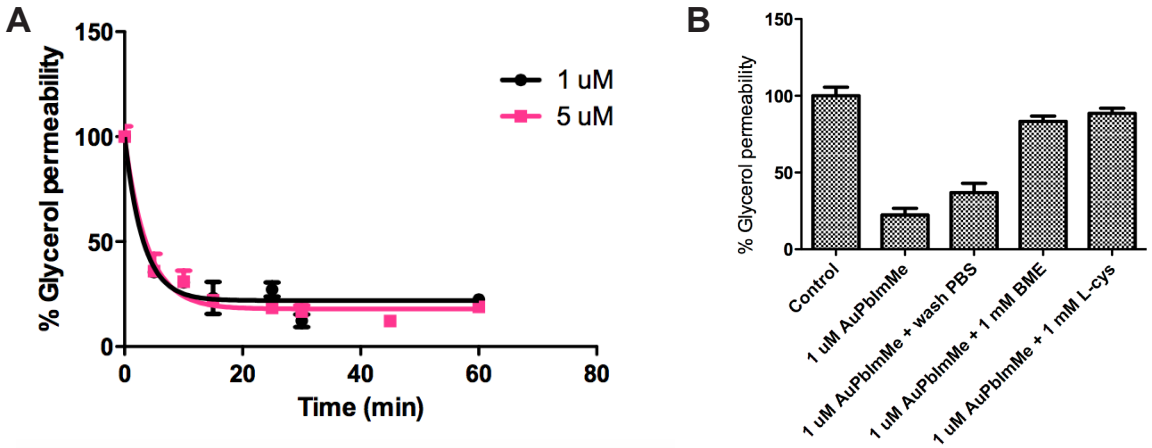

Figure 4. A: Time-dependence glycerol inhibition (% of control) for two concentrations of AuPbImMe; B: Inhibition of glycerol permeability (% of control) of hRBCs after AuPbImMe treatment (30 min at RT, 1 μM), and reversibility by incubation with 2-mercaptoethanol (BME) and L-Cys (1 mM for 30 min). The results shown represent the average of, at least, three independent experiments ± SE.

1.2.3. Mechanism of Aquaporins Inhibition by Gold(III) compounds

Our group has previously reported a model for the selective inhibition of AQP3 by Au(III) channel blockers, including Auphen [15]. The resulting mechanistic hypothesis suggests that the metal coordinates to a specific nucleophilic site, namely the side chain of Cys40, which is located at the extracellular side of AQP3 in close proximity to the selectivity filter (SF) region, therefore, inducing the blockage of the channel upon binding (Figure S2 in Supplementary Material). In AQP1, Cys189 is also located in the protein extracellular domain and is part of the SF region, but it is deeply buried in the channel and its thiol group is poorly available for binding to the bulky Au(III) complexes [15]. In fact, previously reported non-covalent docking studies of Auphen in AQP1 have shown that the side chain of Cys189 is distant from the gold ion (12-14 Å) and not favourably oriented for the binding to occur. In this context, the selective inhibition of AQP3 vs AQP1 is mainly related to the lack of possible gold binding sites in the extracellular pocket of AQP1 accessible to such relatively bulky metal complexes [15].

According to the proposed inhibition mechanism, the electrophilicity of the metal centre is expected to play a role in determining the reactivity of the complexes towards AQP3. Therefore, we carried out DFT calculations to characterize the electrophilicity of the considered Au(III), Pt(II) and Cu(II) complexes using the perturbative approach in terms of atomic charges and frontier orbitals proposed by Klopman [21]. Natural atomic orbital population analyses (Table 2) highlight

similar charges on the metal centre for all monocationic Au(III) complexes. A higher charge is observed on the gold(III) center of Auterpy, as expected, for dicationic species, while the metal of neutral Cuphen and Ptphen complexes is almost the same or less positively charged than the gold(III) center of monocationic complexes, respectively (Table 2). Thus, charge factors indicate the following order of reactivity towards nucleophiles: Auterpy > (Auphen, Aubipy analogues) > (Cuphen, Ptphen).

Table 2. Mulliken and natural atomic orbital (NAO) charges.

Compound	M^{n+}	Cl	N
AubipyCl_2	1.09	-0.35	-0.49
AubipyMeCl_2	1.10	-0.36	-0.50
AubipyNH_2Cl_2	1.10	-0.37	-0.53
Auterpy	1.22	-0.38	-0.48, -0.49[a]
Auphen	1.09	-0.35	-0.49
Cuphen	0.66	-0.44	-0.50
Ptphen	1.10	-0.65	-0.52

[a] The two values reported for Auterpy N refer to the two reciprocal trans and the one Cl-trans pyridyl nitrogens, respectively.

On the other hand, the analysis of frontier orbitals (see Figure S3 in Supplementary Material) shows similar LUMO energies for all monocationic Au(III) complexes. Auterpy shows a significant lower LUMO energy, whereas Cuphen and Ptphen are characterized by the highest LUMO. Thus, frontier orbital factors suggest an order of reactivity towards nucleophiles substantially inverse to that indicated by charge factors: (Cuphen, Ptphen) > (Auphen, Aubipy analogues) > Auterpy. The charge and orbital factors probably compensate for each other in the Au(III) compounds, thus leading to similar reactivity towards cysteine, while the charge factors seems to prevail for the Cu(II) and Pt(II) complexes which are much less reactive, in agreement with the observed AQP3 inhibition potency, see Table 1.

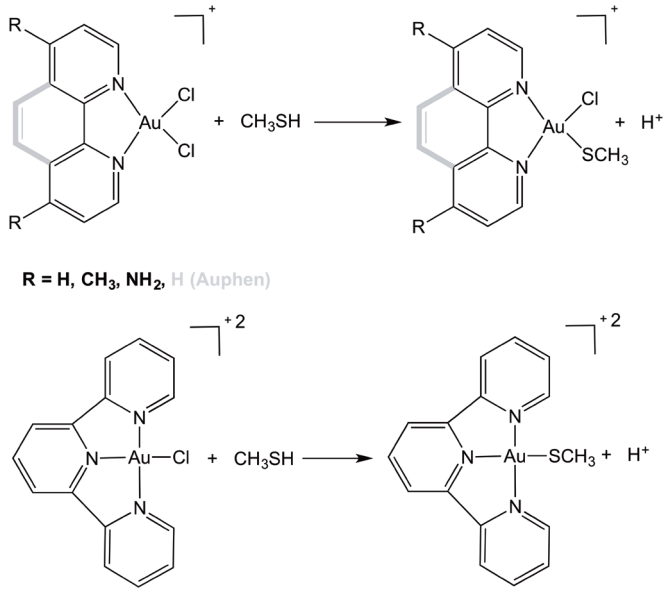

Figure 5. Reaction scheme of the considered Au(III) complexes with the Cys40 side-chain model leading to the final Au(III)-thiolate complexes.

The thermodynamics of the ligand exchange process leading to covalently bound Au(III)-AQP3 adducts was then investigated at DFT level of theory, which has been recently shown to give good results for the reactivity of Au(III) compounds [22]. In particular, the exchange of the Cl-anion, by using CH_3SH as a model of the Cys40 side-chain, was analyzed (See Figure 5). As previously reported, in physiological conditions (pH 7.4) the cysteine residue (pK_a = 8.3) is prevalently, but not exclusively, protonated and this process can be considered as result of: either the initial nucleophilic attack of the neutral cysteine

with formation of an Au(III)-thiol complex followed by its easy deprotonation, or the initial cysteine deprotonation followed by the attack of the more nucleophilic thiolate anion giving the final Au(III)-thiolate complex. In any case, the whole reaction is thermodynamically favoured for all the gold(III) complexes, with binding energies to Cys40 similar to those previously calculated for Auphen [15] (See Table 3) accounting for the good AQP3 inhibition potency observed for all these cationic Au(III) compounds.

Table 3. Calculated free energies for the reaction of the investigated Au(III) complexes with the cysteine side-chain model. All values are in kJ mol^{-1}.

Compound	ΔG_{tot}
$AubipyCl_2$	-48
$AubipyMeCl_2$	-46
$AubipyNH_2Cl_2$	-35
Auterpy	-36
Auphen	-48

We also investigated the initial approach of the various metal complexes to the Cys40 residue in the channel pore from the extracellular side and the possible formation of non-covalent adducts with Cys40 itself or other neighbouring residues within the active site. To this purpose, quantum mechanics/molecular mechanics (QM/MM) calculations at DFT level of theory were performed by using the previously proposed AQP3 homology model [15], and by optimizing several possible initial poses of the complexes in the extracellular pocket around the Cys40 residue. In Figure 6A, the calculated most stable binding mode of AubipyMe at the AQP3 extracellular binding pocket is reported. The complex lies perpendicular to the membrane plane and the Au-S(Cys40) distance is around 5.8 Å. As detailed in the interaction diagram depicted in Figure 6B, the compound establishes π-π stacking interactions with Tyr212 and Phe63, two of the residues representing the arginine-aromatic (ar/R) constriction (the selectivity filter, SF) typical of AQPs [23]. Along with π-π interactions, the gold(III) complex also interacts via further hydrophobic contacts of the bipy methyl substituents with Ile59, Val67 and Val199. The results also show the proximity of the complex to the Arg218 side-chain, whose positive charge might play a role in stabilizing the leaving chloride in the binding of the metal centre to Cys40. Thus, calculations showed how the placement of the metal complexes in the AQP3 extracellular pocket is controlled by both covalent anchoring to Cys40 and by non-covalent interactions; the latter may be crucial in the channel blockage by favouring the bury of the constriction region of the channel.

1.3. Conclusions

Numerous reports have highlighted the possible areas where AQP modulators could be useful in treating human diseases. Yet, only a few pharmaceutically relevant compounds have been identified to date. We described here the selective and potent inhibitory effect of a series of Au(III) complexes bearing nitrogen donor ligands on AQP3, which together with their high water solubility makes them suitable candidates for future *in vivo* studies. AQP3 has been shown to mediate most of the glycerol movements across RBCs membranes. In addition to its expression in hRBCs,

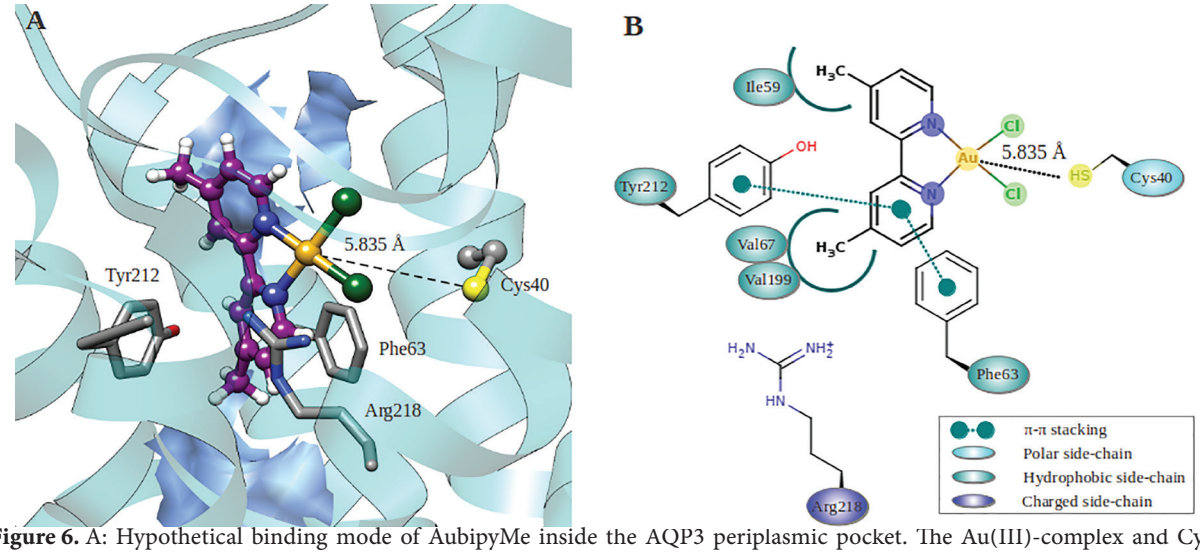

Figure 6. A: Hypothetical binding mode of AubipyMe inside the AQP3 periplasmic pocket. The Au(III)-complex and Cys40 side chain are shown in ball and sticks. Side-chains of SF domain residues are reported as grey sticks. Residues interacting through hydrophobic contacts with the ligand are displayed as surfaces. B: Interaction diagram of AubipyMe inside the AQP3 extracellular pocket.

AQP3 has a wide tissue distribution in the epithelial cells of kidney, airways and skin, suggesting a role in water reabsorption, mucosal secretions, skin hydration and cell volume regulation [24]. Moreover, recent studies demonstrated an aberrant AQP3 expression in tumor cells of different origins, particularly aggressive tumors [24-27] suggesting this enhanced protein expression to be of diagnostic and prognostic value.

Interestingly, the gold(III) complexes herewith described possess cytotoxic anticancer properties *in vitro*, and in recent years several gold compounds have shown promising anticancer effects related to the inhibition of different protein targets, such as the thioredoxin reductases, the proteasome and certain zinc-finger proteins [28-30]. In this context, we cannot exclude that inhibition of AQP3 might also contribute to the biological effects of the gold(III) compounds towards cancer cells, although other studies are on-going in our labs to validate such a hypothesis. Moreover, the inhibition properties of the compounds towards the other aquaglyceroporin isoforms involved in essential physiological pathways should be further investigated in order to optimize the drug design and to achieve highly selective molecules with reduced risks of side effects.

Finally, it is worth mentioning that, although the only organometallic Au(III) complex did not show AQP3 inhibitor ($(py^b\text{-}H)AuCl_2$), other families of gold compounds containing a direct metal-carbon bond should be tested before discarding them as suitable AQPs modulators. As a matter of fact, organometallic compounds have the advantage over classical coordination complexes (e.g. with only N-donor ligands bound to the metal centre) to be more stable and with a reactivity that can be fine-tuned by appropriate modifications of the ligand scaffold, i.e. an essential requisite to design biologically active compounds.

1.4. Experimental Section

Chemistry: Gold compounds were prepared according to literature procedures [19, 20, 31]. The purity of the compounds was confirmed by elemental analysis, and all of them showed purity greater than 98%. Copper and platinum 1,10-phenantroline and 2-mercaptoethanol were from Sigma.

Ethics Statement: Venous blood samples were obtained from healthy human volunteers following a protocol approved by the Ethics Committee of the Faculty of Pharmacy of the University of Lisbon. Informed written consent was obtained from all participants.

Erythrocyte sampling and preparation: Venous blood samples were collected in citrate anticoagulant (2.7 % citric acid, 4.5 % trisodium citrate and 2% glucose). Fresh blood was centrifuged at 750 xg for 5 min at 4 °C and plasma and buffy coat were discarded. Packed erythrocytes were washed three times in PBS (KCl 2.7 mM, KH_2PO_4 1.76 mM, Na2HPO4 10.1 mM, NaCl 137 mM, pH 7.4), diluted to 0.5% haematocrit and immediately used for experiments. hRBC mean volume in isotonic solution was determined using a CASY-1 Cell Counter (Schärfe System GmbH, Reutlingen, Germany) and was calculated as 82 fL.

Stopped-flow light scattering experiments: Stopped-flow experiments were performed on a HI-TECH Scientific PQ/SF-53 apparatus, with 2 ms dead time, temperature controlled and interfaced with a microcomputer. Experiments were performed at 23 °C for glycerol permeability and at 10 °C for water permeability; for activation energy measurements temperatures were ranged from 10 °C to 37 °C. For each experimental condition, 5-7 replicates were analysed. For measuring the osmotic water permeability (P_f), 100 mL of a suspension of fresh erythrocytes (0.5%) was mixed with an equal volume of PBS containing 200 mM sucrose as a non-permeable osmolyte to produce a 100 mM inwardly directed sucrose gradient. The kinetics of cell shrinkage was measured from the time course of 90° scattered light intensity at 400 nm until a stable light scatter signal was attained.

P_f was estimated by $P_f = k\ (V_o/A)(1/V_w(osm_{out})_\infty)$, where V_w is the molar volume of water, V_o/A is the initial cell volume to area ratio and $(osm_{out})_\infty$ is the final medium osmolarity after the applied osmotic gradient and k is the single exponential time constant fitted to the light scattering signal of erythrocyte shrinkage.

For glycerol permeability (P_{gly}), 100 mL of erythrocyte was mixed with an equal volume of hyperosmotic PBS containing 200 mM glycerol creating a 100 mM inwardly directed glycerol gradient. After the first fast cell shrinkage due to water outflow, glycerol influx in response to its chemical gradient was followed by water influx with subsequent cell reswelling. P_{gly} was calculated as $P_{gly} = k\ (V_o/A)$, where k is the single exponential time constant fitted to the light scattering signal of glycerol influx in erythrocytes. For inhibition experiments cells were incubated with different concentrations of complexes, from freshly prepared stock aqueous solutions, for various times at room temperature before stopped-flow experiments. A time dependent inhibition assay for all the tested compounds over several hours incubation with hRBC showed no further increase of inhibition after 30 min at r.t. Inhibitors' reversibility was tested by 30 min incubation of hRBCs with the compounds followed by further incubation with 1 mM 2-mercaptoethanol (EtSH) for 30 min at room temperature. The reversibility assays were also performed under the same conditions, using 1 mM L-cysteine. The inhibitor concentration necessary to achieve 50% inhibition (IC_{50}) was calculated by nonlinear regression of dose-response curves (Graph Pad Prism, Inc) to the equation: $y=y_{min}+(y_{max}-y_{min})/(1+10((LogIC_{50}-Log[Inh])\ H))$, where y is the percentage inhibition obtained for each concentration of inhibitor [Inh] and H is the Hill slope. The activation energy (E_a) of water and glycerol transport was calculated from the slope of the Arrhenius plot (lnP_f or lnP_{gly} as a function of 1/T) multiplied by the gas constant R. All solution osmolarities were determined from freezing point depression on a semi-micro osmometer (Knauer GmbH, Berlin, Germany) using standards of 100 and 400 mOsM.

Statistic analysis: Data were presented as mean ± standard error of the mean (SEM) of at least four independent experiments, and were analysed with either the paired Student's t-test or one-way analysis of variance (ANOVA) followed by Tukey's test. A value of P = 0.01 was considered to be statistically significant.

QM calculations: The structures of Au(III), Cu(II) and Pt(II) complexes were investigated at DFT level of theory with the B3LYP hybrid functional [32, 33]. The core electrons of the chloride and metal atoms were described with the Hay and Wadt core-valence relativistic effective core-potential (ECP) leaving the outer electrons to be treated explicitly through the basis set denoted as LACVP** in Jaguar, while for the remaining atoms the 6-31G** basis set was used [34]. Each structure was optimized in the gas phase (a=0) and frequency calculations were performed to verify the correct nature of the stationary points and to estimate zero point energy (ZPE) and vibrational entropy corrections at room temperature. Single point energies of all stationary points were calculated by using the larger 6-311++G** set for the main group elements, and the LACV3P++** set for the metal and the chloride atoms. At this level of theory, Mulliken [34] and natural atomic orbital[40] population analyses were also performed. The Poisson-Boltzmann (PB) continuum solvent method was employed to simulate the aqueous medium (ε = 80) [35]. The values of DGII for methanethiol species have been calculated by using a thermodynamic cycle as previously reported [15]. The Jaguar 7.9 quantum chemistry package (Jaguar, version 7.9, Schrödinger, LLC, New York, NY, 2012) was used for all calculations.

QM/MM calculations: Hybrid quantum mechanics molecular mechanics (QM/MM) calculations have been performed with the Qsite 5.8 software package (QSite, version 5.8, Schrödinger, LLC, New York, NY, 2012). As, to date, no crystallographic information about the AQP3 is available, we performed the studies by using a AQP3 homology model [15], which has been previously reported and built by using the crystal structure of the Escherichia coli glycerol facilitator (GlpF) [36] as template (PDB ID code: 1LDF).

The starting complexes have been set up manually by placing the Au(III) centre in the proximity of the Cys40 side-chain, which is expected to react with the metal centre. To sped up the calculations, the QM region as been limited to

the Au(III) complex and has been treated at DFT level of theory with the B3LYP functional [M1, M2] and the LACVP** basis set [37], whereas the MM system, consisting of protein atoms, has been described with the OPLSA_2001 force field [38, 39]. Protein atoms have been kept frozen at their initial coordinates and only the side-chain atoms of Cys40, Phe63, Tyr212 and Arg218 have been allowed to relax during the optimization.

References

[1] L.S. King, D. Kozono, P. Agre, Nat Rev Mol Cell Biol, 5 (2004) 687-698.
[2] A.S. Verkman, Annual Review of Medicine, 63 (2012) 303-316.
[3] E. Beitz, Biol Cell, 97 (2005) 373-383.
[4] G.M. Preston, T.P. Carroll, W.B. Guggino, P. Agre, Science, 256 (1992) 385-387.
[5] G.M. Preston, J.S. Jung, W.B. Guggino, P. Agre, J Biol Chem, 268 (1993) 17-20.
[6] Y. Yukutake, S. Tsuji, Y. Hirano, T. Adachi, T. Takahashi, K. Fujihara, P. Agre, M. Yasui, M. Suematsu, Biology of the cell, 100 (2008) 355-363.
[7] M. Zelenina, S. Tritto, A.a. Bondar, S. Zelenin, A. Aperia, J Biol Chem, 279 (2004) 51939-51943.
[8] H.L. Brooks, J.W. Regan, A.J. Yool, Mol Pharmacol, 57 (2000) 1021-1026.
[9] A.J. Yool, A.M. Weinstein, News Physiol Sci, 17 (2002) 68-72.
[10] F.J. Detmers, B.L. de Groot, E.M. Muller, A. Hinton, I.B. Konings, M. Sze, S.L. Flitsch, H. Grubmuller, P.M. Deen, J Biol Chem, 281 (2006) 14207-14214.
[11] Y. Yukutake, Y. Hirano, M. Suematsu, M. Yasui, Biochemistry, 48 (2009) 12059-12061.
[12] V.J. Huber, M. Tsujita, T. Nakada, Mol Asp Med, 33 (2012) 691-703.
[13] D. Seeliger, C. Zapater, D. Krenc, R. Haddoub, S. Flitsch, E. Beitz, J. Cerdà, B.L. de Groot, ACS Chem biol, 8 (2013) 249-256.
[14] S. Jelen, S. Wacker, C. Aponte-Santamaría, M. Skott, A. Rojek, U. Johanson, P. Kjellbom, S. Nielsen, B.L. de Groot, M. Rützler, J Biol Chem, 286 (2011) 44319-44325.
[15] A.P. Martins, A. Marrone, A. Ciancetta, A. Galán Cobo, M. Echevarría, T.F. Moura, N. Re, A. Casini, G. Soveral, PloS one, 7 (2012) e37435.
[16] E. Campos, T.F. Moura, A. Oliva, P. Leandro, G. Soveral, Biochem Biophys Res Comm, 408 (2011) 477-481.
[17] D.F. Savage, R.M. Stroud, J Mol Biol, 368 (2007) 607-617.
[18] C.M. Niemietz, S.D. Tyerman, FEBS letters, 531 (2002) 443-447.
[19] A. Casini, M.C. Diawara, R. Scopelliti, S.M. Zakeeruddin, M. Grätzel, P.J. Dyson, Dalton Trans, 39 (2010) 2239-2245.
[20] M.A. Cinellu, A. Zucca, S. Stoccoro, G. Minghetti, M. Manassero, M. Sansoni, Dalton Trans (1996) 4217-4225.
[21] G. Klopman, J Am Chem Soc, 90 (1968) 223-234.
[22] H.F. Dos Santos, D. Paschoal, J.V. Burda, Chemical Physics Letters, 548 (2012) 64-70.
[23] D.F. Savage, J.D.O. Connell, L.J.W. Miercke, J. Finer-moore, R.M. Stroud, PNAS, 107 (2010) 17164-17169.
[24] M. Hara-Chikuma, A.S. Verkman, Mol Cell Biol, 28 (2008) 326-332.
[25] M. Kusayama, K. Wada, M. Nagata, S. Ishimoto, H. Takahashi, M. Yoneda, A. Nakajima, M. Okura, M. Kogo, Y. Kamisaki, Cancer Sci, 102 (2011) 1128-1136.
[26] W. Liu, K. Wang, K. Gong, X. Li, K. Luo, Mol Med Rep, 6 (2012) 607-610.
[27] L. Gao, Y. Gao, X. Li, P. Howell, R. Kumar, X. Su, A.V. Vlassov, G.A. Piazza, A.I. Riker, D. Sun, Y. Xi, Mol Oncol, 6 (2012) 81-87.
[28] F. Mendes, M. Groessl, A.a. Nazarov, Y.O. Tsybin, G. Sava, I. Santos, P.J. Dyson, A. Casini, J Med Chem, 54 (2011) 2196-2206.
[29] L. Dalla Via, C. Nardon, D. Fregona, Future Med Chem, 4 (2012) 525-543.
[30] M. Serratrice, F. Edafe, F. Mendes, R. Scopelliti, S.M. Zakeeruddin, M. Grätzel, I. Santos, M.A. Cinellu, A. Casini, Dalton Trans (Cambridge, England : 2003), 41 (2012) 3287-3293.
[31] L.S. Hollis, S.J. Lippard, J Am Chem Soc, 105 (1983) 4293-4299.
[32] A.D. Becke, J Chem Phys, 98 (1993) 5648-5652.
[33] A.D. Becke, Physical review. A, 38 (1988) 3098-3100.
[34] R.S. Mulliken, J Chem Phys, 23 (1955) 1833-1840.
[35] D.J. Tannor, B. Marten, R. Murphy, R.A. Friesner, D. Sitkoff, A. Nicholls, B. Honig, M. Ringnalda, W.A. Goddard, J Am Chem Soc, 116 (1994) 11875-11882.
[36] D. Fu, A. Libson, R. Stroud, in: Ion Channels - from atomic resolution physiology to functional genomics, 2002, pp. 51-65.
[37] J. E. D. Glendening, K. Badenhoop, A. E. Reed, J. E. Carpenter, J. A. Bohmann, C. M. Morales, and F. Weinhold, in, Theoretical Chemistry Institute, University of Winsconsin, Madison, 2001.
[38] W.L. Jorgensen, D.S. Maxwell, J. Tirado-Rives, J Am Chem Soc, 118 (1996) 11225-11236.
[39] R.A.F. G. Kaminski, J. Tirado-Rives, W. L. Jorgensen, J. Phys. Chem. B, (2001) 6474-6487.

A2. Gold Compounds as Aquaglyceroporin-7 inhibitors

This chapter is published:

Ana Madeira*, Andreia de Almeida*, Chris de Graaf, Marta Camps, Antonio Zorzano, Teresa F. Moura, Angela Casini and Graça Soveral

Gold coordination compounds as chemical probes to unravel aquaporin-7 function

Chem.Bio.Chem. (2014) 15: 1487-1494

Supplementary information available: DOI: 10.1002/c bic.201402103

*Authors contributed equally to this work

Abstract

Aquaporins (AQPs) are membrane water/glycerol channels that are involved in many physiological functions. Aquaporin-based modulators are predicted to have potential utility in the treatment of several diseases, as well as chemical tools to assess AQPs function in biological systems. We recently reported gold(III) compounds as human AQP3 inhibitors, with Auphen as the most potent of the series. In this work, we assessed the modulation of aquaporin-7 (AQP7) expressed in an adipocyte cell model and show that Auphen significantly inhibits mouse and human AQP7. By homology modeling and molecular docking it was possible to identify the thioether groups of methionine residues, in particular Met47, as likely candidates for binding to the gold(III) complex. Our data point to Auphen as a useful chemical tool to detect AQP7 function. It might constitute a basis to develop inhibitors with improved affinity towards different aquaglyceroporin isoforms.

2.1. Introduction

Aquaporins (AQPs) belong to a highly conserved group of membrane proteins that are involved in the transport of water and small solutes and that play a variety of important physiological roles. The 13 human AQP isoforms (AQP0–12) are differentially expressed in many types of cells and tissues in the body and can be divided into two major groups: those strictly selective for water (orthodox aquaporins), and those that are also permeable to other small solutes including glycerol (aquaglyceroporins), namely isoforms AQP3, AQP7, AQP9, and AQP10 [1].

At the cellular level, aquaporin-mediated osmotic water transport across cell plasma membranes facilitates transepithelial fluid transport, cell migration, and neuroexcitation; aquaporin-mediated glycerol transport regulates cell proliferation, adipocyte metabolism, and epidermal water retention [2]. Much of our understanding of AQP functions in mammalian physiology has come from relatively recent phenotype analysis of mice lacking one of the AQPs. These studies have confirmed the involvement of AQPs in the urinary-concentrating mechanism and glandular fluid secretion, and led to the discovery of unanticipated roles of AQPs in various processes, including cell migration (angiogenesis, tumour metastasis, wound healing), cell proliferation, neural function, epidermal hydration and ocular function. Specifically, the aquaglyceroporins, regulate glycerol content in epidermal, fat and other tissues, and are involved in skin hydration, cell proliferation, carcinogenesis and fat metabolism [3].

In spite of the numerous studies on AQPs, the lack of small-molecule compounds with potent and selective aquaporin inhibiting activity (for use as chemical probes) is a major issue in this field. Such inhibitors are necessary to gain new insights into aquaporin activity and function. With this aim, we recently reported the potent inhibition of glycerol transport through human aquaglyceroporin-3 (hAQP3) by a water-soluble gold(III) coordination compound [Au(phen)Cl_2]Cl (phen = 1,10-phenantroline; Auphen) (Figure 1), and by other gold(III) complexes bearing N-donor ligands [4]. Notably, Auphen was shown to inhibit glycerol transport in human red blood cells while exhibiting no effect on water permeability mediated by AQP1 [5]. Importantly, no cell toxicity was observed upon incubation with the compound, thus pointing to a nontoxic inhibitory effect.

In order to investigate the inhibition of other aquaglyceroporin isoforms by gold(III)

coordination complexes, we studied Auphen modulation of the plasma membrane protein aquaporin-7 (AQP7) expressed in adipocytes. Inhibition of the AQP7 channel was evaluated by assessing both glycerol and water permeability in the stable murine adipocyte cell line, 3T3-L1. As it was previously demonstrated that AQP7 is a functional water and glycerol channel when expressed in these cells [6, 7], this cell model can be considered valuable in screening for modulators of AQP7 function. Our approach included characterization of the effect of Auphen on the transport properties of the murine isoform, mAQP7. Moreover, by overexpressing human AQP7 in 3T3-L1 adipocytes (and, therefore, assembling a gain-of-function model), we aimed at determining the effect of Auphen on the human isoform (hAQP7). Interestingly, the gold compound proved to be a good inhibitor of glycerol permeability in this model. Thus, a homology model of human AQP7 was built and compared to one we previously created for human AQP3 [8], in order to highlight possible differences in the mechanisms of inhibition of glycerol permeation. Our molecular modelling also allowed identification of putative reactive sites for gold ions (thus, also crucial to glycerol transport), and molecular docking studies predicted plausible Auphen binding modes.

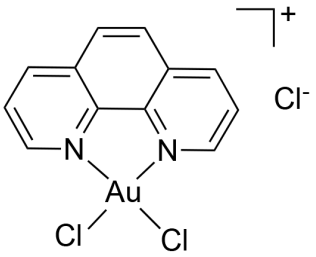

Chart 1. Formula of the gold(III) coordination compound Auphen.

2.2. Results and Discussion

2.2.1. Inhibition of mouse AQP7 water and glycerol permeability by Auphen

We recently reported the potent and selective inhibition of AQP3 by a water-soluble gold(III) coordination compound, Auphen [5]. To test the effect of this metallodrug on AQP7 activity, water and glycerol permeability of 3T3-L1 adipocytes expressing mouse AQP7 (control) and with overexpression of hAQP7 were evaluated. For this purpose, calcein-loaded adipocytes were incubated for 20 min with Auphen immediately before the permeability assays and challenged with hypertonic mannitol (nondiffusible solute) or glycerol (diffusible solute) solutions. Representative time-course traces of the change in cell volume (V/V_o) for control adipocytes subjected to an osmotic shock with mannitol are shown in Figure 1A (inducing water outflow and cell shrinkage). In the presence of 15 μM Auphen, cells presented a slower volume change.

In order to assess glycerol permeability (P_{gly}), cell volume changes following glycerol osmotic shock were monitored (Figure 1B). This methodology was validated in our previous work assessing AQP7 as a functional water and glycerol channel when expressed in 3T3-L1 cells [7]. In this experimental setup, after the perturbation was applied, water and glycerol fluxes occured concomitantly. Figure 1B shows the cell volume change for control cells when subjected to a glycerol challenge, either in the presence or absence of Auphen.

Following these promising results we investigated the effect of Auphen on glycerol transport through mouse AQP7 by performing a dose-response assay (Figure 1C). Control cells were incubated with increasing Auphen concentration (0 to 50 μM) until maximum inhibition was

reached. The half-maximal effective concentration (EC_{50}) was (6.5 ± 3.7) μM.

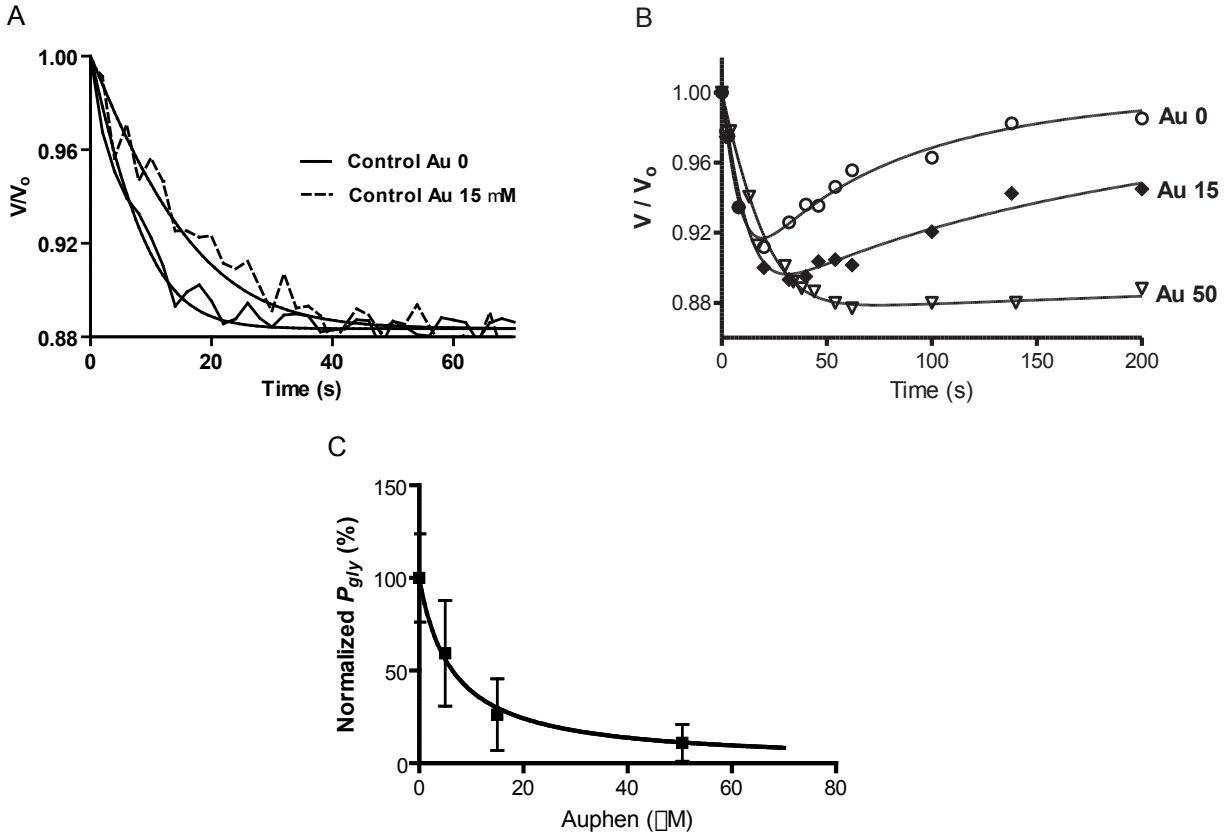

Figure 1. Effect of Auphen on water and glycerol permeation through mouse AQP7. Representative time course of the relative cell volume change (V/Vo) for control adipocytes (basal mouse AQP7) after (A) a mannitol or (B) a glycerol osmotic shock, in presence or absence of Auphen. (C) Dose-response curve of Auphen in control adipocytes; EC_{50} = (6.5 ± 3.7) μM.

2.2.2. Effect of Auphen on human AQP7

To further investigate the effect of Auphen on human AQP7 we used a 3T3-L1 cell line overexpressing the human AQP7 isoform (described in ref. [7]). We selected an Auphen concentration (15 μM) of approximately twice the EC_{50} value obtained for control cells (basal expression of mAQP7), to ensure inhibition of both AQP7 isoforms.

The enhancement of permeability conferred by hAQP7 overexpression was characterized in detail in a previous work [7]: hAQP7 cells showed a two-fold increase in permeability compared to control cells (Figure 2A). Upon treatment with 15 μM Auphen, a reduction of water permeability (P_f) in both control (37% inhibition, $P<0.05$) and hAQP7-overexpressing adipocytes (63% inhibition, $P<0.01$) was observed. The smaller effect in water permeability in control cells can be explained by the relatively high contribution of the lipid bilayer to water permeation (diffusion permeability), which masks the effect of Auphen. However, by increasing the number of active channels through overexpression of hAQP7, the inhibitory effect was more pronounced. The calculated P_f values for control and hAQP7-overexpressing adipocytes in the absence and presence of Auphen are given in Table 1.

In glycerol permeability assays, 15 μM Auphen drastically reduced P_{gly} in both control and hAQP7-overexpressing adipocytes, (~74 and 79%, respectively; $P<0.001$; Figure 2B). Given that in adipocytes overexpressing hAQP7, both mouse and human isoforms are present and contribute simultaneously to water and glycerol permeation, we calculated the effect of Auphen on hAQP7

by subtracting the contribution of the mouse isoform: 82% inhibition for hAQP7 was obtained, independently from the water or glycerol experiments. Altogether, these data clearly indicate that Auphen inhibits human AQP7 channel activity.

Table 1. Water and glycerol permeability of control and human AQP7-overexpressing (hAQP7) adipocytes

Compound	P_f x 10^{-3} (cm.s^{-1})		P_{gly} x 10^{-6} (cm.s^{-1})	
Cell line	[a]	+ Auphen [b]	[a]	+ Auphen [b]
Control	0.76 ± 0.06	0.48 ± 0.04	3.98 ± 0.04	0.36 ± 0.11
hAQP7	1.80 ± 0.01	0.67 ± 0.08	10.28 ± 1.35	2.16 ± 0.05

Each value represents the mean ± SEM derived from 30-50 cells analyzed. [a] Data from ref. [7]. [b] 15 μM, data from this work.

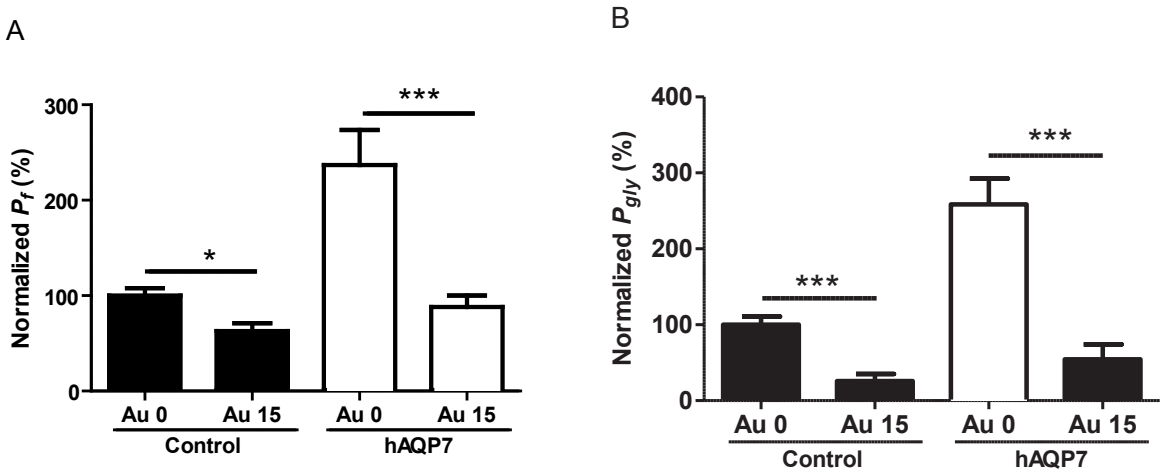

Figure 2. Effect of Auphen on AQP7 water (P_f) and glycerol permeability (P_{gly}) in control adipocytes (basal mouse AQP7) and hAQP7 adipocytes (with hAQP7 overexpression). (A) Water and (B) glycerol permeability of control and hAQP7 after treatment with 15 μM Auphen. Permeability values are normalized to control cells without Auphen. Bars show mean ± SEM from 30-50 cells. * $P < 0.05$, *** $P < 0.001$.

2.2.3. Mechanisms of AQP7 inhibition by Auphen

To investigate the mechanisms of AQP7 inhibition by Auphen at the molecular level we performed protein homology modelling and molecular docking studies. Three computational steps were used: homology model preparation, binding site identification, and molecular docking studies. The homology model of hAQP7 (see the Experimental Section) was constructed by using the *Escherichia coli* glycerol facilitator (bGlpF) structure as the template, previously solved by X-ray crystallography [9]. In the obtained hAQP7 model (Figure 3A) the main distinctive features of aquaglyceroporins can be seen, specifically the hydrophilic and hydrophobic residues typical of the glycerol channel lining (Figure S1 in the Supporting Information), as well as two constriction sites.

The aquaporin family and the aquaglyceroporin subfamily share a common protein fold comprising six transmembrane helices and two half-helices located inside the channel. These helices surround the amphipathic AQP channel (~ 20 Å long and 3-4 Å wide). AQPs have two constriction sites (the "selectivity filters", SFs) [10]. The first, a constricted region, is formed by a few residues near the extracellular entrance, and provides distinguishing features of the subfamilies. It is an aromatic/Arg (ar/R) constriction site (ar/R SF), the diameter of which determines which solutes (e.g. glycerol, methylamine), in addition to water, can pass through the AQP [10-12]. This region is the narrowest point in the channel; in water selective AQPs it is polar, whereas in

aquaglyceroporins it is slightly wider and more hydrophobic, with two conserved aromatic residues (Phe74 and Tyr223 in hAQP7; Figure 3B) [10].

The second constriction site is characterized by asparagine-proline-alanine (NPA) motifs at the ends of the two semi-helices; this motif is highly conserved in AQPs [13], although in hAQP7 the first sequence is NAA and the second is NPS (Figure 3B). The helix dipole moments have one net positive charge, and the resulting electrostatic field poses another energy barrier for cations [14].

Sequence alignment of human AQP7 and AQP3 with bacterial bGlpF (Figure S2) shows

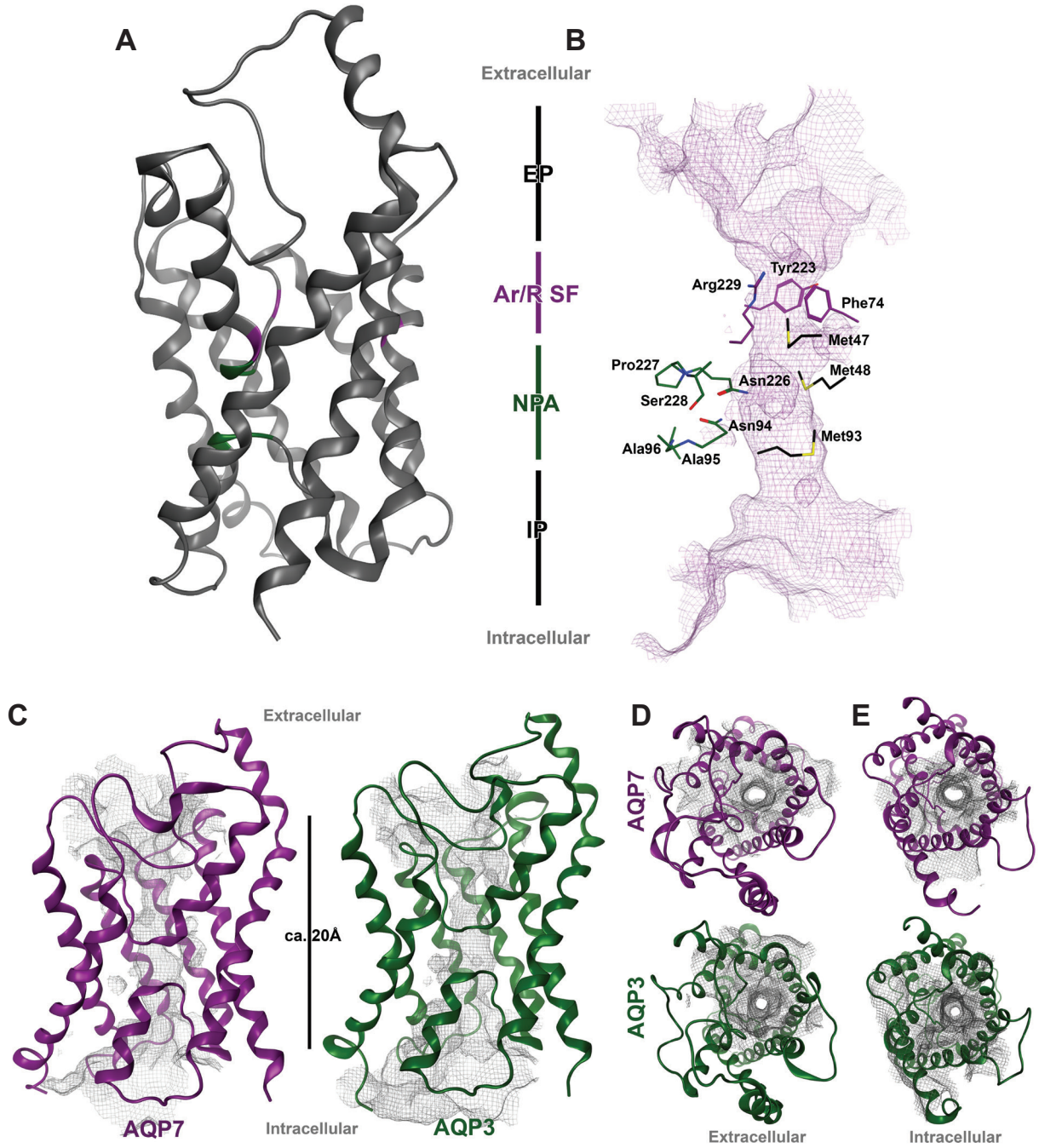

Figure 3. Top pannel: Homology model of hAQP7 in (A) cartoon representation of tertiary structure and (B) surface representation of residues lining the channel (purple mesh). The main protein regions are identified as extracellular pocket (EP), aromatic/arginine selectivity filter (Ar/R SF), NPA motif and intracellular pocket (IP), respectively. Ar/R SF residues are coloured in purple, while NPA residues (NAA and NPS) are coloured in green. The identified methionines are represented in black with the sulphur atom in yellow. Lower pannel: Cartoon representation of the homology models of hAQP7 (purple) and hAQP3 (green) with surface representation of the residues lining the channel (grey mesh). The different panels show lateral (C), extracellular (D) and intracellular (E) views of the channels. Figures generated with MOE [15].

that, although the ar/R SF of the two human glycerol channels have the same composition, the one of bGlpF differs by one residue (Tyr223 in hAQP7, Trp48 bGlpF), while retaining the two hydrophobic residues and the conserved arginine (Arg229 in hAQP7), which is present in all isoforms. Concerning the balance of hydrophobic/hydrophilic residues, the two human isoforms share the same composition in residues lining the channel, whereas bGlpF is almost 15% richer in hydrophobic residues. A detailed comparison was performed between the obtained homology model of hAQP7, the previously obtained hAQP3 model [8], and the X-ray structure of bGlpF (PDB ID: 1FX8). Of note, in the case of hAQP7 and hAQP3, although the overall structures of the proteins are similar (Figure 3C-E), ar/R SF is 1 Å broader in hAQP7. Moreover, both the cytosolic and extracellular entrances of the pore show considerable differences in size and shape: in hAQP3 both entrances are round (extracellular entrance 50% larger), whereas in hAQP7 they are elliptical and have the same area (Figure 3C-E). The bGlpF channel has elliptical entrances (as hAQP7) but with different areas (as for hAQP3, although smaller; Table S1).

Our analysis also highlighted key differences between human AQP7 and AQP3 isoforms. In detail, the channel composition is slightly different in the two human isoforms: in hAQP7 four methionines (Met219, Met47, Met48, and Met93) are located throughout the channel (in the extracellular pocket (EP), ar/R SF and NPA pockets; Figure 3A-B), whereas in hAQP3 these residues are leucines.

The importance of these methionine residues was revealed when identification of the main amino acidic residues involved in glycerol binding was attempted, by superposing the hAQP7 and hAQP3 homology models with the structures of bGlpF and the Plasmodium falciparum glycerol facilitator (pfAQP, PDB ID: 3C02; both crystal structures contain glycerol molecules inside the channel) [16, 17].

Based on the positions of the glycerol molecules in the aquaglyceroporins channels, four possible binding pockets were identified: in the EP and in the ar/R SF and NPA regions for AQP7 and CP (cytoplasmic pocket) region for AQP3 (Figure 5). According to our analysis, the hydrophobic/hydrophilic composition and surface of the channel are maintained between the two human isoforms, as well as in GlpF (sequence alignment Figure S2). Interestingly, the four methionine residues in the lining of the hAQP7 channel are located in three of the glycerol binding pockets, EP, ar/R SF and NPA (Figure 4).

Glycerol transport requires specific H-bonds and hydrophobic interactions with side-chains located along the channel, in the various pockets. From our hAQP7 model we predicted crucial H-bond interactions that are evident in the bGlpF structure (e.g. Arg229 in the hAQP7 ar/R SF region), but also different H-bond acceptors, such as methionine residues. For example, given the position of the glycerol molecules in the hAQP7 model, interactions between the sulphur atoms of Met47 and Met93 (Figure S1) and the glycerol molecule located in the NPA binding pocket were predicted to be involved in the transport of glycerol.

The hydrogen bonding capability of Met residues in proteins were re-evaluated in recent studies. For example, detailed investigations of small, isolated, intermolecular complexes have suggested that H-bonds to sulphur can be as strong as their oxygen counterparts [18, 19]. Most importantly an investigation into the strength of the H-bond in Met-containing peptides [20] concluded that these interactions can be crucial as the classical intra-backbone NH···O=C H-Bonds to stabilize the protein structure.

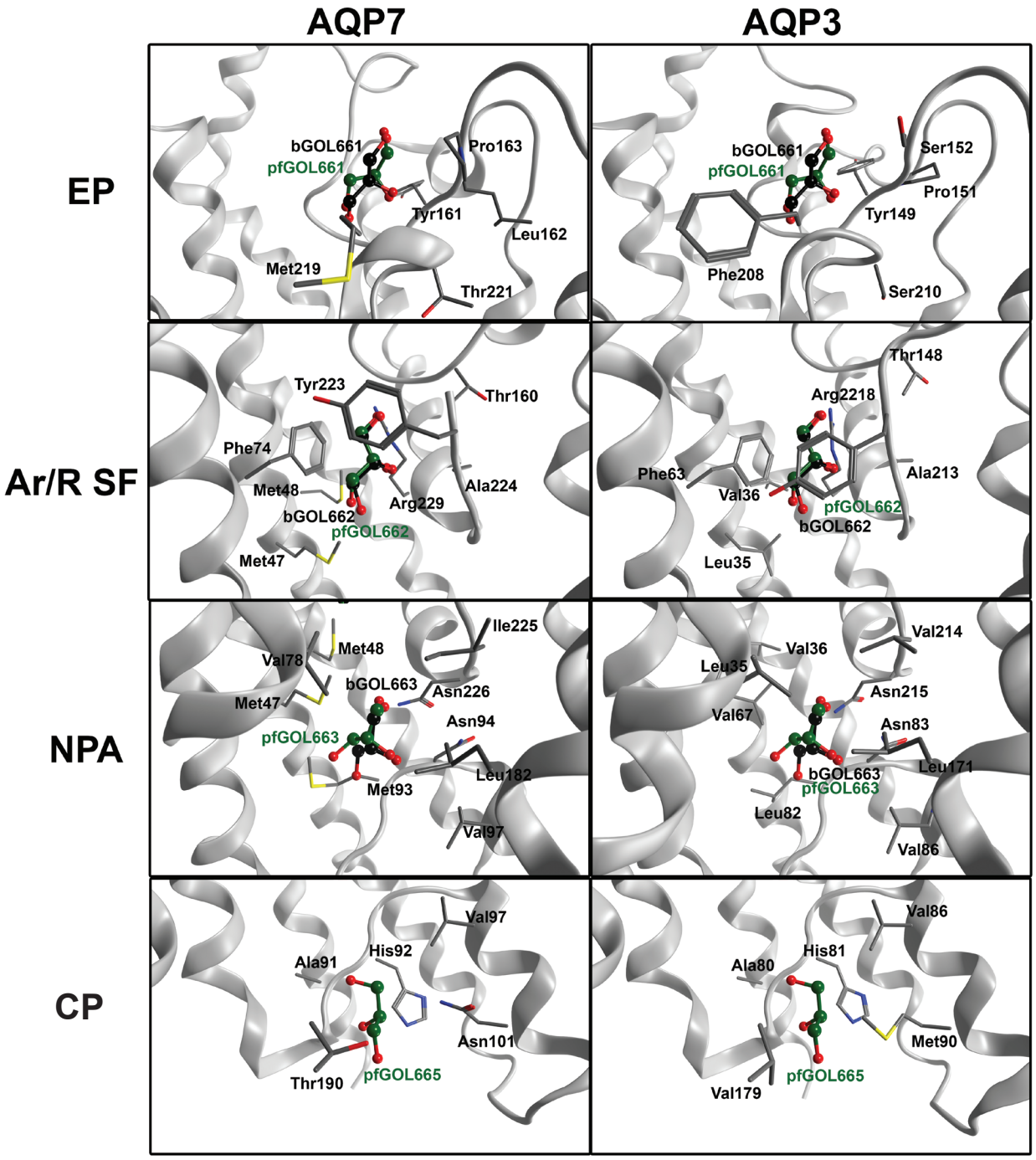

Figure 4. Glycerol molecules from the structures of bGlpF (PDB ID: 1FX8, black) and pfAQP (PDB ID: 3C02, green) superposed inside the channels of hAQP7 and hAQP3 models. The glycerol molecules (GOL): b (bacterial) or pf (P. falciparum), with original PDB numbering. The four identified glycerol pockets are extracellular pocket (EP), aromatic/arginine selectivity filter (ar/R SF), NPA motif (NPA) and cytoplasmic pocket (CP), respectively. The figures were generated with MOE [15].

Interestingly, these Met residues are not present in hAQP3 (Figure 4). In hAQP3 a methionine residue is only present in the CP region (Met90), and it is not predicted to be involved in the interactions with glycerol. Overall, these differences between isoforms could lead to different mechanisms of action by inhibitor molecules.

The mechanism of gold inhibition in hAQP3 is possibly attributable to the ability of AuIII to interact with sulphur donor groups of proteins, such as the thiolate of cysteine or the thioether methionine. In fact, we previously reported a model for the selective inhibition of AQP3 by gold(III) channel blockers, including Auphen. In this model, the metal coordinates to a specific nucleophilic site side chain of Cys40) at the extracellular side of AQP3, thereby inducing blockage of the channel upon binding [5]. Thus, to explain the mechanism of inhibition of hAQP7 by Auphen, we analysed in detail the positions and the chemical environment of the most likely gold-ion binding sites, such as cysteine and methionine side chains, in our homology model. Interestingly, although no cysteine residues are found in the hAQP7 channel, Met47 and Met93 have the side chains pointing towards the inside of the channel and could thus be accessible for gold binding. According to our model, if gold(III) binding occurs at these sites, efficient inhibition of glycerol transport could occur, as these two residues are involved in substrate binding. To confirm our hypothesis, docking calculations were carried out to evaluate the accessibility of the proposed Met binding sites to Auphen. Specifically, we evaluated non-covalent binding poses and possible steric clashes of the compound approaching the Met residues. As these residues are below the first constriction site, their side chains are inaccessible for gold binding from the extracellular pocket, as the Ar/R SF is very narrow. Thus, we docked the compound from the cytosolic side of the channel, as close as possible to the constriction pore of the protein below the SF domain (Figure S3).

Automated docking studies suggest that Auphen binds close to the constriction pore and interacts with the sulphur atom of Met47 via its AuIII centre (Figure 5). Along with the possible formation of a coordination bond between AuIII-S(Met47) upon release of a chloride, the gold(III) complex is also predicted to interact through further hydrophobic contacts with residues in the channel. For example, the phenantroline ligand of Auphen could interact with Val78 and the backbone of Asn94. These results show how the placement of a metal complex in the hAQP7 intracellular pocket is potentially controlled by both covalent anchoring to Met47 and by non-covalent interactions.

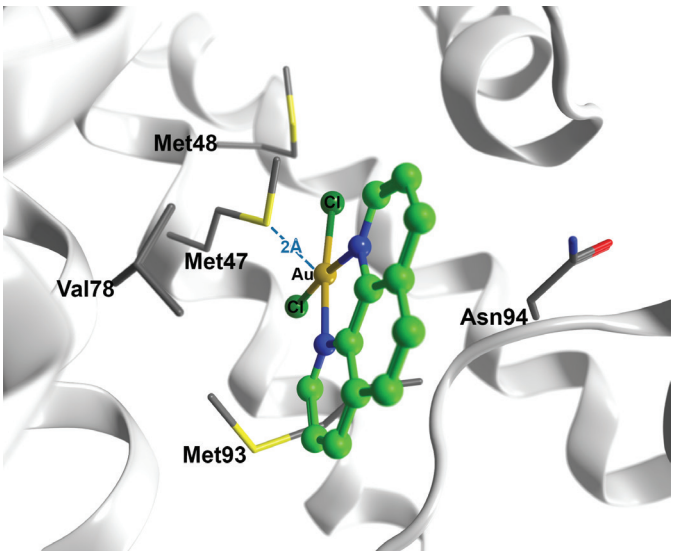

Figure 5. Molecular docking of the gold(III) complex Auphen (green) inside the NPA pocket of hAQP7 (grey) Location of the NPA pocket is shown on Figure 5. Side chains of Met47, Met48, Val78, Met93, and Asn94 are depicted in sticks. Generated with MOE [15].

It must be noted that gold(III) coordination compounds with N-donor ligands have been reported to undergo reduction to gold(I) with concomitant ligand loss upon protein binding [21-23]. Thus, we cannot exclude the possibility that reduction of the gold(III) ion in the Auphen complex might also occur. Nevertheless, other studies investigating the reactivity of gold(III) complexes, including Auphen, with models of zinc-finger (ZF) domains showed that gold remains in oxidation state 3^+ when binding

to four residues in a ZF peptide [24]. Thus, stabilization of AuIII ions might occur if the compound has the possibility of fulfilling the tetracoordinate geometry ideal to maintain the 3^+ oxidation state upon ligand substitution reactions with various residues in the protein channel.

Finally, it was shown experimentally (Figures 1B, C and 2B) that Auphen also inhibits glycerol transport in 3T3-L1 adipocytes with basal expression of mAQP7. Thus, to investigate if inhibition of glycerol transport by gold ions in mAQP7 could be possible through the same mechanism as that discussed for hAQP7, we performed a full sequence alignment between the two isoforms by using UniProt database (Figure S4). The two proteins have 67% sequence identity and 93% of similarity for residues lining the binding pockets, with the identified methionine residues in the same positions. This additional information leads us to conclude that hAQP7 and mAQP7 may share the same inhibition mechanism by Auphen.

2.3. Conclusions

Our broader goal has been to find selective agents capable of blocking glycerol and water transport through aquaglyceroporins. Following previous results on the inhibition of human AQP3 by gold(III) coordination compounds, herein investigated the ability of one of our most potent inhibitors, Auphen, to exert its effects on another important glycerol channel, AQP7.

AQP7 has been shown to be a functional water and glycerol channel in 3T3-L1 adipocytes [7]. In the present work, we showed that Auphen significantly inhibits glycerol and water transport by both mouse and human AQP7. By homology modelling and molecular docking studies, it was possible to identify the side chains of sulphur-donor methionine residues (Met47 and Met93) as crucial interacting sites for gold in hAQP7. Non-covalent docking studies supported the hypothesis of AQP7 channel blockage by Auphen through direct binding to Met47. Interestingly, in our previous work, molecular modelling suggested binding of Auphen to Cys40 in the AQP3 extracellular pocket. In contrast, in hAQP7 the most favourable binding residue is located in the channel entrance facing the cytoplasm, thus implying that the gold compound has to enter the cell before reaching its putative binding site. Similar binding to the internal pore, with consequent reduction of AQP permeability, was proposed for small-molecule blockers of AQP1 and AQP4 [25, 26], but mechanisms of inhibition were not fully determined.

Notably, our modelling approach has so far proven to be predictive of the Auphen inhibition mechanism of human AQP3. As our recently published site-directed mutagenesis studies [27] showed that point mutation of the Cys40 residue (hypothesized by us to be the most favourable binding site in AQP3 for Auphen) [5] resulted in almost complete loss of the inhibitory effects of this compound.

Several studies have described the importance of AQP7 in adipose tissue, pancreatic insulin secretion, as well as in energy production in skeletal muscle and heart [28-31], therefore, further work is necessary to validate AQP7 as a potential drug target. Interestingly, an improved insulin-secretion profile with reduced pancreatic cell mass in AQP7-deficient mice [32] suggests promising applications for *in vivo* AQP7 inhibitors.

The use in research of tools like these potent AQP7 inhibitors could also contribute to broadening our understanding of AQP7 and other glycerol channels in the onset of human diseases. In this context, our results on the inhibitory effect of the gold compound, Auphen, on AQP7 and

AQP3 – but with different predicted mechanisms - constitute a basis to develop inhibitors with improved affinity towards different aquaglyceroporin isoforms.

2.4. Experimental Section

Cell culture: 3T3-L1 fibroblasts (CCL 92.1; American Type Culture Collection, Manassas, VA) were grown to confluence and induced to differentiate into adipocytes essentially as described [33]. Fully mature adipocytes were used 10-15 days after initiation of differentiation. The 3T3-L1 stable cell line overexpressing human AQP7 was obtained by lentiviral infection of 3T3-L1 preadipocytes, as previously detailed [7].

Permeability assays: Water (P_f) and glycerol (P_{gly}) permeabilities were measured in individual adherent cells on a coverslip as previously described [7]. Briefly, 3T3-L1 adipocytes were loaded with 5 μM calcein acetoxymethyl ester (calcein-AM) (Sigma® Aldrich, Saint Louis, MO) (a volume sensitive fluorescence probe) for 90 min at 37°C in 5% CO2/95% air. The coverslips with the adhered cells were mounted in a closed perfusion chamber (Warner Instruments, Hamden, USA) on the stage of a Zeiss Axiovert 200 inverted microscope (Carl Zeiss, Thornwood, NY). Fluorescence was excited at wavelength 495/10 nm and the emission fluorescence was collected with a 535/25nm bandpass filter coupled with a 515 nm dichroic beam splitter. Images were captured using a ×40/1.6 epifluorescence oil immersion objective and a digital camera (CoolSNAP EZ, Photometrics, Tucson, AZ) and were recorded by the Metafluor Software (Molecular Devices, Downingtown, PA). Cells were perfused with HEPES (135 mM NaCl, 5 mM KCl, 2.5 mM CaCl2, 1.2 mM $MgCl_2$, 10 mM Glucose, 5 mM Hepes, pH 7.4, $(osm_{out})_o$ = 300 mosM) for 60 s. The osmotic challenges were performed by adding mannitol or glycerol to the HEPES solution achieving an external osmolarity of $(osmout)\infty$ = 600 mosM and thus a tonicity of the osmotic shock of Λ=2 (defined as the ratio between final and initial media osmolarities, $\Lambda = (osm_{out})\infty/(osm_{out})_o$). For the inhibition studies, cells were incubated with 5 μM Auphen for 20 minutes at 37°C in 5% CO_2/95% air, prior to the permeability assays.

Osmotic and Glycerol Permeability coefficients: Permeability coefficients P_f and P_{gly} were evaluated from the measured time dependent volume changes, $v_{rel}=V/V_o$, obtained by adding mannitol (P_f) or glycerol (P_{gly}) to the external media achieving an osmotic challenge of Λ=2. For these calculations the values for the solute reflection coefficient were considered constant and equal to one (σS=1) [7]. The relative non-osmotic volume $\beta=VN_{osm}/V_o$ was considered in all calculations. For each cell population the values of Pf and β were obtained from the mannitol osmotic shocks and these values were used for evaluating P_{gly} in the glycerol experiments. Parameters (P_f, P_{gly} and β) were evaluated by numerically integrating and curve fitting the time dependent vrel data, using the model equations detailed in the Supplementary Information and the Berkeley Madonna software (http://www.berkeleymadonna.com/).

Cell volumes and fluorescence output: A linear relationship between relative changes in cell osmotic volume $(V-\beta)/(V_o-\beta)$ (thus of V/V_o) and calcein fluorescence intensity (F/F_o) was previously validated [34].Taking this into account, and following the strategy detailed in [7], for the mannitol experiments the cell fluorescence traces F/Fo were converted into (V/V_o) after subtracting the bleaching given by the initial fluorescence decay before the mannitol osmotic shock. F_o was calculated in each signal as the averaged initial values of fluorescence prior to the osmotic challenge. For the glycerol experiments and as previously discussed in [7], the measured cell volumes were used to calculate V/V_o.

Cell volume V was measured at selected time points from 2D images obtained during the permeability assay protocols (V_o is the initial volume prior to the osmotic challenge). For each coverslip with adhered cells, 6 or 18 pictures with 10-13 cells each were analyzed for selected time points for the water and the glycerol permeability studies, respectively. For each experimental condition four coverslips from two different cell platings were assayed, making an average of 40-50 cells analyzed per condition. The cross sectional area of calcein-AM loaded cells was measured using the Image J software and cells were assumed to have a spherical shape for volume calculations.

Statistical Analysis: The results were expressed as mean ± SEM of n individual experiments. Statistical analysis between groups was performed by unpaired t-test. P values < 0.05 were considered statistical significant. Statistical analyses were performed using the Prism software (GraphPad Software Inc., San Diego, CA).

Molecular Modeling: The 3D structure of hAQP7 was obtained by homology modeling using Molecular Operating Environment (MOE 2012.10) (CCG 2012) [15]. The choice of a template structure was based on the sequence identity between hAQP7 and the sequence of the AQPs with available resolved structures from human, bacteria and Plasmodium falciparum (UniProt 2013 codes O14520, C8TK05 and Q8WPZ6, respectively). The isoform that shows to have the highest sequence similarity with hAQP7 is the bacterial isoform Glycerol Facilitator (GlpF), which was then chosen as a template structure. Three resolved structures for bGlpF, crystalized either with or without glycerol and solved by X-Ray diffraction, were retrieved from the Protein Data Bank [9]. Among them, the template was chosen according to the best available resolution (2.70 Å) without any substrate (pdb 1LDI) and the structure was prepared and protonated at pH 7 under forcefield Amber12EHT. Thus, the human AQP7 model was built under the same force field: 50 intermediate models were generated and merged into one final homology model.

The obtained model was checked for rotamers of side chains in the regions of Ar/R SF and NPA, by comparison with the available crystal structures of all the other AQP isoforms (pdb codes 1H6I, 36D8, 3D9S, 1RC2, 1LD1 and 3C02). The structure was protonated at pH 7 and an energy minimization refinement was performed, also under Amber12EHT force field, fixing the Cα.

Measurements of the size of the channels were performed using MOE 2012.10 (CCG 2012) [15]. For the intra and extracellular entrances the measurements were done transversally in the channel, fixing as entrance the point where the channel starts narrowing. A second measurement was performed in the same plane rotating 90º. The selected points for measurement were approximately the same in all the structures. The longitudinal measurement was performed using residues located in the planes defined as intra and extracellular entrances.

Non-covalent Docking: Non–covalent docking was performed on the hAQP7 homology model described before using MOE [15]. 50 poses were generated using the virtual screening method and scored by the London dG scoring function using placement triangle matcher. The binding pocket was defined as the sulphur atom of Met47 generating 50 possible docking positions. All other default MOE docking settings were used. Plausible docking poses were selected according to docking score, the position of the Auphen gold atom with respect to methionine side-chains, favourable interactions with the residues lining the pocket. After careful analysis, one pose was chosen according to the orientation of the compound inside the pocket and of the gold atom in order to avoid possible steric hindrance with other atoms from the protein, and to favour possible stabilization of the compound's position by side chain/backbone interactions with Auphen. The compound's orientation was later optimized by energy minimization of side-chains of residues forming clashes in the NPA pocket with Auphen, also using Amber12EHT forcefield. For this energy minimization all the atoms were fixed, except for the side-chains of Asn94 and Met93.

References

[1] A. Rojek, J. Praetorius, J. Frokiaer, S. Nielsen, R.A. Fenton, Annu Rev Physiol, 70 (2008) 301-327.
[2] A.S. Verkman, Annu Rev Med, 63 (2012) 303-316.
[3] A.S. Verkman, J Exp Biol, 212 (2009) 1707-1715.
[4] A.P. Martins, A. Ciancetta, A. de Almeida, A. Marrone, N. Re, G. Soveral, A. Casini, ChemMedChem, 8 (2013) 1086-1092.
[5] A.P. Martins, A. Marrone, A. Ciancetta, A. Galán Cobo, M. Echevarría, T.F. Moura, N. Re, A. Casini, G. Soveral, PloS one, 7 (2012) e37435.
[6] K. Kishida, H. Kuriyama, T. Funahashi, I. Shimomura, S. Kihara, N. Ouchi, M. Nishida, H. Nishizawa, M. Matsuda, M. Takahashi, K. Hotta, T. Nakamura, S. Yamashita, Y. Tochino, Y. Matsuzawa, J Biol Chem, 275 (2000) 20896-20902.
[7] A. Madeira, M. Camps, A. Zorzano, T.F. Moura, G. Soveral, PLoS One, 8 (2013) e83442.
[8] A.P. Martins, A. Marrone, A. Ciancetta, A. Galan Cobo, M. Echevarria, T.F. Moura, N. Re, A. Casini, G. Soveral, PLoS One, 7 (2012) e37435.
[9] E. Tajkhorshid, P. Nollert, M.O. Jensen, L.J. Miercke, J. O'Connell, R.M. Stroud, K. Schulten, Science, 296 (2002) 525-530.
[10] D.F. Savage, J.D. O'Connell, 3rd, L.J. Miercke, J. Finer-Moore, R.M. Stroud, Proc Natl Acad Sci U S A, 107 (2010) 17164-17169.
[11] J.S. Hub, B.L. de Groot, Proc Natl Acad Sci U S A, 105 (2008) 1198-1203.
[12] E. Beitz, B. Wu, L.M. Holm, J.E. Schultz, T. Zeuthen, Proc Natl Acad Sci U S A, 103 (2006) 269-274.
[13] Y. Fujiyoshi, K. Mitsuoka, B.L. de Groot, A. Philippsen, H. Grubmuller, P. Agre, A. Engel, Curr Opin Struct Biol, 12 (2002) 509-515.
[14] H. Chen, B. Ilan, Y. Wu, F. Zhu, K. Schulten, G.A. Voth, Biophys J, 92 (2007) 46-60.
[15] in, Molecular Operating Environment (MOE), 2012.10; Chemical Computing Group Inc., 1010 Sherbooke St. West, Suite #910, Montreal, QC, Canada, H3A 2R7, 2012.
[16] D. Fu, A. Libson, L.J. Miercke, C. Weitzman, P. Nollert, J. Krucinski, R.M. Stroud, Science, 290 (2000) 481-486.
[17] Z.E. Newby, J. O'Connell, 3rd, Y. Robles-Colmenares, S. Khademi, L.J. Miercke, R.M. Stroud, Nat Struct Mol Biol, 15 (2008) 619-625.
[18] H.S. Biswal, S. Wategaonkar, J Phys Chem. A, 113 (2009) 12763-12773.
[19] D.L. Howard, H.G. Kjaergaard, PCCP, 10 (2008) 4113-4118.
[20] H.S. Biswal, E. Gloaguen, Y. Loquais, B. Tardivel, M. Mons, J Phys Chem letters, 3 (2012) 755-759.
[21] A. Casini, M.A. Cinellu, G. Minghetti, C. Gabbiani, M. Coronnello, E. Mini, L. Messori, J Med Chem, 49 (2006) 5524-5531.
[22] A. Casini, M.C. Diawara, R. Scopelliti, S.M. Zakeeruddin, M. Grätzel, P.J. Dyson, Dalton Trans, 39 (2010) 2239-2245.
[23] M.D. Durovic, Z.D. Bugarcic, F.W. Heinemann, R. van Eldik, Dalton Trans, 43 (2014) 3911-3921.
[24] F. Mendes, M. Groessl, A.a. Nazarov, Y.O. Tsybin, G. Sava, I. Santos, P.J. Dyson, A. Casini, J Med Chem, 54 (2011) 2196-2206.
[25] E. Migliati, N. Meurice, P. DuBois, J.S. Fang, S. Somasekharan, E. Beckett, G. Flynn, A.J. Yool, Mol Pharmacol, 76 (2009) 105-112.
[26] M. Ozu, R.A. Dorr, M. Teresa Politi, M. Parisi, R. Toriano, Eur Biophys J, 40 (2011) 737-746.
[27] A. Serna, A. Galan-Cobo, C. Rodrigues, I. Sanchez-Gomar, J.J. Toledo-Aral, T.F. Moura, A. Casini, G. Soveral, M. Echevarria, Journal of cellular physiology, 229 (2014) 1787-1801.
[28] N. Maeda, Mol Aspects Med, 33 (2012) 665-675.
[29] C. Delporte, Biochim Biophys Acta, (2013).
[30] T. Hibuse, N. Maeda, H. Nakatsuji, Y. Tochino, K. Fujita, S. Kihara, T. Funahashi, I. Shimomura, Cardiovasc Res, 83 (2009) 34-41.

[31] A. Rodriguez, V. Catalan, J. Gomez-Ambrosi, G. Fruhbeck, Cell Cycle, 10 (2011) 1548-1556.
[32] K. Matsumura, B.H. Chang, M. Fujimiya, W. Chen, R.N. Kulkarni, Y. Eguchi, H. Kimura, H. Kojima, L. Chan, Mol Cell Biol, 27 (2007) 6026-6037.
[33] S.C. Frost, M.D. Lane, J Biol Chem, 260 (1985) 2646-2652.
[34] S. Hamann, J. Kiilgaard, T. Litman, F. Alvarez-Leefmans, B. Winther, T. Zeuthen, J Fluoresc, 12 (2002) 139-145.

A3. The inhibition of glycerol permeation through Aquaglyceroporin-3 induced by mercury(II): a molecular dynamics study

This chapter is published:

Angelo Spinello, Andreia de Almeida, Angela Casini and Giampaolo Barone
The inhibition of glycerol permeation through Aquaglyceroporin-3 induced by mercury(II): a molecular dynamics study
J.Inorg.Biochem. (2015) in press
Supplementary information available: DOI: 10.1016/j.jinorgbio.2015.11.027

Abstract

Mercurial compounds are known to inhibit water permeation through aquaporins (AQPs). Although in the last years some hypotheses were proposed, the exact mechanism of inhibition is still an open question and even less is known about the inhibition of the glycerol permeation through aquaglyceroporins. Molecular dynamics (MD) simulations of human aquaporin-3 (AQP3) have been performed up to 200 ns in the presence of Hg^{2+} ions. For the first time, we have observed the unbiased passage of a glycerol molecule from the extracellular to cytosolic side. Moreover, the presence of Hg^{2+} ions covalently bound to Cys40 leads to a collapse of the aromatic/arginine selectivity filter (ar/R SF), blocking the passage of both glycerol and water. Interestingly, the local conformational changes of the protein follow mercury coordination by water and by aminoacidic donor atoms. Overall, the obtained results are important to improve the design of selective AQP inhibitors for future therapeutic and imaging applications.

3.1. Introduction

Aquaporins (AQPs) are trans-membrane proteins that permeate water and other small molecules through biological membranes [1] and [2]. Thirteen AQP isoforms have been identified in humans (AQP0–12), which can be divided into two groups, according to their permeated substrates: selective for water, named orthodox aquaporins (AQP0, AQP1, AQP2, AQP4, AQP5), while aquaglyceroporins can permeate water and small uncharged solutes such as glycerol (AQP3, AQP7, AQP9, AQP10 and AQP11) [3]. A few special cases have been reported: AQP8 is permeable to water, but also to ammonia [4] and can be expressed in intracellular vesicles, mitochondria or cell membrane, while AQP6 is an anion channel with low water permeability and is exclusively expressed in intracellular vesicles [5]. Two other aquaporin isoforms are exclusively intracellular, AQP11 and AQP12, and even though AQP11 was described as a glycerol channel [6], the permeated solutes of AQP12 are still unknown. AQPs are organized as tetramers on membranes and there is some information about the AQP structure from electron and X-ray crystallography [7] showing AQP monomers (~ 30 kDa) containing six membrane-spanning helical domains surrounding a narrow aqueous pore. The most remarkable feature of the aquaporin channels is their high selectivity and efficiency on water or glycerol permeation. It was found that AQPs have two selectivity filters that constitute the main solute barriers: the first one, named aromatic/arginine selectivity filter (ar/R SF), is responsible for size selectivity, and it is formed by three (in aquaglyceroporins) or four (in orthodox aquaporins) residues near the periplasmic/extracellular entrance. A second selectivity filter, composed of two conserved asparagine–proline–alanine (NPA SF) sequence motifs, generates an electrostatic barrier, fundamental for the exclusion of charged ions from the channel, and it is located at the N-terminal ends of two half-helices, at the centre of the channel. In this context, computational methods, in particular classic molecular dynamics (MD) showed to be a useful tool to investigate, with an atomistic detail, the machinery of these macromolecular systems. In fact, several MD simulations were performed on aquaporins in the past years in order to obtain a deep understanding of AQP permeation [8]. For example, some of these studies revealed a pronounced water dipole orientation pattern across the channel, with the NPA region as its symmetry centre [9]. Interestingly, water molecules were found to rotate by 180° on their pathway through the pore.

Moreover, it was demonstrated that the electric field, which prevents the passage of protons, is generated by the half helices B and E, containing the NPA motifs [10].

It is well known that mercurial compounds, such as $HgCl_2$, are able to inhibit water permeation in AQPs [11] and [12]. Mercury(II), due to its high affinity towards sulphur atoms, usually binds to accessible cysteine and methionine residues. Indeed, when *Xenopus* oocytes were transfected with Cys-mutated AQP1 isoforms and the effects of mercury inhibition were evaluated, only one Cys residue, among the mutated ones, was shown to confer sensitivity to the mercurial salt $HgCl_2$, namely Cys189 [13] and [14]. Moreover, cells expressing the Cys189Ser mutant lost sensitivity to $HgCl_2$, and did not show significant inhibition by $HgCl_2$ up to a concentration of 3 mM. Later on, as the atomic-resolution structure of human AQP1 was solved, Cys189 resulted to be positioned inside the channel, just above the ar/R SF [15]. Therefore, it was hypothesised that Hg^{2+} binding to this site was likely to prevent passage of water molecules via steric effects.

Several attempts to investigate the mechanism of AQP inhibition by mercury at a molecular level were performed in the last years. As an example, Savage et al. have reported the crystal structures of two AQPZ mutants, the bacterial homologue of AQP1, in the presence of Hg^{2+} ions, namely Thr183Cys and Leu170Cys [16]. These mutants were introduced to mimic the positions of the two cysteines present in the channel of AQP1. According to the obtained structural information, one Hg^{2+} ion appears to be positioned inside the channel, just below the ar/R SF, suggesting a steric blockage of the channel upon metal binding, while no conformational changes upon metal binding could be observed. However, it should be noted that the bond distance between the Hg^{2+} atom and Thr183Cys in the reported structure is not ideal to demonstrate binding to the thiol residue (ca. 5.6 Å). In the same structure, another Hg^{2+} ion is outside the pore, pointing towards Cys183 (distance of ca. 4.0 Å) and residing in a hydrophilic pocket formed by conserved Glu138 and Ser177, where it makes favourable electrostatic interactions at 2.6 Å and 3.1 Å distances, respectively. Interestingly, Glu138 appears to be important for maintaining the orientation of the backbone carbonyl oxygen of Gly190, Cys191, and Gly192. This may imply that a conformational change can also occur in Thr183Cys-AQPZ bound to mercury, although this mechanism has still to be confirmed.

On the other hand, Hirano et al., using MD simulations, showed that binding of mercury may lead to conformational changes in the ar/R region of bovine AQP1, with a consequential collapse of the selectivity filter, leading to channel blockage [17]. Moreover, another MD study of the Leu170Cys AQPZ mutant [18] showed a shell of five to six water molecules strongly attracted by the mercury atoms, and authors postulated that such cluster of water molecules might cause steric occlusion of the channel. However, this conclusion is questionable due to the labile bonds of metal coordinated water molecules in physiological environment.

Overall, the current literature provides support to two main mechanisms of inhibition of AQPs by mercury: i) the simple occlusion of the water pore by the mercury atoms/ions found in the proximity of the cysteine residues lining the water channel wall and ii) the conformational change (collapse of the water pore) at the ar/R SF region, induced by mercury bound to a neighbouring cysteine residue. Within this frame, several open questions remain to be addressed concerning binding of mercury to AQPs, in particular those regarding the coordination chemistry of $Hg^{2+}$and how this affects the inhibition of water permeation.

In the present study, we have performed MD simulations on the human aquaglyceroporin-3 (hAQP3) in the presence of Hg^{2+} ions covalently bound to a selected cysteinato residue. Our

simulations, due to availability of Graphics Processing Unit (GPU) computing, were significantly longer than the reported ones and allowed us to obtain new insights on the mechanism of AQP inhibition by Hg^{2+}. Several MD studies were performed in the past years, to clarify the energetics and the orientation of glycerol permeation, in particular in AQPZ and glycerol facilitator (GlpF) [15]. However, some bias (usually by using steered molecular dynamics, SMD, or interactive molecular dynamics, IMD) was always included to accelerate a process that was otherwise too slow to be seen within the timescale accessible to classical MD simulations [19], [20], [21] and [22]. Notably, in the present study, for the first time, we also observed the unbiased passage of a glycerol molecule through the channel of hAQP3.

It is worth mentioning that the AQP3 isoform has been selected among others since it is expressed in a wide variety of organs such as the kidney and urinary tract. Interestingly, AQP3 is also highly expressed in skin tumours and AQP3 deficiency or blockage inhibits cell proliferation and reduces tumour growth in mice [23]. Moreover, the involvement of AQP3 expression and functional activity in cell proliferation was further demonstrated using a human epidermoid carcinoma cell line [24], suggesting that the modulation of AQP3 expression or function could be explored for cancer therapeutics. Thus, elucidation of the mechanisms of AQP3 inhibition by mercury could lead to new ideas for the development of selective inhibitors to be used as therapeutic agents and as chemical probes to study AQP3 function in health and disease.

3.2. Results and Discussion

In the following sections, we have evaluated by MD the glycerol permeation of hAQP3 and the effect of Hg^{2+} on both water and glycerol transport in this isoform.

3.2.1. AQP3 permeation by water and glycerol

The quaternary structure of AQP3 was prepared via homology modelling as described above. Thus, 200 ns MD simulations were performed on hAQP3, with and without Hg^{2+}, in the presence of explicit water molecules and of 110 molecules of glycerol, randomly added inside the box (see Figure S1) to mimic its physiological concentration of ca. 0.1–0.2 mM [41]. During the MD simulation we were able to observe the crossing of a glycerol molecule (see Figure 1 and the video file M1.mpg in the supplementary material). In detail, after the passage through the first selectivity filter (at about 40 ns), the glycerol molecule stays nearby the NPA filters until the end of the simulation. This is due to the occurrence of several hydrogen bonds between the glycerol hydroxyl groups and the asparagine residue of the NPA filter. Interestingly, the orientation of the glycerol molecule is retained during the passage. This is not surprising since the channel is for half hydrophilic and half hydrophobic. In detail, the glycerol molecule tries to adopt different molecular geometries to cross the ar/R SF, but the spontaneous passage can only occur when the molecule is oriented with the hydroxyl groups pointing towards Arg218 and the backbone oxygen atoms of Tyr212 (Figure 1), as previously observed in steered molecular dynamics simulation of the *Escherichia coli* glycerol facilitator (Glpf) channel [20]. During the downhill pathway, glycerol is guided by a series of hydrogen bonds with the oxygen backbone atoms of Gly211, Tyr212 and Ala213 until it reaches the NPA SF. Notably, concerning the water transport, the water flipping in the proximity of the NPA filter is correctly reproduced, as it can be seen in Figure 1c, as well as the

hydrogen bond line connecting the water molecules.

hAQP3 is a passive water and glycerol channel, therefore, under equilibrium conditions, the inward and outward transport rates should be the same. Although we have observed several attempts of glycerol molecules to cross the channel in the opposite direction, none of them was able to pass the ar/R SF within the chosen simulation time.

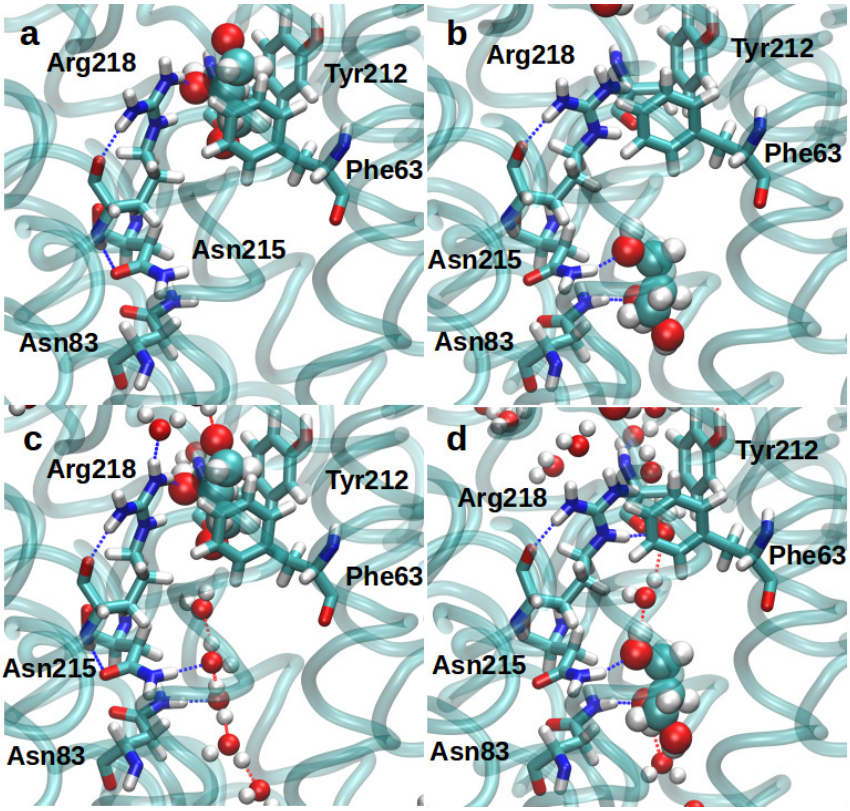

Figure 1. The passage of a glycerol molecule through hAQP3. Glycerol and water are shown in a ball representation. Glycerol is in the proximity of the ar/R filter (a,c) and of the NPA filter (b,d). In c and d the water line is also shown.

3.2.2. AQP3–Hg interaction

Afterwards, the interaction of mercury with hAQP3 was also investigated by MD. Thus, Hg^{2+} ions were bound to deprotonated Cys40 in each AQP monomer. Cys40 is an accessible cysteine residue near the extracellular entrance of the channel in a position close to Cys189 in hAQP1 [26]. The overall conformation of the protein is conserved upon Hg^{2+} binding, as shown by the root mean square displacement (RMSD) plots reported in Figure 2; however several local conformational changes have been observed. Figure 3 shows that, on average, three channels (**2**, **3** and **4**) are closed during the MD simulation of hAQP3, while in one channel (**1**) water flux is only partly reduced (Figure 3). Glycerol molecule is considerably larger in comparison to water and, due to the reduced dimension of the AQP3 channels upon metal binding, its permeation is practically impossible. In all the channels, Hg^{2+} ions adopt an octahedral geometry and the coordination sphere involves the sulphur atom of Cys40 and a

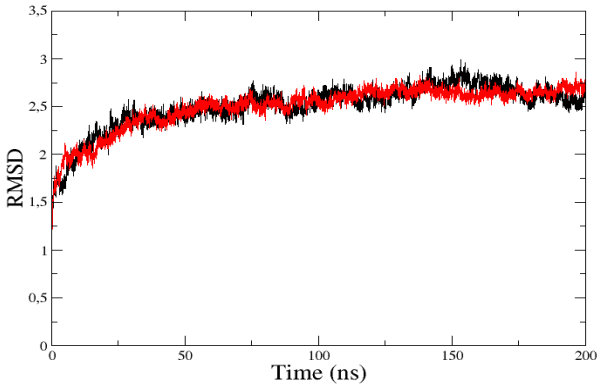

Figure 2. RMSD (Å) of the protein backbone atoms of AQP3 (red) and of the Hg–AQP3 adduct (black).

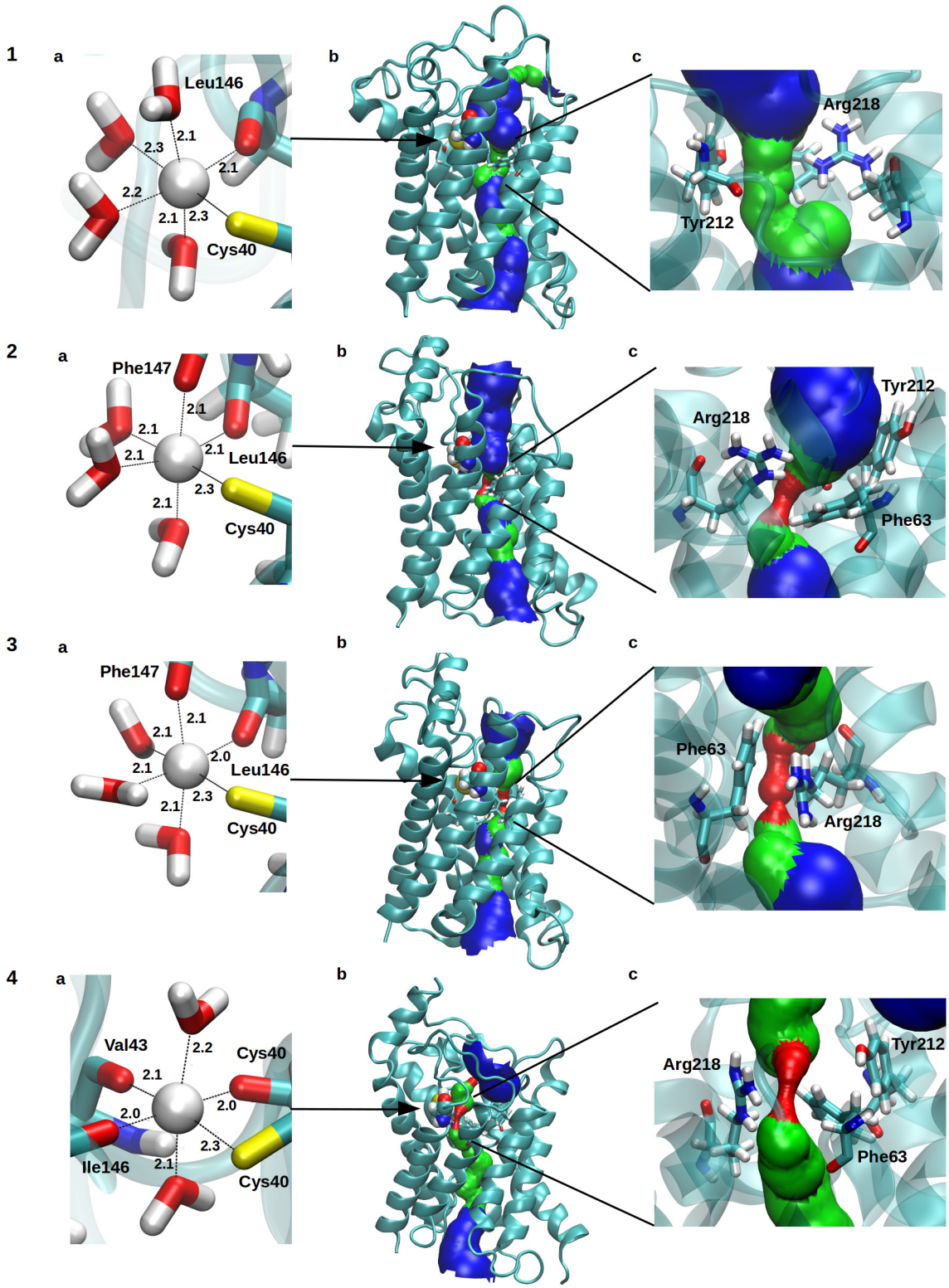

Figure 3. Representative snapshots of the four channels (labelled **1–4**) in AQP3–Hg along the MD simulation. From left to right: the Hg coordination (distances in Å) (a), a picture of the AQP monomer with Cys40 and the channel highlighted (b) and a closer view of the ar/R filter (c). Red colour indicates a pore radius smaller than the size of a water molecule; green colour indicates a pore size enough to allow the entrance of a single water molecule. Blue colour indicates a pore radius double than the green pore.

variable number of carbonyl oxygen atoms and of "labile" water molecules. As an example, such distorted octahedral coordination of mercury has been confirmed by X-ray crystallography investigations on $Hg[Cu(C_{17}H_{16}N_2O_2)SCN]_2$ and $Hg[Cu(C_{18}H_{18}N_2O_2)SCN]_2$ compounds [42]. Other previous examples of this metal coordination can be found in the literature [43-46].

Interestingly, the mechanism of channel closure is different for each channel. After a closer inspection of the structure, this behaviour could be correlated to the different coordination environments for mercury (Figure 3, panel a). In all cases, the Hg^{2+} ion adopts an octahedral geometry, but the ligands vary depending on the monomer channel. In the case of the channel labelled **1**, the coordination sphere of mercury is constituted by the sulphur atom of Cys40, four water molecules and the carbonyl oxygen of Leu146. Interestingly, channel **1** remains always open during the MD simulations, although it undergoes size reduction due to the presence of Arg218 (Figure 3-1c). In the case of channels **2** and **3**, mercury binding induces complete blockage of the pore due to protein conformational changes. The mercury coordination is similar in these two cases, with Cys40, three water molecules and the backbone carbonyl oxygen of Leu146 and Phe147. Specifically, closure of the channels is due to the steric hindrance of Phe63 in channel 2 and of Arg218 in channel 3. In fact, in normal conditions, Phe63 is located near the channel wall, but, upon binding of Hg^{2+} (Figure 3-2c), a rotation of the phenyl ring of about 90° is clearly visible, leading to the pore closure (see also Figure S2c). Concerning channel **3**, its radius along the Z axis is plotted in Figure 4. This picture clearly shows that the pore radius reaches a minimum of ca. 1.5 Å in AQP3-wt (red line), and of less than 0.5 Å in AQP3–Hg (black line). The channel is closed in the region of the ar/R filter, while other parts of the channel seem to be only slightly affected by the presence of the Cys-Hg^{+} residues.

Finally, channel **4** is completely closed, due to the participation of both Arg218 and Phe63, as observed in the case of channels **2** and **3**. Interestingly, in this case (Figure 3-4a) only two water molecules are involved in mercury coordination plus the carbonyl oxygen atom of Cys40, Val43 and Ile146. In general, it was observed that the increase in the number of coordinated amino acids to Hg^{2+} dramatically increases the distortion of AQP3 conformation, leading to a collapse of the ar/R filter and to pore closure, as previously observed also in the case of bovine AQP1 [17].

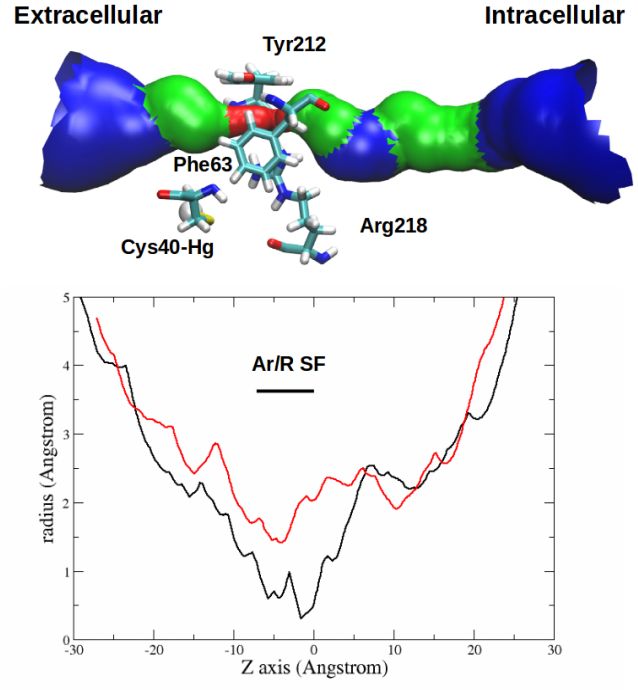

Figure 4. Channel 3 pore radius, comparison between AQP3-Hg (black) and AQP3-wt (red). The AQP3-Hg channel 3 is shown on the top.

Concerning the closure of channel **3**, it is interesting to notice the displacement of Arg218 due to the presence of the Hg^{2+} ion from the very first steps of the simulation (see Figure 5). For example, in AQP3-wt, Arg218 is anchored in its position by hydrogen bonds established with its backbone and with Phe147 (Fig. 6b). This keeps this residue near the channel wall under physiological conditions. After a few MD steps we observed the coordination of Hg^{2+} by Phe147 (see both channels **2** and **3**,

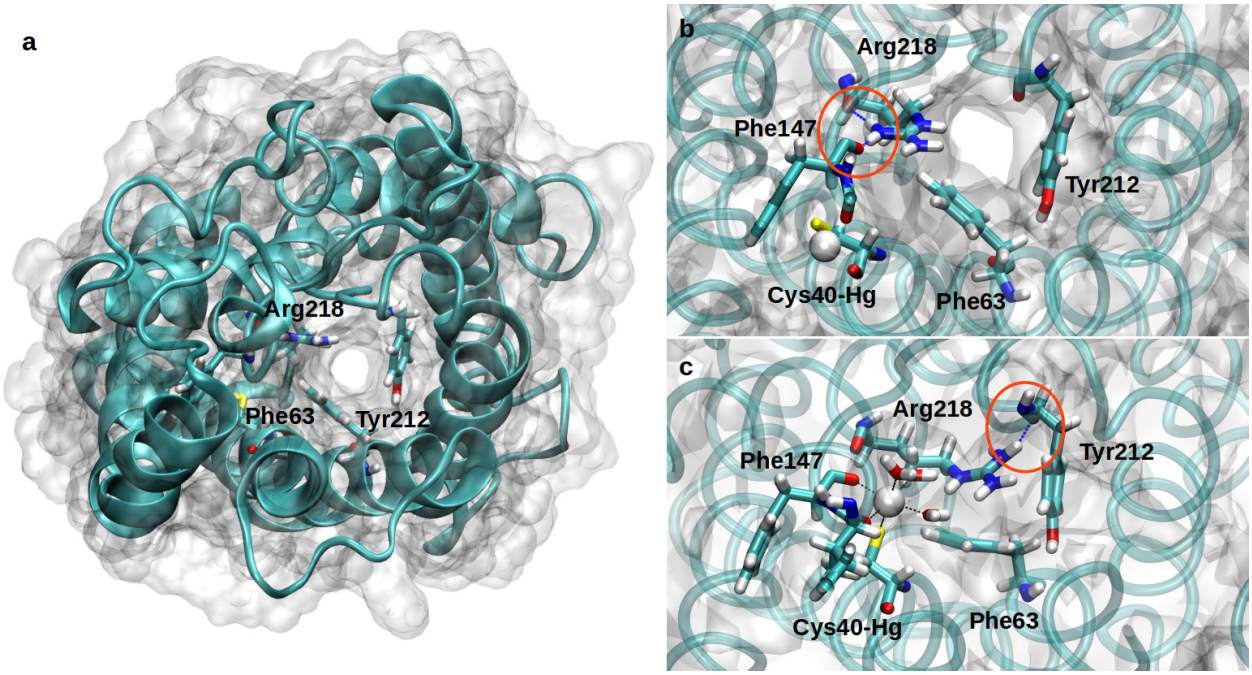

Figure 5. Mechanism of Arg218 displacement in channel 3. Hydrogen bonds between Arg218, Tyr212, Phe147 are shown and highlighted by circles. (a,b) Top view of the starting structure of the open channel (extracellular opening). (c) Representative snapshot at the equilibrium, showing the occlusion of the channel by the displacement of Arg218.

Figures 3-2 and 3-3). When the hydrogen bond between Ar218 and Phe63 is lost, Arg218 moves towards the channel establishing new hydrogen bonds with other residues, such as Tyr212, leading to a complete occlusion of the pore (Figures 3-3c and 5c).

Finally, we have also observed a movement of a flexible loop near the extracellular entrance that partially closes channel **1** (Figure 6). Although in this case water flux in channel is only partially reduced, it is impossible for glycerol to pass through the membrane when the channel adopts this conformation. A similar closure was recently reported in the case of spinach plasma membrane aquaporin SoPIP2 [47]. This may be correlated with the presence of the mercury since no such loop movement was observed in the Hg-free AQP3 trajectory.

As an example, in channel **1** two glycerol molecules remain trapped between the ar/R filter and the closed loop for more than 150 ns (not shown). This is another proof that, although water is still flowing, glycerol permeation is completely inhibited by the presence of the mercury.

Interestingly, AQP3's water and glycerol permeation has been reported to be inhibited by endogenous metals, such as copper and nickel [48] and [49]. Notably, two of the three Cu^{2+} and Ni^{2+}-sensitive residues are located in extracellular loops, which gives further indication that protein conformational changes may be crucial for the mechanism of AQP3 inhibition.

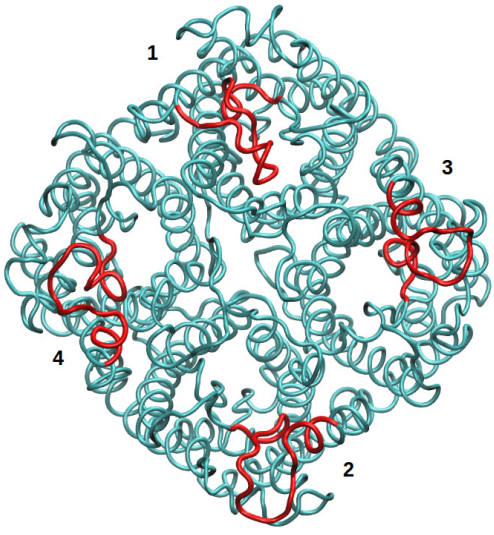

Figure 6. Snapshot of AQP3-Hg tetramer (Top view), with extracellular flexible loops highlighted in red and channels labelled 1-4.

3.3. Conclusions

In the present paper we report on the mechanism of inhibition by mercury of hAQP3, studied by MD. Our *in silico* approach suggests that the coordination

environment of Hg^{2+} ions is determinant for the inhibition of AQP3 water/glycerol flux, since it may induce major conformational changes in the protein structure leading to pore closure. The multiplicity of structures observed in the four channels of hAQP3–Hg is essentially related to two different mechanisms of pore closure: one involving the rotation of the aromatic ring of Phe63 (see Figure 3-2c); and the other concerning the displacement of Arg218 (see Figures 3-3c and 5c). These two mechanisms correspond to a specific octahedral coordination environment of Hg^{2+}, involving the sulphur of Cys40, the carbonyl oxygen atoms of Leu146 and Phe147, and three water molecules (Figures 3-2a and 3-3a). It is interesting to notice that the different Hg^{2+} coordination observed in channel **1**, involving the Cys40 sulphur, the carbonyl oxygen atom of Leu146 and four water molecules, leaves channel 1 open to water permeation. The closure of channel 4 to both glycerol and water is the result of the coexistence of the two mechanisms described above, while flexible loops near the extracellular entrance may also hinder glycerol permeation (Figure 6).

An example of the biological effect of Hg^{2+} coordination is water flux reduction related to the displacement of Arg218 after the breaking of the important hydrogen bond with Phe147. On the other hand, with the same mechanism, glycerol permeation in AQP3–Hg is completely inhibited by the presence of Hg^{2+} ions coordinated by cysteine residues.

Interestingly, the degree of pore closure follows the decrease of the number of labile water molecules coordinated to the Hg^{2+} ion, substituted by carbonyl ligands: four water molecules for a partial pore closure (Figure 3-1); three for an intermediate closure (Figures 3-2 and 3-3); and two for a complete pore closure to both glycerol and water (Figure 3-4).

Overall, due to the broad range of functions of AQPs in physiology and in disease states, the necessity of selective modulators (inhibitors) of AQP channels that could be used as either chemical probes to detect AQP function in biological systems, or as innovative therapeutic agents in a variety of disease states, is impellent. In this context, the understanding of the mechanisms of inhibition by mercury may open the way to new strategies to selectively target different AQPs and to achieve optimization of other metal-based inhibitors, such as the recently reported gold(III) compounds, and selective inhibitors of aquaglyceroporin isoforms [26, 50, 51]. In fact, gold compounds have also been hypothesised to bind to Cys40 in AQP3, which may also cause protein distortion towards a closed channel state, more than direct steric blockage by the gold(III) ions.

3.4. Experimental section

Homology modelling: The 3D structure of hAQP3 was obtained by homology modelling using the Molecular Operating Environment (MOE 2012.10) (CCG 2012) [25]. The choice of a template structure was based on the sequence identity between hAQP3 and the sequence of the AQPs with available resolved structures from human, bacteria and *Plasmodium falciparum*. The isoform showing the highest sequence similarity with hAQP3 is the bacterial isoform GlpF, which was then chosen as a template structure to generate a homology model of hAQP3, following the same approach as previously reported [26]. Three resolved structures for bGlpF, crystallized either with or without glycerol and solved by X-ray diffraction, were retrieved from the Protein Data Bank. Among them, the template was selected that had the best resolution (2.70 Å) without any substrate (pdb 1LDI) [27]. The tetrameric form was assembled and the structure was prepared and protonated at pH 7 by using the Amber12EHT force field. 50 intermediate models of AQP3 were generated and averaged to obtain the final homology model. The model obtained was checked for reliable rotamers involving the side chains in the regions of ar/R SF and NPA, by comparison with the available crystal structures of all the other human and microbial AQP isoforms (pdb codes 1H6I, 3GD8, 3D9S, 1RC2, 1LD1 and 3C02). The structure was protonated at pH 7 and an energy minimization refinement was performed, with fixed Cα atoms.

Molecular dynamics: The mechanism of water and glycerol flux inhibition in AQP3 by mercury was investigated by MD simulations, following a recently reported procedure [28], [29] and [30]. MD simulations were carried out through the GROMACS 5.0.4 software package [31], using the Amber ff99SB-ILDN force field [32]. The parameters for the

Cys-Hg^+ adduct were taken from a previous study [17]. AQP models were embedded into a membrane formed by 166 POPC lipid using the charmm-gui online server [33] and [34].

Glycerol molecules were randomly inserted inside the water layers using the PACKMOL software [35]. The charge of the protein was neutralized with 8 Cl^- in the case of AQP1 and with 4 Na^+ in the case of AQP3. Explicit solvent simulations were performed in the isothermal-isobaric NPT ensemble, at the temperature of 300 K. Explicit solvent simulations were performed in the NPT ensemble, at a temperature of 300 K, under control of a Nosé–Hoover thermostat [36]. Pressure was maintained at 1 atm using a Parrinello–Rahman barostat [37] and semiisotropic pressure coupling. The particle mesh Ewald method was used to describe long-range electrostatic interactions [38]. The timestep for integration was 2 fs and all covalent bonds constrained with the LINCS algorithm. Preliminary energy minimizations were run for 5000 steps with the steepest descend algorithm. During a 10 ns equilibration AQP atoms were harmonically restrained with a force constant of 1000 kJ mol^{-1} nm^{-2}. For each system a 200 ns molecular dynamics simulation was performed. The MD trajectories were analysed using the VMD software [39]. The radii of the cylindrical channels of AQPs were determined using the HOLE2 software [40].

Refererences

[1] G.M. Preston, T.P. Carroll, W.B. Guggino, P. Agre, Science. 256 (1992) 385–387.
[2] M. Borgnia, S. Nielsen, A. Engel, P. Agre, Annu. Rev. Biochem. 68 (1999) 425–458.
[3] G. Benga, Mol. Aspects Med. 33 (2012) 514–517.
[4] L.R. Soria, E. Fanelli, N. Altamura, M. Svelto, R.A. Marinelli, G. Calamita, Biochem. Biophys. Res. Comm. 393 (2010) 217–221.
[5] M. Yasui, A. Hazama, T.H. Kwon, S. Nielsen, W.B. Guggino, P. Agre, Nature 402 (1999) 184–187.
[6] A. Madeira, S. Fernández-Veledo, M. Camps, A. Zorzano, T.F. Moura, V. Ceperuelo-Mallafré, J. Vendrell, G. Soveral, Obesity 22 (2014) 2010–2017.
[7] T. Gonen, T. Walz, Q. Rev. Biophys. 39 (2006) 361–396.
[8] A.R. Binesh, R. Kamali, Biophys. Chem. in press, doi: 10.1016/j.bpc.2015.10.002.
[9] B.L. de Groot, H. Grubmüller, Science. 294 (2001) 2353–2357.
[10] E. Tajkhorshid, P. Nollert, M.Ø. Jensen, L.J.W. Miercke, J. O'Connell, R.M. Stroud, K. Schulten, Science. 296 (2002) 525–530.
[11] R.I. Macey, R.E. Farmer, Biochim. Biophys. Acta. 211 (1970) 104–106.
[12] A.S. Verkman, M.O. Anderson, M.C. Papadopoulos, Nat. Rev. Drug Discov. 13 (2014) 259–277.
[13] G.M. Preston, J.S. Jung, W.B. Guggino, P. Agre, J. Biol. Chem. 268 (1993) 17–20.
[14] R. Zhang, A.N. van Hoek, J. Biwersi, A.S. Verkman, Biochemistry (Mosc.). 32 (1993) 2938–2941.
[15] H. Sui, B.G. Han, J.K. Lee, P. Walian, B.K. Jap, Nature. 414 (2001) 872–878.
[16] D.F. Savage, R.M. Stroud, J. Mol. Biol. 368 (2007) 607–617.
[17] Y. Hirano, N. Okimoto, I. Kadohira, M. Suematsu, K. Yasuoka, M. Yasui, Biophys. J. 98 (2010) 1512–1519.
[18] Y. Zhang, Y. Cui, L.Y. Chen, Biophys. Chem. 160 (2012) 69–74.
[19] Y. Wang, K. Schulten, E. Tajkhorshid, Struct. 13 (2005) 1107–1118.
[20] M.Ø. Jensen, S. Park, E. Tajkhorshid, K. Schulten, Proc. Natl. Acad. Sci. 99 (2002) 6731–6736.
[21] P. Grayson, E. Tajkhorshid, K. Schulten, Biophys. J. 85 (2003) 36–48.
[22] J. Hénin, E. Tajkhorshid, K. Schulten, C. Chipot, Biophys. J. 94 (2008) 832–839.
[23] M. Hara-Chikuma and A. S. Verkman, Mol. Cell. Biol. 28 (2008), 326–332.
[24] A. Serna, A. Galán Cobo, C. Rodrigues, I. Sanchez-Gomar, J. J. Toledo-Aral, T. F. Moura, A. Casini, G. Soveral, M. Echevarrıa, J. Cell. Physiol. 229 (2014) 1787–1801.
[25] M.O.E. (MOE), Chemical Computing Group Inc., Montreal, Quebec, Canada, https://www.chemcomp.com.
[26] A.P. Martins, A. Marrone, A. Ciancetta, A. Galán Cobo, M. Echevarría, T.F. Moura, N. Re, A. Casini, G. Soveral, PLoS ONE. 7 (2012) e37435.
[27] D. Fu, A. Libson, R. Stroud, The Structure of G1pF, A Glycerol Conducting Channel, in: G.B. Organizer, J.A. Goode (Eds.), Ion Channels: From Atomic Resolution Physiology to Functional Genomics, John Wiley & Sons, Ltd, 2002: pp. 51–65. http://onlinelibrary.wiley.com/doi/10.1002/0470868759.ch5/summary (accessed September 15, 2015).
[28] A. Spinello, M.G. Ortore, F. Spinozzi, C. Ricci, G. Barone, A. Marino Gammazza, A. Palumbo Piccionello, RSC Adv. 5 (2015) 49871–49879.
[29] A. Terenzi, R. Bonsignore, A. Spinello, C. Gentile, A. Martorana, C. Ducani, B. Högberg, A.M. Almerico, A. Lauria, G. Barone, RSC Adv. 4 (2014) 33245–33256.
[30] L. Lentini, R. Melfi, A. Di Leonardo, A. Spinello, G. Barone, A. Pace, A. Palumbo Piccionello, I. Pibiri, Mol. Pharm. 11 (2014) 653–664.
[31] D. Van Der Spoel, E. Lindahl, B. Hess, G. Groenhof, A.E. Mark, H.J.C. Berendsen, J. Comput. Chem. 26 (2005) 1701–1718.
[32] K. Lindorff-Larsen, S. Piana, K. Palmo, P. Maragakis, J.L. Klepeis, R.O. Dror, D.E. Shaw, Proteins. 78 (2010) 1950–1958.
[33] S. Jo, T. Kim, V.G. Iyer, W. Im, J. Comput. Chem. 29 (2008) 1859–1865.
[34] E.L. Wu, X. Cheng, S. Jo, Huan Rui, K.C. Song, E.M. Dávila-Contreras, Y. Qi, J. Lee, V. Monje-Galvan, R.M. Venable, J.B. Klauda, W. Im, J. Comput. Chem. 35 (2014) 1997–2004.
[35] L. Martínez, R. Andrade, E.G. Birgin, J.M. Martínez, J. Comput. Chem. 30 (2009) 2157–2164.
[36] W.G. Hoover, Phys. Rev. A. 31 (1985) 1695–1697.
[37] M. Parrinello, A. Rahman, J. Appl. Phys. 52 (1981) 7182–7190.
[38] T. Darden, D. York, L. Pedersen, J. Chem. Phys. 98 (1993) 10089–10092.
[39] W. Humphrey, A. Dalke, K. Schulten, J. Mol. Graph. 14 (1996) 33–38.

[40] O.S. Smart, J.G. Neduvelil, X. Wang, B.A. Wallace, M.S.P. Sansom, J. Mol. Graph. 14 (1996) 354–360.
[41] E.F. Coyle, J.M. Hagberg, B.F. Hurley, W.H. Martin, A.A. Ehsani, J.O. Holloszy, J. Appl. Physiol. Respir. Environ. Exerc. Physiol. 55 (1983) 230–235.
[42] L.T. Yıldırım, R. Kurtaran, H. Namli, A.D. Azaz, O. Atakol, Polyhedron. 26 (2007) 4187–4194.
[43] M. Sandström, Persson Ingmar, S. Ahrland, Acta Chem. Scand. 32 (1978) 607–625.
[44] J.A. Carrabine, M. Sundaralingam, Biochemistry (Moscow) 10 (1971) 292–299.
[45] K. Krot, A.L. Llamas-Saiz, N. Vembu, K.B. Nolan, Z. Anorg. Allg. Chem. 633 (2007) 1900–1910.
[46] S.A. Al-Jibori, Z.S. Afandi, K. Merzweiler, C. Wagner, H. Schmidt, S. Basak-Modi, G. Hogarth, Polyhedron. 81 (2014) 442–449.
[47] S. Törnroth-Horsefield, Y. Wang, K. Hedfalk, U. Johanson, M. Karlsson, E. Tajkhorshid, R. Neutze, P. Kjellbom Nature 439 (2006) 688–694.
[48] M. Zelenina, S. Tritto, A.A. Bondar, S. Zelenin, A. Aperia, J. Biol. Chem. 279 (2004) 51939–51943.
[49] M. Zelenina, A.A. Bondar, S. Zelenin, A. Aperia, J. Biol. Chem. 278 (2003) 30037–30043.
[50] A.P. Martins, A. Ciancetta, A. de Almeida, A. Marrone, N. Re, G. Soveral, A. Casini, ChemMedChem 8 (2013) 1086–1092.
[51] A. Madeira, A. de Almeida, C. de Graaf, M. Camps, A. Zorzano, T.F. Moura, A. Casini, G. Soveral, ChemBioChem. 15 (2014) 1487–1494.

A4. Exploring the gating mechanisms of aquaglyceroporins: new clues for inhibitors design?

This chapter is adapted from two submitted manuscripts:

Andreia de Almeida*, Ana P. Martins*, Andreia Mósca, Hein J. Wijma, Catarina Prista, Graça Soveral, Angela Casini
Exploring the gating mechanisms of aquaporin-3: new clues for inhibitors' design?
Mol.Biosyst.(2016) Accepted
Supplementary information available: DOI: 10.1039/C6MB00013D

Paula Martins*, Andreia de Almeida*, Andreia Mósca*, Hein J. Wijma, Ana Madeira, Maria C. Loureiro-Dias, Angela Casini, Teresa F. Moura, Catarina Prista, Graça Soveral
Human aquaporin-7 expressed in yeast reveals pH gating
(submitted)

*Authors contributed equally to this work

Mol.Biosyst.

Abstract

Aquaporins (AQPs) are membrane channels that facilitate the transport of water and/or other small molecules such as glycerol across cellular membranes having important roles in physiology and homeostasis. Mechanisms of water flux gating through classical AQPs have been described. However less is known about the regulation of glycerol transport through members of the aquaglyceroporin subfamily. In this study, the pH gating of human AQP3 and its effects on both water and glycerol permeability has been fully characterized for the first time using a human red blood cell model (hRBC). For comparison, the effects of pH on the gating of rat AQP3 have also been characterized in yeast. The obtained results highlight similarities as well as differences between the two isoforms. We also investigated the molecular mechanism of hAQP3 pH gating *in silico*, which may disclose new pathways to AQP regulation by small molecule inhibitors, and therefore may be important for drug development. Additionally we used a yeast heterologous expression system for expression and functional analysis of the human AQP7 (hAQP7) isoform. hAQP7 showed to transport water and glycerol in the yeast system and its activity was confirmed by inhibition with the gold(III) compound Auphen. Importantly, we disclose for the first time hAQP7 regulation by external pH changing from an open to closed state when pH drops from 7.5 to 5. Also here, *in silico* studies allowed to identify the putative amino acidic residues involved in pH gating and important monomer-monomer interactions within the hAQP7 tetramer, which could explain the achievement of maximal protein permeation ability at mammalian physiological pH range. The obtained results are discussed in terms of the possible physiological roles of pH gating in aquaglyceroporins.

4.1. Introduction

Aquaporins (AQPs) are a family of small membrane proteins belonging to the Major Intrinsic Protein (MIP) superfamily. They are expressed in almost every organism and are involved in the bidirectional transfer of water and small solutes across cell membranes in response to osmotic and hydrostatic pressure gradients, having important roles in physiology and homeostasis.

The presently known mammalian AQPs (AQP0-AQP12) can be divided into three groups according to their primary structure and permeability [1]: i. orthodox or classical AQPs, considered to be water selective (AQPs 0, 1, 2, 4, 5, 6 and 8). Although AQP6 has been proved to be a pH-sensitive chloride channel or possibly a nitrate channel and AQP8 has been found permeable to urea, they are both classified under the classical AQP group; ii. aquaglyceroporins (AQP3, 7, 9, 10) permeable to glycerol and other small solutes, in addition to water; and iii. superaquaporins (AQP11, 12), with lower sequence homology to the other mammalian AQPs and unique subcellular localization [2], whose permeability specificity has been difficult to establish, although AQP11 was recently reported to transport both water and glycerol [3].

AQPs are considered crucial to maintain the water homeostasis in many epithelia and endothelia involved in fluid transport [4]. In addition, due to their unique ability to transport glycerol, aquaglyceroporins have important roles in glycerol metabolism in non-fluid transport tissues such as in skin, fat and liver [5-7]. In particular, AQP7, a member of aquaglyceroporin subgroup, has been associated with the adipose tissue, where is the major source of glycerol efflux from adipocytes [7-9] but it is also involved in maintenance of sperm quality and motility in human

testis [10]. Remarkably, AQP7 is also found in cardiac tissue, where information about the role of aquaporins is scarce [11]. A recent study reported that glycerol transported intracellularly by AQP7 could be used as an alternative substrate for energy production in cardiomyocytes, under cardiac stress [12].

Interestingly, AQPs, as many other channels and transporters, can be subjected to regulation. Indeed, it has been shown that the function of various eukaryotic water selective aquaporins are regulated by post-translational modifications, such as phosphorylation [13-16], pH [17, 18], divalent cations [19, 20], or membrane surface tension [14, 21-23].

Less is known about the regulation of aquaglyceroporins and glycerol transport. Only a few studies have shown regulation of permeability of AQP3 by pH, copper and nickel [24-26], indicating that aquaglyceroporins may also be subjected to pH gating. In general, we believe that a better understanding of human aquaglyceroporin regulation in biological environments would facilitate the identification of mechanisms of water/glycerol fluxes modulation, which may lead to the design of novel inhibitors with potential therapeutic applications for human health.

The other gated mammalian aquaporins, AQP0, expressed in the lens, and AQP6, expressed in the intercalated cells of the kidney collecting ducts, appear to have low permeability at physiological pH, increasing below pH 7 and with a maximum of permeability at about and below pH 6.5, respectively [20, 27]. On the other hand, rat AQP3 showed the opposite behavior, with an overall maximum of permeability for water and glycerol above pH 6.5, decreasing with lower pH, until completely closed at pH 5 [28, 29]. As AQP0 and AQP6 are both orthodox aquaporins and AQP3 permeates glycerol, these differences may be correlated to protein function.

In this context we decided to focus our investigation on two isoforms: AQP3 and AQP7. AQP3 has a wide tissue distribution in the epithelial cells of kidney, airways and skin, suggesting a role in water reabsorption, mucosal secretions, skin hydration, and cell volume regulation [30]. Moreover, recent studies demonstrated an aberrant AQP3 expression in tumor cells of different origins, particularly aggressive tumors [31], suggesting this enhanced protein expression to be of diagnostic and prognostic value. On the other hand, AQP7 is expressed in tissues related to metabolism, such as liver and adipocytes, which indicates an important role of this isoform in energy metabolism [32].

Thus, in collaboration with the group of Prof. G. Soveral (University of Lisbon) two different models were used : i) human red blood cells (hRBC), expressing human AQP3, and ii) yeast cells expressing hAQP7 and rAQP3 - to investigate the pH gating of the two aquaglyceroporin isoforms.

It is worth mentioning that due to its intrinsic low water plasma membrane permeability, yeast has been reported as a suitable system for heterologous individual aquaporin expression [33]. Yeasts are easily and permanently transformed (an advantage to transient transfection in *Xenopus laevis* oocytes and mammalian cell lines), have short doubling times, can be maintained in diverse environments and even the composition of the intracellular medium can be controlled, creating a variety of conditions to study aquaporin regulation [18, 21, 23]. On the other hand, hRBC have been shown to be a very good natural model to assess AQP3 function since they only express one orthodox aquaporin (AQP1) and one aquaglyceroporin isoform (AQP3) [34].

Therefore, we selected *Saccharomyces cerevisiae* strains, silenced on endogenous orthodox aquaporins (Aqy1 and Aqy2) to overexpress hAQP7. In our experimental conditions, the endogenous aquaglyceroporins YFL054c and Fps1 are inactive since the first does not seem to

mediate glycerol entry and the second is in a closed state induced by high external osmolarity in the permeability assays [35]. In addition, we used hRBC to assess hAQP3 function. Water and glycerol permeability was assessed in both cases by stopped flow spectroscopy. It is worth mentioning that the activity of heterologous aquaporins anchored in the membrane of aquaporin-null strains has been powerfully characterized by this method [18, 23, 36]. Moreover, the use of a fluorescence self-quenching methodology for assessing cell volume changes in yeast walled cells [37] induced by solute gradients represents an added value for the study of aquaglyceroporins. This methodology opens new perspectives to measure aquaglyceroporin activity in minimally disturbed cells that are quite stable during a rather long experiment.

Overall, we were able to unravel for the first time the gating of hAQP7 by external pH, to confirm previously reported studies on rAQP3, and to study the gating of glycerol transport in hAQP3, described here for the first time. Our results show that all three isoforms (hAQP3, rAQP3 and hAQP7) are gated by pH, important differences are observed among AQP3 and AQP7 isoforms. Through molecular modeling studies, we investigated the pH dependent closure/opening of both human channels at a molecular level, allowing us to predict gating mechanisms of the two isoforms and possibly other aquaglyceroporins. The obtained results are discussed in terms of the putative physiological roles of pH gating in aquaglyceroporins.

4.2. Results and Discussion

4.2.1. pH gating of AQP3

Rat aquaporin-3 (rAQP3) has been described to be gated by pH, when expressed in *Xenopus* oocytes [29] and other authors identified the key residues for pH gating in human AQP3 [28]. However, the details of the pH gating of the human isoform of AQP3 are not known, as well as there is no information if the gating affects the glycerol transport, in this isoform, in the same manner. Thus, we started by evaluating the gating of rat AQP3, in a yeast cell model, well characterized by our group [36], followed by the characterization of the pH gating of human AQP3, in a human red blood cell model (hRBC), also well characterized by us as a model for AQP3 function [34].

Following the evaluation of AQP3 function upon pH changes, we used *in silico* approaches to investigate, in detail, the mechanism of pore closure.

4.2.1.1. pH gating of rat AQP3 in yeast

In our study we first evaluated rAQP3 gating, in a yeast model, using stopped-flow spectroscopy. Functional aquaporin studies, performed using heterologous expression of aquaporins in an *aqy*-null strain of *Saccharomyces cerevisiae*, have been previously described by our group [38]. This yeast strain expresses also two endogenous aquaglyceroporins, which were not silenced: Fps1 and YFL054c. Fps1 is crucial for yeast osmotic adaptation being inactivated within seconds after a hyper-osmotic shock to ensure intracellular retention and accumulation of glycerol [39]. Thus, in our experimental conditions it remains in a closed state induced by high external osmolarity in the permeability assays. Additionally, YFL054c is not permeated by glycerol under normal conditions or when subjected to hyper or hypo osmotic stress [35]. Moreover, deletion of the two aquaglyceroporins can cause changes in cell membrane content, lead to cell wall stress and

increased temperature sensitivity, which could influence the output in our experimental setup.[35] Therefore, we optimized an expression system where only the orthodox aquaporins were silenced.

Yeast cells were transformed with either the empty plasmid (control cells) or the plasmid containing the rat AQP3 gene (mentioned as rAQP3 cells, for clarity). The expression of rAQP3 in the S. cerevisiae model was assessed by fluorescence microscopy, using GFP tagging. In transformed cells, rAQP3-GFP is localized at the cellular membrane, while cells with empty plasmid have a homogeneous cytoplasmic distribution (Figure 1).

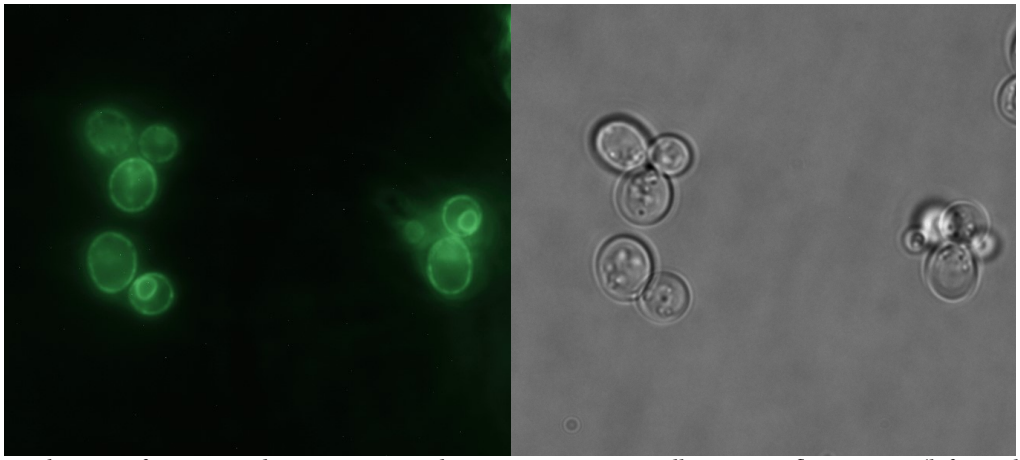

Figure 1. Localization of GFP-tagged rAQP3 expressed in S. cerevisiae aqy-null strain. Epifluorescence (left panel) and phase contrast (right panel) images of *S. cerevisiae* aqy-null strains transformed with rAQP3.

Stopped-flow technique allows volume monitoring of cells subjected to hypo and hyperosmotic stress: when cells are exposed to hyperosmotic shock with impermeant solutes, water outflow induces cell shrinkage. Conversely, when the osmotic shock is provided by a permeable solute as glycerol, cells first shrink due to water outflow and afterwards swell again due to glycerol passage. Thus, water and glycerol permeability is then evaluated according to cell swelling or shrinkage monitored by 90° light scattering, detected by the stopped-flow. In the case of the yeast cell model, the cells are pre-loaded with carboxifluorescein, and the fluorescence intensity reflects volume changes.

At first, in order to evaluate if the observed effect was due to AQP3 being expressed in the yeast cells, both groups of control and rAQP3 were incubated at two different pH values, namely pH 5 and 7. These pH conditions were chosen based on previous literature [28, 29], to have closed (pH 5) and open (pH 7) AQP3.

In Figure 2 the water and glycerol permeability (P_f and P_{gly}, respectively) of control and rAQP3 cells are shown. It is possible to observe that, while control cells have no glycerol permeability, they do show basal water permeability at both tested pH conditions, due to the intrinsic water permeability of the membrane lipid bilayer. Interestingly, from panel C of Figure 2 it is evident that, at pH 5, there is no permeation by glycerol, with a significant increase at pH 7, which clearly demonstrate the close and open states of rAQP3.

Since the control cells present a basal water permeability that is not altered by the expression of rAQP3 when incubated at pH 5, it is possible to normalize the P_f that corresponds to the permeability of rAQP3 alone. Knowing from these results (Figure 2) and previous studies that hAQP3 is in a closed state at low pH (ca. 5),[29] the normalized water permeability via rAQP3 was obtained by subtracting the permeability values of control cells at each pH value. For P_{gly}, this subtraction was not necessary since the control cells show no glycerol permeability at any pH. The

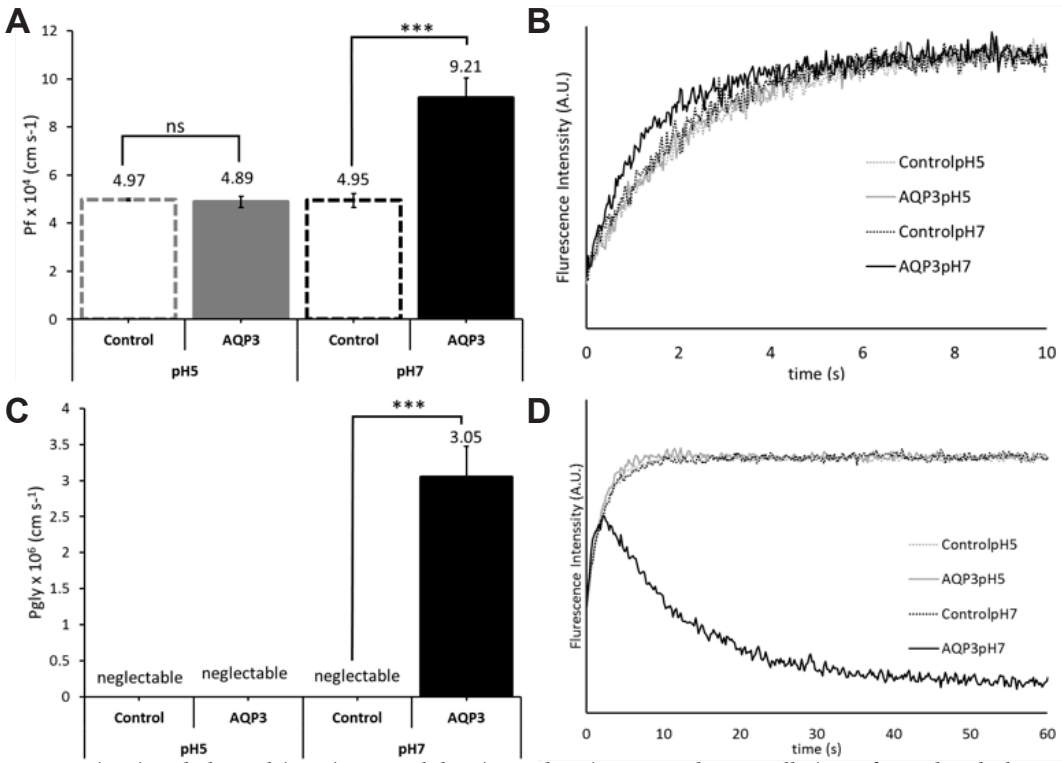

Figure 2. Water (A,B) and glycerol (C, D) permeability (P_f and P_{gly}) in control yeast cells (transformed with the empty vector PUG) (dashed) and in yeast expressing rAQP3 (solid) at pH 5 (grey) and 7 (black). Panel A shows the water permeability (P_f) of control and AQP3-expressing cells, at pH 5 and pH 7. Panel B shows the changes in fluorescence intensity obtained when yeast transformants are confronted with a hyperosmotic sorbitol solution of tonicity 1.25 triggering cell shrinkage due water outflow. Panel C shows the glycerol permeability (P_{gly}) of control and AQP3-expressing cells, at pH 5 and pH 7, while panel D shows the changes of fluorescence intensity obtained when cells are confronted with a hyperosmotic glycerol solution. After a first water outflow due to the osmotic gradient, the AQP3-expressing cells re-swell due to glycerol entrance at pH7. *** p<0.001

rAQP3 permeability for both water and glycerol are shown in Figure 3. We can observe that the channel is closed for both water and glycerol between pH 5 and 6 and has maximum permeability at pH 6.5 (glycerol) and pH 7 (water), respectively. This behaviour and Hill slope values found for water and glycerol in the rAQP3 isoform (see Table 1) are similar to those reported previously [29].

4.2.1.2. pH gating of human AQP3

Afterwards, we evaluated hAQP3 gating in hRBC. hRBC co-express hAQP1 (selective for water) and hAQP3 (permeating water and glycerol) and thus both isoforms contribute for water permeability. Previous studies showed that human AQP1 is not gated by pH [20, 29], and thus any pH-dependent effect on hRBC water permeability would be due to individual gating of hAQP3. Knowing that pH does not influence water permeation via lipid bilayer nor via hAQP1, water permeability corresponding exclusively to hAQP3 was obtained by subtracting the total cell permeability at pH 5 (where

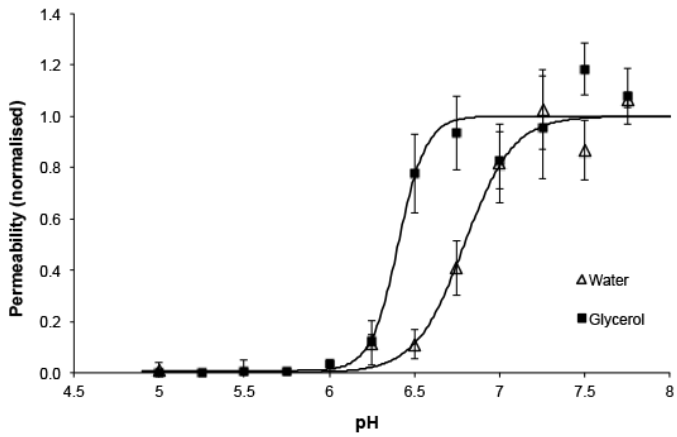

Figure 3. Water and glycerol permeability (P_f and P_{gly} normalized)) in yeast cells expressing rAQP3 *versus* pH. The fit is according to Hill equation.

AQP3 is in the closed state [28, 29]) from the total permeability at each pH value (Figure 4).

In accordance with previous studies [28, 29], we observed a maximum permeability for both water and glycerol between pH 6.5 and 7.5, and a decreased permeability and pore closure at lower pH, with the pore completely closed at pH 5.

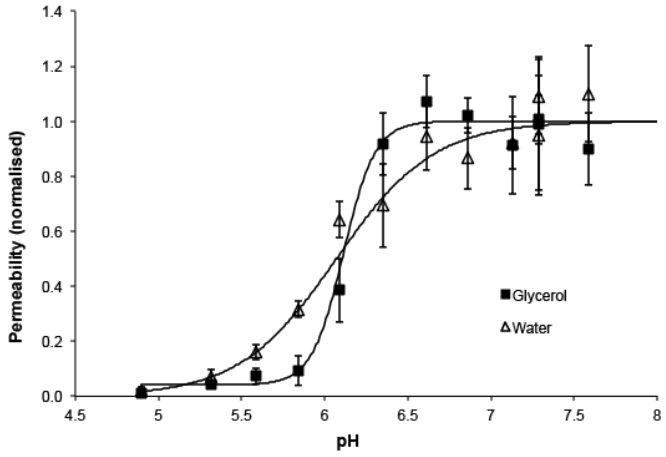

Figure 4. Water and glycerol permeability (P_f and P_{gly} normalized) in human red blood cells (hRBC) *versus* pH. The fit is according to Hill equation.

The calculated pK_a values for both water and glycerol were found to be approximately the same, ca. 6.1, with Hill slopes of about 2 and 4, respectively. While the pK_a for glycerol permeability is in accordance with our data on rAQP3, the pK_a value for water is slightly lower (6.1 *vs* 6.8). Notably, while the Hill coefficients vary from those calculated for rAQP3 - which may be due to both differences in protein sequence or in the selected cellular model -they have the same 2-fold difference (Table 1). It is worth mentioning that in spite of the strong sequence homology (ca. 95%) between the two isoforms (see Figure S3 in supplementary information) still the 5% difference in sequence may account for a different mechanism of inhibition, as will be discussed further.

Hill coefficients, as black boxes parameters, may be subjected to different interpretations. One explanation found in literature for this difference of half the value for water, when compared to glycerol, is based on the Eyring energy barrier model [40], and explained by the differences in activation energy (E_a) of both solutes. Interestingly, the measured activations energies for water and glycerol in hRBC evidenced a two-fold value for glycerol permeability [41]. It was hypothesized that, as E_a for water permeability is low, water molecules cross the channel by forming a single line of hydrogen bonds, while glycerol, with higher E_a, and having three OH groups, will establish more hydrogen bonds than water molecules when passing through the channel [40]. In fact, such hydrogen bond network for both water and glycerol is evidenced by X-ray studies of the bacterial glycerol facilitator (bGlpF) channel [42] and of the *Plasmodium falciparum* isoform (pfAQP) [43] (Figure 5). Moreover, glycerol molecules have their OH groups pointing towards the hydrophilic side of the channel, favouring such hydrogen bond network. In the case of hAQP3, we can also observe this phenomenon in molecular dynamics (MD) simulations.[44] Remarkably, in this latter study the number of hydrogen bonds in the crystal structures, as well as in the MD simulations, is similar to the Hill slopes found by us for hAQP3 in hRBC, approximately 1.5 for water and 4 for

Table 1. pK_a and Hill slope values for water and glycerol, of human and rat AQP3. Obtained by fitting the data presented in Figures 3 and 4.

AQP3 variant	pK_a		Hill Slope	
	Water	*Glycerol*	*Water*	*Glycerol*
rat	6.80 ± 0.15	6.40 ± 0.20	3.00 ± 0.31	5.30 ± 0.62
human	6.08 ± 0.01	6.12 ± 0.01	1.64 ± 0.21	3.93 ± 0.91

glycerol.

Although the importance of H-bonding interactions between substrates and amino acid residues inside the AQP3 channel cannot be underestimated, and certainly plays a role in determining the activation energies of each substrate, recent experimental findings from our groups on the pH gating of aquaglyceroporin-7 (hAQP7) (described in the following sections) indicate that the Hill slope is similar for water and glycerol. Therefore, other factors may influence the overall pH gating mechanisms of AQPs, in addition to the number of H-bonds between substrates and the protein channel.

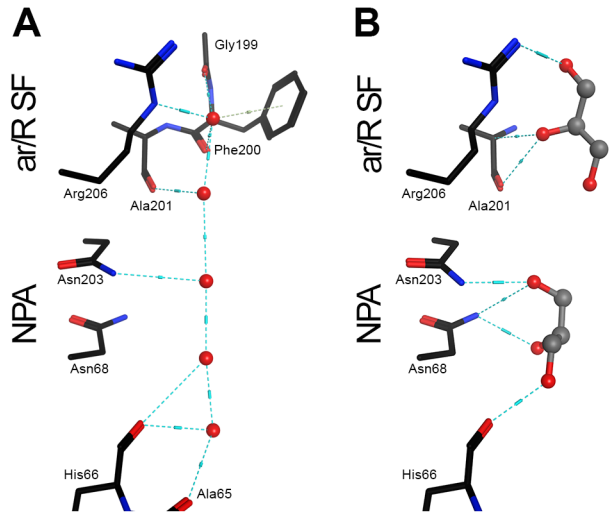

Figure 5. H-bond network of (A) water and (B) glycerol permeation. X-ray structure of bacterial glycerol facilitator (bGlpF) with water (A), pdb1LDA, and glycerol, pdb1FX8.

A second explanation for the observed difference in Hill coefficient values is the amount of titrable residues inside the channel, as postulated previously by Zeuthen et al. [29] This theory is based on the possible competition between the H^+ and glycerol molecules for the protonable side-chains. A phenomenon of non-competitive inhibition of glycerol binding, by two protons, has been observed in hRBC [45]. The limitation of this theory is the fact that the titrable residues would be located in the channel lining, where they could affect glycerol H-bond formation. Later work on aquaporin sequencing and structure showed that hydrophilic and hydrophobic sides constitute the aquaporin lining and few to no residues are actually titrable.

4.2.1.3. Investigation of the pH gating mechanism of hAQP3 by molecular modelling

In order to investigate the molecular mechanism of pH gating of hAQP3, a molecular modelling approach previously developed by our group was used [9]. However, in the case of the present study, a homology model of human AQP3 in the tetrameric form was built, instead of the monomeric form, based on the available structure of the bacterial glycerol facilitator (GlpF, pdb code 1LDI) [46]. The final model was obtained by averaging 50 individual models, using MOE software (MOE 2012.10; CCG 2012) [47], as described in the experimental section.

Analysis of the model shows the common fold, shared by the aquaporin family, containing six transmembrane helices and two half-helices, for each monomer. The two half-helices are located inside of the pore of each monomer and contain the typical NPA (Asp-Pro-Ala) motif that constitutes one of the aquaporin's selectivity filters. The residues in these two NPA motifs are Asn83-Pro84-Ala85, and Asn215-Pro216-Ala217 (Figure S2 in supplementary information). Another selectivity filter, the narrowest part of the channel lining, is located near the extracellular entrance and is named ar/R SF (aromatic/arginine selectivity filter). This selectivity filter is an important structural feature of aquaporins, where the arginine is fully conserved in all mammalian aquaporins (Figure S2). The ar/R SF also serves as a distinctive feature among aquaporins, as the composition in aminoacids

may vary in water and glycerol channels: classical aquaporins have an ar/R SF formed by 4 residues, including, commonly a phenylalanine and histidine, while aquaglyceroporins' ar/R SF comprises only three residues. Thus, these differences account for pore size and selectivity among aquaporin isoforms. All these features are observed in our model of hAQP3, where Phe63, Tyr212 and Arg218 constitute the ar/R SF (Figure S2).

According to the previously reported site-directed mutagenesis studies, the molecular mechanism behind the gating of AQP3 involves four titrable residues, namely His53, Tyr124, Ser152 and His154 [28]. However, the lack of structural information about this isoform led the authors only to speculate on the type of interactions these residues could possibly establish with unknown surrounding residues, based on possible similar behaviours of histidines, tyrosines and serines in enzymes. Using our homology model of the tetrameric form of hAQP3, it is possible to locate the pointed residues at the interface of the monomers, closer to the extracellular side of the protein (Figure 6). These residues may be involved in important monomer-monomer interactions and their protonation/deprotonation may affect the overall assembly of the tetramer and, consequently, of the water and glycerol permeability. In detail, at pH 7 in our model His53 is located at the central pore lining and its side-chain appears to have the possibility to form H-bonds with residues Thr58, Thr52 and Gln45 in the same monomer while interacting also with the aromatic ring of Phe56, located in an adjacent monomer. These interactions are different in each monomer. Interestingly, mimicking the protonation state of the protein at pH 5 leads to the formation of new H-bonds, namely a second H-bond with Thr52 (this time with its side-chain) Thr204, Gly51 and Thr62. The formation of the new H-bonds may cause loop A to move closer to the monomer pore and cause structural modifications in transmembrane-helix 5 (TM5).

On the other hand, Tyr124 does not appear to have a clear role or to be particularly sensitive to pH changes. Due to its very high pK_a (typical range for a Tyr side-chain in proteins is 9-12 [48]), it is unlikely that its side-chain is affected by changes in the pH range from 5 to 8. In addition, the side-chain of Tyr124 appears to be pointing out in the direction of the membrane, not participating in any interaction with other residues. The only apparent interactions of this residue are between its backbone and the backbones of Trp128 and Phe120, contributing to the maintenance of the helical structure. Interestingly, at pH 5, in one monomer is possible to see the formation of a new H-bond with the backbone of Ile127. This cannot explain the influence of pH on Tyr124 and the possible changes it may induce.

Regarding Ser152 and His154, these residues are located in the region between two adjacent monomers. At pH 7, while the backbone of His154 is forming an H-bond with the backbone of Ser152, located in the same loop (Loop C), the His154 side-chain is forming an H-bond with the side-chain of His129, in opposite end of loop C of another monomer (Figure 6B).

At lower pH, the same interactions appear to be maintained and a new H-bond may be formed with the backbone of Gly153. The formation of this new bond in the same loop may weaken the interaction between the two histidines, leading to a movement of loop C towards the channel opening. This disruption, together with the above-described movement of loop A due to protonation of His53, may be the cause for blockage of the channel for water and glycerol permeability. This structural change of movement of loop C was also observed in the MD studies on mercury inhibition of hAQP3, which leads to a collapse of the ar/R SF [44]. This movement may not be simultaneous as, due to neighbouring amino acid side-chains, the pK_a of His53 and His154

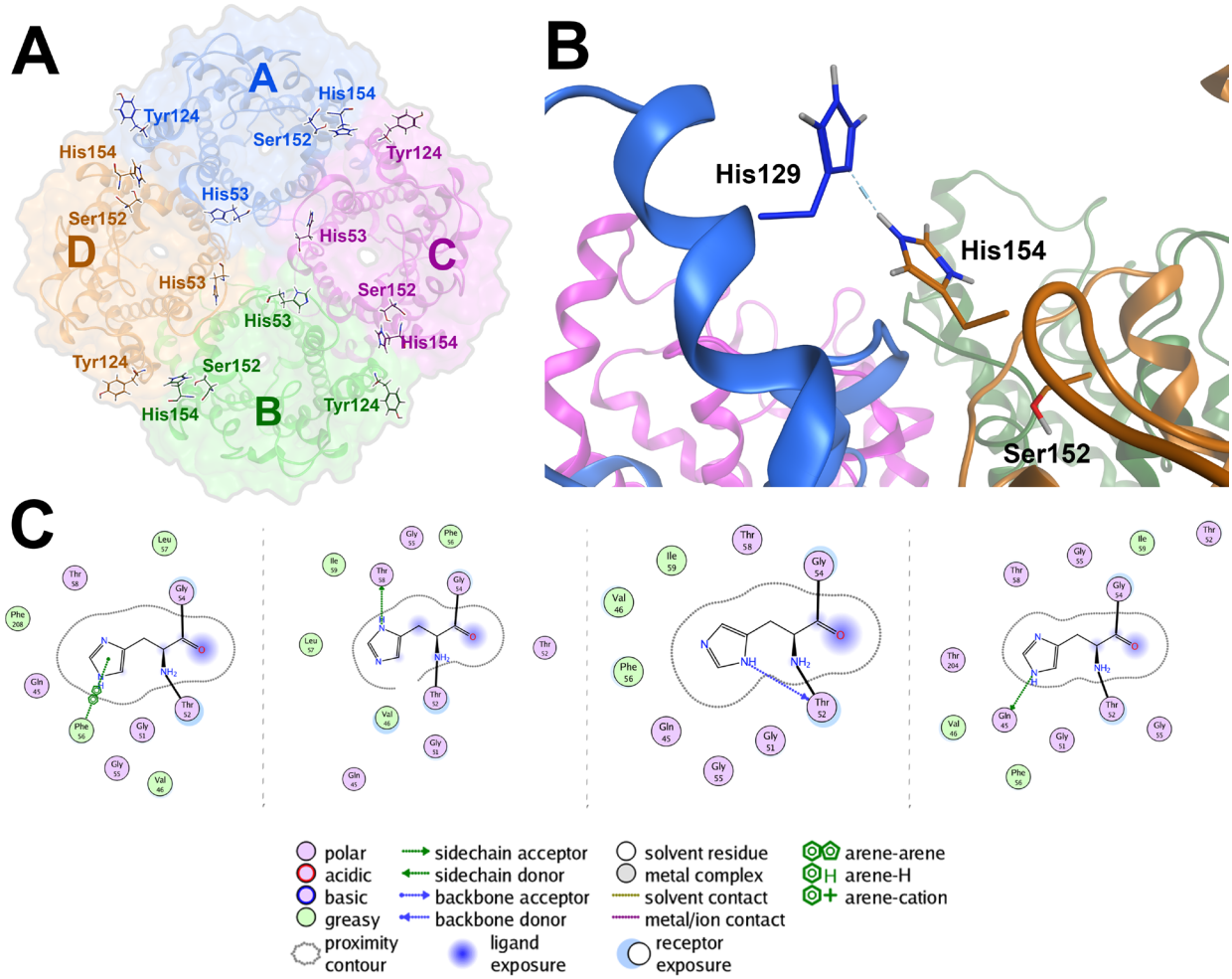

Figure 6. Homology model of tetrameric human AQP3. A: Extracellular top view of the tetrameric form of hAQP3 and position of residues involved in pH regulation. (B) Positions of His129 from monomer A and His154 from monomer D, as well as Ser152. The dashed blue line represents the H-bond formed between the two histidines at pH 7. C: Scheme of the interactions of His154 with neighboring residues, at pH 7, for each of the 4 monomers.

may be subjected to small variation, causing a gradual conformational change with pH decrease (or increase).

Previous studies by Zelenina et al. show that a mutation of His129 to an alanine residue does not affect water permeability or change the pH sensitivity range [28]. However, glycerol permeability was not measured and the contribution of this residue for the mechanism of inhibition of hAQP3 by pH, regarding glycerol permeability, cannot be excluded.

Interestingly, loop movement upon pH changes was also observed for the orthodox water channel bovine AQP0 (bAQP0). This isoform has a maximum of permeability similar to that of hAQP3 at pH 6.5, however it is closed at pH 8.5 [49]. The residues responsible for pH sensibility were identified by site-directed mutagenesis as two histidines: His40 and His122, in loops A and C, respectively. While His40 in bAQP0 is in a similar position as His53 in our model of hAQP3, His122 is in the position corresponding to Ser152 (and close to His154) in hAQP3 (Figure S4 in supplementary information). Overall, as described for bAQP0, we propose that key histidines in loops A and C that span the outer vestibule contribute to pH sensitivity in hAQP3. Moreover, insertion of two histidines in similar positions in hAQP1, a non pH-gated aquaporin, induced pH sensitivity in the same range as bAQP0 [49], further confirming the key role of these residues in pH gating.

As observed for the MD study on Hg^{2+} inhibition of hAQP3, by Spinello et al. [44], the closed state of bAQP0 involves movement of a loop (in this case loop A) and a collapse of the ar/R SF (Figure S5, in supplementary information), shown in the X-ray structures of the open and closed bAQP0 [50]. This collapse in the SF appears to be different than the one described for hAQP3, most likely due to differences in amino acid composition and diameter of the channel. Mutations in the histidine of loop A - His40 in AQP0 [49] and His53 in AQP3 [28] - showed a shift of the pH sensitivity towards a more alkaline range. This effect supports the idea that the pK_a of histidine residues in different regions of the same protein may be very different, leading to different levels of channel regulation.

Other studies reported that the orthodox water channel AQP4 also shows pH-sensitivity, which was recently attributed to one particular histidine residue, His95, predicted by *in silico* methodologies [51]. His95, located inside the channel and facing the intracellular side, is conserved in all aquaporins, including those that do not show pH-sensitivity, such as AQP1. Therefore, it is difficult to conclude that it is the only one responsible for the observed pH gating mechanism.

4.2.1.4. rAQP3 vs hAQP3

Molecular modelling was useful also to explain observed differences among the Hill slope values of hAQP3 with respect to rAQP3 (see Table 1). Human AQP3 shares a sequence identity higher than 80% with most mammalian AQP3 isoforms. Nonetheless, changes in key residues may change permeability and regulatory features. When compared human and rat AQP3 isoforms, although a sequence similarity of about 95% is observed, they do not share one of the residues that may be involved in the pH gating of the hAQP3, namely His129, which is substituted by an alanine (Figure 7). Even though this mutation does not seem to affect water permeability of hAQP3 [28], its effect on glycerol permeability is unknown. Moreover, a mutation of the same residue on a human and rat isoform may not have the same effect, as a network of hydrogen bonds is a very delicate system and is highly dependent on the neighbouring residues. Therefore, we can

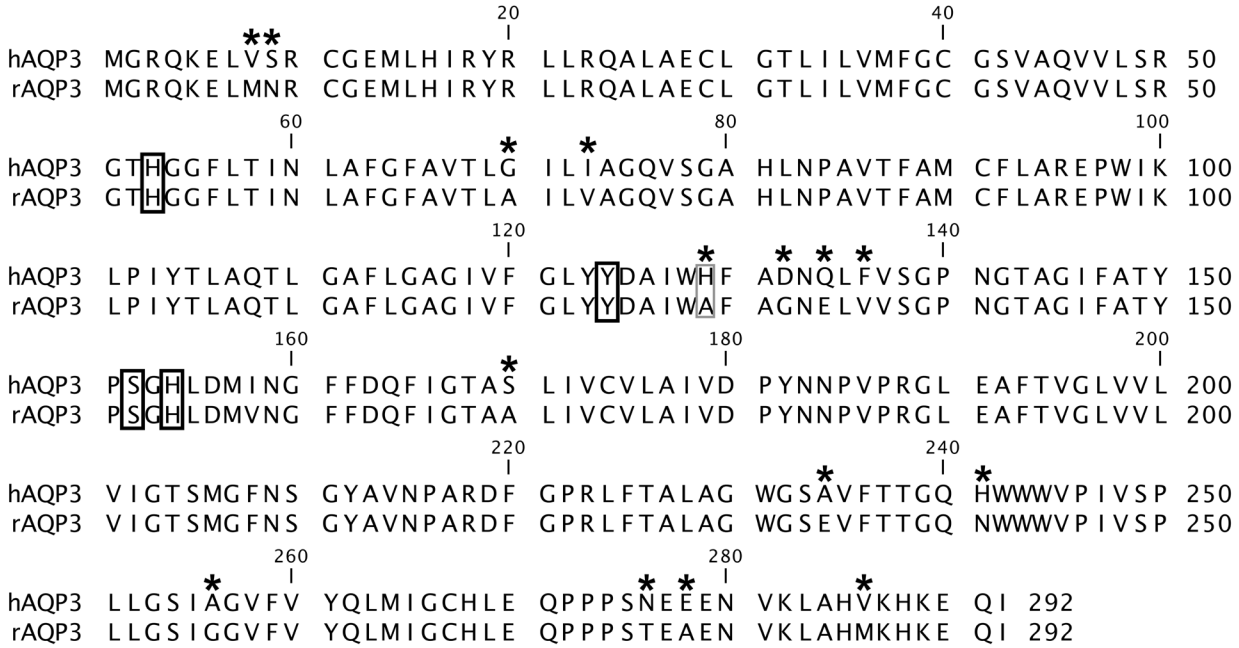

Figure 7. Sequence alignment of rat and human aquaporin-3. The black boxes highlight the pH-sensitive residues, while the grey box highlights His129 in hAQP3. * represents the residues that are not conserved in the two isoforms.

only conclude that the mutation H129A is able to produce a functional rAQP3 glycerol and water channel. Additionally, it is possible that the differences in the observed pK_a and Hill slope for the human and rat isoforms are due to species differences, even though we cannot exclude the possibility of cell-model differences.

4.2.2 Gating of human AQP7

Following our studies on the gating of human AQP3, we proceeded by investigating the possible pH gating of another aquaglyceroporin, human AQP7. Just as hAQP3, hAQP7 also has an important role in human physiology, namely in glycerol metabolism in adipocytes and liver [32]. Thus, here we investigate the pH gating of hAQP7, expressed in a yeast model and following the same approaches as described in section **4.2.1**. Even though both isoforms have similar permeability properties, their mechanism of gating may be different, as observed for other aquaporins [16, 52-54]. Thus, we investigated the molecular mechanism of pH gating, using *in silico* methodologies, and described, for the first time, the gating of hAQP7 by pH.

4.2.2.1. Cloning and heterologous expression of hAQP7

Expression and subcellular localization of hAQP7 in yeast transformants was confirmed by cytoplasmic fluorescence (Figure 8A), while yeast cells expressing hAQP7-GFP show membrane-localized fluorescence, confirming hAQP7 localization at the plasma membrane (Figure 8B). In addition, GFP-tagged hAQP7 was also observed in internal membranes, probably endoplasmic reticulum or in vesicles of the secretory pathway in an early stage of the protein trafficking to the cell membrane. Because proper folding of GFP fused to the C-terminus of a target protein depends on the correct folding of the latter, only folded fusion GFP will become fluorescent [55]. The observed fluorescence shows that GFP is properly folded.

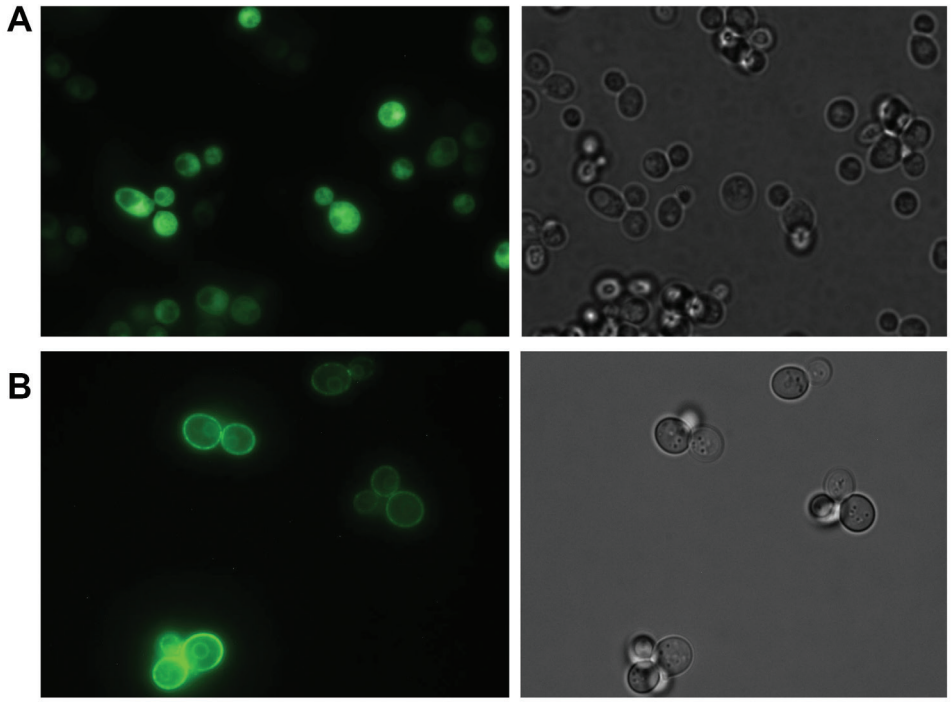

Figure 8. Localization of GFP-tagged hAQP7 expressed in *S. cerevisiae* aqy-null strain. Epifluorescence (left panels) and phase contrast (right panels) images of *S. cerevisiae aqy*-null strains transformed with (A) the empty plasmid pUG35 and (B) hAQP7. Localization at the yeast plasma membrane is depicted for hAQP7-yeast strain.

4.2.2.2. Functional characterization of hAQP7 expressed in yeast

The activity of hAQP7 expressed in *S. cerevisiae aqy*-null strains was assessed through stopped flow fluorescence spectroscopy by challenging cells equilibrated in isosmotic solution at pH 7.4 (mammalian physiological pH) with sorbitol (impermeant solute, inducing water fluxes) or glycerol gradients.

As expected, in the case of sorbitol hyperosmotic shock, the relative cell volume decreases till cells reach a new osmotic equilibrium volume (Figure 9A). At low temperature (11 °C), it is clear that hAQP7-expressing cells (named hAQP7 cells for clarity) show a faster volume equilibration ($P < 0.05$) with higher osmotic permeability coefficient P_f ($(2.0 \pm 0.1) \times 10^{-4}$ cm s^{-1}) than cells transfected with the empty plasmid (named pUG35 cells) ($(1.50 \pm 0.08) \times 10^{-4}$ cm s^{-1}). However, at higher temperatures (37 °C), the two traces almost overlap and similar P_f values were obtained ($(1.15 \pm 0.07) \times 10^{-3}$ cm s^{-1}) for hAQP7 cells and ($(1.05 \pm 0.09) \times 10^{-3}$ cm s^{-1}) for pUG35 cells, $P > 0.1$). Such temperature dependent behaviour is better analysed in the Arrhenius plot (ln P_f *vs* 1/T) shown in Figure 9B, used to calculate the activation energy E_a for water transport, a valuable parameter indicating the contribution of protein-channels for permeation. Here, it is observed that at a higher temperature range (23 to 36 °C) the E_a values are similar (15.2 ± 0.85 kcal mol^{-1}), while for the lower temperature range (11 to 23 °C) E_a decreases (10.3 ± 0.74 kcal mol^{-1}) only for hAQP7

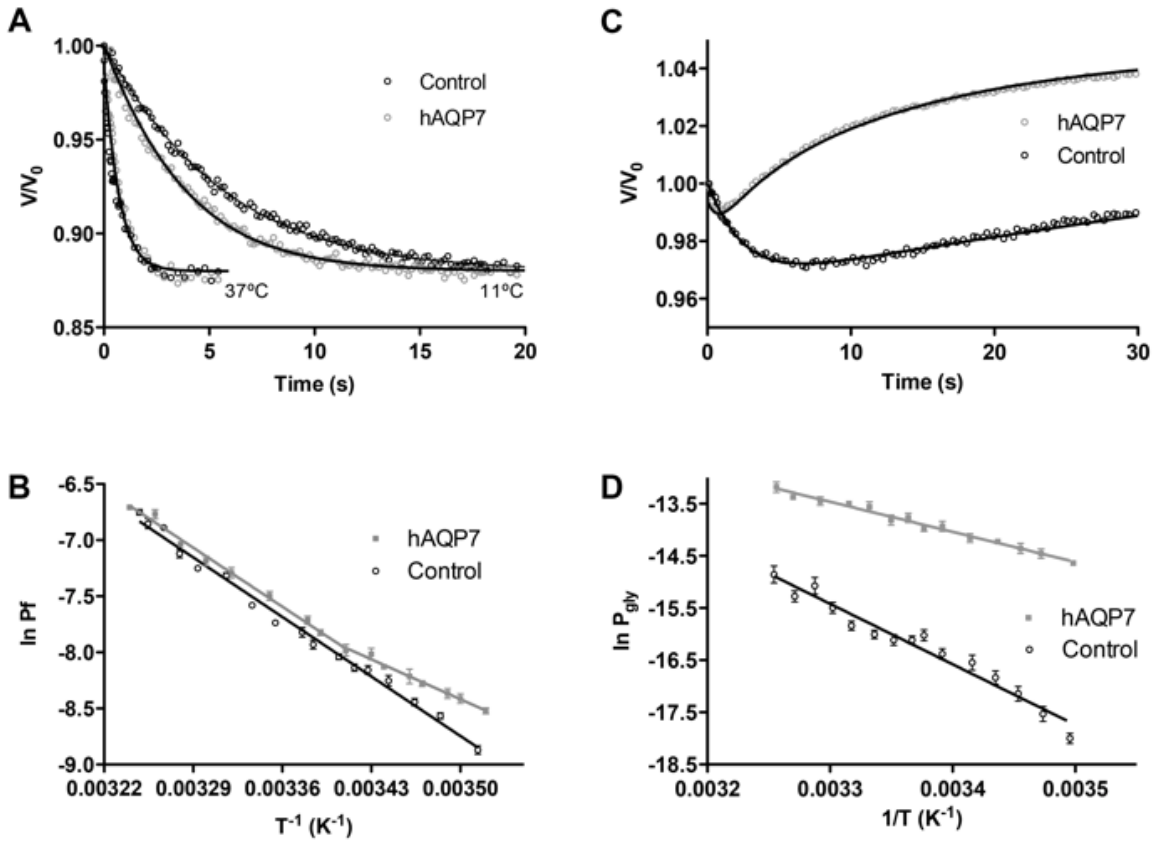

Figure 9. Water and glycerol permeability in control and cells expressing hAQP7. (A) Representative time course of the relative cell volume (V/V_0) changes after a sorbitol hyperosmotic shock (pH 7.4). Signals are illustrative of ten traces for each temperature (11 and 37 °C) obtained from cells expressing hAQP7 and control cells (transformed with pUG35 empty plasmid). (B) Arrhenius plot for calculation of the activation energy (E_a) for water transport. Data are mean ± SD of three independent experiments with at least ten traces each. (C) Representative time course of the relative cell volume (V/V_0) change after a glycerol hyperosmotic shock (pH 7.4). Signals are illustrative of ten traces (23 °C) obtained from cells expressing hAQP7 and pUG35 cells. (D) Arrhenius plot for calculation of the activation energy (E_a) for water transport. Data are mean ± SD of three independent experiments with at least ten traces each.

expressing cells, unmasking the channel contribution to water permeation.

The undetectable increase in water transport and concomitant decrease in E_a at a high temperature range can be explained by the relatively high contribution of the lipid bilayer to the total water permeation across the cell membrane. Conversely, at lower temperatures the lipid pathway becomes almost impermeable and water permeation through aquaporins can be discriminated. Thus, yeast cells expressing hAQP7 show a significant increase in P_f in parallel with a 36% decrease in E_a at low temperatures confirming the contribution of the channel pathway to water permeation [56].

Regarding glycerol permeability, a clear difference between the control pUG35 and hAQP7 strain is well recognised. Figure 9C shows the relative volume changes caused by glycerol gradients used to calculate P_{gly} and E_a for glycerol transport. Since glycerol is a permeant solute, upon a glycerol osmotic shock both water and glycerol fluxes take place concomitantly. After the initial cell shrinkage due to the faster water outflow in response to the initial osmotic gradient, cells re-swell caused by the glycerol influx in response to its chemical gradient. pUG35 and hAQP7 expressing cells show a large difference in the rate of volume changes. Using the P_f value previously estimated for each yeast strain, the calculated P_{gly} of AQP7 cells (8.59 ± 0.06) x10^{-7} cm s^{-1}) was eight-fold the control (1.1 ± 0.10) x 10^{-4} cm s^{-1}). Accordingly, we obtained an E_a value of 23.2 ± 3.1 kcal mol^{-1} for control pUG35 cells and 11.5 ± 0.97 kcal mol^{-1} for hAQP7 expressing cells (Figure 9D), thus confirming hAQP7 glycerol channel activity in the yeast expression system.

4.2.2.3. Inhibition of hAQP7 by Auphen

Previous studies by our group have detected the strong and selective inhibitory effect of the gold(III) coordination compound Auphen [Au(phen)Cl_2]Cl (phen=1,10-phenantroline) on hAQP3 and hAQP7 expressed in human erythrocytes and mammalian cultured cells [57-60]. To evaluate the inhibitory effect of Auphen on hAQP7 activity in our yeast model, water and glycerol permeability of pUG35 and hAQP7 strains were estimated at pH 7.4 in the presence and absence of the gold compound. Thus, yeast cells were incubated for 30 min with Auphen (at 70 μM, a concentration higher than that reported to saturate hAQP7 in adipocytes [60]) prior to the permeability assays and compared with non-treated cells. In the case of pUG35 control cells, Auphen did not induce any significant inhibition ($P > 0.1$) in water and in glycerol permeability (Figure 10A and 10B). Instead, for cells expressing hAQP7, a marked inhibitory effect of the compound (70 μM) was detected, with a decrease of 34% and 84% for P_f and P_{gly}, respectively. It is worth mentioning that the measured permeabilities represent the total water or glycerol fluxes across the yeast cell membrane, i.e., through the lipid bilayer plus hAQP7 and yeast endogenous glycerol facilitators. To discriminate the fluxes across the hAQP7 channel, P_f and P_{gly} values of pUG35 control cells were further subtracted from those obtained for hAQP7 expressing cells ($P_{Channel} = P_{AQP7} - P_{pUG35}$) giving only the contribution of the hAQP7 channel. Therefore, it can be concluded that Auphen inhibited water and glycerol transport via hAQP7 by approximately 92% (as depicted in Figure 10C for the highest Auphen concentration).

A dose-response curve for P_{gly} inhibition was obtained by incubation of cells with increasing concentrations of Auphen (from 0 to 70 μM) and showed a half-maximal effective concentration (EC_{50}) of 12.95 ± 0.35 μM (Figure 10C). Interestingly, this calculated EC_{50} value is slightly higher

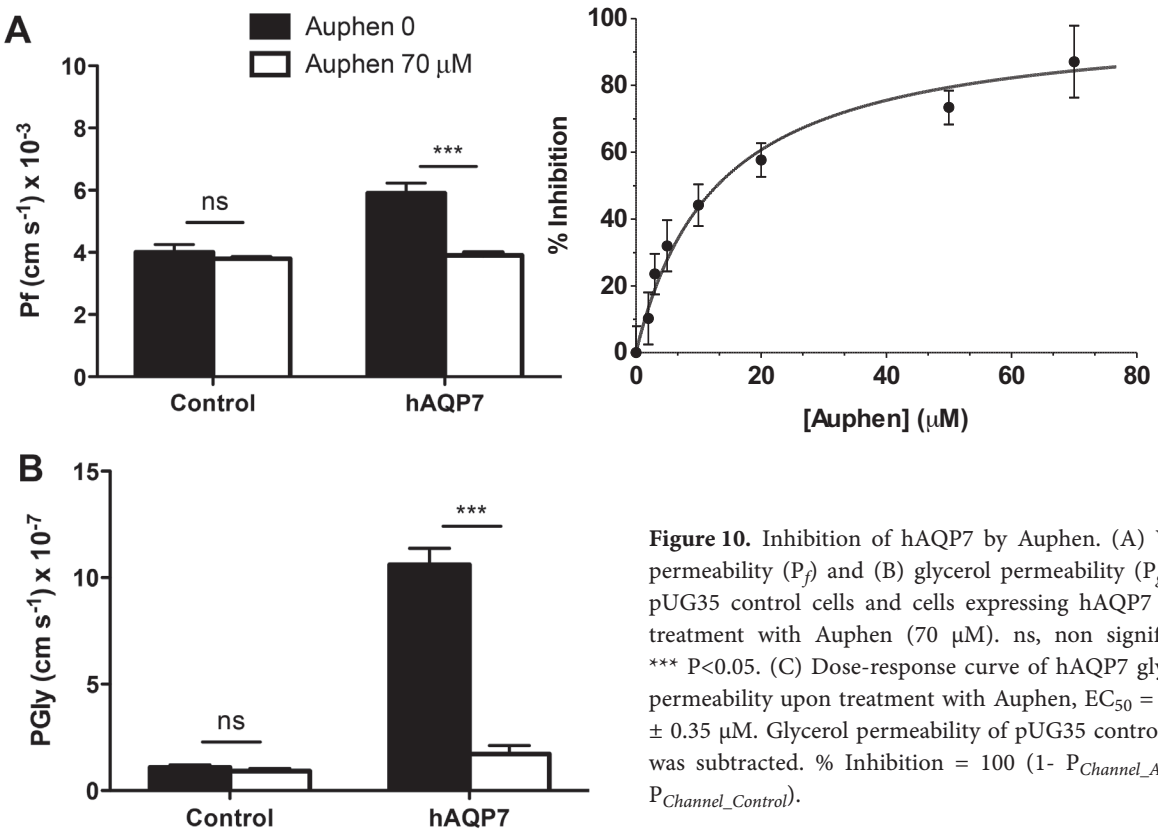

Figure 10. Inhibition of hAQP7 by Auphen. (A) Water permeability (P_f) and (B) glycerol permeability (P_{gly}) of pUG35 control cells and cells expressing hAQP7 upon treatment with Auphen (70 μM). ns, non significant, *** $P<0.05$. (C) Dose-response curve of hAQP7 glycerol permeability upon treatment with Auphen, EC_{50} = 12.95 ± 0.35 μM. Glycerol permeability of pUG35 control cells was subtracted. % Inhibition = 100 (1- $P_{Channel\_Auphen}$/ $P_{Channel\_Control}$).

than the one previously calculated for hAQP7 in the adipocyte model (6.5 ± 3.7 μM) [60]. This discrepancy may be due to differences in cell membrane constitution of each cell model, which may have an effect on Auphen's uptake. In fact, as previously postulated [60] the most favourable Auphen binding sites in hAQP7 are methionine residues facing the cytoplasmic side of the channel, which implies that the gold compound needs to enter the cell before reaching its putative binding site in the protein channel. Moreover, we cannot exclude differences due to the distinct methodologies applied, i.e., stopped-flow for cells suspensions *vs* fluorescence microscopy in cultured adipocytes.

4.2.2.4. AQP7 permeability is dependent on external pH

In a second series of experiments, we investigated the pH dependence of hAQP7 permeability in the selected yeast model. Thus, water and glycerol permeability experiments were performed at 23 ºC varying pH from 5 to 7.5. Permeability of the hAQP7 channel ($P_{Channel}$) is represented in Figure 11A as a function of external pH. Remarkably, a strong pH dependence of both water and glycerol permeability was detected, showing that at pH 5 hAQP7 is completely inactive, while the maximal activity is reached when pH is raised to 6.5.

The pH dependence of hAQP7 channel activity was analysed by fitting the experimental data (P_f and P_{gly} channel corrected values) to a to a Hill equation from where the Hill coefficients and pK_a values for channel gating were estimated. The obtained pK_a value (corresponding to 50% channel activity) of 5.9 and the Hill coefficient around 3, suggest the involvement of 3 proton-binding residues or, alternatively, 3 protein subunits in the pH dependent gating mechanism.

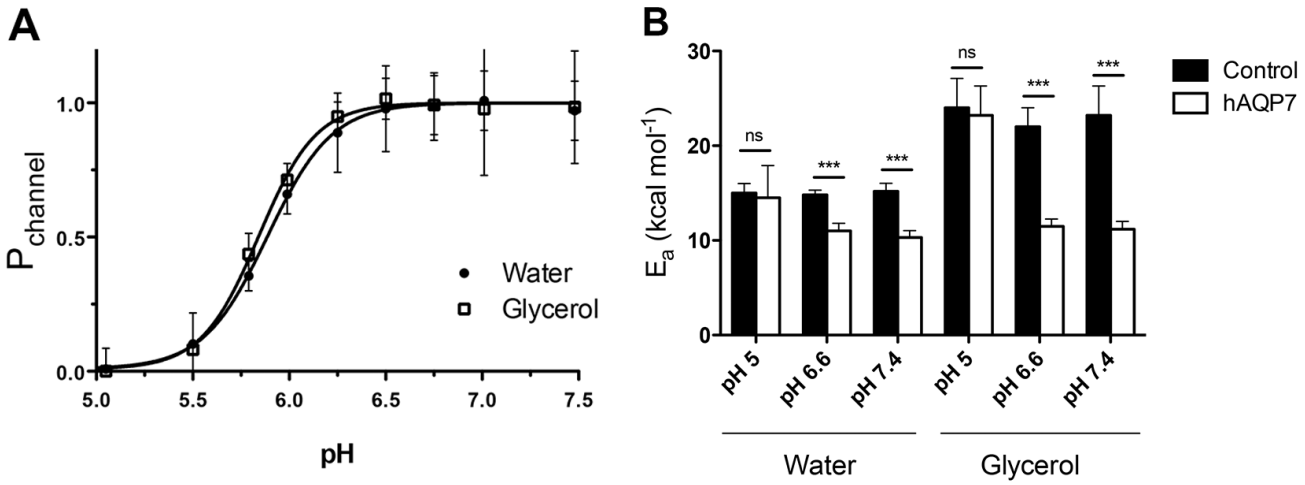

Figure 11. pH dependence of hAQP7 activity. (B) Permeability normalized for each data set and expressed as % of their maximal values ($P_{Channel\_Pf}$ and $P_{Channel\_Pgly}$). Hill coefficient = 3.09 and 2.89 and p*K*s = 5.87 and 5.9, for water and glycerol transport, respectively. (C) Activation energy E_a of glycerol transport of hAQP7 (calculated as $P_{Channel} = P_{AQP7} - P_{pUG35}$) at pH 5 (17.4 ± 2.4 Kcal mol^{-1}), pH 6.5 (11.0 ± 1.5 Kcal mol^{-1}), and pH 7.5 (10.2 ± 1.2 Kcal mol^{-1}).

To further confirm the pH dependence of hAQP7 channel activity, the E_a values for glycerol permeation were estimated at three distinct pH values (pH 5, 6 and 7.5) at which the channel is expected to be on fully closed and open configurations. As shown in Figure 11B, the E_a for glycerol permeation significantly decreased from pH 5 (17.4 ± 2.4 kcal mol-1) to pH 6.5 (11.0 ± 1.5 kcal mol^{-1}) and pH 7.5 (10.2 ± 1.1 kcal mol^{-1}), corroborating the proposed channel closure/opening transition.

The effect of pH on hAQP7 has been assessed in a recent study [61] that explored the kinetic features of hAQP7 expressed in Madin-Darby canine kidney (MDCKII) cells. By measuring cellular ^{14}C-glycerol uptake in the range of pH 5 to 8, the authors did not observe any meaningful change in solute transport via hAQP7 activity although the uptake was significantly reduced at the lowest pH of 5, and thus concluded that H^+ was not important for AQP7 operation. Conversely, taking advantage of the yeast cell system to measure glycerol influx trough hAQP7, we could demonstrate that pH-gating mechanisms take place for this isoform.

4.2.2.5. Investigation of the pH gating mechanism of hAQP7 by molecular modelling

As for hAQP3, we developed a homology model of hAQP7 in a tetrameric form (see detailed information in the methodology section), which allowed once more to visualize the common fold shared by the aquaporin family, comprising six transmembrane helices and two half-helices, with their N-terminal ends located in the center of the pore. These two half-helices contain distinctive central motifs, which in the case of hAQP7 are NAA (Asn94, Ala95, Ala96) and NPS (Asn226, Pro227, Ser228) instead of the classical NPA (asparagine-proline-alanine) sequence (Figure 13). Moreover, three residues, Phe74, Tyr223 and Arg229, constitute the ar/R SF of hAQP7 as for hAQP3.

As previously mentioned, in the case of AQP7, we obtained a Hill coefficient of approximately 3 for pH gating for both water and glycerol transport. This suggests that there are, at least, three protonatable sites that are cooperatively involved in regulation and that the same mechanism inhibits transport of both permeants. Previous research by Zelenina et al. [25] using site directed mutagenesis, demonstrated that four residues might be involved in the regulation of human AQP3

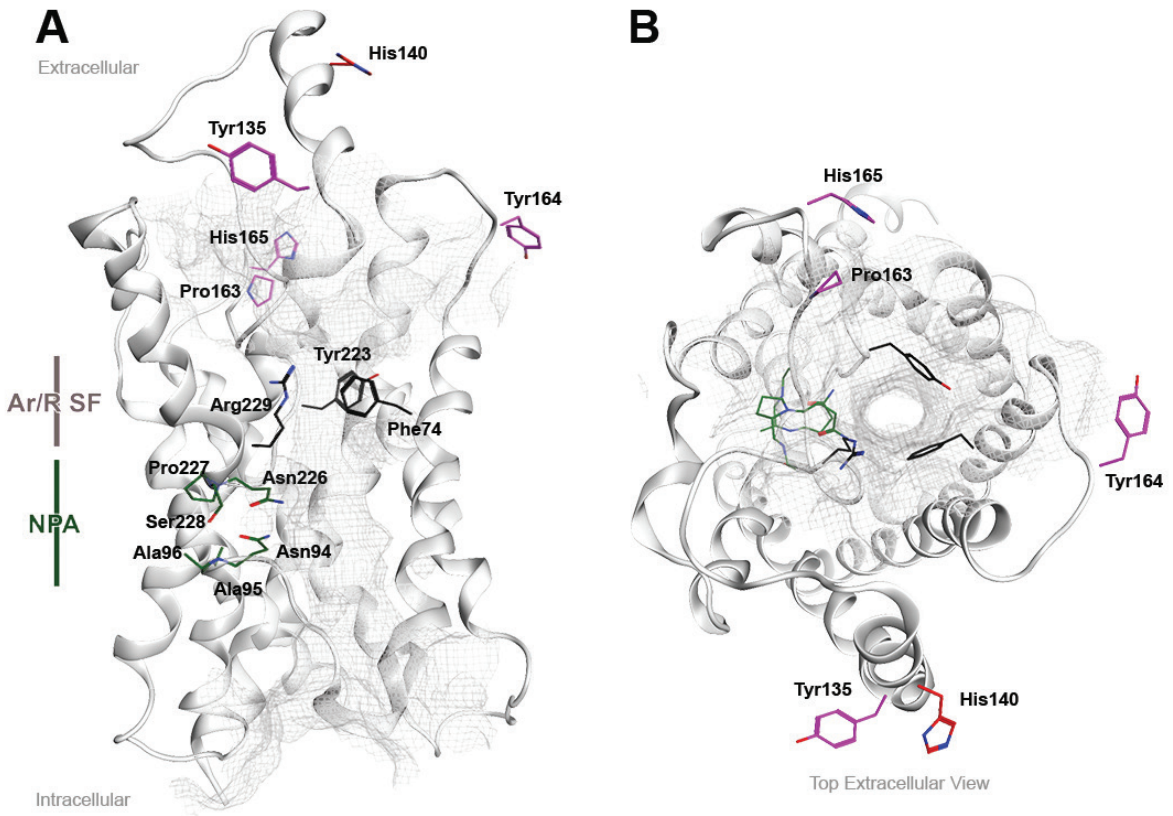

Figure 12. Homology model of human AQP7, showing the conserved aromatic/Arginine selectivity filter (ar/R SF) and NPA motifs. In magenta are highlighted the residues corresponding to those previously identified as pH-sensitive in hAQP3 [28] and in red is shown the His140, hypothesized to be interacting, via H-bonds, with His165.

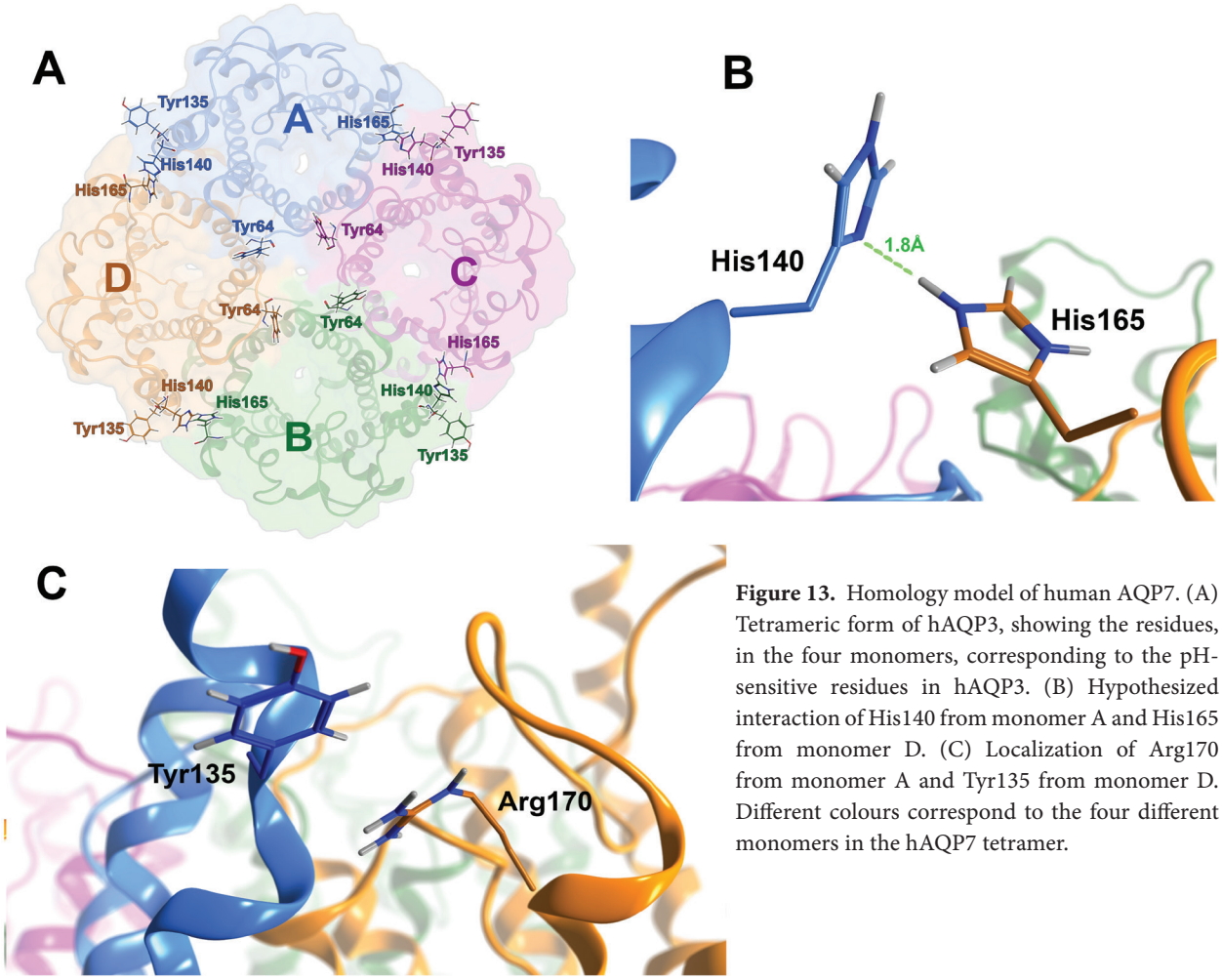

Figure 13. Homology model of human AQP7. (A) Tetrameric form of hAQP3, showing the residues, in the four monomers, corresponding to the pH-sensitive residues in hAQP3. (B) Hypothesized interaction of His140 from monomer A and His165 from monomer D. (C) Localization of Arg170 from monomer A and Tyr135 from monomer D. Different colours correspond to the four different monomers in the hAQP7 tetramer.

by pH.

Interestingly, this mechanism appears to be different from the one described for hAQP3 in section 4.2.1. In the case of hAQP3, water and glycerol are not gated in the same manner upon pH changes. Nonetheless, sequence alignment of hAQP3 and hAQP7 shows that hAQP7 shares most of the pH-sensitive residues of hAQP3 (His53, Tyr124, Ser152 and His154), namely in hAQP7 Tyr64, Tyr135, Pro163 and His165 (Figure 12). Analysing the hAQP7 monomer, it is hard to predict how these residues alone can be so important for pH sensitivity, as they do not appear to share any interaction with other neighbour residues (Figure 12). Thus, we decided to further analyse these residues in the context of the hAQP7 overall tetrameric assembly, as performed for hAQP3 described earlier in this subchapter. Notably, in our model, all the residues corresponding to those indicated by Zelenina et al. for hAQP3 [25], are located in extracellular loops or helices and may have contact with other monomers (Figure 13A).

As we observe an effect of pH on the gating of hAQP7, that is similar for water and glycerol, the first theory described by previous authors for hAQP3, where the H-bonding network is higher for glycerol, explaining the differences in Hill slope can be applied. In fact, this theory can explain the behavior of hAQP3 in the permeation of water and glycerol, with Hill slopes of approximately 2 and 4, respectively, but fails at explaining why this Hill slope is the same for both solutes in the case of hAQP7, as both channels transport both solutes in a similar fashion. Instead, our attempt to explain the Hill slope differences in hAQP3 may serve to elucidate the similarities in hAQP7. Even though both channels transport both water and glycerol, structural changes induced by pH may be different, as the involved residues are not exactly the same.

Thus, we hypothesize that the protonation of a residue in one or more of the protein subunits may trigger a change in the structure of the entire tetramer. In the most simple model, if the change is symmetric over all subunits, there would be two states of the tetramer, one in which the protonated state is favored and one in which the deprotonated state in all four subunits is favorable. This would explain the Hill coefficient of 3, which nearly corresponds to the number of subunits or to the number of identified titrable residues.

In detail, His165 (corresponding to His154 in AQP3) is located in loop C and interacts via a hydrogen bond with His140, which itself is located in transmembrane-helix 3 from the next monomer (Figure 13B). At physiological pH (7.4), the software predicted His165 to be protonated, while His140 is in a deprotonated state. Given a possible interaction between these two side-chains, it is hypothesized that protonation of the highly accessible His140 would cause these side-chains to repel each other, causing loop C to move closer to the channel entrance. Interestingly, movement of loop C in hAQP3, and consequent closure of the channel, was described for hAQP3 inhibition by mercury, using molecular dynamics simulations [44]. Thus it is possible that the mechanism of gating by extracellular pH and inhibition by metals share some structural features.

Similarly to the described histidines, Tyr135 in AQP7 (the crucial Tyr124 in AQP3) can contribute to inter-monomer interactions, as it may form an H-bond with the positively charged Arg170 of the next monomer (Figure 13C). This H-bond is expected to strongly stabilize the deprotonated state of Tyr135, thereby possibly lowering its pK_a to the observed value of 6.1. It is well established that strong H-bonding can shift the pK_a of protein sidechains outside their usual window [62]. Indeed, the commonly observed pK_a range for tyrosine is 9-12, while for histidine it is 5-8 [63]. None of the other tyrosines studied in the homology model had similar H-bonding

features that could lower the pK_a so strongly.

Another residue involved in pH sensitivity in AQP3 is His53. In that position, AQP7 does not have a histidine residue, but a tyrosine residue instead (Tyr64) (Figure 13A). Tyr64 in AQP7 is located in an accessible position from the extracellular side in Loop A, and appears to be contributing to monomer-monomer interactions in the central pore. However, its environment does not present any feature that could account for an unusually low pK_a of this residue. Ser152 in AQP3 was also shown to be involved in pH gating, but it is not present in hAQP7 where it is substituted by a non-protonatable residue (Pro163). Hence, this residue is not suitable to be involved in the pH gating of hAQP7.

4.3. Conclusions

The main objective of the present studies was to assess regulation the permeability properties of two human aquaglyceroporins, hAQP3 and hAQP7, by pH, as well as to investigate the pH gating of rat AQP3, expressed in a yeast cell-model. This was achieved in cellular models where analysis was unlikely to be compromised by the co-expression of other aquaporin isoforms. In the case of hAQP3, we used a hRBC model, well-described as a good model for functional studies of this aquaglyceroporin. Furthermore, due to their easy molecular genetics as well as availability of a wide range of mutants, we selected the yeast *S. cerevisiae* devoided of endogenous aquaporins to express hAQP7 and rAQP3.

In our yeast cells, hAQP7 and rAQP3 localized at the plasma membrane and it was possible to measure increased water permeability at low temperature where the fluidity of the lipid bilayer is reduced [56]. Moreover, compared to control cells, yeast expressing hAQP7 and rAQP3 displayed considerably higher glycerol permeability at mammalian physiological pH (pH 7.4), confirming their function as a glycerol channel. The concomitant lower E_a for glycerol transport corroborated this observation and assured that the yeast cell system can be used for assessment of aquaporin regulation. Additionally, the inhibitory effect of Auphen towards hAQP7 was also confirmed in this model. Importantly, the yeast cell model herein optimized allowed disclosing for the first time the pH dependence of hAQP7 activity, showing that this channel changes from an open to closed state when pH drops from 7.5 to 5.

In the present study we investigated the pH gating of rat and human AQP3 by stopped flow spectroscopy. For the first time we were able to fully characterize not only the effects of pH gating on water, but also on glycerol permeability in this human isoform. In the case of water, the obtained results confirm the previous observations of hAQP3 gating in oocytes [29]. Interestingly, previous reports on rAQP3 pH gating were confirmed in our yeast model, which highlighted differences with the human isoform. In fact, while hAQP3 shows the same pK_a for both water and glycerol, the pK_a values are similar for water, but different for glycerol in the rAQP3 system. These differences may be due to species differences, even though we cannot exclude that the selected investigational system itself may partly lead to this variation.

In the light of the experimental Hill slope values for water and glycerol, a few theories on differences in the pH gating mechanisms of aquaporin permeation have been postulated. Current knowledge about aquaporin sequence and structure allows us to discard the hypothesis of protonation of residues inside the channel.

According to our data the maximum of protein function, for both aquaglyceroporins, is achieved at the expected mammalian physiological pH range of 6 to 7.5. Reflecting upon the possible reasons for such phenomenon, the cellular and tissue distribution of these aquaporins may shed some light on the physiologic meaning of its regulation. For example, glycerol metabolism and hAQP7 regulation is well documented in adipose tissue and liver [6, 7], while in the kidney AQP7 is important for glycerol reabsorption preventing glyceroluria [64]. However, less is known about AQP7 regulation in tissues where it is also moderately expressed, such as pancreatic β-cells controlling insulin secretion [65] and in skeletal muscle and heart importing glycerol for energy production [12, 66, 67]. In the male reproductive system, AQP7 is present particularly in the spermatids, as well as in the testicular and epididymal spermatozoa, suggesting that AQP7 has some role in late spermatogenesis [10, 68].

The role of hAQP3, in post-copulatory sperm osmoadaptation and migration has also been recently suggested [69]. Notably, a number of reports indicate that pH gradients and the concentration of bicarbonate in the lumen of the extratesticular ducts are involved in the regulation of sperm metabolism and motility [70] and thus have a direct physiological role in reproductive function. It is tempting to speculate that the pH gating of human AQP7 and AQP3 has biological relevance for sperm maturation and quiescence.

Notably, metal compounds have also been shown to modulate the function of AQPs. For example, among the endogenous transition metal ions, Cu^{2+} and Ni^{2+} ions, in the form of CuSO4 and $NiCl_2$, have been demonstrated to cause water and glycerol permeability decrease in cells expressing human AQP3-GFP in a dose-dependent manner and the effect was rapid and reversible, Pb^{2+} and Zn^{2+} ions had no effect in AQP3 permeability [28, 71]. Moreover, the effect of Ni^{2+} was pH-dependent: at neutral and acidic pH, the AQP3-mediated water permeability was completely inhibited by 1 mM $NiCl_2$. At pH 7.4 and 8.0, the P_f in transfected cells was decreased by Ni^{2+}, but remained significantly higher than that in non-transfected cells. Site-directed mutagenesis studies identified three residues, Trp128 and Ser152 in the second extracellular loop and His241 in the third extracellular loop of AQP3, as determinants of Ni^{2+} inhibition effects [28]. These Ni^{2+}-sensitive residues are the same as for Cu^{2+}, which suggests the same binding site and mechanism of inhibition [71]. Interestingly, Ser152 was identified as a common determinant of both Ni^{2+} and pH sensitivity.

These findings confirm our idea that knowledge of the physiological mechanisms of AQPs gating may open the way to new strategies to selectively target different AQPs and to achieve optimization of inhibitors, such as the recently reported gold-based compounds [34, 58, 59] potentially active also as His binders. Finally, considering the importance of glycerol in multiple vital physiological processes, regulation of its permeation across hydrophobic cell membranes via AQPs may be crucial for cell proliferation, adaptation and survival, and future research to untangle the biological relevance of aquaglyceroporins' pH gating in health and disease conditions ought to be conducted.

4.4. Experimental section

Strains, plasmids and growth conditions: Plasmid with human aquaporin-7 (hAQP7) cDNA (pWPi-DEST-AQP7) [9] was used for AQP7 cDNA amplification.

The centromeric plasmid pUG35 was used for cloning human AQP7, conferring C-terminal GFP tagging, MET25

promoter and CYC1-T terminator.

Escherichia coli DH5α [72] was used as host for routine propagation of the plasmids. *E. coli* transformants were maintained and grown in Luria-Bertani broth (LB) at 37 ºC; ampicillin (100 μg/ml) [73]. Plasmid DNA from *E. coli* was isolated using a GenElute^{TM} Plasmid Miniprep Kit (Sigma-Aldrich).

Saccharomyces cerevisiae, 10560-6B MATα leu2::hisG trp1::hisG his3::hisG ura352 aqy1D::KanMX aqy2D::KanMX (YSH1770, further indicated as aqy-null) was used as a host strain for heterologous expression of human AQP7 and for functional studies. Yeast strains were grown and maintained at 28 ºC with orbital shaking in YNB (yeast nitrogen base) without amino acids (DIFCO), with 2% (w/v) glucose (and 2% (w/v) agar for solid medium) supplemented with the adequate requirements for prototrophic growth [74]. For stopped-flow assays, the same medium was used.

Cloning of human AQP7 gene in pUG35: *E. coli* DH5α was transformed with (pWPi-DEST_lnAQP7) and used for propagation of the plasmid. Plasmidic DNA was isolated and purified.

hAQP7 specific primers modified to incorporate restriction sites for *Spe*I (underlined) and ClaI (underlined) (5'-GGACTAGTCCTATGGTTCAAGCATCCGGGCACAG-3' and 5'-CCATCGATGGAGAAGTGCTCTAGGGCCATGGATTCAT -3' respectively) were designed and used for PCR amplification of hAQP7 cDNA. PCR amplification was carried out in an Eppendorff thermocycler with Taq Change DNA polymerase (NZYTech). A temperature gradient PCR was previously performed to determine the optimum annealing temperature. The PCR product was digested with *Spe*I and *Cla*I restriction enzymes (Roche Diagnostics®), purified using Wizard® SV Gel and PCR Clean-Up System kit (Promega) and cloned into the corresponding restriction sites of pUG35 digested by the same restriction enzymes, behind MET25 promoter and in frame with GFP sequence and CYC1-T terminator, using T4 DNA Ligase (Roche). Cloning was performed according to standard protocols [73] to construct the expression plasmid pUG35-hAQP7. The plasmid were used to transform DH5α *E. coli* strain, propagated and subjected to extraction and purification. Fidelity of constructs and correct orientation were verified by PCR amplification, restriction analysis and DNA sequencing. Agarose gel electrophoresis and restriction site mapping were performed according to standard methods [73, 75].

Transformation of the *S. cerevisiae* aqy-null strain: Transformation of the aqy-null strain with pUG35-AQP7 was performed by the lithium acetate method described in [75]. The same strain was also transformed with an empty pUG35 vector (which does not contain hAQP7 cDNA) to be used as a control (further indicated as pUG35 cells). Transformants were selected on YNB medium without uracil as auxotrofic marker.

Subcellular localization by fluorescence microscopy: For subcellular localization of GFP-tagged AQP7 in S. cerevisiae, yeast transformants in mid-exponential phase were observed with a Zeiss Axiovert 200 fluorescence microscope, at 495 nm excitation and 535 nm emission wavelengths. Fluorescence microscopy images were captured with a digital camera (CoolSNAP EZ, Photometrics, USA) and using the Metafluor software (Molecular Devices, Sunyvale, CA).

Fluorophore loading: Yeast transformants were grown up to $OD_{640nm} \approx 1$, harvested by centrifugation (5000×g; 10 min; 4 °C), washed and re-suspended in ice cold sorbitol (1.4 M) K^+-citrate buffer (50 mM, pH 7.4) up to a concentration of 0.33 g ml^{-1} wet weight and kept on ice for at least 90 minutes. Prior to the osmotic challenges the cell suspension was pre-loaded with the nonfluorescent precursor 5-and-6-carboxyfluorescein diacetate (CFDA, 1 mM for 10 min at 30 ºC) that is cleaved intracellularly by nonspecific esterases and generates the impermeable fluorescent form known to remain in the cytoplasm [37].

Stopped-flow fluorescence assays: Stopped-flow was used to monitor cell volume changes of cells loaded with a concentration-dependent self-quenching fluorophore [37]. Experiments were performed on a HI-TECH Scientific PQ/SF-53 stopped-flow apparatus, which has a 2 ms dead time, temperature controlled, interfaced with an IBM PC/AT compatible 80386 microcomputer. Experiments were performed at temperatures ranging from 7 to 38 °C. Five runs were usually stored and analysed in each experimental condition. In each run 0.1 ml of cell suspension (1:10 dilution in resuspension buffer) was mixed with an equal amount of iso (baseline) or hyperosmotic solutions (of sorbitol or glycerol) of 1.25 tonicity (($\Lambda = (osm_{out})_\infty/(osm_{out})_o$)). Fluorescence was excited using a 470 nm interference filter and detected using a 530 nm cut-off filter and the changes in fluorescence due to carboxyfluorescein (CFDA) fluorescence quenching were recorded.

Cell volume measurements: Equilibrium cell volumes were obtained by loading cells with CFDA under a fluorescent microscope equipped with a digital camera as previously described [37]. Cells were assumed to have a spherical shape with a diameter calculated as the average of the maximum and minimum dimensions of each cell.

Calibration of the fluorescence signals into relative volume: The fluorescence traces obtained were corrected by subtracting the baseline trace that reflects the bleaching of the fluophore. The calibration of the resulting traces for the two strains followed our previous strategy [21], where a linear relationship between relative volume and F was obtained

(v_{rel} =a F/F_o+b); the values of a and b were estimated individually for each sorbitol osmotic shocks, considering the initial and final fluorescence values and the correspondent relative volumes obtained previously by our group for the same tonicity shock. These values were then used for the calibration of the traces in the glycerol osmotic shock preformed under the same experimental conditions, tonicity and temperature.

Permeability and activation energies evaluation: The experimental protocols to assess aquaporin function were designed to keep the membrane surface tension to a minimum in order to maintain aquaporin activity at its maximum as previously found in our laboratory [21]. This was accomplished by equilibrating cells in 1.4 M sorbitol solution (considering sorbitol a non-diffusible solute) followed by the application of low tonicity hyperosmotic shocks (Λ = 1.25) with sorbitol or glycerol. Under these experimental conditions and immediately prior ($t=0^-$) the osmotic shocks the intracellular non-diffusible species ($C_{ND\_in\_0}$) and glycerol ($C_{Gly\_in\_0}$) concentrations were 1.4 M and 0 M respectively. Upon the introduction of the hyperosmotic shocks (t=0+) the extracellular medium osmolarity changes to 1.75 M and the initial extracellular solute concentrations and the concentration gradients (ΔC=Cin-Cout) change accordingly: i) for the sorbitol shock, the extracellular sorbitol (C_{Sor_out}) concentration is 1.75 M and the initial gradient of non-diffusible species ($\Delta C_{Total}=C_{ND\_in}-C_{Sor\_out}$) is -0.35M and ii) for the glycerol shock, the extracellular media is composed by a mixture of sorbitol 0.7 M (C_{Sor_out}) and glycerol 1.05 M (C_{Gly_out}) and the initial gradients are ΔC_{ND_0}=+0.7 M and ΔC_{Gly_0}=-1.05 M, ΔC_{Total}=-0.35 M. Using the analysis described in [9] that incorporates all these osmotic and concentration gradients and their respective water and glycerol fluxes, together with the value of 0.4 for the relative non-osmotic volume previously determined [21], the permeability coefficients for water (P_f) and glycerol (P_{gly}) transport were evaluated.

For this end, the calibrated experimental curves v_{rel}, were fitted to their theoretical curves, considering the water and glycerol fluxes and the resulting changes in cell volume and intracellular concentrations of solutes. Optimization of permeability values was accomplished by numerical integrations using the mathematical model implemented in the Berkeley Madonna software (http://www.berkeleymadonna.com/). The activation energy (Ea) of water transport was evaluated from the slope of the Arrhenius plot (ln P_f as a function of 1/T).

Inhibition with Auphen: Inhibition experiments were carried out in the same way as above. Intact cell suspensions equilibrated in isotonic solution (sorbitol 1.4 M) were incubated with fluorescent probe (CFDA) in the absence or presence of Auphen (70 μM), at room temperature for 30 minutes.

Similarly to above, cell suspension is confronted with a hypertonic solution by the addition of sorbitol or glycerol, to characterize the water and glycerol transport, respectively. Acquisition and calibration of fluorescence signals was as described above, at 23 ºC. Estimation of P_f and P_{gly} was done by fitting the theoretical curves following the same method described above. Inhibitory effect of Auphen was evaluated by comparing values of P_f and P_{gly} at 23 ºC with and without incubation with Auphen.

External pH dependence: In order to further characterize the pH dependence on hAQP7 channel status (open/closed), yeast transformants cells were grown up as previously described and incubated in isotonic solution (sorbitol 1.4 M) under different pH values (varying from 5 to 7.5) at least 90 minutes. In these conditions, cells deprived of carbon source and incubated in ice for a long period, are considered in starvation and unable to maintain an internal pH gradient. Thus, the internal pH equals the external pH [76].

After the incubation with the fluorescence probe, stopped-flow experiments were performed at 23 ºC for both water and glycerol transport at different external pH. For each pH buffer the osmotic challenges, isotonic (to access baseline), and hyper-osmotic with sorbitol (for water) and glycerol (for glycerol) were performed sequentially, in order to secure that data points for water and glycerol transport through the AQP7 channel were obtained under the same temperature and pH conditions for both control cells and expressing hAQP7 cells.

Statistical Analysis: The results were expressed as mean ± SEM of n individual experiments. Statistical analysis between groups was performed by the unpaired t-test. P values < 0.05 were considered statistical significant. Statistical analyses were performed using the Prism software (GraphPad Software Inc., San Diego, CA).

Molecular modeling: The 3D structure of hAQP7 and hAQP3 were obtained by homology modeling using Molecular Operating Environment (MOE 2012.10) (CCG 2012) [47]. The choice of a template structure was based on the sequence identity between the isoforms and the sequence of the AQPs with available resolved structures from human, bacteria and Plasmodium falciparum (UniProt 2013 codes O14520, C8TK05 and Q8WPZ6, respectively). The isoform that has the highest sequence similarity with hAQP7 and hAQP3 is the bacterial isoform Glycerol Facilitator (GlpF), which was then chosen as a template structure. Three resolved structures for bGlpF, crystalized either with or without glycerol and solved by X-Ray diffraction, were retrieved from the Protein Data Bank [46]. Among them, the template was selected that had the best resolution (2.70 Å) without any substrate (pdb 1LDI). The tetrameric form was assembled according to directions given in the pdb file and the structure was prepared and protonated at pH 7 under forcefield

Amber12EHT. Thus, the tetrameric form of human AQP7 model was built: 50 intermediate models were generated and averaged to obtain the final homology model.

The obtained models were checked for more realistic rotamers of side chains in the regions of Ar/R SF and NPA, by comparison with the available crystal structures of all the other AQP isoforms (pdb codes 1H6I, 36D8, 3D9S, 1RC2, 1LD1 and 3C02). The structures were protonated at pH 7 and an energy minimization refinement was performed, also under the Amber12EHT force field, during which the Cα atoms were fixed. After identification of the residues of interest for the mechanism of pH gating, the same energy minimization procedure was used to further refine them.

References

[1] G. Benga, Mol Aspects Med, 33 (2012) 514-517.
[2] K. Ishibashi, Y. Tanaka, Y. Morishita, Biochim Biophys Acta, 1840 (2014) 1507-1512.
[3] A. Madeira, S. Fernandez-Veledo, M. Camps, A. Zorzano, T.F. Moura, V. Ceperuelo-Mallafre, J. Vendrell, G. Soveral, Obesity (Silver Spring), 22 (2014) 2010-2017.
[4] M.L. Kortenoeven, R.A. Fenton, Biochim Biophys Acta, 1840 (2014) 1533-1549.
[5] M. Hara-Chikuma, A.S. Verkman, Cell Mol Life Sci, 63 (2006) 1386-1392.
[6] A. Rodriguez, V. Catalan, J. Gomez-Ambrosi, G. Fruhbeck, Cell Cycle, 10 (2011) 1548-1556.
[7] A. Madeira, T.F. Moura, G. Soveral, Cell Mol Life Sci, 72 (2015) 759-771.
[8] A. Rojek, J. Praetorius, J. Frokiaer, S. Nielsen, R.A. Fenton, Annu Rev Physiol, 70 (2008) 301-327.
[9] A. Madeira, M. Camps, A. Zorzano, T.F. Moura, G. Soveral, PLoS One, 8 (2013) e83442.
[10] K. Saito, Y. Kageyama, Y. Okada, S. Kawakami, K. Kihara, K. Ishibashi, S. Sasaki, The Journal of urology, 172 (2004) 2073-2076.
[11] T.L. Butler, C.G. Au, B. Yang, J.R. Egan, Y.M. Tan, E.C. Hardeman, K.N. North, A.S. Verkman, D.S. Winlaw, Am J Physiol Heart Circ Physiol, 291 (2006) H705-713.
[12] T. Hibuse, N. Maeda, H. Nakatsuji, Y. Tochino, K. Fujita, S. Kihara, T. Funahashi, I. Shimomura, Cardiovasc Res, 83 (2009) 34-41.
[13] K. Kalman, K.L. Nemeth-Cahalan, A. Froger, J.E. Hall, J Biol Chem, 283 (2008) 21278-21283.
[14] G. Fischer, U. Kosinska-Eriksson, C. Aponte-Santamaria, M. Palmgren, C. Geijer, K. Hedfalk, S. Hohmann, B.L. de Groot, R. Neutze, K. Lindkvist-Petersson, PLoS Biol, 7 (2009) e1000130.
[15] S. Tornroth-Horsefield, K. Hedfalk, G. Fischer, K. Lindkvist-Petersson, R. Neutze, FEBS Lett, 584 (2010) 2580-2588.
[16] L. Janosi, M. Ceccarelli, PLoS One, 8 (2013) e59897.
[17] C. Tournaire-Roux, M. Sutka, H. Javot, E. Gout, P. Gerbeau, D.T. Luu, R. Bligny, C. Maurel, Nature, 425 (2003) 393-397.
[18] L. Leitao, C. Prista, T.F. Moura, M.C. Loureiro-Dias, G. Soveral, PLoS One, 7 (2012) e33219.
[19] L. Verdoucq, A. Grondin, C. Maurel, Biochem J, 415 (2008) 409-416.
[20] K.L. Nemeth-Cahalan, J.E. Hall, J Biol Chem, 275 (2000) 6777-6782.
[21] G. Soveral, A. Madeira, M.C. Loureiro-Dias, T.F. Moura, Biochim Biophys Acta, 1778 (2008) 2573-2579.
[22] M. Ozu, R.A. Dorr, F. Gutierrez, M.T. Politi, R. Toriano, Biophys J, 104 (2013) 85-95.
[23] L. Leitao, C. Prista, M.C. Loureiro-Dias, T.F. Moura, G. Soveral, Biochem Biophys Res Commun, 450 (2014) 289-294.
[24] T. Zeuthen, D.A. Klaerke, J Biol Chem, 274 (1999) 21631-21636.
[25] M. Zelenina, A.A. Bondar, S. Zelenin, A. Aperia, J Biol Chem, 278 (2003) 30037-30043.
[26] M. Zelenina, S. Tritto, A.A. Bondar, S. Zelenin, A. Aperia, J Biol Chem, 279 (2004) 51939-51943.
[27] M. Yasui, A. Hazama, T.-H. Kwon, S. Nielsen, W.B. Guggino, P. Agre, Nature, 402 (1999) 184-187.
[28] M. Zelenina, A.a. Bondar, S. Zelenin, A. Aperia, J Biol Chem, 278 (2003) 30037-30043.
[29] T. Zeuthen, D.a. Klaerke, Journal of Biological Chemistry, 274 (1999) 21631-21636.
[30] M. Hara, A.S. Verkman, P Natl Acad Sci USA, 100 (2003) 7360-7365.
[31] A. de Almeida, G. Soveral, A. Casini, MedChemComm, 5 (2014) 1444-1453.
[32] N. Maeda, T. Funahashi, I. Shimomura, Nature clinical practice. Endocrinol Metab, 4 (2008) 627-634.
[33] N. Pettersson, J. Hagstrom, R.M. Bill, S. Hohmann, Curr Genet, 50 (2006) 247-255.
[34] A.P. Martins, A. Marrone, A. Ciancetta, A. Galán Cobo, M. Echevarría, T.F. Moura, N. Re, A. Casini, G. Soveral, PloS one, 7 (2012) e37435.
[35] D. Ahmadpour, C. Geijer, M.J. Tamas, K. Lindkvist-Petersson, S. Hohmann, Biochim Biophys Acta, 1840 (2014) 1482-1491.
[36] F. Sabir, M.J. Leandro, A.P. Martins, M.C. Loureiro-Dias, T.F. Moura, G. Soveral, C. Prista, PloS one, 9 (2014) e102087.
[37] G. Soveral, A. Madeira, M.C. Loureiro-Dias, T.F. Moura, Appl Environ Microbiol, 73 (2007) 2341-2343.
[38] L. Leitão, C. Prista, T.F. Moura, M.C. Loureiro-Dias, G. Soveral, PloS one, 7 (2012) e33219.
[39] M.J. Tamas, K. Luyten, F.C. Sutherland, A. Hernandez, J. Albertyn, H. Valadi, H. Li, B.A. Prior, S.G. Kilian, J. Ramos, L. Gustafsson, J.M. Thevelein, S. Hohmann, Molecular microbiology, 31 (1999) 1087-1104.
[40] J. Nieto-Frausto, B. Kleutsch, Biochim Biophys Acta, 1111 (1992) 81-92.
[41] E. Campos, T.F. Moura, A. Oliva, P. Leandro, G. Soveral, Biochem Biophys Res Comm, 408 (2011) 477-481.
[42] D. Fu, A. Libson, R. Stroud, in: Ion Channels - from atomic resolution physiology to functional genomics, 2002, pp. 51-65.
[43] Z.E.R. Newby, J. O'Connell Iii, Y. Robles-Colmenares, S. Khademi, L.J. Miercke, R.M. Stroud, Nat Struct Mol Biol, 15 (2008) 619-625.
[44] A. Spinello, A. de Almeida, A. Casini, G. Barone, J Inorg Biochem, (2015).
[45] W.D. Stein, Biochim Biophys Acta, 59 (1962) 47-65.
[46] E. Tajkhorshid, P. Nollert, M.O. Jensen, L.J. Miercke, J. O'Connell, R.M. Stroud, K. Schulten, Science, 296 (2002) 525-530.
[47] M.O.E. (MOE), Chemical Computing Group Inc. Montreal, QC, Canada), 2012.10.
[48] D.G. Herries, Biochem Educ, 13 (1985) 146-146.

[49] K.L. Németh-Cahalan, K. Kalman, J.E. Hall, J Gen Physiol, 123 (2004) 573-580.
[50] T. Gonen, Y. Cheng, P. Sliz, Y. Hiroaki, Y. Fujiyoshi, S.C. Harrison, T. Walz, Nature, 438 (2005) 633-638.
[51] S. Kaptan, M. Assentoft, H.P. Schneider, R.A. Fenton, J.W. Deitmer, N. MacAulay, B.L. de Groot, Structure, 23 (2015) 2309-2318.
[52] A. Frick, M. Järvå, S. Törnroth-horsefield, FEBS letters, 587 (2013) 989-993.
[53] S. Törnroth-Horsefield, Y. Wang, K. Hedfalk, U. Johanson, M. Karlsson, E. Tajkhorshid, R. Neutze, P. Kjellbom, Nature, 439 (2006) 688-694.
[54] C. Tournaire-Roux, M. Sutka, H. Javot, E. Gout, P. Gerbeau, D.-T. Luu, R. Bligny, C. Maurel, Nature, 425 (2003) 393-397.
[55] D.E. Drew, G. von Heijne, P. Nordlund, J.W. de Gier, FEBS Lett, 507 (2001) 220-224.
[56] G. Soveral, A. Veiga, M.C. Loureiro-Dias, A. Tanghe, P. Van Dijck, T.F. Moura, Microbiology, 152 (2006) 1515-1521.
[57] A.P. Martins, A. Marrone, A. Ciancetta, A. Galan Cobo, M. Echevarria, T.F. Moura, N. Re, A. Casini, G. Soveral, PLoS One, 7 (2012) e37435.
[58] A.P. Martins, A. Ciancetta, A. de Almeida, A. Marrone, N. Re, G. Soveral, A. Casini, ChemMedChem, 8 (2013) 1086-1092.
[59] A. Serna, A. Galan-Cobo, C. Rodrigues, I. Sanchez-Gomar, J.J. Toledo-Aral, T.F. Moura, A. Casini, G. Soveral, M. Echevarria, J Cell Physiol, 229 (2014) 1787-1801.
[60] A. Madeira, A. de Almeida, C. de Graaf, M. Camps, A. Zorzano, T.F. Moura, A. Casini, G. Soveral, Chembiochem : a European journal of chemical biology, 15 (2014) 1487-1494.
[61] T. Katano, Y. Ito, K. Ohta, T. Yasujima, K. Inoue, H. Yuasa, Drug Metab Pharmacok, 29 (2014) 244-248.
[62] E. Krieger, J.E. Nielsen, C.A. Spronk, G. Vriend, J Mol Graph Model, 25 (2006) 481-486.
[63] A. Fersht, Enzyme Structure and Mechanism, 2nd Ed ed., W.H. Freeman and company, New York.
[64] E. Sohara, T. Rai, J. Miyazaki, A.S. Verkman, S. Sasaki, S. Uchida, Am J Physiol Renal Physiol, 289 (2005) F1195-1200.
[65] K. Matsumura, B.H. Chang, M. Fujimiya, W. Chen, R.N. Kulkarni, Y. Eguchi, H. Kimura, H. Kojima, L. Chan, Mol Cell Biol, 27 (2007) 6026-6037.
[66] M.T. Skowronski, J. Lebeck, A. Rojek, J. Praetorius, E.M. Fuchtbauer, J. Frokiaer, S. Nielsen, Am J Physiol Renal Physiol, 292 (2007) F956-965.
[67] A. Rutkovskiy, G. Valen, J. Vaage, Basic Res Cardiol, 108 (2013) 393.
[68] E. Sohara, S. Uchida, S. Sasaki, Handb Exp Pharmacol, (2009) 219-231.
[69] Q. Chen, H. Peng, L. Lei, Y. Zhang, H. Kuang, Y. Cao, Q.X. Shi, T. Ma, E. Duan, Cell Res, 21 (2011) 922-933.
[70] N. Newcombe, J. Clulow, S.Y. Man, R.C. Jones, Int J Androl, 23 (2000) 46-50.
[71] M. Zelenina, S. Tritto, A.a. Bondar, S. Zelenin, A. Aperia, J Biol Chem, 279 (2004) 51939-51943.
[72] D. Hanahan, Techniques for transformation of Escherichia coli, Oxford: IRL Press, 1985.
[73] J. Sambrook, E.F. Fritsch, T. Maniatis, Molecular Cloning: A Laboratory Manual, 2nd edn ed., Cold Spring Harbor, NY, 1989.
[74] J.T. Pronk, Appl Environ Microb, 68 (2002) 2095-2100.
[75] R.D. Geitz, R.H. Schiestl, Methods in Mol Cell Biol, 5 (1995) 255–269.
[76] M. Henriques, C. Quintas, M.C. Loureiro-Dias, Microbiology, 143 (1997) 1877-1883.

Part B

Gold Compounds as Anticancer Agents

B1. Gold(I) Organometallic Compounds with Biological Activity in Cancer Cells

This chapter is published:

Benoit Bertrand*, Andreia de Almeida*, Evelien P.M. van der Burgt, Michel Picquet, Anna Citta, Alessandra Folda, Maria Pia Rigobello, Pierre Le Gendre, Ewen Bodio and Angela Casini

New Gold(I) Organometallic Compounds with Biological Activity in Cancer Cells

Eur.J.Inorgn.Chem. (2014) 27:4532-4536

Supplementary information available: 10.1002/ejic.201402248

*Authors contributed equally to this work

Abstract

N-Heterocyclic carbene gold(I) complexes bearing a fluorescent coumarin ligand were synthesized and characterized by various techniques. The compounds were examined for their antiproliferative effects in normal and tumor cells *in vitro*; they demonstrated moderate activity and a certain degree of selectivity. The compounds were also shown to efficiently inhibit the selenoenzyme thioredoxin reductase (TrxR), whereas they were poorly effective towards the glutathione reductase (GR) and glutathione peroxidase enzymes. Notably, {3-[(7-methoxy-2-oxo-*2H*-chromen-4-yl)methyl]-1-methylimidazol-2-ylidene}(tetra-O-acetyl-1-thio-β-d-glucopyranosido)gold(I) (3) showed a pronounced inhibition of TrxR also in cell extracts, and it appeared to activate GR. Mechanistic information on the system derived from biotin-conjugated iodoacetamide assays showed selective metal binding to selenocysteine residues. Preliminary confocal fluorescence microscopy experiments proved that **3** enters tumor cells, where it reaches the nuclear compartment.

1.1. Introduction

Following the clinical success of cisplatin, many platinum and non-platinum metallodrugs are currently investigated as experimental antitumor agents with different mechanisms of action and improved pharmacological properties with respect to existing drugs [1]. However, major challenges must be faced to reach such a goal, including the identification of the actual biological targets for metal compounds, as well as the determination of their distribution in tissues, cells and subcellular compartments, to achieve an understanding of the possible mechanisms of biological activity [2].

It is worth mentioning that gold complexes belonging to various families have drawn attention in the last years as new generation of experimental anticancer agents, and have shown to possess anticancer properties *in vitro* and *in vivo* [3, 4]. Notably, various organometallic gold complexes were synthesized in which the presence of a direct carbon-gold bond greatly stabilizes the gold oxidation state and guarantees more controlled chemical speciation in biological systems. In general, both organometallic gold(I) and gold(III) compounds have increased stability compared to the classical gold-based coordination complexes, allowing to design compounds in which the redox properties and ligand exchange reactions can be modulated to achieve selective activation in diseased cells.

Mechanistic studies showed that interactions of gold complexes with DNA are not as tight as found for platinum(II) drugs, suggesting the occurrence of different pathways to cytotoxicity [5-7]. Indeed, several studies supported the idea that mitochondria and pathways of oxidative phosphorylation are among the primary intracellular targets [8]. Moreover, inhibition of the seleno-enzyme thioredoxin reductase (TrxR) appears as a common mechanistic trait to explain (at least partially) the cytotoxic actions of gold complexes, as strong TrxR inhibition may eventually lead to apoptosis through a mitochondrial pathway [9, 10]. TrxRs are large homodimeric proteins playing a crucial role in the intracellular redox balance [11]. Two major isoforms are known, a cytosolic (TrxR1) and a mitochondrial one (TrxR2); their main function is the reduction of 12 kDa disulfide protein thioredoxin (Trx) to its dithiolic form [9]. Interestingly, the view that TrxRs are

effective "druggable" targets for inorganic compounds is supported, for example, by mechanistic investigation of arsenic trioxide, a potent TrxR inhibitor now approved for promyelocytic leukaemia treatment [12].

Within this frame, in the last years, gold(I) N-heterocyclic carbenes (NHCs) have transformed from niche compounds to some of the most popular scaffolds in medicinal inorganic chemistry [13, 14]. For example, studies by our group, et al., confirmed that many gold(I) NHC complexes with the 1,3-substituted imidazol-2-ylidene and benzimidazol-2-ylidene ligands of the type NHC-Au-L (L = Cl or 2-mercapto-pyrimidine) can potently inhibit both of the cytosolic and mitochondrial isoforms of the TrxR enzyme [15]. The compounds showed potent and selective TrxR inhibition properties in particular in cancer cell lines.

On the basis of these promising results, we report here on the synthesis and characterization of three new gold(I) NHC complexes bearing a coumarin moiety. This functionalization was chosen because coumarin derivatives are one of the most studied fluorophore for *in vitro* imaging. They display a good chemical and photochemical stability, relatively high absorption coefficients and quantum yields, and are very easily available. Moreover, two of the new derivatives bear 1-thio-β-D-glucose-type ligands, which may affect the uptake of the compounds as previously observed for other gold(I) complexes [16].

All compounds were tested *in vitro* against different human cancerous cell lines (i.e. A2780, MCF7, and A549) along with non-cancerous cells (i.e. HEK-293T). To gain preliminary mechanistic insights, we screened the interactions of compounds 1–4 with TrxR. The compounds were also screened for inhibition of glutathione reductase (GR), a pyridine disulfide oxidoreductase able to maintain glutathione in its reduced state, as well as of the seleno-enzyme glutathione peroxidase (Gpx). Additional complementary information regarding the enzyme metallation process and possible binding sites was obtained through the application of a specific biochemical assay that relies on the thiol-tagging reagent, BIAM (biotin-conjugated iodoacetamide). Furthermore, fluorescence confocal microscopy has been used to study compounds' uptake in cancer cells.

1.2. Results and Discussion

1.2.1. Synthesis

The chlorido gold carbene was efficiently synthesized in three steps by adapting literature procedures (Scheme 1) [17, 18]. Thus, 1-methylimidazole was alkylated by the commercially available 4-bromomethyl-7-methoxycoumarin to obtain the imidazolium salt **1** in 95% yield. Afterwards, **1** was treated with silver oxide at room temperature in the dark to generate the silver carbene which was transferred to gold by reaction with the precursor [AuCl(tht)]. The formation of the gold carbene complex **2** was assessed by ^{1}H and $^{13}C\{^{1}H\}$ NMR spectroscopy. The singlet corresponding to the imidazolium proton disappeared and a significant shift of the signal of the C-2 carbon was observed going from 138.2 ppm in the imidazolium salt to 173.5 ppm in the complex (carbenic carbon). This behaviour is in agreement with already reported data in the literature ([19] and references cited therein).

Replacing the chlorido ligand on some phosphine gold(I) complexes by 1-thio-β-D-glucose tetraacetate was reported to result in an enhancement of both the cytotoxic effects and uptake [16].

Thus, we decided to substitute the chlorido ligand of **2** by both thio-β-D-glucose tetraacetate and thio-β-D-glucose (Scheme 1). While the tetraacetate derivative **3** was obtained by deprotonation of the thiol using 1 M NaOH in acetone [20], the thio-β-D-glucose complex **4** was synthesized by direct reaction of the commercially available sodium thiolate-β-D-glucose with the chlorido gold carbene **2**. All compounds were fully characterized by ^{1}H and $^{13}C\{^{1}H\}$ NMR, IR, high-resolution MS and their purity was checked by elemental analysis. A far infrared spectrum confirmed the formation of an S-Au bond in both cases, displaying a novel absorption band around 370 cm^{-1} and the absence of the band at 330 cm^{-1} corresponding to the ν_{Au-Cl} stretching [21]. The ^{1}H NMR spectra of **3** and **4** show the expected 1/1 ratio of the signals of the NHC with respect to the sugar moiety. The signal of the carbenic carbon in the $^{13}C\{^{1}H\}$ NMR spectrum of **3** resonates downfield from 2 (Dd = -3.6 ppm) and is not observed in case of **4**. However, by 1H-13C correlation NMR spectroscopy, we observe a correlation spot between both the N-methyl and the methylene bridge signals in the 1H spectrum and a signal at around 181 ppm in the $^{13}C\{^{1}H\}$ spectrum of **4** (see ^{1}H-^{13}C HMBC spectrum in the Supplementary Material, Figure S1). Noteworthy, the elemental analysis of **4** shows that it is in the form of adduct with one equivalent of NaCl, probably through the hydroxyl groups of the glucose moiety as already reported for different sugars [22]. The photophysical characterization was performed for the four compounds (see details of the study in the Supplementary Material). No significant change was observed between the imidazolium salt **1** and the Au(I) NHC complexes **2-4**. The compounds display a maximum of absorption around 325 nm, a maximum of emission around 400 nm, and the molar absorption coefficient remains almost the same for the different compounds. The quantum yields are low, maybe due to a photoinduced electron transfer (PET) between the coumarin and the imidazolium/carbine [23, 24].

1.2.2. In vitro cell viability assays

The antiproliferative properties of the imidazolium salt **1** and the Au(I) NHC complexes **2-4** (with cisplatin used as comparison) were assessed by monitoring their ability to inhibit cell growth using the classical MTT assay in human ovarian cancer A2780 cell line, in human mammary carcinoma MCF7 cells, as well as in the human lung cancer A549 cell line. In addition, in order to evaluate the compounds' selectivity for cancerous compared to healthy cells, these coumarin derivatives were also tested in human embryonic kidney HEK-293T cells. Overall, the compounds are markedly less effective in all the selected cell lines in comparison to cisplatin. Only in the case of the MCF7 cells, compound **3** shows a better activity (IC_{50} = 11.6 ± 0.8 µM) than cisplatin. Notably, **3**, bearing the 1 thio-β-D-glucose tetraacetate ligand, is also the most active of the series in A2780 and MCF7 cells, as well as the one relatively selective for cancer cells with

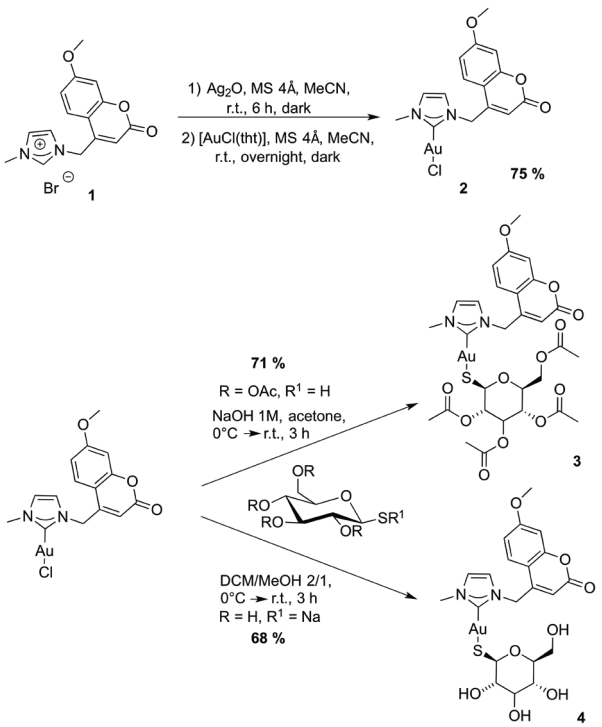

Scheme 1. Synthesis of the investigated gold(I) NHC complexes.

respect to non-cancerous ones. The inactivity of 4 in all tested cells, rules out the idea that the 1 thio-β-D-glucose ligand may enhance the compound's uptake via GLUT-1 transporters.

Table 1. Effects of compounds **1-4** on cell viability in human ovarian carcinoma A2780 cells, in human lung cancer A549 cells, in human mammary carcinoma MCF7 cells, and in embryonic kidney cells (HEK-293T) after 72 h incubation

	IC_{50} (μM) [a]			
Compound	**A2780**	**A549**	**MCF7**	**HEK-293T**
1	46.9 ± 13.3	52.5 ± 17.9	71.2 ± 5.2	>100
2	45.5 ± 7.5	95.8 ± 5.3	39.7 ± 11.8	48.0 ± 8.4
3	11.6 ± 0.8	55.6 ± 12.6	12.9 ± 3.8	15.2 ± 1.7
4	>100	>100	64.5 ± 11.5	>100
Cisplatin	1.9 ± 0.6	8.0 ± 0.5	20.0 ± 3.1	11.0 ± 2.9

[a] Values are the mean ± SE of at least three determinations.

Because TrxR is a potential target for gold compounds, *in vitro* inhibition of rat TrxR by **1-4** was studied using an established protocol. The results summarized in Figure 1 and Table 2 show that the gold(I) NHC complexes inhibit both TrxR1 and TrxR2, although less efficiently than the gold(I) compound auranofin. Notably, ligand **1** is ineffective as inhibitor at least until 30 μM concentration (Table 2). Moreover, the new complexes are much less efficient with respect to both the closely related selenium enzyme glutathione peroxidase (Gpx), and the Se-free glutathione reductase (GR) having IC_{50} values >10000 nM. Notably, minor Gpx inhibition was shown for different gold(I) NHC complexes previously reported [25].

Additional complementary information on the interaction of TrxR with compound **1-3**, and possible binding sites was obtained through the application of a specific biochemical assay relying on the thiol-tagging reagent BIAM (biotin-conjugate iodoacetamide). BIAM selectively alkylates TrxR in a pH dependent manner; at pH 6.0 only seleno-cysteines and low pK_a cysteines are alkylated. In our experiments, TrxR1 was treated with metal complex, and afterwards, sample aliquots were treated with BIAM at pH 6.0. Thus, the samples were analysed by SDS-PAGE. BIAM-labelled proteins were detected with horseradish peroxidase-conjugated streptavidin (see Figure S3 and Experimental Section for further details). The immunoblotting indicated that the tested gold complexes are able to target, although to slightly varying extents, the seleno-cysteine residues

Table 2. IC_{50} values for TrxRs, GR and Gpx inhibition calculated for compounds **1-4**.

	IC_{50} (nM) [a]			
Compound	**A2780**	**A549**	**MCF7**	**HEK-293T**
1	>10000	>10000	>10000	>10000
2	16.38 ± 1.32	76.52 ± 3.2	>1000	>500
3	17.90 ± 1.8	78.66 ± 1.2	>1000	>500
4	6.49 ± 0.2	54.02 ± 1.3	>1000	>1000
Auranofin	1.5 ± 0.2	24.3 ± 1.2	>1000	>1000

[a] Values are the mean ± SE of at least three determinations.

present in the enzyme redox-active motif.

To assess whether TrxR inhibition by the compounds under study could contribute to the observed antiproliferative effects on cells, enzyme activity was also evaluated on protein extracts obtained from A2780 cells, pre-treated with 10 μM of the compound **3** (close to the IC_{50} for the antiproliferative effects) for 48 h. In this case we observed an inhibition of thioredoxin reductase activity of ca. 30% with respect to control samples (Figure S4 in the supplementary material). Conversely glutathione reductase, tested in the same cell lysates, appears to be largely stimulated. This fact can be explained as a response to the stress that cells are subjected to after inhibition of the thioredoxin system. In fact, as a control, isolated GR is not inhibited by this compound.

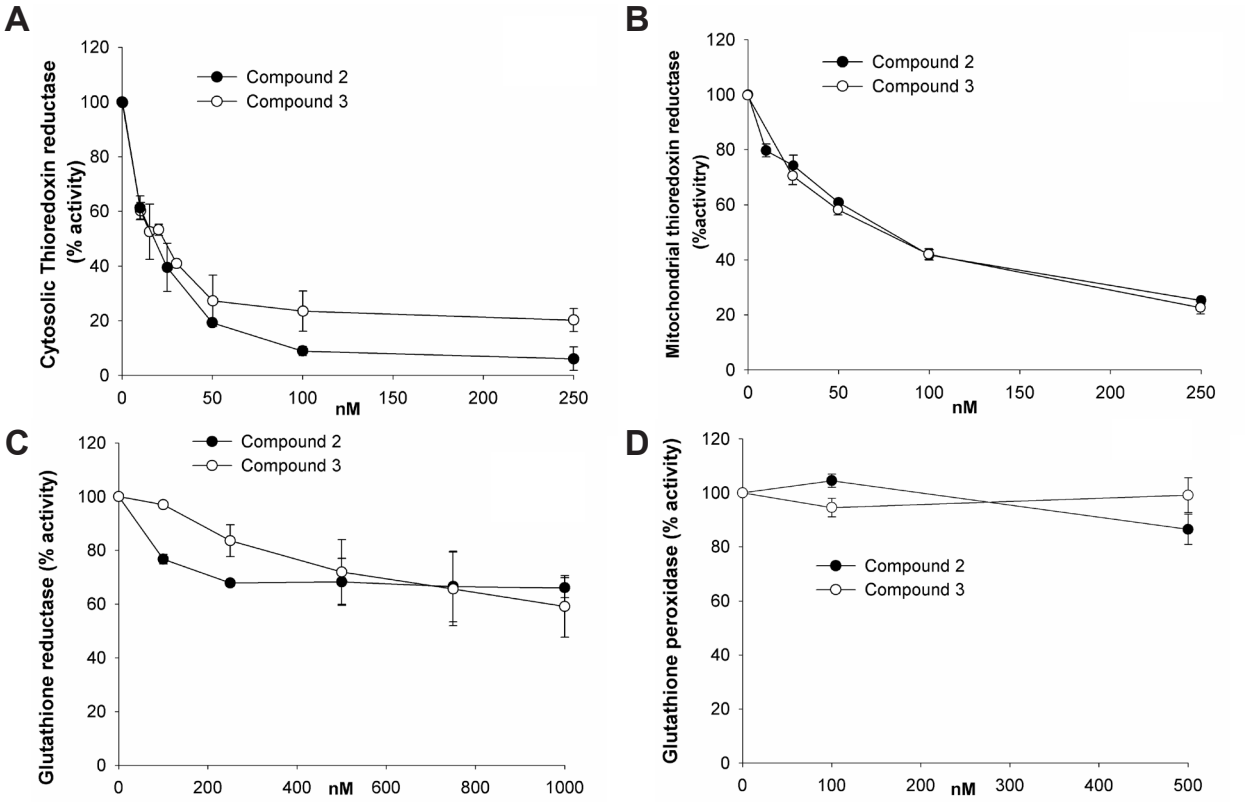

Figure 1. Effect of compounds **2-3** on cytosolic (A) and mitochondrial (B) TrxRs, (C) GR and (D) Gpx enzymes. The compounds were tested in isolated and purified enzymes.

B1

1.2.3. Fluorescence microscopy

It is worth mentioning that, among the various strategies to achieve metal compounds imaging in biological environments, fluorescence microscopy is certainly one of the most explored, and an increasing number of publications has appeared reporting on bifunctional metal compounds bearing fluorescent moieties for both therapeutic and imaging applications [26, 27]. Thus, recently, we described a gold(I) NHC complex bearing a fluorescent anthracenyl ligand whose cytotoxic effects were investigated *in vitro* in different lines of normal and cancerous human cells [28].

Similarly, the uptake of **3** was evaluated in A2780 cells by using fluorescence confocal microscopy. Figure 2 shows typical fluorescence images of cells treated with 3 (50 μM) for 2 h at 37 °C. Unfortunately, the low fluorescence of the compounds allowed visualization only at 50 μM or higher. We avoided longer incubation times due to the relatively high tested concentrations of compounds, which may have induced rapid cell death. In the obtained images, preserved cell morphology confirms viability after treatment, and compound's uptake is evident, as well as its accumulation in the nuclei (colocalization with PI staining).

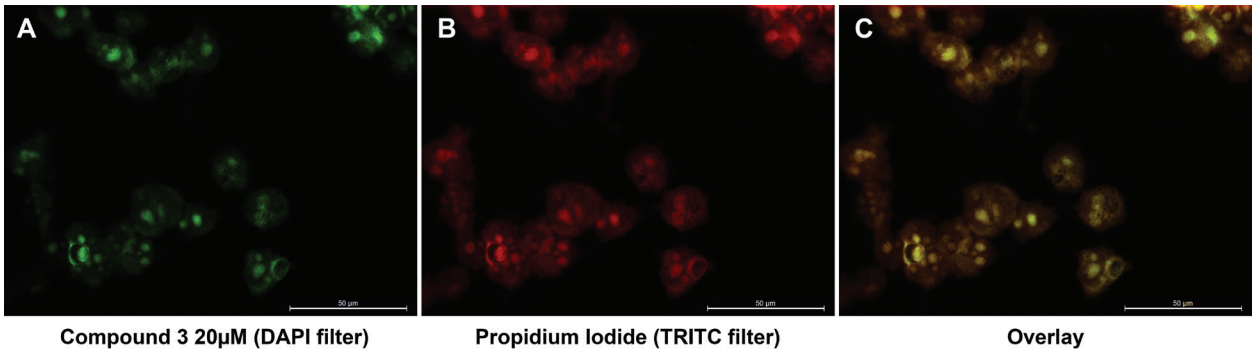

Figure 2. Visualization of gold(I)–NHC compound using confocal microscopy. A2780 cells were incubated for 2 h with 50 µM of 3 at 37 °C. A: fluorescence of the compound; B: propidium iodide localization; C: merge.

1.3. Conclusions

In summary, we have synthesized and characterized a new family of gold(I) NHC complexes bearing a fluorescent coumarin-type carbene ligand, using a limited number of steps (2-3). Two of the reported compounds bear thio-*β*-D-glucose groups as second ligand. Notably, this study was initiated in the frame of ongoing studies in our laboratories aiming at developing new organometallic gold compounds as anticancer agents. In fact, as demonstrated by numerous studies, regulating the reactivity of gold compounds *via* the optimization of an appropriate organometallic scaffold may constitute a strategy to achieve selectivity for cancer tissues, a feature that is often lacking with other types of coordination gold complexes.

Thus, the new compounds have been tested in different cancer cell lines showing moderate antipoliferative properties, in particular the derivative bearing the 1-thio-*β*-D-glucose tetraacetate ligand (3), which was also uptaken in cancer cells as shown by fluorescence microscopy. Preliminary mechanistic studies have demonstrated that the compounds are able to inhibit the cancer relevant enzyme thioredoxin reductase, most likely targeting the seleno-cysteine residue in the active site. Presently, further studies are ongoing in our labs to validate this protein target, since other interactions may occur between the gold(I) compounds and other relevant biomolecules. As an example, a recent study described for the first time the properties of a cationic gold(I) bis-NHC complex containing a caffeine-based ligand as DNA G-quadruplex stabilizing agent with exquisite quadruplex-over-duplex DNA selectivity [29].

1.4. Experimental Section

General Remarks: All reactions were carried out under an atmosphere of purified argon using Schlenk techniques. Solvents were dried and distilled under argon before use. The precursor [AuCl(tht)] (Uson R. et al, Inorg Synth. 1989, 26, 85-91) has been synthesized according to literature procedure. All other reagents were commercially available and used as received. All the analyses were performed at the "Plateforme d'Analyses Chimiques et de Synthèse Moléculaire de l'Université de Bourgogne". The identity and purity (≥ 95%) of the complexes were unambiguously established using high-resolution mass spectrometry, elemental analysis, NMR and IR spectrometries. Exact mass of the synthesized complexes were obtained on a Thermo LTQ Orbitrap XL. Elemental analyses were performed on a Thermo Electron Flash EA 1112 Series analyzer. ^{1}H- (300.13, 500.13 or 600.23 MHz) and 13C- (125.77 or 150.90 MHz) NMR spectra were recorded on Bruker 300 Avance III, 500 Avance III or 600 Avance II spectrometers. Chemical shifts are quoted in ppm (δ) relative to TMS (1H and 13C) using the residual protonated solvent (1H) or the deuterated solvent (^{13}C) as internal standards. Infrared spectra were recorded on a Bruker Vector 22 FT-IR spectrophotometer (Golden Gate ATR) and far infrared spectra were recorded on a Bruker Vertex 70v FT-IR spectrophotometer (ATR Diamant).

• **3-[(7-methoxy-2-oxo-2H-chromen-4-yl)methyl]-1-methylimidazolium bromide (1)**

A two-neck round-bottom flask was charged under argon with 1 g of 4 (bromomethyl) 7 methoxy-2H-chromen-2-one (3.76 mmol) which was suspended in THF (50 mL). 1-methylimidazole (0.31 mL, 3.76 mmol) was added dropwise

and the mixture was refluxed overnight. After removing of the THF under vacuum, the obtained white powder was suspended into dry dichloromethane and a large amount of diethyl ether. The suspension was filtered and the residue was dried under vacuum to afford the pure product as a white powder (1.26 g, 96 % yield).

^{1}H NMR (DMSO-d6, 300.13 MHz, 300 K): 3.88 (s, 3 H, N-Me), 3.89 (s, 3 H, O-Me), 5.78 (s, 2 H, N-CH_2), 5.89 (s, 1 H, CH^A), 7.02 (dd, 1 H, $^3J_{H-H}$ = 9.0 Hz, $^4J_{H-H}$ = 2.7 Hz, CH^C), 7.08 (d, 1 H, $^4J_{H-H}$ = 2.7 Hz, CH^B), 7.76 (d, 1 H, $^3J_{H-H}$= 9.0 Hz, CH^D), 7.80 (s, 1 H, CH^{Im}), 7.84 (s, 1 H, CH^{Im}), 9.22 (s, 1 H, N=CH-N^+).

^{13}C{1H} (DMSO-d6, 75.78 MHz, 300 K): 36.6 (s, N-CH3), 48.8 (s, N-CH2), 56.6 (s, O-CH3), 101.6 (s, CHB), 110.7 (s, CHA), 113.1 (s, CHC), 123.4 (s, CHIm), 124.7 (s, CHIm), 126.1 (s, CHD), 138.2 (s, N=CH-N+), 149.8 (s, Cquat-CHD), 155.5 (s, Cquat-OC(O)), 160.2 (s, C(O)), 163.4 (s, Cquat-OMe).

FT-IR (ATR, cm^{-1}): 3122, 3064, 2847, 1705, 1607, 1564, 1515, 1464, 1439, 1400, 1342, 1286, 1270, 1211, 1169, 1137.

ESI-MS (DCM/MeOH), positive mode exact mass for $C_{15}H_{15}N_2O_3^+$ (271.10772): measured *m/z* 271.10664 $[M\ Br]^+$.

Anal. Calc. for $C_{15}H_{15}N_2O_3Br$: C, 51.30, H, 4.31, N, 7.98 %. Found: C, 51.27, H, 4.05, N, 8.03 %.

• 3-[(7-methoxy-2-oxo-2H-chromen-4-yl)methyl]-1-methylimidazol-2-ylidene gold(I) chloride (2)

A round-bottom flask was charged with **1** (200 mg, 0.57 mmol) and Ag_2O (106 mg, 0.46 mmol) which were suspended in dichloromethane (150 mL). The mixture was reacted for 6 h at room temperature in the dark. [AuCl(tht)] (182 mg, 0.57 mmol) was then added and the reaction was stirred overnight at room temperature in the dark. After filtration through Celite, the filtrate was concentrated under reduced pressure. Upon addition of a large amount of diethyl ether, a pale yellow precipitate was formed and was collected by filtration. The residue was dried under vacuum to afford the pure product as a pale yellow powder (215 mg, 75 % yield).

^{1}H NMR ($CDCl_3$, 300.13 MHz, 300 K): 3.89 (s, 3 H, N-Me), 3.92 (s, 3 H, O-Me), 5.55 (s, 2 H, N CH_2), 5.68 (s, 1 H, CH^A), 6.85 (d, 1 H, $^4J_{H-H}$ = 2.7 Hz, CH^B), 6.89 (dd, 1 H, $^3J_{H-H}$ = 9.0 Hz, $^4J_{H-H}$ = 2.7 Hz, CH^C), 7.00 (d, 1 H, $^3J_{H-H}$ = 1.8 Hz, CH^{Im}), 7.06 (s, 1 H, $^3J_{H-H}$ = 1.8 Hz, CH^{Im}), 7.52 (d, 1 H, $^3J_{H-H}$ = 9.0 Hz, CH^D).

^{13}C{1H} ($CDCl_3$, 75.78 MHz, 300 K): 38.6 (s, N-CH_3), 51.1 (s, N-CH_2), 55.9 (s, O-CH_3), 101.5 (s, CHB), 110.3 (s, CH^A), 110.8 (s, C_{quat}-CH_2), 112.9 (s, CH^C), 120.9 (s, CH^{Im}), 122.9 (s, CH^{Im}), 124.5 (s, CH^D), 148.8 (s, C_{quat}-CH^D), 155.6 (s, C_{quat}-OC(O)), 160.2 (s, C(O)), 163.4 (s, C_{quat}-OMe), 173.5 (s, $C_{carbene}$).

FT-IR (ATR, cm^{-1}): 3129, 2943, 1709, 1610, 1558, 1515, 1465, 1429, 1397, 1348, 1331, 1288, 1245, 1207, 330.

ESI-MS (DCM/MeOH), positive mode exact mass for $C_{15}H_{15}N_2O_3AuClNa^+$ (525.02507): measured *m/z* 525.02328 $[M+Na]^+$.

Anal. Calc. for $C_{15}H_{15}N_2O_3AuCl$: C, 35.84, H, 2.81, N, 5.57 %. Found: C, 35.74, H, 3.00, N, 5.50 %.

• 3-[(7-methoxy-2-oxo-2H-chromen-4-yl)methyl]-1-methylimidazol-2-ylidene gold(I) (thio-β-D-glucose tetraacetate) (3)

A Schlenk tube was charged under argon with thio-*β*-D-glucose tetraacetate (36 mg, 0.10 mmol) which was dissolved in degassed acetone (3 mL). 1 M NaOH (0.1 mL, 0.10 mmol, 1 eq.) was added and the mixture was stirred for 30 min at room temperature. The mixture was then transferred onto a solution of 1 (50 mg, 0.10 mmol) in 5 mL of degassed acetone at 0°C. At the end of the addition, the ice bath was withdrawn and the mixture was stirred for 3 h at room temperature in the dark. The solvent was removed under vacuum. Dichloromethane was added and the mixture was filtered through Celite. The filtrate was concentrated under reduced pressure. An off-white precipitate was formed after addition of a large amount of n-pentane. The precipitate was filtered and dried under vacuum to give the pure product as an off-white powder (58 mg, 71 % yield).

^{1}H NMR ($CDCl_3$, 300.13 MHz, 300 K): 1.95 (s, 3 H, CH_3-COO), 2.00 (s, 3 H, CH_3-COO), 2.02 (s, 6 H, 2 CH_3-COO), 3.67-3.72 (m, 1 H, CH_{sugar}), 3.87 (s, 3 H, N-Me), 3.95 (s, 3 H, O-Me), 4.06 (dd, 1 H, $^2J_{H-H}$ = 12.3 Hz, $^3J_{H-H}$ = 2.4 Hz, $CH_{A-B,sugar}$), 4.20 (dd, 1 H, $^2J_{H-H}$ = 12.3 Hz, $^3J_{H-H}$ = 4.8 Hz, $CH_{A-B,sugar}$), 4.99-5.11 (m, 4 H, 4 CH_{sugar}), 5.57 (dd, 1 H, $^2J_{H-H}$ = 16.8 Hz, $^3J_{H-H}$ = 1.2 Hz, CH_{A-B}-N), 5.67 (d, 1 H, $^2J_{H-H}$ = 16.8 Hz, CH_{A-B}-N), 5.75 (s, 1 H, CH^A), 6.86 (d, 1 H, $^4J_{H-H}$ = 2.4 Hz, CH^B), 6.92 (dd, 1 H, $^3J_{H-H}$ = 8.7 Hz, $^4J_{H-H}$ = 2.4 Hz, CH^C), 6.96 (d, 1 H, $^3J_{H-H}$= 1.8 Hz, CH^{Im}), 7.03 (d, 1 H, $^3J_{H-H}$ = 1.8 Hz, CH^{Im}), 7.67 (d, 1 H, $^3J_{H-H}$ = 8.7 Hz, CH^D).

^{13}C{1H} ($CDCl_3$, 125.77 MHz, 300 K): 20.6 (s, CH_3-COO), 20.7 (s, CH_3-COO), 20.8 (s, CH_3-COO), 21.2 (s, CH_3-COO), 38.3 (s, CH_3-N), 50.9 (s, CH_2-N), 55.9 (s, CH_3-O), 63.0 (s, CH_2-$_{sugar}$), 69.0 (s, CH_{sugar}), 74.3 (s, CH_{sugar}), 75.8 (s, CH_{sugar}), 77.6 (s, CH_{sugar}), 83.1 (s, CH_{sugar}), 101.4 (s, CH^B), 110.6 (s, C_{quat}-CH2), 111.0 (s, CH^A), 112.9 (s, CH^C), 120.7 (s, CH^{Im}), 122.8 (s, CH^{Im}), 125.0 (s, CH^D), 149.3 (s, C_{quat}-CH^D), 155.6 (s, C_{quat}-OC(O)), 160.4 (s, C(O)coum.), 163.3 (s,

C_{quat}-OMe), 169.6 (s, $C(O)_{sugar}$), 169.9 (s, Ccarbene), 170.2 (s, $C(O)_{sugar}$), 170.7 (s, $C(O)_{sugar}$).

FT-IR (ATR, cm^{-1}): 2946, 1735, 1613, 1561, 1463, 1430, 1368, 1288, 1219, 1147, 1031, 373.

ESI-MS ($CDCl_3$/MeOH), positive mode exact mass for $C_{29}H_{33}N_2O_{12}AuSNa^+$ (853.13119): measured *m/z* 853.12907 $[M+Na]^+$.

Anal. Calc. for $C_{29}H_{33}N_2O_{12}AuS$: C, 41.93, H, 4.00, N, 3.37, S, 3.86 %. Found: C, 41.54, H, 4.20, N, 3.27, S, 3.09 %.

• 3-[(7-methoxy-2-oxo-2H-chromen-4-yl)methyl]-1-methylimidazol-2-ylidene gold(I) (thiolato-β-D-glucose) (4)

A flame-dried Schlenk tube was charged under argon with sodium thiolate-*β*-D-glucose (26 mg, 0.12 mmol) which was suspended in methanol (3 mL). This mixture was transferred onto a solution of 2 (60 mg, 0.12 mmol) in 6 mL of dichloromethane at 0°C. After the end of the addition, the ice bath was withdrawn and the mixture was stirred for 3 h at room temperature. The solution was filtered under argon through Celite using a flame-dried sintered glass. Upon concentration under reduced pressure, and addition of a large amount of a mix diethylether/n pentane, a white precipitate was formed. The precipitate was filtered and dried under vacuum to afford the product as an adduct with one equivalent of NaCl (58 mg, 68 % yield).

^{1}H NMR (DMSO-d6, 600.23 MHz, 300 K): 2.50 (dt, 1 H, $^3J_{H-H}$ = 9.0 Hz, $^3J_{H-H}$ = 3.6 Hz, CH_{sugar}), 2.93-3.04 (m, 3 H, 3 CH_{sugar}), 3.24-3.28 (m, 1 H, CH_2-sugar), 3.55 (ddd, 1 H, $^2J_{H-H}$ = 11.4 Hz, $^3J_{H-H}$ = 5.4 Hz, $^3J_{H-H}$ = 1.8 Hz, CH_{sugar}), 3.82 (s, 3 H, NCH_3), 3.87 (s, 3 H, OCH_3), 3.97 (broad s, 1 H, OH), 4.35 (pseudo t, 1 H, $^3J_{H-H}$ = 5.7 Hz, CH_2-OH), 4.47 (d, 1 H, $^3J_{H-H}$ = 9.0 Hz, CH_{sugar}), 4.71-4.73 (m, 2 H, 2 OH), 5.59 (s, 1 H, CH^A), 5.64 (s, 2 H, NCH_2), 7.01 (dd, 1 H, J_{H-H}= 8.4 Hz, $^4J_{H-H}$= 1.8 Hz, CH^C), 7.05 (s, 1 H, CH^B), 7.52 (s, 2 H, 2 CH^{Im}), 7.86 (d, 1 H, $^3J_{H-H}$ = 8.4 Hz, CH^D).

^{13}C{1H} NMR (DMSO-d6, 125.77 MHz, 300 K): 37.5 (broad s, NCH_3), 49.9 (broad s, NCH_2), 56.0 (s, OCH_3), 61.4 (s, CH_2-sugar), 70.5 (s, CH_{sugar}), 77.4 (s, CH_{sugar}), 80.1 (s, CH_{sugar}), 81.1 (s, CH_{sugar}), 85.1 (s, CH_{sugar}), 101.2 (s, CH^B), 109.3 (broad s, C_{quat}-CH_2), 110.5 (s, CH^A), 112.4 (s, CH^A), 121.9 (broad s, CH^{Im}), 123.3 (broad s, CH^{Im}), 125.8 (s, CH^D), 151.5 (s, C_{quat}-CH^D), 154.9 (s, C_{quat}-OC(O)), 159.8 (s, C(O)), 162.8 (s, C_{quat}-OMe), ca. 171 (Ccarbene not directly observed, see below).

FT-IR (ATR, cm^{-1}): 3365, 2909, 1710, 1610, 1559, 1515, 1463, 1399, 1349, 1289, 1146, 1020, 840, 558, 179, 171.

ESI-MS (MeOH), positive mode exact mass for $C_{21}H_{25}N_2O_8AuSNa^+$ (685.08893): measured *m/z* 685.08564 $[M+Na]^+$, ESI-MS (MeOH), negative mode exact mass for $C_{21}H_{25}N_2O_8AuSCl^-$ (697.06802): measured *m/z* 697.07103 $[M+Cl]^-$.

Anal. Calc. for $C_{21}H_{25}N_2O_8AuS.NaCl$: C, 34.99, H, 3.50, N, 3.89, S, 4.45 %. Found: C, 34.38, H, 3.64, N, 4.08, S, 3.21 %.

Remark: ^{13}C{^{1}H} NMR signals of 4 corresponding to the carbons of the imidazole ring appeared very broad and no signal of the carbenic carbon appeared. However, by ^{1}H-^{13}C HMBC correlation NMR spectroscopy, we could observe a correlation spot between both the N-methyl and the methylene bridge signals in the ^{1}H spectrum and a signal at around 181 ppm in the ^{13}C{1H} spectrum.

Fluorescence measurements: The steady-state fluorescence emission and excitation spectra were obtained by using a JASCO FP8560 spectrofluorometer instrument. All fluorescence spectra were corrected for instrument response. The fluorescence quantum yield (Φ_F) was calculated from equation 1.

$$\frac{\Phi_F}{\Phi_{FR}} = \frac{n^2}{n_R^2} \times \frac{\int_0^\infty I_F(\lambda_E,\lambda_F)d\lambda_F}{\int_0^\infty I_{FR}(\lambda_E,\lambda_F)d\lambda_F} \times \frac{1-10^{-A_R(\lambda_E)}}{1-10^{-A(\lambda_E)}}$$

Equation 1

Φ_F and Φ_{FR} are fluorescence quantum yields of the compound and the reference respectively. $A(\lambda_E)$ and $AR(\lambda_E)$ are the absorbance at the excitation wavelength, and n is the refractive index of the medium. I_F and I_{FR} are fluorescent intensities of the compound and the reference respectively. The reference system used was 9,10-diphenylanthracene (φ = 0.955 in cyclohexane, λ_{ex} = 366 nm).3 The data are shown in Table 1. Absorption and emission spectra of compound **1** are displayed in Figure S2 (the same behaviour was observed for complexes 2, 3 and 4).

Cell viability assay: The human lung cancer cell line A549, human breast cancer MCF-7 cells and human ovarian cancer A2780 cells, (obtained from the European Centre of Cell Cultures ECACC, Salisbury, UK) were cultured in DMEM (A549, MCF-7) and RPMI (A2780) both containing GlutaMax-I supplemented with 10% FBS and 1% penicillin/streptomycin (all from Invitrogen), at 37° C in a humidified atmosphere of 95% of air and 5% CO2 (Heraeus, Germany). Non-tumoral human embryonic kidney cells HEK-293T were cultivated in DMEM medium with GlutaMax-I, 10% FBS and 1% penicillin/streptomycin, incubated in the same conditions as other cell lines. For evaluation of growth inhibition, cells were seeded in 96-well plates (Costar, Integra Biosciences, Cambridge, MA) at a

concentration of 10000 cells/well and grown for 24 h in complete medium. Solutions of the compounds were prepared by diluting a freshly prepared stock solution (10 2 M in DMSO) of the corresponding compound in aqueous media (RPMI or DMEM depending on the cell lines). The percentage of DMSO in the culture medium never exceeded 0.2%: at this concentration DMSO has no effect on the cell viability. Cisplatin (Sigma-Aldrich) stock solutions were prepared in MilliQ water. Afterwards, the intermediate dilutions of the compounds were added to the wells (200 µL) to obtain a final concentration ranging from 0 to 200 µM, and the cells were incubated for 72 h. Following 72 h drug exposure, 3 (4,5-dimethylthiazol-2-yl)-2,5-diphenyltetrazolium bromide (MTT) was added to the cells at a final concentration of 0.50 mg.ml-1 incubated for 3-4 h, then the culture medium was removed and the violet formazan dissolved in DMSO. The optical density of each well (96-well plates) was quantified in quadruplicate at 540 nm using a multi-well plate reader and the percentage of surviving cells was calculated from the ratio of absorbance between treated and untreated cells. The IC50 value was calculated as the concentration reducing the proliferation of the cells by 50% and is presented as a mean (± SE) of at least three independent experiments.

Estimation of enzyme activities inhibition *in vitro*: Highly purified cytosolic thioredoxin reductase (TrxR1) was prepared from rat liver, according to Luthman and Holmgren, (M. Luthman and A. Holmgren, Biochemistry, 1982, 21, 6628-6633) Mitochondrial thioredoxin reductase (TrxR2) was purified from isolated rat liver mitochondria following the procedure of Rigobello et al. (M. P. Rigobello and A. Bindoli, Methods Enzymol., 2010, 474, 109-122.) Thioredoxin reductases activity was determined by measuring the ability of the enzyme to directly reduce DTNB in the presence of NADPH. (M. Luthman and A. Holmgren, Biochemistry, 1982, 21, 6628-6633) Aliquots of highly purified TrxR1 (30 nM) and TrxR2 (30 nM) in 0.2 M Na, K-phosphate buffer (pH 7.4), 5 mM EDTA, 0.25 mM NADPH were pre-incubated for 5 min with the Au-NHC coumarin derivatives. Afterwards, the reaction was started with 1 mM DTNB, and monitored spectrophotometrically at 412 nm for about 10 min.

Yeast glutathione reductase was obtained from Sigma (St. Louis Mo, USA) and used without further purification. Glutathione reductase activity was measured in 0.2 M Tris HCl buffer (pH 8.1), 1 mM EDTA, and 0.25 mM NADPH after 5 min pre-incubation with the gold complexes. The assay was initiated by the addition of 1 mM GSSG and followed spectrophotometrically at 340 nm.

Glutathione peroxidase activity was performed by the following procedure: (X Liu, K E Pietsch, S J Sturla, Chem. Res. Toxicol., 24 (2011) 726–736) aliquots of GPx from bovine erythrocytes (0.02 U) were incubated with gold compounds in a total volume of 0.5 mL of 50 mM Hepes buffer (pH 7.0) containing 3 mM EDTA and 0.3 mM NADPH at 25°C. After 5min, 4 mM GSH and 25 nM glutathione reductase were added. After 2 min of incubation the reaction was started by the addition of 200 µM tert-butyl hydroperoxide and monitored spectrophotometrically at 340 nm as decrease of NADPH.

BIAM assay: TrxR (1 µM) pre-reduced in presence of NADPH was incubated with different concentrations of complexes for 30 min at room temperature, in 20mM Tris-HCl buffer (pH 7.4) containing 200 µM NADPH, and 1 mM EDTA. After incubation, 8 µL of the reaction mixture was removed and added to 50 µM biotinylated iodoacetamide (BIAM) in 0.1 M Hepes- Tris pH 6.0.(J. Fang and A. Holmgren J. Am. Chem. Soc., 2006, 128 (6), pp 1879–1885) Samples were incubated at room temperature for additional 30 min to alkylate the remaining SH groups in the enzyme. Then, BIAM-modified enzyme was mixed with loading buffer and the mixture was subjected to sodium dodecyl sulfate–polyacrylamide gel electrophoresis (SDS–PAGE) on a 7.5 % gel, and the separated proteins were transferred to a nitrocellulose membrane. Proteins labelled with BIAM were detected with horseradish peroxidase-conjugated streptavidin and enhanced chemiluminescence detection.

Determination of TrxR and GR activities in cell lysates: A2780 cells (1x106) were incubated for 48 h with 10 µM of compounds 1-4, with refresh at 24 h. After incubation, cells were harvested and washed twice with ice-cold PBS. Each sample was lysed with a modified RIPA buffer. After 40 min of incubation at 0 °C, lysates were centrifuged at 14000 x g for 5 min. The obtained supernatants were tested for enzyme activities. Aliquots (50 µg) of lysates were subjected to thioredoxin reductase determination in a final volume of 250 µl of 0.2 M Na, K-phosphate buffer (pH 7.4), 5 mM EDTA, and 2 mM DTNB. After 2 min the reaction was started with 0.3 mM NADPH. In cell lysates glutathione reductase activity was also estimated using 50 µg protein/ml as reported above.

Fluorescence microscopy: Cells (A2780) were seeded (5 x 105 for each sample) and grown on 8 well microscope plates, coated with Poly-L-Lysine hydrobromide (Sigma-Aldrich, P6516) with a complete medium. After 24 h, cells were incubated with various concentrations of the complexes in RPMI, without FCS for 2 h at 37 °C and 4°C. At the end of incubation, cells were rapidly washed with cold PBS and then fixed with 2% paraformaldehyde for 30 min at 4°C. For the visualization of PI, cells were permeabilized with 0.2% Triton X-100 for 20 min at 4°C and treated with 1µg/µl of PI for 10 min at room temperature. Cells were washed once with PBS and then analyzed by confocal microscopy. As preparation for visualization, the plate wells were removed and glycerol was used to cover the slide with a glass cover slip. The fluorescence was analysed using a Leica DM4000 B Automated Upright Microscope, equipped with the appropriate filters. PI was excited at 547 nm (emission wavelength 572 nm) and the compounds at 358 nm (emission

wavelength 461 nm, DAPI filter). The acquired images were obtained using individual filters and a combined image, overlaying the fluorescence acquired with the two filters, was obtained using the Leica microscope software.

References

[1] S. Komeda, A. Casini, Curr Top Med Chem, 12 (2012) 219-235.
[2] L.E. Wedlock, S.J. Berners-Price, Aust. J. Chem., 64 (2011) 692-704.
[3] E.M. Nagy, L. Ronconi, C. Nardon, D. Fregona, Mini-Rev Med Chem, 12 (2012) 1216-1229.
[4] L. Messori, A. Casini, Curr Top Med Chem, 11 (2011) 2647-2660.
[5] A. de Almeida, B.L. Oliveira, J.D.G. Correia, G. Soveral, A. Casini, Coord Chem Rev, 257 (2013) 2689-2704.
[6] L. Ronconi, D. Fregona, Dalton Trans., (2009) 10670-10680.
[7] A. Casini, C. Hartinger, C. Gabbiani, E. Mini, P.J. Dyson, B.K. Keppler, L. Messori, J. Inorg. Biochem., 102 (2008) 564-575.
[8] J.L. Hickey, R.A. Ruhayel, P.J. Barnard, M.V. Baker, S.J. Berners-Price, A. Filipovska, J. Am. Chem. Soc., 130 (2008) 12570-12571.
[9] A. Bindoli, M.P. Rigobello, G. Scutari, C. Gabbiani, A. Casini, L. Messori, Coord. Chem. Rev., 253 (2009) 1692-1707.
[10] S.J. Berners-Price, A. Filipovska, Metallomics, 3 (2011) 863-873.
[11] Y.M. Go, D.P. Jones, Antioxid Redox Sign, 13 (2010) 489-509.
[12] J. Lu, E.H. Chew, A. Holmgren, Proc. Natl. Acad. Sci. U. S. A., 104 (2007) 12288-12293.
[13] B. Bertrand, A. Casini, Dalton Trans, 43 (2014) 4209-4219.
[14] L. Oehninger, R. Rubbiani, I. Ott, Dalton Trans, 42 (2013) 3269-3284.
[15] E. Schuh, C. Pfluger, A. Citta, A. Folda, M.P. Rigobello, A. Bindoli, A. Casini, F. Mohr, J. Med. Chem., 55 (2012) 5518-5528.
[16] E. Vergara, E. Cerrada, C. Clavel, A. Casini, M. Laguna, Dalton Trans., 40 (2011) 10927-10935.
[17] J. Lemke, N. Metzler-Nolte, Eur.J. Inorg.Chem., 21 (2008) 3359-3366.
[18] H.M.J. Wang, I.J.B. Lin, Organometallics, 17 (1998) 972-975.
[19] B. Bertrand, E. Bodio, P. Richard, M. Picquet, P. Le Gendre, A. Casini, J. Organomet. Chem., (2014) 10.1016/j.jorganchem.2014.1003.1020.
[20] S.S. Gunatilleke, A.M. Barrios, J. Med. Chem., 49 (2006) 3933-3937.
[21] E.A. Allen, W. Wilkinson, Spectrochim Acta a-M, A 28 (1972) 2257-2262.
[22] J.A. Rendleman Jr, Complexes of Alkali Metals and Alkaline-Earth Metals with Carbohydrates, in: L.W. Melville, R.S. Tipson (Eds.) Advances in Carbohydrate Chemistry, Academic Press, 1967, pp. 209-271.
[23] N. Saleh, Y.A. Al-Soud, W.M. Nau, Spectrochim Acta A, 71 (2008) 818-822.
[24] P. Datta, D. Sardar, P. Mitra, C. Sinha, Polyhedron, 30 (2011) 1516-1523.
[25] R. Rubbiani, S. Can, I. Kitanovic, H. Alborzinia, M. Stefanopoulou, M. Kokoschka, S. Monchgesang, W.S. Sheldrick, S. Wolfl, I. Ott, J. Med. Chem., 54 (2011) 8646-8657.
[26] S. Tasan, O. Zava, B. Bertrand, C. Bernhard, C. Goze, M. Picquet, P. Le Gendre, P. Harvey, F. Denat, A. Casini, E. Bodio, Dalton Trans., 42 (2013) 6102-6109.
[27] F. Schmitt, P. Govindaswamy, O. Zava, G. Suss-Fink, L. Juillerat-Jeanneret, B. Therrien, J. Biol. Inorg. Chem., 14 (2009) 101-109.
[28] A. Citta, E. Schuh, F. Mohr, A. Folda, M.L. Massimino, A. Bindoli, A. Casini, M.P. Rigobello, Metallomics, (2013) 1006-1015.
[29] B. Bertrand, L. Stefan, M. Pirrotta, D. Monchaud, E. Bodio, P. Richard, P. Le Gendre, E. Warmerdam, M.H. de Jager, G.M. Groothuis, M. Picquet, A. Casini, Inorg Chem, 53 (2014) 2296-2303.
[30] A. Casini, M.C. Diawara, R. Scopelliti, S.M. Zakeeruddin, M. Grätzel, P.J. Dyson, Dalton Trans, 39 (2010) 2239-2245.
[31] M.A. Cinellu, A. Zucca, S. Stoccoro, G. Minghetti, M. Manassero, M. Sansoni, Journal of the Chemical Society, Dalton Trans, (1996) 4217-4225.
[32] L.S. Hollis, S.J. Lippard, J Am Chem Soc, 105 (1983) 4293-4299.
[33] A.D. Becke, J Chem Phys, 98 (1993) 5648-5652.
[34] A.D. Becke, Physical review. A, 38 (1988) 3098-3100.
[35] R.S. Mulliken, J Chem Phys, 23 (1955) 1833-1840.
[36] D.J. Tannor, B. Marten, R. Murphy, R.A. Friesner, D. Sitkoff, A. Nicholls, B. Honig, M. Ringnalda, W.A. Goddard, J Am Chem Soc, 116 (1994) 11875-11882.
[37] A.P. Martins, A. Marrone, A. Ciancetta, A. Galán Cobo, M. Echevarría, T.F. Moura, N. Re, A. Casini, G. Soveral, PloS one, 7 (2012) e37435.
[38] D. Fu, A. Libson, R. Stroud, in: Ion Channels - from atomic resolution physiology to functional genomics, 2002, pp. 51-65.
[39] J. E. D. Glendening, K. Badenhoop, A. E. Reed, J. E. Carpenter, J. A. Bohmann, C. M. Morales, and F. Weinhold, in, Theoretical Chemistry Institute, University of Wisconsin, Madison, 2001.
[40] W.L. Jorgensen, D.S. Maxwell, J. Tirado-Rives, J Am Chem Soc, 118 (1996) 11225-11236.
[41] R.A.F. G. Kaminski, J. Tirado-Rives, W. L. Jorgensen, J. Phys. Chem. B, (2001) 6474-6487.

B2. New Luminescent Polynuclear Metal Complexes with Anticancer properties

This chapter is published:

Margot Wenzel*, Andreia de Almeida*, Emilia Bigaeva, Paul Kavanagh, Michel Picquet, Pierre Le Gendre, Ewen Bodio and Angela Casini

New luminescent polynuclear metal complexes with anticancer properties: towards structure–activity relatioships

Eur.J.Inorgn.Chem. (2016) in press

DOI: 10.1021/acs.inorgchem.5b02910

*Authors contributed equally to this work

Abstract

A series of new heterodinuclear luminescent complexes with two different organic ligands have been synthesized and characterized. A luminescent Ru^{II}(polypyridine) moiety and a metal-based anticancer fragment (AuCl, (p-cymene)$RuCl_2$, (p-cymene)$OsCl_2$, (Cp*)$RhCl_2$ or Au-thioglucose) are the two general features of these complexes. All of the bimetallic compounds have been evaluated for their antiproliferative properties *in vitro* in human cancer cell lines. Only the complexes containing an Au(I) fragment exhibit antiproliferative activity in the range of cisplatin or higher. The photophysical and electrochemical properties of the bimetallic species have been investigated, and fluorescence microscopy experiments have been performed successfully. The most promising bimetallic cytotoxic complexes (i.e. with the Au-thioglucose scaffold) have shown to be easily taken up by cancer cells at 37 °C in the cytoplasm and/or in specific organelles. Interestingly, experiments repeated at 4 °C showed no uptake of the bimetallic species inside cells, which confirms involvement of active transport processes. To evaluate the role of glucose transporters in the cell uptake of the gold complexes, inhibition of the GluT-1 (glucose transporter isoform with high level of expression in cancer cells) was achieved, showing only scarce influence on the compounds' uptake. Finally, the observed absence of interactions with nucleic acid model structures suggests that the gold compounds may have different intracellular targets with respect to cisplatin.

2.1. Introduction

Cancer is the second most frequent cause of death in the industrialized world after cardiovascular diseases. In this area, several research efforts have demonstrated that the unique properties of metal ions can be exploited in the design of new anticancer drugs that have different mechanisms of pharmacological activity, with respect to classical organic drugs, and can be used for cancer cell-targeted approaches [1-5]. Within this field, polynuclear compounds are a relatively new and successful approach in metal-based cancer chemotherapy, as shown for example by the trinuclear Pt(II) compound BBR3464 evaluated in clinical trials (Figure 1) [6]. This concept of multinuclearity has also been envisaged with Au(I) and Au(III)-based compounds (Figure 1) [7-9]. In most cases, the polynuclear compounds were shown to be potent inhibitors of cancer cells proliferation with a significant improvement compared with their mononuclear parent complexes [10, 11].

A greater challenge in this concept of multinuclearity consists in the combination of two (or more) different metal containing moieties, requiring a design of suitable ligands to coordinate selectively one metal and the other. The idea is that the combination of two different metal-based compounds into a unique structure might improve their anticancer properties thanks to the multiplication of the potential biological targets and to the new physico-chemical properties of the generated bimetallic species. In recent years, a few successful examples have been described in the literature by us and others (Figure 1) [12-20]. In some cases, a significant improvement of the cytotoxic activity of the heterobimetallic entity has been observed in comparison with the parent monometallic complexes or with an equimolar mixture of both of them.[15]

In this context, the synthesis of a series of heterobimetallic complexes based on Pt(II) and Au(I) units was described by us [17]. Cell viability studies have shown potent antiproliferative

activity towards cancer cells for both the mono- and di-nuclear complexes. Interestingly, the biological properties were significantly improved by replacement of the chlorido ligand of Au(I) by 1-thio-β-D-glucose tetraacetate, as previously observed for other Au(I) cytotoxic complexes [21, 22].

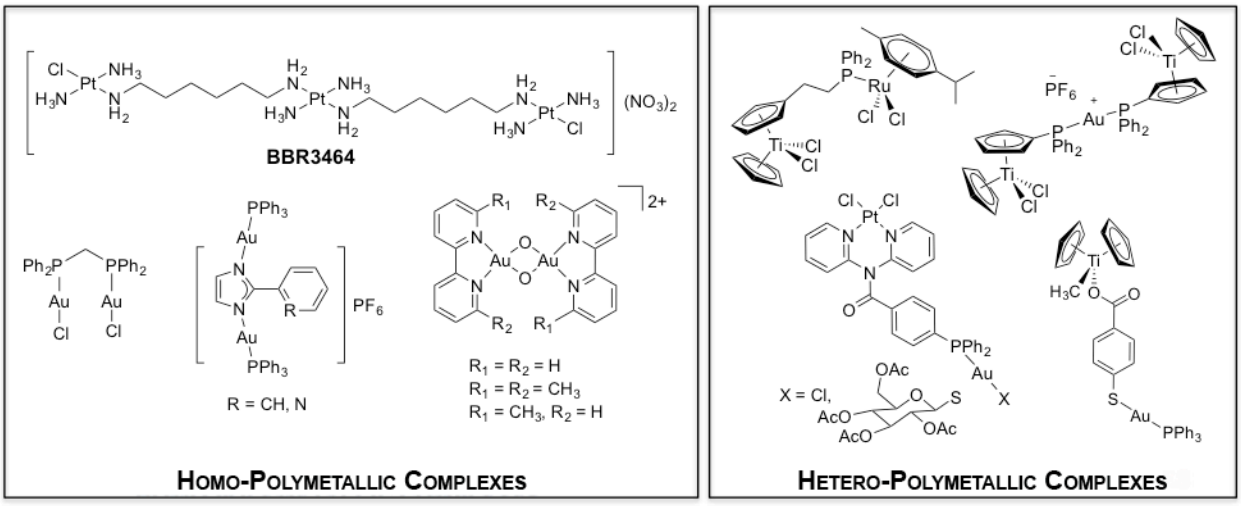

Figure 1. Examples of homo- and hetero-polymetallic complexes described as anticancer agents.

Exploration of the cellular uptake, subcellular distribution, as well as the fate of these metallodrugs (mono or poly-nuclear) inside cells is of major importance to get insights into their mechanism of action. Thus, there is an increasing need for imaging methods that allow the direct mapping of the subcellular distribution of metal-based therapeutics, while preserving important morphological information of the cell.

Among the various strategies to achieve metal compounds imaging in biological environments, fluorescence microscopy is certainly one of the most explored, and an increasing number of publications reporting on bifunctional metal compounds bearing fluorescent moieties for both therapeutic and imaging applications (so called *theranostic* agents) have appeared [23-26]. Thus, several examples of such fluorescent metal complexes are present in the literature, including Pt(II) complexes tagged with fluorescent rhodamine-type moieties [27], gold [28], zinc [29] and copper [30] complexes bearing both fluorescent and cytotoxic ligands, cobalt complexes with coumarin ligands [31], as well as organometallic ruthenium compounds [32]. Within this frame we recently developed series of cytotoxic metal compounds featuring a porphyrin [33, 34] or the dipyrromethene fluorophore (BODIPY)[35, 36] as highly fluorescent coordinating ligands (Figure 2). Moreover, some of us reported on cytotoxic silver(I) and gold(I) N-heterocyclic carbene (NHC) complexes bearing a fluorescent anthracenyl ligand [37], and on gold(I) NHC [38] or phosphine

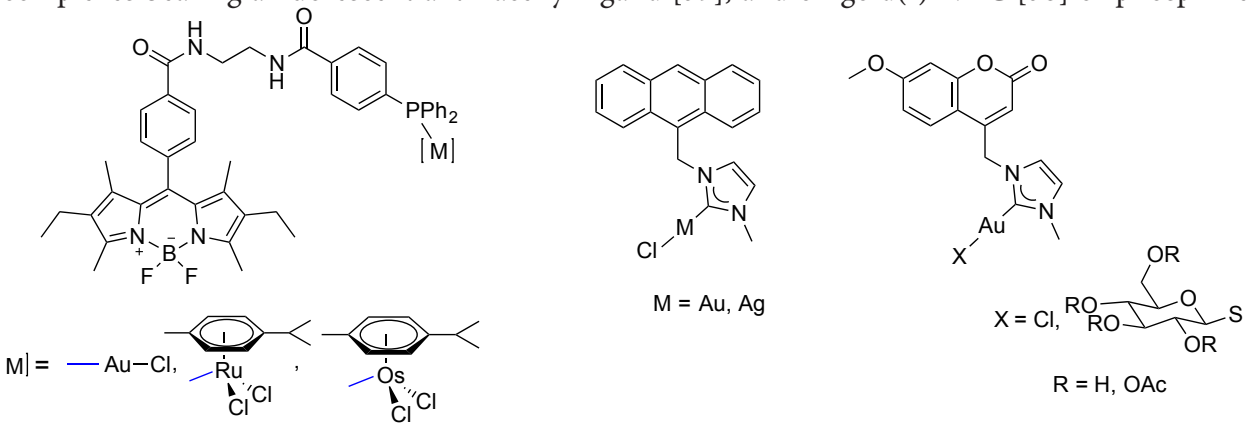

Figure 2. Luminescent metal-based complexes with biological activity.

[39] compounds bound to a coumarin moiety (Figure 2).

Following these promising results, we describe here a new series of dinuclear heterobimetallic compounds featuring a luminescent $Ru(bipy)_2(N^N)$ moiety and a second metal-based unit with potential as anticancer agents (Figure 3). To link these two metal-based fragments together, we designed two bifunctional ligands bearing both a phosphine scaffold as well as a bidentate N^N ligand. Specifically, the first ligand (**1**) is based on a bipyridine (bipy) moiety while the second one (**2**) is based on a dipyridylamine (dipy) skeleton and has been recently described by us [17]. Both ligands are able to coordinate Ru(II) ions via their N-donor groups to achieve the corresponding luminescent ruthenium polypyridyl complexes $Ru(bipy)_3$ and $Ru(bipy)_2(dipy)$, respectively. Afterwards, coordination of the phosphine unit in the mononuclear ruthenium complexes to Ru(II), Os(II), Au(I) and Rh(III)-based scaffolds has been envisaged and resulted in the synthesis of two series of heteronuclear complexes: series I based on the $Ru(bipy)_3$ moiety, and series II based on the $Ru(bipy)_2(dipy)$ scaffold, respectively (Figure 3).

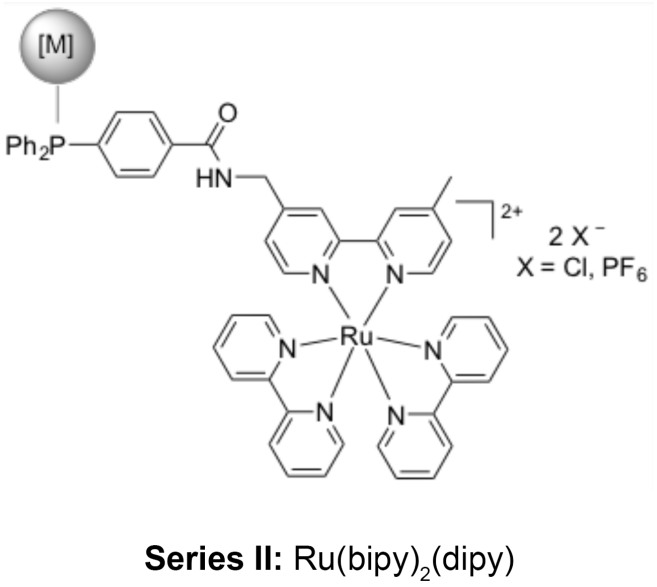

Series II: $Ru(bipy)_2(dipy)$

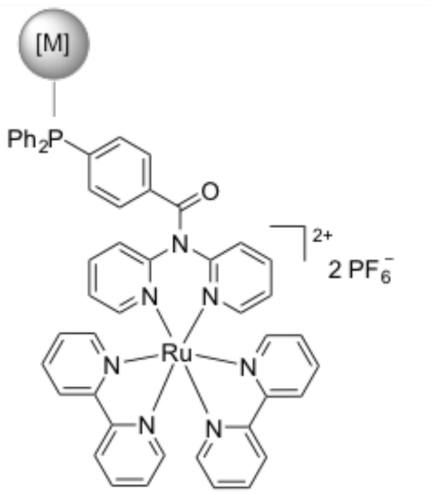

Series I: $Ru(bipy)_3$

Bimetallic complexes	[M]				
	Au Cl	Ru Cl Cl	Os Cl Cl	Rh Cl Cl	OAc, Au, O, S, AcO, OAc, AcO
$Ru(bipy)_3$ Series I[a]	**1A-PF_6** **1A-Cl**	**1B**	**1C**	-	**1D**
$Ru(bipy)_2(dipy)$ Series II	**2A**	**2B**	-	**2C**	**2D**

[a] **1B**, **1C**: X = PF_6; **1D**: X = Cl

Figure 3. Structure of the investigated luminescent bimetallic complexes.

In addition, the replacement of the chlorido ligand bound to Au(I) ions by 1-thio-β-D-glucose 2,3,4,6-tetraacetate allowed the generation of auranofin-like derivatives within both series. Auranofin is an anti-arthritic drug currently being investigated for potential therapeutic application including cancer [40]. Interestingly, it has been hypothesized that the thio-sugar unit

in auranofin, and in other metal compounds, is acting as a true substrate for the glucose active-transport system, and can be used to increase the uptake of the resulting metallodrugs [41]. Thus, the two new series of bimetallic compounds have been tested for their cytotoxic effects on various cancer cell lines (A2780S, A2780R and A549) in comparison to cisplatin. The possibility of an interaction of representative compounds with DNA has also been assessed by gel electrophoresis. Moreover, fluorescence microscopy studies of some of the bimetallic complexes were performed to evaluate the metal uptake via GLUT-1 transporters and distribution in cancer cells.

2.2. Results and Discussion

2.2.1. Synthesis and characterization

Initially, the synthesis of the ruthenium monometallic complexes **1-PF$_6$** and **1-Cl** was achieved, which requires the generation of the non-commercially available (4'-methyl-[2,2'-bipyridin]-4-yl)methanamine **3** in three steps as described in the literature [42]. Then, the reaction proceeds in three additional steps, starting with the coupling reaction of **3** with 4-iodobenzoyl chloride and followed by the complexation of the ruthenium precursor (Ru(bipyridyl)$_2$Cl$_2$ with the functionalized bipyridine derivative **4** via the exchange of the two chlorido ligands (Scheme 1) [43]. At this stage, counter-anion exchange reaction can be performed by addition of aqueous saturated KPF_6 solution, giving rise to the complex **1-PF$_6$**. The pallado-catalysed coupling reaction between the iodo derivatives **5** (**5-PF$_6$** or **5-Cl**) and diphenylphosphine gave the desired phosphines **1-Cl** and **1-PF$_6$** in 83% yield (Scheme 1).

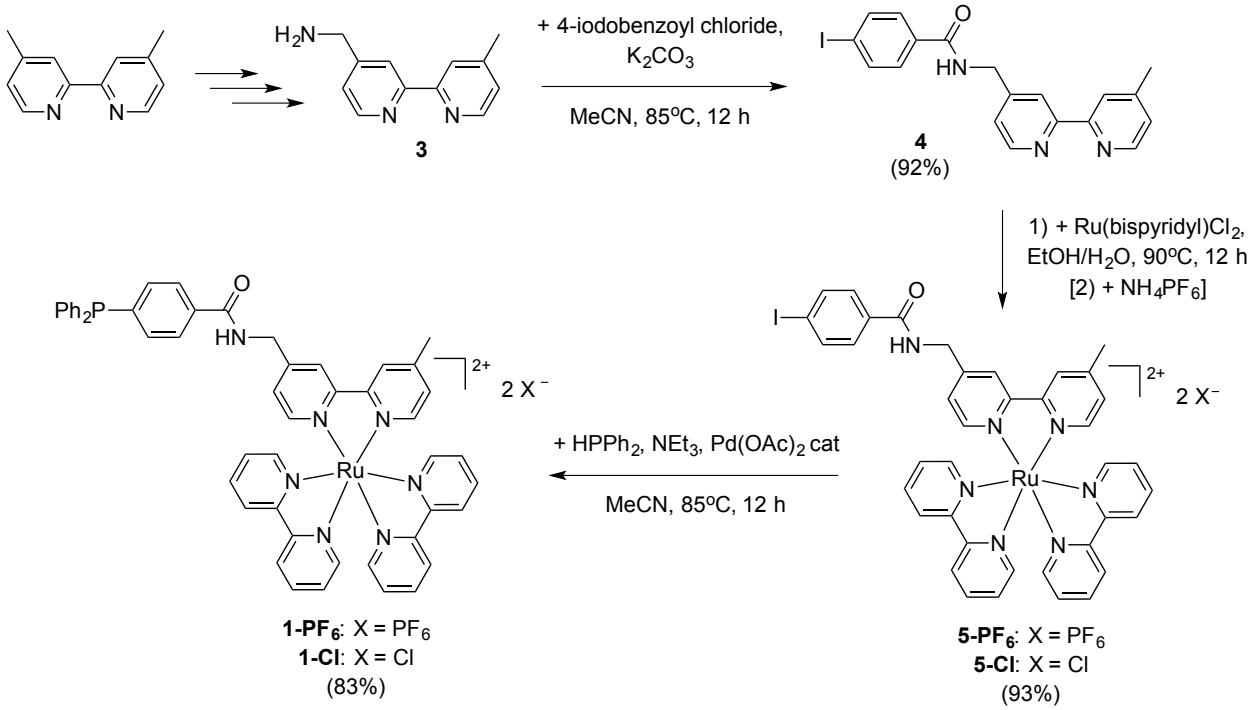

Scheme 1. Synthetic routes for the production of **1-PF6** (and **1-Cl**).

The same strategy was applied to the synthesis of the dipyridylamine-phosphine based ruthenium complex **2** starting from compound **6**, whose synthesis has been recently described by us (Scheme 2) [17]. The desired product **2** was obtained in more than 81% (global yield).

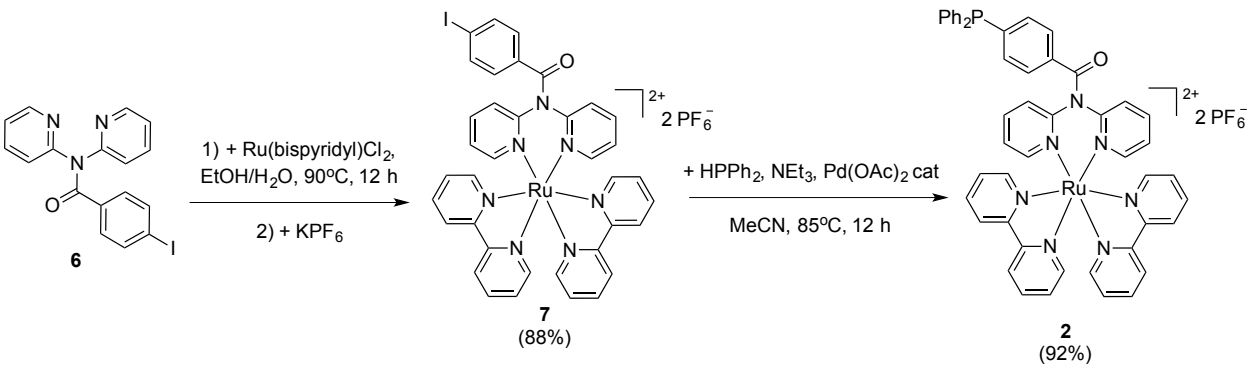

Scheme 2. Synthetic routes for the obtainment of **2**.

Afterwards, the ruthenium mononuclear complexes **1-PF$_6$**, **1-Cl** and **2** were metallated at the terminal phosphine with gold, arene-ruthenium, pentamethylcyclopentadienyl rhodium or arene-osmium derivatives under mild conditions. The complexation reactions were monitored by ^{31}P NMR, and a significant chemical shift was observed going from the free phosphines in **1-PF$_6$**, **1-Cl** and **2** (singlet at around -5 ppm) to the desired bimetallic complexes (singlet at around 33 ppm for Au derivatives, 26 ppm for the Ru ones, 31 ppm for the Rh one and -12 ppm for the Os one). All complexation reactions afforded the bimetallic complexes in good to excellent yields (Table 1).

Table 1. Route to the synthesis of the bimetallic luminescent compounds.

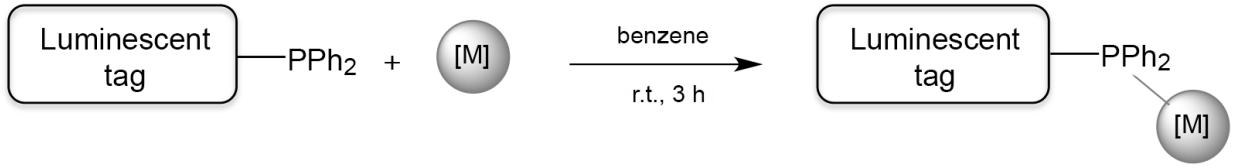

Monometallic complex (1 or 2) **Metallic percursor** **Bimetallic product**

Entry	Ligand	Metallic precursor	Product	Yield (%)
1	**1-PF$_6$ / 1-Cl**	Au(tht)Cl	**1A-PF$_6$ / 1A-Cl**	92
2	**1-PF6**	[(*p*-cymene)RuCl$_2$]$_2$	**1B**	93
3	**1-PF6**	[(Cp*)RhCl$_2$]$_2$	**1C**	87
4	**2**	Au(tht)Cl	**2A**	84
5[a]	**2**	[(*p*-cymene)RuCl$_2$]$_2$	**2B**	77
6	**2**	[(*p*-cymene)OsCl$_2$]$_2$	**2C**	99

[a] Reactions stirred 4 h at r.t.

In previous studies, we and others noticed that replacing the chlorido ligand of a phosphine gold chloride complex by a thioglucose tetraacetate could lead to a moderate to dramatic increase of its cytotoxicity [17, 21]. Thus, we decided to perform the same experiment on the gold compounds **1A-Cl** and **2A** by reaction with one equivalent of thioglucose tetraacetate and sodium hydroxide to obtain respectively the complexes **1D** and **2D** (Scheme 3). The reactions were monitored by ^{31}P NMR, and a chemical shift of +5 ppm was observed between the starting phosphine-gold-chloride complexes and the phosphine-gold-thioglucose products. Noteworthy, the shape of the signal goes from a sharp singlet to a broad one, characteristic feature of this exchange of ligands on phosphine gold complexes [44].

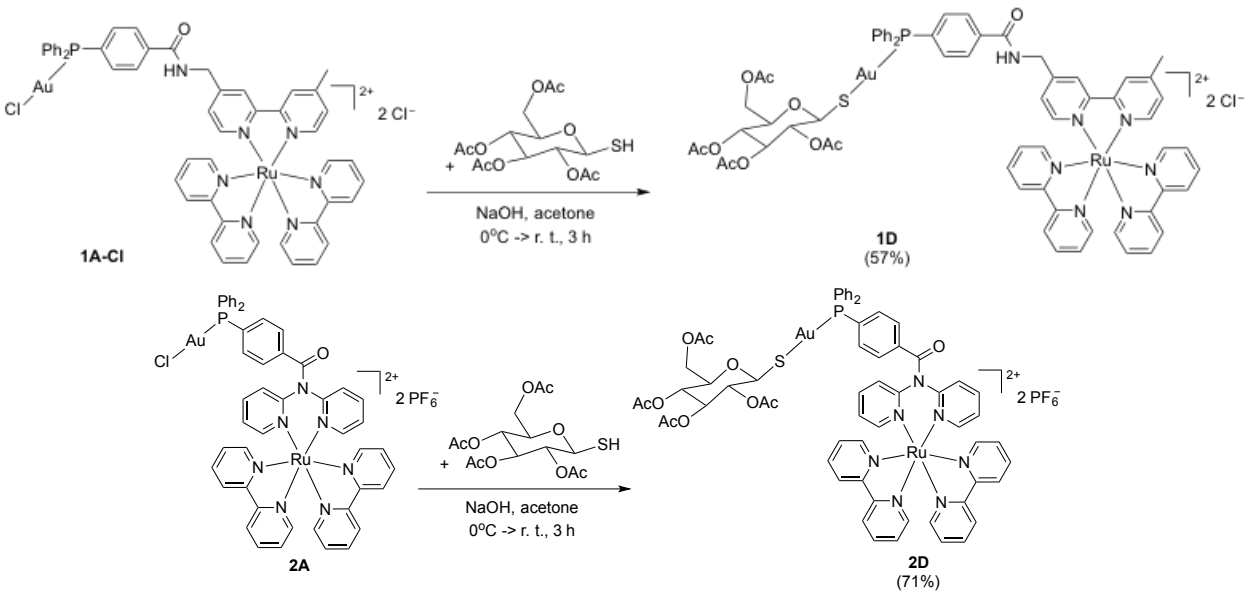

Scheme 3. Synthetic routes for the synthesis of the complexes **1D** and **2D**.

2.2.2. Photophysical and electrochemical properties

The mononuclear ruthenium complexes **1-PF$_6$** and **2** exhibit in DMSO a typical MLCT absorption band at 457 and 433 nm and a luminescence emission band at 535 and 539 nm, respectively (Table 2). These absorption and emission wavelengths are globally insensitive to further metal complexation of **1-PF$_6$** and **2** (less than 15 nm of variation). However, the emission wavelengths in series I have appeared to be relatively sensitive to the nature of the counter anion of the bimetallic complex. As a matter of fact, it is worth mentioning that the emission of the complexes can be tuned from around 535 nm with PF_6^- as counter anion (complexes **1A-PF$_6$**, **1B** and **1C**) to 595 nm with Cl^- (complexes **1A-Cl** (data not shown) and **1D**). Nevertheless, this observation isn't of great relevance in a biological context, where the counter-ion of each compound will be rapidly exchanged, most likely by chlorido anions.

The quantum yield of luminescence of the mononuclear complex **1-PF$_6$** (19%) is in agreement with the reported values for $Ru(bipy)_3$ complexes [46]. Interestingly, the luminescence is only slightly affected upon complexation with the second metallic moiety (complexes **1A-PF$_6$** to **1D**,

Table 2. Absorption and emission wavelengths and quantum yields of luminescence of the mono- (**1-PF$_6$** and **2**) and bimetallic (**1A-PF$_6$-1D** and **2A-2D**) complexes measured in degassed DMSO at 298 K, using $[Ru(bipy)_3]Cl_2$ as internal reference.

Complexes	λ_{abs} (nm)	λ_{em}(nm)	Φ (%)
$[Ru(bipy)_3]Cl_2$[a]	454	630	8
1-PF$_6$	457	535	19
1A-PF$_6$	457	533	14
1B	456	533	14
1C	457	536	15
1D	456	593	13
2	433	539	12
2A	432	531	<1

[a] Values taken from reference [45]

quantum yields of 13 to 15%). Notably, for these compounds, the quantum yield is still sufficient enough to produce well-resolved images in vitro.

In the $Ru(bipy)_2(dipy)$ series, the quantum yield of **2** is slightly reduced (12%) in comparison with its analog in the $Ru(bipy)_3$ series (**1-PF_6**). This phenomenon might be linked to the fact that the dipyridylamine ligand is less rigid and less symmetric than bipyridine. Unfortunately, the complexation of a second metal center by the mononuclear complex **2** results in a dramatic decrease of the quantum yield of luminescence (from 12% to less than 1%). In this case, the structure of the organic linker seems to play an important role. On the other side, the presence of a CH_2 between the bipyridine and the coordinating phosphine in the series I seem to isolate and contain the luminescence properties of the ruthenium-based fragment. Due to their poor quantum yields, complexes **2A-2C** appear clearly not suitable for *in vitro* fluorescence imaging. Notably, replacing the chlorido ligand on gold by the thioglucose tetraacetate moiety allows the partial recovery of the luminescence (Φ = 6%) and the possible use of **2D** for fluorescence imaging.

It is worth mentioning that cyclic voltammetric (CV) measurements on the Ru-Au bimetallic compound **1D** also indicate the absence of an effect of the coupling of two redox active centers (Ru(II) and Au(I)) within the same molecule. Figure S4 (in supplementary information) shows the CV of compound **1D** recorded in DMSO solvent containing 0.1 M TBAP as supporting electrolyte. Clearly, the redox couples I, II, II and IV can be attributed to $Ru^{3+/2+}$ (metal based), $Ru^{2+/1+}$, $Ru^{1+/0}$ and $Ru^{0/1-}$ (ligand based) redox transitions, respectively [47]. The redox potential (E°') of +0.81 V vs. Fc^+/Fc evaluated for the metal centered $Ru^{3+/2+}$ couple, shown in Table 3, is close to the value of +0.8 V vs. Fc^+/Fc recorded for $[Ru(bipy)_3]^{3+/2+}$ in DMF (0.1 M Bu_4NPF_6) [47]. The slight discrepancy in redox potential (+0.01 V) observed is likely due to sensitivity of the Fc^+/Fc redox couple (used as an internal reference) [48] to the different solvent and electrolyte composition employed [49]. In addition, the presence of additional functional groups on the coordinating bipyridine ligand linking to the Au moiety complicates direct electrochemical comparison to $[Ru(bipy)_3]^{3+/2+}$. For example, the electron-donating 4'-methyl group located on the bipyridine ligand is expected to shift E°' by approximately -0.03 V, compared to $[Ru(bipy)_3]^{3+/2+}$, as predicted by the Lever ligand electrochemical series.[50] All redox couples (I, II, II and IV) are quasi-reversible (ΔEp values range from ca. 0.07 V to 0.09 V), with similar ΔEp values to those of $[Ru(bipy)_3]^{3+/2+}$ for corresponding redox couples [47]. This suggests that the relatively rapid heterogeneous electron transfer rates for these redox couples are not altered by attachment to the Au moiety. Further evidence that the metal centers remain electronically independent (uncoupled) is indicated by the lack of significant change in voltammetric response between compound **1D** and $[Ru(bipy)_3]^{3+/2+}$. Strong electronic coupling of metal centers would be expected to alter the voltammetric response for one or both metal centers, compared to their mononuclear forms, as observed for electronically coupled binuclear complexes [51]. The scarcely defined voltammetric peak at -1.06 V vs. Fc^+/Fc that can be tentatively attributed to Au(I) reduction [52] suggests that the Au metal center is relatively inaccessible to heterogeneous electron transfer in DMSO solvent within this potential range (-2.3 V to 1.2 V vs. Fc^+/Fc), thereby restricting Ru-Au cooperative effects.

Preliminary stability studies of the complexes have been performed by ^{31}P NMR and UV-visible spectrophotometry in PBS buffer over 48 h (see Supplementary Information for details). Most of the complexes showed no significant change in the resulting spectra. In some cases, a slight decrease of the MLCT band appeared, due to a partial precipitation of the compounds in solution.

Table 3. Voltammetric parameters evaluated for **1D** recorded in DMSO containing 0.1 M TBAP. Scan were recorded at a glassy carbon working electrode (3 mm diameter) at a scan rate of 0.1 V/s. All potentials (V) were measured vs. Fc^+/Fc redox couple.

Redox Couple	Assignment	E_p^a (V)	E_p^c (V)	ΔE_p (V)	$E^{o'}$ (V)
I	$Ru^{3+/2+}$	0.85	0.77	0.077	0.81
II	$Ru^{2+/1+}$	-1.65	-1.73	0.086	-1.69
III	$Ru^{1+/0+}$	-1.82	-1.91	0.088	-1.87
IV	$Ru^{0/1-}$	-2.06	-2.15	0.091	-2.11

Fortunately, even after 48 h, the absorbance decreased less than 30%. Noteworthy, neither new band appearance nor band disappearance has been noticed. Therefore, we can conclude that there is few or no degradation of the luminescent ruthenium-based moiety of the reported fluorescent metal compounds within the time frame of the experiment (few hours). Regarding the phosphine metal part, the stability of analogues has been investigated in previous works by UV-Visible spectroscopy as well as ^{31}P and ^{1}H NMR, which showed no decomposition after 48 hours [17, 36].

2.2.3. Antiproliferative effects and DNA interaction studies

The bimetallic complexes **1A-PF_6-1D** and **2A-2D** were initially tested for their antiproliferative properties using the classical MTT [3-(4,5-dimethylthiazol-2-yl)-2,5-diphenyltetrazolium bromide] assay against various cancer cell lines, including the human ovarian carcinoma sensitive (A2780S) and cisplatin-resistant (A2780cisR) cells and the human lung carcinoma (A549) cell lines. The obtained results are reported in Table 4. Overall, the cytotoxic effect of these complexes appears to be dependent on different factors.

The insertion of Rh, Ru and Os groups to be coupled to the Ru(polypyridyl) compounds resulted in complexes with poor or no activity in the tested cell lines, independently on the type of luminescent tag moiety and linker type. This observation is consistent with the previous findings that similar ruthenium and rhodium complexes are, in general, less cytotoxic than platinum-based

Table 4. IC_{50} values of complexes of series I and II against various cancer cell lines compared to cisplatin after 72 h incubation at 37° C.

Compound	IC_{50} (μM) [a]		
	A2780S	A2780R	A549
1A-PF_6	> 100	> 100	> 100
1B	> 100	> 100	> 100
1C	> 300	> 300	> 300
1D	2.7 ± 0.9	6.4 ± 1.0	26.5 ± 2.6
2A	12.0 ± 3.7	12.7 ± 1.4	40 ± 7
2B	> 50	> 50	> 50
2C	> 50	> 50	> 50
2D	1.4 ± 0.3	3.1 ± 0.9	5.7 ± 0.5

[a] Values are mean ± SEM of at least three independent determinations.

anticancer agents [53, 54]. On the other hand, the luminescent tag linker seems to play an important role in the case of the heteronuclear Ru-Au complexes: in fact, **1A-PF_6**, with the "bipy" linker, has no toxic effects on the tested cell lines, while **2A**, bearing the "dipy" linker, is moderately toxic in most cell lines.

Interestingly, the only complexes displaying significant antiproliferative effects were the heteronuclear Ru-Au complexes **1D**, **2A** and **2D** and these compounds were more effective on the cisplatin-resistant cell line A2780cisR than cisplatin itself, indicating lack of cross-resistance and a different mechanism of action from the platinum drug. This hypothesis has been confirmed by DNA electrophoresis experiment (Figure 4), which demonstrated the absence of interaction between complex **2D** and plasmid pUC19 DNA.

Moreover, compound **2D** has a similar potency in all tested cell lines, while compound 1D has an IC_{50} against A549 cells of one order of magnitude higher. This fact may indicate that the mechanism of activity of the two metal compounds may be different in this cell line. Furthermore, among these three Ru-Au derivatives, the most lipophilic compounds **1D** and **2D**, containing a conjugated bioactive molecule (thioglucose moiety) were even more toxic against all cell lines than the parent compounds, **1A-PF_6** and **2A** respectively (with chloride as ancillary ligand). This observation suggests that the increase of cytotoxic potency of complexes **1D** and **2D**, with respect to the other complexes, might derive from an improved uptake in cancer cells.

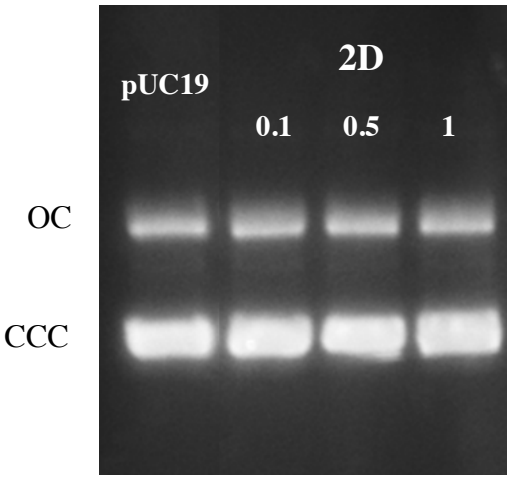

Figure 4. Gel electrophoresis of pUC19 plasmid DNA treated with different concentrations of **2D** (r = 0.1, 0.5 and 1; r = bimetallic complex: DNA base pairs) after overnight incubation at 37°C. (CCC = super-coiled DNA; OC = open circular DNA).

2.2.4. Fluorescence microscopy

In order to assess the imaging properties of our heteronuclear complexes in vitro, fluorescence microscopy was used, allowing us to gain insights into the uptake and localization of these luminescent compounds. Thus, the gold(I)-ruthenium(II) compounds **1D**, **2A** and **2D** were selected, due to their promising cytotoxic effects and sufficient fluorescence quantum yields. The human ovarian A2780 and lung A549 cells were grown onto a sterile chamber slides and treated with the luminescent compounds as described in the Experimental Section.

Evaluation of active transport mechanisms which may be involved in the uptake of the complexes was performed incubating cells with the metal complexes at either 37 ºC or 4 ºC, respectively. At low temperatures, active and facilitated passive transport mechanisms are commonly inhibited. Figure 5 shows the low fluorescence of complex **2A** on A2780 at 4 ºC in A2780 cells after 3 h incubation. At this temperature the luminescence of the compound is very low and this is representative for all the tested complexes in both cell lines (data not shown). Therefore, the uptake of the complexes should occur by active or facilitated transport. Figure 6 shows that complex **1D** has enhanced intracellular fluorescence intensity in both cell lines. Complex **2D** is the most cytotoxic compound of the series despite being one of the least luminescent. Thus, the low fluorescence intensity of this complex may lead to scarce detection by fluorescence microscopy, rather than the low uptake, although the need

of longer incubation times for uptake cannot be excluded.

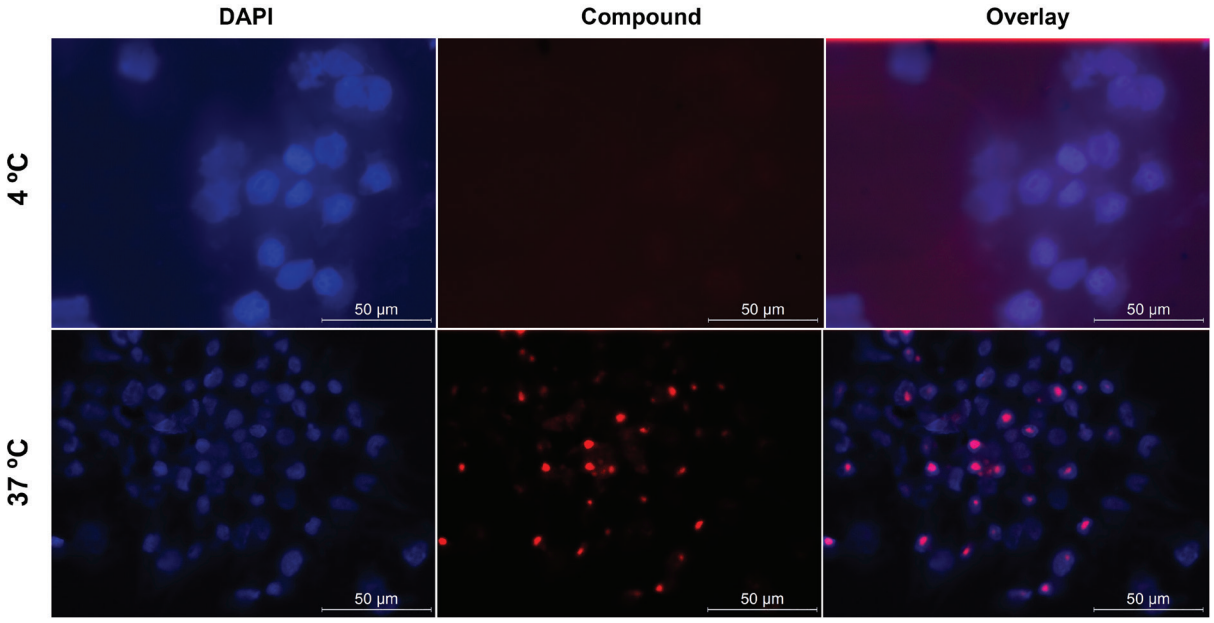

Figure 5. Visualization of the complex **2A** by confocal microscopy, with DAPI nuclear staining. A2780 cells were incubated with 100 µM of **2A** at 4 °C or 37 °C for 3 h.

Interestingly, compounds **1D** and **2D** present quite different intracellular localization: while **2D** appears to have a diffuse localization in the cytoplasm, complex **1D** seems to accumulate in organelles in the nuclei, in both A2780 and A549 cells. This is different for example from what has been observed in the case of previously reported lipophilic mononuclear $Ru(bipy)_3^{2+}$ complexes which showed membrane localization [55]. Interestingly, Gottschald et al. presented ruthenium polypyridyl complexes with peripherally attached sugar substituents [56]. In this case, fluorescence microscopy revealed that D-glucose conjugated complexes possess a clear intracellular distribution with a granular pattern as observed for complex **1D**. Adding a targeting moiety to a complex, such as thioglucose, may increase its uptake by aiming at the glucose transporters. GluT-1 is a glucose transporter isoform known by having a high level of expression on A549 cells. To investigate the transport of our Ru-Au complexes via this isoform, we used a known inhibitor (WZB117) for this transporter and expected to see a decrease in uptake of the complexes bearing the targeting moiety, complexes **1D** and **2D**. Unfortunately, due to its fluorescent properties, complex **2D** was not detected in these cells. As shown in Figure 6, a 30 min pre-incubation of cells with 50 µM of the inhibitor did not affect the uptake of complex **1D**. These results argue against the role of the GluT-1 isoform as transporter in the uptake of the Ru-Au complexes bearing the thioglucose targeting moiety but do not exclude the possibility that other isoforms are involved.

Since the uptake of compound **2D** could not be followed by fluorescence microscopy, we investigated the effect of WZB117 in the toxicity of complex **2D** in A2780 cells. Thus, the toxicity of both the Glut-1 inhibitor and compound **2D** were evaluated at 24 and 72 h, by measuring the cell viability using an MTT assay. The cells were incubated with either WZB117 and compound **2D**alone or co-incubation of compound **2D** with several concentrations of WZB117. The inhibitor was not toxic up to a concentration of 0.5 µM at 24 h and very low toxicity up to 20 µM at 72 h. The concentrations of complex **2D** used were 1 and 5 µM for both incubation times. Our results show that co-incubation of the Ru(II)-Au(I) complex with the GluT-1 inhibitor didn't affect the toxicity of the complex (data not shown), suggesting that GluT-1 transporter is not involved in the uptake

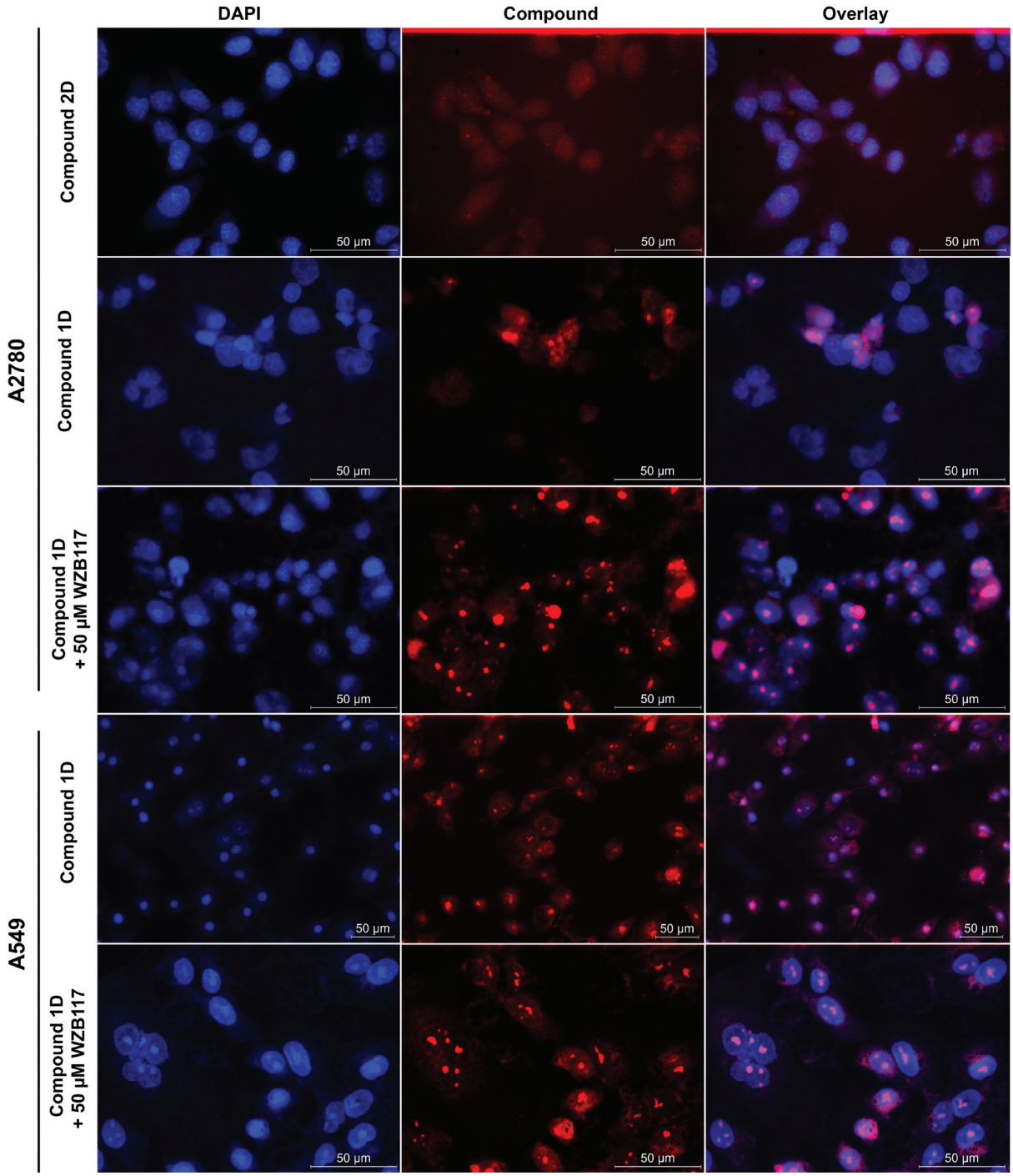

Figure 6. Visualization of the Ru-Au complexes by fluorescence microscopy, with DAPI nuclear staining. A2780 and A549 cells were incubated with the complexes (50 or 100 µM) at 37°C for 3 h, with or without 30 min pre-incubation with 50 µM WZB117.

of this complex, as shown for complex 1D by fluorescence microscopy.

2.3. Conclusions

Two series of novel heterobimetallic complexes possessing a luminescent Ru(polypyridine) scaffold have been synthetized and characterized. All the compounds have been studied for their photophysical properties, showing typical MLCT absorption bands between 420 and 460 nm, and emission bands centered around 535 nm (595 nm when possessing the chloride counter-anion). While the quantum yield of the complexes in series I (**1A-PF_6-1D**) is only slightly affected by the presence of the metal-based fragment coordinated on the phosphine, the luminescence of the

second series of compounds (**2A-2D**) is dramatically quenched. Interestingly, initial electrochemical data evaluated for the bimetallic complex **1D** suggest that the Ru(II) and Au(I) metal centers are electronically independent based on the similarity of voltammetric response compared to that of mononuclear $[Ru(bipy)_3]^{3+/2+}$. All complexes have been evaluated for their antiproliferative properties and their activity has shown to be highly dependent on the nature of the metal-based fragment coordinated on the phosphine moiety. The gold-based complexes have demonstrated the highest cytotoxic activity, especially when replacing the chlorido ligand by a thioglucose tetraacetate. DNA gel electrophoresis experiments also support the idea of a mechanism of action non-related to interactions with nucleic acids, as in the case of other Au(I)-based complexes.[17] Fluorescence microscopy experiments have been performed with the most promising luminescent and/or cytotoxic complexes and demonstrated a remarkable uptake of the compound at 37 °C with targeting of organelles in the cytoplasm or in the nuclei. However, the uptake is dramatically reduced at 4 °C, suggesting the implication of active transport mechanisms in the compounds' intracellular accumulation. Inhibition experiments of a glucose transporter isoform, GluT-1, could not confirm the involvement of this transporter in the mechanism of uptake of the complexes inside cells, but other isoforms of the same family cannot be excluded.

It should be noted that even if the binuclear complexes may present improved cytotoxic properties with respect to their monometallic components, the possible cooperative effect does not necessarily involve a chemical "communication" between the two metal centers, but could be the result of different overall chemical-physical properties (e.g. lipophilic/hydrophilic balance, overall charge etc.) of the resulting binuclear scaffold which favors compounds' uptake and intracellular localization. This is actually a possibility in the case of complex **1D**, where while the two metal centers seem not to interfere with each other, as evidenced by spectroscopic and electrochemical data, the complex is still much more cytotoxic than the monometallic Ru derivative. Overall, these observations support the hypothesis that polynuclear gold-based complexes may be promising anticancer agents, provided that their design allow improving their selective accumulation in cancer cells. Further studies are ongoing in our lab in order to enhance this selectivity.

2.4. Experimental Section

General Information: All solvents were dried and distilled under argon before use. $[(p\text{-cymene})RuCl_2]_2$ and $[(p\text{-cymene})OsCl_2]_2$ dimers were obtained following Bennett's protocol [57]. The gold (I) tetrahydrothiphene precursor Au(tht)Cl has been synthetized according to Laguna's procedure [58]. The compounds 3 and 6 have been obtained as described in the literature [42, 17]. All other reagents were commercially available and used as received. The analyses were performed at the "Plateforme d'Analyses Chimiques et de Synthèse Moléculaire de l'Université de Bourgogne". The identity and purity (≥ 95%) of the complexes were unambiguously established using high-resolution mass spectrometry and multinuclear NMR spectroscopy. The exact mass of the complexes were obtained on a Thermo LTQ Orbitrap XL ESI-MS. ^1H (300.13, 500.13, or 600.23 MHz), ^{13}C (75.5, 125.8, or 150.9 MHz), 11B (192.5 MHz) and ^{31}P (121.5, 202.5, or 242.9 MHz) NMR spectra were recorded on Bruker 300 Avance III, Bruker 500 Avance III, or Bruker 600 Avance II spectrometers. Chemical shifts are quoted in parts per million (δ) relative to tetramethylsilane, TMS (^1H and ^{13}C), using the residual protonated solvent (^1H) or the deuterated solvent (^{13}C) as an internal standard. Alternatively, 85% H_3PO_4 (^{31}P) and 15% $BF_3.OEt_2$ (11B) in $CDCl_3$ were used as external standards. The coupling constants are reported in Hertz. All aromatic positions: ortho, meta, para are defined using phosphorus as main group. All aromatic positions in pyridines are numbered as follow:

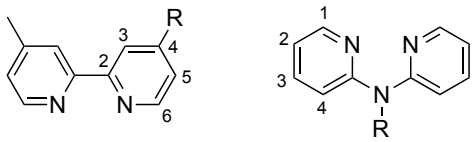

Infrared spectra were recorded on a Bruker Vector 22 FT-IR spectrophotometer (transmission mode) equipped with the ATR 'golden gate' or on a Bruker Vertex 70v FT-IR spectrophotometer. Elemental analyses were performed on a Thermo Electron Flash EA 1112 Series analyzer. UV-Visible absorption spectra were recorded on a JASCO V630BIO spectrometer. The steady-state fluorescence emission spectra were obtained by using a JASCO FP8560 spectrofluorometer instrument.

Synthesis: 1-PF_6 (or 1-Cl): In a round-bottom flask under argon and equipped with a cooling system, were introduced 461 mg (or 372 mg) (0.407 mmol, 1 eq.) of 5-PF_6 (or 5-Cl) and 0.18 mg (0.0008 mmol, 0.002 eq.) of $Pd(OAc)_2$, dissolved in 20 mL of distilled acetonitrile. 113 µL (0.814 mmol, 2 eq.) of distilled triethylamine and 71 µL (0.407 mmol, 1 eq.) of diphenylphosphine were then added, and the reaction mixture was stirred at 85° C overnight. After cooling at room temperature, the solvent was removed by rotary evaporation, and the crude product purified by column chromatography on silica (eluent: 100 acetonitrile/10 distilled water/1 KNO3 aq. saturated); yield 403 mg (or 328 mg) (0.338 mmol, 83%). ^{1}H NMR (500.13 MHz, CD_2Cl_2): δ = 8.51 (m, 1 H, CH (3)), 8.44 (m, 4 H, 4 x CH-bipyridine), 8.34 (m, 1 H, CH (5)), 8.07 (m, 4 H, 4 x CH-bipyridine), 7.96 (m, 1 H, CH (5')), 7.87 (td, 2 H, $^3J_{H-H}$ = 8.9 Hz and $^4J_{H-H}$ = 1.4 Hz, 2 x CH-Ar), 7.79-7.68 (m, 4 H, 4 x CH-bipyridine), 7.62-7.32 (m, 18 H, 2 x CH-Ar + 10 x CH-PPh_2 + 6 x CH-bipyridine), 7.25 (m, 1 H, CH (3')), 4.81 (d, 2 H, $^3J_{H-H}$ = 5.6 Hz, CH_2), 2.57 (s, 3 H, CH_3). $^{31}P\{^1H\}$ NMR (151.74 MHz, CD_2Cl_2): δ = -5.40 (s, PPh_2) (-144.5 (hept, $^1J_{P-F}$ = 712.5 Hz, PF_6)). $^{13}C\{^1H\}$ NMR (125.76 MHz, CD_2Cl_2): δ = 167.6 (s, CO), 157.5 (s, CIV-bipyridine), 157.4 (s, CIV-bipyridine), 157.2 (s, 2 x CIV-bipyridine), 157.1 (s, CIV-bipyridine), 157.0 (s, CIV-bipyridine), 156.9 (s, CIV-bipyridine), 152.7 (s, CH-bipyridine), 152.1 (s, CH-bipyridine), 151.4 (s, 2 x CH-bipyridine), 151.6 (s, CH-bipyridine), 151.3 (s, CIV-bipyridine), 150.7 (s, CH-bipyridine), 150.5 (s, CH-bipyridine), 142.5 (s, CIV-CCONH), 138.3 (s, CH-bipyridine), 138.2 (s, CH-bipyridine), 138.1 (s, 2 x CH-bipyridine), 138.0 (s, CH-bipyridine), 137.0 (d, $^1J_{C-P}$ = 10.8 Hz, 2 x CIV-PPh_2), 134.3 (d, $^2J_{C-P}$ = 20.5 Hz, 4 x CH-PPh_2 ortho), 134.1 (d, $^1J_{C-P}$ = 11.5 Hz, CIV-Ar), 133.7 (d, $^2J_{C-P}$ = 19.3 Hz, 2 x CH-Ar), 129.4 (s, 2 x CH-PPh_2 para), 129.0 (d, $^3J_{C-P}$ = 6.4 Hz, 4 x CH-PPh_2 meta), 128.5 (s, CH-bipyridine), 128.3 (s, CH-bipyridine), 128.2 (s, CH-bipyridine), 128.1 (s, CH-bipyridine), 128.0 (d, $^3J_{C-P}$ = 6.4 Hz, 2 x CH-Ar), 127.5 (s, CH-bipyridine), 126.0 (s, CH-bipyridine), 124.8 (s, CH-bipyridine), 124.7 (s, CH-bipyridine), 124.6 (s, CH-bipyridine), 124.3 (s, CH-bipyridine), 46.7 (s, CH_2), 8.8 (s, CH_3). ESI-MS (CH_2Cl_2/MeOH, positive mode) exact mass for $C_{51}H42N7O2P1Ru1$ ($[M^+O]^{2+}$, theoretical *m/z* 458.60920): found *m/z* 458.60857 (err. 0.138 ppm). UV-Vis (DMSO): λ_{max} (nm) (ε, mol^{-1} cm^{-1}) 457 (7200). IR (golden gate diamant): ῡ (cm^{-1}) 3409 (ν_{NH} amide), 3065 (ν_{CH} Ar), 1638 ($\nu_{C=O}$ amide), 1619 ($\nu_{C=N}$).

2: In a round-bottom flask under argon and equipped with a cooling system, were introduced 1.414 g (1.280 mmol, 1 eq.) of 7 and 0.6 mg (0.0026 mmol, 0.002 eq.) of $Pd(OAc)_2$, dissolved in 20 mL of distilled acetonitrile. 356 µL (2.559 mmol, 2 eq.) of distilled triethylamine and 222 µL (1.280 mmol, 1 eq.) of diphenylphosphine were then added, and the reaction mixture was stirred at 85°C overnight in the dark. After cooling at room temperature, the solvent was removed by rotary evaporation, and the crude product purified by column chromatography on silica (eluent: 100 acetonitrile/10 distilled water/1 KNO3 aq. saturated); yield 1.364 mg (1.173 mmol, 92%).

^{1}H NMR (300.13 MHz, CD_2Cl_2): δ = 8.56 (broad d, 2 H, $^3J_{H-H}$ = 5.7 Hz, 2 x CH-bipyridine), 8.49 (broad d, 2 H, $^3J_{H-H}$ = 8.1 Hz, 2 x CH-bipyridine), 8.39 (broad d, 2 H, $^3J_{H-H}$ = 8.3 Hz, 2 x CH-bipyridine), 8.19 (td, 2 H, $^3J_{H-H}$ = 8.0 Hz and $^4J_{H-H}$ = 1.5 Hz, 2 x CH (2 and 2')), 8.07 (broad t, 1 H, $^3J_{H-H}$ = 7.9 Hz, CH (1')), 7.99 (td, 2 H, $^3J_{H-H}$ = 7.8 Hz and $^4J_{H-H}$ = 1.4 Hz, 2 x CH (3 and 3')), 7.73 (broad d, 2 H, $^3J_{H-H}$ = 7.0 Hz, 2 x CH-Ar), 7.68 (m, 2 H, 2 x CH-bipyridine), 7.54-7.50 (m, 2 H, 2 x CH-bipyridine), 7.45-7.35 (m, 12 H, 10 x CH-PPh_2 + 2 x CH-Ar), 7.28-7.22 (m, 2 H, 2 x CH-bipyridine), 7.13 (dd, 2 H, $^3J_{H-H}$ = 6.1 Hz and $^4J_{H-H}$ = 1.5 Hz, 2 x CH (4 and 4')), 6.94 (m, 2 H, 2 x CH-bipyridine), 6.77 (m, 2 H, 2 x CH-bipyridine), 6.26 (broad d, 1 H, $^3J_{H-H}$ = 7.5 Hz, CH (1)). $^{31}P\{^1H\}$ NMR (202.46 MHz, CD_2Cl_2): δ = -5.14 (s, PPh_2), -144.4 (hept, $^1J_{P-F}$ = 714.1 Hz, PF_6). $^{13}C\{^1H\}$ NMR (75.47 MHz, CD_2Cl_2): δ = 168.8 (s, CIV-CO), 157.7 (s, CIV-dipyridyl), 157.5 (s, 2 x CIV-bipyridine), 157.4 (s, 2 x CIV-bipyridine), 155.8 (d, $^1J_{C-P}$ = 27.8 Hz, 2 x CIV-PPh_2), 153.8 (s, CIV-dipyridyl), 152.7 (s, 2 x CH-bipyridine), 151.8 (s, 2 x CH-bipyridine), 149.6 (s, 2 x CH (4 and 4')), 139.0 (s, CIV-CCONH), 138.7 (s, CH (1')), 138.5 (s, 2 x CH (2 and 2')), 138.1 (s, CH (3')), 136.1 (d, $^1J_{C-P}$ = 30.3 Hz, CIV-Ar), 134.4-134.2 (m, CH-bipyridine + 4 x CH-PPh_2 ortho), 133.6 (s, CH-bipyridine), 133.4 (s, CH-bipyridine), 133.0 (s, 2 x CH-PPh_2 para), 132.2 (s, CH-bipyridine), 129.5 (s, CH (3)), 129.2-128.9 (m, 4 x CH-PPh_2 meta + 2 x CH-Ar), 128.2 (s, CH-bipyridine), 128.0 (s, CH-bipyridine), 127.7 (s, CH (1)), 124.7 (s, 2 x CH-bipyridine), 124.6 (s, 2 x CH-bipyridine), 120.2 (s, 2 x CH-bipyridine), 116.1 (s, 2 x CH-Ar). ESI-MS (CH_2Cl_2/MeOH, positive mode) exact mass for C49H38N7O1P1Ru1 ($[M]^{2+}$, theoretical *m/z* 436.59606): found *m/z* 436.59712 (err. 3.941 ppm). UV-Vis (DMSO): λ_{max} (nm) (ε, mol^{-1} cm^{-1}) 433 (7400). IR (golden gate diamant): ῡ (cm^{-1}) 3413 (ν_{NH} amide), 3089 (ν_{CH} Ar), 1677 ($\nu_{C=O}$ amide), 1600 ($\nu_{C=N}$).

1A-PF_6 (or 1A-Cl): In a Schlenk tube under argon were introduced 106 mg (or 87 mg) (0.089 mmol, 1 eq.) of 1-PF_6 (or 1-Cl) and 29 mg (0.089 mmol, 1 eq.) of Au(tht)Cl. Degassed benzene (3 mL) was added, and the reaction was stirred at room temperature in the dark during 3 hours. The desired coordination product directly precipitated from the mixture. The red precipitate was isolated by filtration and dried to get 1A-PF_6 (or 1A-Cl) as a red powder; yield 117 mg (or 99 mg) (0.082 mmol, 92%). ^{1}H NMR (500.13 MHz, CD_2Cl_2): δ = 8.50 (m, 1 H, CH (3)), 8.45 (m, 4 H, 4 x CH-bipyridine), 8.35 (broad s, 1 H, CH(5)), 8.10-8.02 (m, 5 H, 4 x CH-bipyridine + CH (5')), 7.78-7.71 (m, 4 H, 4 x CH-

bipyridine), 7.65-7.44 (m, 20 H, 4 x CH-Ar + 10 x CH-PPh_2 + 6 x CH-bipyridine)), 7.26 (m, 1 H, CH (3')), 4.84 (d, 2 H, $^3J_{H-H}$ = 5.8 Hz, CH_2), 2.60 (s, 3 H, CH_3). $^{31}P\{^1H\}$ NMR (202.46 MHz, CD_2Cl_2): δ = 32.9 (s, PPh_2) (-144.5 (hept, $^1J_{P-F}$ = 715.3 Hz, PF_6)). $^{13}C\{^1H\}$ NMR (125.76 MHz, CD_2Cl_2): δ = 161.6 (s, CO), 157.0 (s, CIV-bipyridine), 156.8 (s, CIV-bipyridine), 156.7 (s, 2 x CIV-bipyridine), 156.6 (s, CIV-bipyridine), 156.2 (s, CIV-bipyridine), 152.8 (d, $^1J_{C-P}$ = 29.6 Hz, CIV-Ar), 151.5 (s, CH-bipyridine), 151.3 (s, 2 x CH-bipyridine), 151.2 (d, $^1J_{C-P}$ = 35.0 Hz, 2 x CIV-PPh_2), 151.2 (s, CH-bipyridine), 150.5 (s, 2 x CH-bipyridine), 150.1 (s, 2 x CH-bipyridine), 137.9-137.8 (m, 4 x CH-bipyridine + 2 x CH-Ar), 134.2 (d, $^2J_{C-P}$ = 14.3 Hz, 4 x CH-PPh_2 ortho), 134.3 (d, $^2J_{C-P}$ = 13.7 Hz, 2 x CH-Ar), 133.1 (s, CIV-bipyridine), 132.7 (s, CIV-bipyridine), 132.4 (s, CIV-CCONH), 132.3 (d, $^4J_{C-P}$ = 2.7 Hz, 2 x CH-PPh_2 para), 129.4 (d, $^3J_{C-P}$ = 10.6 Hz, 4 x CH-PPh_2 meta), 128.9 (broad s, CH (3')), 128.2-127.9 (m, 3 x CH (5', 6 and 6')), 125.3 (s, CH (5)), 124.2 (s, CH-bipyridine), 124.1 (s, CH-bipyridine), 124.0 (s, CH-bipyridine), 123.9 (s, CH-bipyridine), 123.4 (s, CH (3)), 42.7 (s, CH_2), 21.1 (s, CH_3). ESI-MS (CH_2Cl_2/MeOH, positive mode) exact mass for $C_{51}H_{42}N_7O_1Au_1Cl_1P_1Ru_1$([M]$^{2+}$, theoretical *m/z* 566.57927): found *m/z* 566.58117 (err. 4.268 ppm). UV-Vis (DMSO): λ_{max} (nm) (ε, mol^{-1} cm^{-1}) 457 (7030). IR (golden gate diamant & FIR): $\bar{\upsilon}$ (cm^{-1}) 3395 (ν_{NH} amide), 3076 (ν_{CH} Ar), 1657 ($\nu_{C=O}$ amide), 1621 ($\nu_{C=N}$), 321 (νAuCl).

1B: In a Schlenk tube under argon were introduced 146 mg (0.123 mmol, 1 eq.) of 1-PF_6 and 38 mg (0.061 mmol, 0.5 eq.) of [(p-cymene)$RuCl_2$]2. Degassed benzene (3 mL) was added, and the reaction was stirred at room temperature in the dark during 3 hours. The desired coordination product directly precipitated from the mixture. The red precipitate was isolated by filtration and dried to get 1B as a red powder; yield 170 mg (0.114 mmol, 93%). ^1H NMR (500.13 MHz, CD_2Cl_2): δ = 8.47 (broad s, 1 H, CH (3)), 8.45-8.41 (m, 4 H, 4 x CH-bipyridine), 8.34 (broad s, 1 H, CH (5)), 8.08-8.03 (m, 4 H, 4 x CH-bipyridine), 7.87-7.70 (m, 11 H, 8 x CH-bipyridine + 2 x CH-Ar + CH (5')), 7.56-7.55 (m, 2 H, 2 x CH-Ar), 7.52-7.42 (m, 12 H, 10 x CH-PPh_2 + 2 x CH (6 and 6')), 7.26 (broad d, 1 H, $^3J_{H-H}$ = 5.5 Hz, CH (3')), 5.27 (d, 2 H, $^3J_{H-H}$ = 6.6 Hz, 2 x CH-Ar p-cymene), 5.03 (d, 2 H, $^3J_{H-H}$ = 6.3 Hz, 2 x CH-Ar p-cymene), 4.76 (broad d, 2 H, $^3J_{H-H}$ = 6.3 Hz, CH_2), 2.78 (hept, 1 H, $^3J_{H-H}$ = 7.0 Hz, CH-iPr), 2.58 (s, 3 H, CH_3), 1.90 (s, 3 H, CH_3), 1.17 (d, 6 H, $^3J_{H-H}$ = 7.0 Hz, 2 x CH_3-iPr). $^{31}P\{^1H\}$ NMR (202.46 MHz, CD_2Cl_2): δ = 25.6 (s, PPh_2), -144.4 (hept, $^1J_{P-F}$ = 711.9 Hz, PF_6). $^{13}C\{^1H\}$ NMR (125.76 MHz, CD_2Cl_2): δ = 159.7 (s, CO), 157.4 (s, CIV-bipyridine), 157.2 (s, CIV-bipyridine), 157.1 (s, CIV-bipyridine), 157.0 (s, 2 x CIV-bipyridine), 156.6 (s, CIV-bipyridine), 152.0 (s, CIV-bipyridine), 151.9 (s, CH-bipyridine), 151.7 (s, CH-bipyridine), 151.6 (m, 4 x CH-bipyridine), 151.5 (d, $^1J_{C-P}$ = 41.4 Hz, CIV-Ar), 151.4 (s, CIV-bipyridine), 150.9 (s, CH-bipyridine), 150.5 (s, CH-bipyridine), 148.8 (s, CIV-CCONH), 138.3 (s, 2 x CH-bipyridine), 138.2 (s, 2 x CH-bipyridine), 134.9 (s, CH (5')), 134.7 (d, $^1J_{C-P}$ = 46.9 Hz, 2 x CIV-PPh_2), 134.6 (m, 2 x CH-Ar), 131.0 (m, 2 x CH-Ar), 129.3 (s, CH (3')), 128.7-128.2 (m, 10 x CH-PPh_2 + 2 x CH (6 and 6')), 125.8 (s, CH (5)), 124.6-124.3 (m, 4 x CH-bipyridine), 123.7 (s, CH (3)), 89.2 (m, 2 x CH-Ar p-cymene), 88.0 (m, 2 x CH-Ar p-cymene), 79.1 (s, CIV-p-cymene), 79.0 (s, CIV-p-cymene), 43.0 (s, CH_2), 30.9 (s, CH-iPr), 22.1 (s, 2 x CH_3), 21.5 (s, CH_3), 18.0 (s, CH_3). ESI-MS (CH_2Cl_2/MeOH, positive mode) exact mass for $C_{61}H_{56}N_7O_1Cl_2P_1Ru_2$ ([M]$^{2+}$, theoretical *m/z* 603.08793): found *m/z* 603.08895 (err. 2.929 ppm). UV-Vis (DMSO): λ_{max} (nm) (ε, mol^{-1} cm^{-1}) 456 (5800). IR (golden gate diamant & FIR): $\bar{\upsilon}$ (cm^{-1}) 3367 (ν_{NH} amide), 3081 (ν_{CH} Ar), 1621 ($\nu_{C=O}$ amide), 1328 (ν_{C-N}), 220 (νRuCl).

1C: In a Schlenk tube under argon were introduced 79 mg (0.066 mmol, 1 eq.) of 1-PF_6 and 26 mg (0.033 mmol, 0.5 eq.) of [(p-cymene)$OsCl_2$]2. Degassed benzene (3 mL) was added, and the reaction was stirred at room temperature in the dark during 3 hours. The desired coordination product directly precipitated from the mixture. The red precipitate was isolated by filtration and dried to get 1C as a red powder; yield 85 mg (0.057 mmol, 87%). ^1H NMR (500.13 MHz, CD_2Cl_2): δ = 8.47 (broad s, 1 H, CH (3)), 8.45-8.42 (m, 4 H, 4 x CH-bipyridine), 8.33 (broad s, 1 H, CH (5)), 8.08-8.04 (m, 4 H, 4 x CH-bipyridine), 7.88-7.70 (m, 11 H, 8 x CH-bipyridine + 2 x CH-Ar + CH (5')), 7.65-7.63 (m, 2 H, 2 x CH-Ar), 7.55-7.42 (m, 12 H, 10 x CH-PPh_2 + 2 x CH (6 and 6')), 7.26 (broad d, 1 H, $^3J_{H-H}$ = 5.7 Hz, CH (3')), 5.46 (d, 2 H, $^3J_{H-H}$ = 5.9 Hz, 2 x CH-Ar p-cymene), 5.22 (d, 2 H, $^3J_{H-H}$ = 5.8 Hz, 2 x CH-Ar p-cymene), 4.79 (broad d, 2 H, $^3J_{H-H}$ = 5.7 Hz, CH_2), 2.70 (hept, 1 H, $^3J_{H-H}$ = 6.8 Hz, CH-iPr), 2.60 (s, 3 H, CH_3), 2.00 (s, 3 H, CH_3), 1.21 (d, 6 H, $^3J_{H-H}$ = 6.8 Hz, 2 x CH_3-iPr). $^{31}P\{^1H\}$ NMR (202.46 MHz, CD_2Cl_2): δ = -11.9 (s, PPh_2), -140.9 (hept, $^1J_{P-F}$ = 711.7 Hz, PF_6). ESI-MS (CH_2Cl_2/MeOH, positive mode) exact mass for $C_{61}H_{56}N_7O_1Cl_2Os_1P_1Ru_1$ ([M]$^{2+}$, theoretical *m/z* 648.61504): found *m/z* 648.61740 (err. 3.058 ppm). UV-Vis (DMSO): λ_{max} (nm) (ε, mol^{-1} cm^{-1}) 457 (8920).

1D: In a Schlenk tube under argon were introduced 210 mg (0.174 mmol, 1 eq.) of 1A-Cl, dissolved in 3 mL of degassed acetone at 0°C. In another Schlenk tube under argon were mixed 64 mg (0.174 mmol, 1 eq.) of thioglucose tetraacetate in 3 mL of acetone and 174 µL of 1 M NaOH (0.174 mmol, 1 eq.). This mixture was stirred 10 minutes at room temperature in the dark, and was then added at 0°C on the bimetallic solution. The reaction was stirred at room temperature in the dark during 3 hours. The solvent was evaporated, and distilled dichloromethane was added (5 mL). The salts were removed by filtration under argon; the filtrate was evaporated and dried to obtain the desired product as a bright red powder; yield 153 mg (0.100 mmol, 57%). ^1H NMR (500.13 MHz, CD_2Cl_2): δ = 9.66 (broad m, 1 H, NH), 8.73 (d, 1 H, $^4J_{H-H}$ = 3.0 Hz, CH (3)), 8.58-8.53 (m, 4 H, 4 x CH-bipyridine), 8.49 (broad s, 1 H, CH (5)), 8.23-8.20 (dd, 2 H, $^3J_{H-H}$ = 8.2 Hz & $^4J_{H-H}$ = 2.0 Hz, 2 x CH-bipyridine), 8.15-8.06 (m, 4 H, 4 x CH-bipyridine), 7.84-7.83 (broad d, 1 H, $^3J_{H-H}$ = 5.6 Hz, CH (5')), 7.80-7.73 (m, 3 H, 3 x CH-bipyridine), 7.68-7.45 (m, 19 H, 4 x CH-Ar + 10 x CH-PPh_2 + 5 x CH-bipyridine)), 7.27 (m, 1 H, CH (3')), 5.20-5.07 (m, 4 H, 4 x CH-glucose), 4.85 (d, 2 H, $^3J_{H-H}$ = 5.9 Hz, CH_2),

3.80 (m, 3 H, CH_2NH & $CHCH_2OAc$), 2.61 (s, 3 H, CH_3), 2.03-1.99 (m, 12 H, 4 x CH_3). $^{31}P\{^1H\}$ NMR (202.46 MHz, CD_2Cl_2): δ = 38.0 (broad s, PPh_2). $^{13}C\{^1H\}$ NMR (125.76 MHz, CD_2Cl_2): δ = 198.7 (s, CIV-CONH), 170.4 (s, CIV-$COCH_3$), 169.9 (s, 2 x CIV-$COCH_3$), 169.4 (s, CIV-$COCH_3$), 157.0 (d, $^1J_{C-P}$ = 43.2 Hz, CIV-Ar), 156.9-156.8 (m, 6 x CIV-bipyridine), 156.7 (m, 2 x CIV-bipyridine & CIV-Ar), 151.7 (s, CH (5')), 151.3 (m, 5 x CH-bipyridine), 150.3-150.2 (m, 2 x CH-bipyridine), 137.9 (s, 2 x CH-bipyridine), 137.8 (s, CH-bipyridine), 137.7 (s, 2 x CH-bipyridine), 136.7 (d, $^1J_{C-P}$ = 40.3 Hz, 2 x CIV-PPh_2), 134.4 (d, $^3J_{C-P}$ = 2.8 Hz, 2 x CH-Ar), 134.3 (d, $^3J_{C-P}$ = 2.9 Hz, 4 x CH-PPh_2 meta), 134.3 (s, 2 x CH-PPh_2 para), 134.1 (s, CH-bipyridine), 131.9 (broad s, CH (3')), 129.3 (d, $^2J_{C-P}$ = 11.6 Hz, 4 x CH-PPh_2 ortho), 128.7 (d, $^2J_{C-P}$ = 8.9 Hz, 2 x CH-Ar), 127.1 (s, 2 x CH-bipyridine), 125.6 (s, CH (5)), 124.4 (s, 2 x CH-bipyridine), 124.3 (s, 2 x CH-bipyridine), 123.9 (s, CH (3)), 75.8 (s, $CHCH_2OAc$), 73.4 (s, 2 x CH-glucose), 70.3 (s, CH-glucose), 56.4 (s, CH_2), 53.0 (s, CH-glucose), 42.7 (s, CH_2), 21.2 (s, CH_3), 20.6 (s, CH_3), 20.5 (s, 3 x CH_3). ESI-MS (H2O, positive mode) exact mass for $C_{65}H_{61}N_7O_{10}Au_1P_1Ru_1S_1$ ($[M]^{2+}$, theoretical *m/z* 730.63269): found *m/z* 730.63453 (err. 3.717 ppm). UV-Vis (DMSO): λ_{max} (nm) (ε, mol^{-1} cm^{-1}) 456 (4350). IR (golden gate diamant & FIR): ῡ (cm^{-1}) 3432 (ν_{NH}amide), 2962 (ν_{CH} Ar), 1741 ($\nu_{C=O}$ amide), 373 (νAuS).

2A: In a Schlenk tube under argon were introduced 75 mg (0.065 mmol, 1 eq.) of Ru(bipy)$_2$(dipy)PPh_2 (2) and 21 mg (0.065 mmol, 1 eq.) of Au(tht)Cl. Degassed benzene (3 mL) was added, and the reaction mixture was stirred 3 hours in the dark at room temperature. The desired coordination product precipitated; it was filtered and dried under vacuum to obtain 2A as a bright red powder; yield 76 mg (0.055 mmol, 84%). ^1H NMR (500.13 MHz, CD_2Cl_2): δ = 8.76-8.26 (m, 8 H, 8 x CH-bipy), 8.08 (m, 3 H, 3 x CH (3, 3' and 4')), 7.95-7.88 (m, 1 H, CH-bipy), 7.74 (m, 3 H, 3 x CH-bipy), 7.65-7.62 (m, 3 H, 3 x CH-bipy), 7.59-7.47 (m, 15 H, 1 x CH-bipy + 4 x CH-Ar + 10 x CH-PPh_2), 7.30-7.26 (m, 2 H, 2 x CH (2 and 2')), 7.22-7.15 (m, 2 H, 2 x CH (1 and 1')), 6.44 (broad d, 1 H, $^3J_{H-H}$ = 7.7 Hz, CH (4)). $^{31}P\{^1H\}$ NMR (202.46 MHz, CD_2Cl_2): δ = 33.1 (s, PPh_2), -144.6 (hept, $^1J_{P-F}$ = 711 Hz, PF_6). $^{13}C\{^1H\}$ NMR (125.76 MHz, CD_2Cl_2): δ = 168.2 (s, CIV-CON), 157.7-157.4 (m, 4 x CIV), 151.7-151.4 (m, 4 x CH-bipy + CIV), 149.6 (s, 2 x CH (1 and 1')), 139.2 (broad s, CIV + CH (4')), 138.8 (broad s, 3 x CH (2', 3 and 3')), 135.9 (d, $^4J_{C-P}$ = 2.8 Hz, CIV-C_6H_4CO), 134.7-134.4 (m, 2 x CH-bipy + 4 x CH-PPh_2 ortho), 134.3 (s, 2 x CH-bipy), 134.2 (s, 2 x CH-bipy), 133.0-132.9 (m, 2 x CH-PPh_2 para + 2 x CH-bipy), 129.9 (s, 2 x CH-bipy), 129.4-129.1 (m, 4 x CH-PPh_2 meta + 2 x CH-Ar), 128.7 (broad s, 2 x CH-bipy), 128.4 (s, CH (2)), 128.3 (s, CH (4)), 128.0 (d, $^1J_{C-P}$ = 15.9 Hz, CIV-$C_6H_4PPh_2$), 127.5 (d, $^1J_{C-P}$ = 15.4 Hz, 2 x CIV-PPh_2), 117.7 (s, 2 x CH-Ar). ESI-MS (CH_2Cl_2/MeOH, positive mode) exact mass for $C_{49}H_{38}Au_1Cl_1N_7O_1P_1Ru_1$ ($[M]^{2+}$, theoretical *m/z* 552.56360): found *m/z* 552.56333 (err. 0.413 ppm). UV-Vis (DMSO): λ_{max} (nm) (ε, mol^{-1} cm^{-1}) 432 (5860). IR (golden gate diamant & FIR): ῡ (cm^{-1}) 3358 (ν_{NH} amide), 3083 (ν_{CH} Ar), 1684 ($\nu_{C=N}$), 321 (νAuCl).

2B: In a Schlenk tube under argon were introduced 69 mg (0.059 mmol, 1 eq.) of Ru(bipy)$_2$(dipy)PPh_2 (2) and 18 mg (0.030 mmol, 0.5 eq.) of [(p-cymene)$RuCl_2$]2. Degassed benzene (3 mL) was added, and the reaction mixture was stirred 4 hours in the dark at room temperature. The desired coordination product precipitated; it was filtered and dried under vacuum to obtain 2B as a red powder; yield 67 mg (0.046 mmol, 77%). ^1H NMR (500.13 MHz, CD_2Cl_2): δ = 8.92-7.75 (m, 10 H, 10 x CH-bipy), 7.71 (m, 3 H, 3 x CH (3, 3' and 4')), 7.60-7.49 (m, 18 H, 4 x CH-bipy + 10 x CH-PPh_2 + 4 x CH-Ar), 7.46 (m, 2 H, 2 x CH (2 and 2')), 7.36-7.24 (m, 2 H, 2 x CH (1 and 1')), 7.16-7.13 (m, 2 H, 2 x CH-bipy), 6.20 (broad d, 1 H, $^3J_{H-H}$ = 7.4 Hz, CH(4)), 5.46 (d, 2 H, $^3J_{H-H}$ = 6.1 Hz, 2 x CH-Ar p-cymene), 5.33 (d, 2 H, $^3J_{H-H}$ = 6.0 Hz, 2 x CH-Ar p-cymene), 2.90 (hept, 1 H, $^3J_{H-H}$ = 6.9 Hz, CH-iPr), 2.15 (s, 3 H, CH_3), 1.31 (d, 6 H, $^3J_{H-H}$ = 7.0 Hz, 2 x CH_3-iPr). $^{31}P\{^1H\}$ NMR (202.46 MHz, CD_2Cl_2): δ = 26.8 (s, PPh_2), -144.6 (hept, $^1J_{P-F}$ = 711 Hz, PF_6). $^{13}C\{^1H\}$ NMR (125.76 MHz, CD_2Cl_2): δ = 168.2 (s, CIV-CON), 157.8-157.6 (m, 4 x CIV), 151.9-151.6 (m, 4 x CH-bipy + CIV), 150.4 (s, 2 x CH (1 and 1')), 139.2 (broad s, CIV + CH (4')), 138.7 (broad s, 3 x CH (2', 3 and 3')), 135.1 (s, 2 x CH-bipy), 135.0 (s, 2 x CH-bipy), 134.6-134.5 (d, $^2J_{C-P}$ = 8.8 Hz, 2 x CH-PPh_2 ortho), 134.4-134.3 (m, 2 x CH-PPh_2 ortho + 2 x CH-PPh_2 para), 133.9 (s, CIV-C_6H_4CO), 132.6 (d, $^1J_{C-P}$ = 42.0 Hz, CIV-$C_6H_4PPh_2$), 131.6 (s, 2 x CH-bipy), 131.4 (s, 2 x CH-bipy), 128.9-128.8 (m, 4 x CH-PPh_2 meta + 2 x CH-Ar), 128.7 (broad s, 4 x CH-bipy), 128.3 (s, CH (2)), 127.0 (s, CH (4)), 126.4 (d, $^1J_{C-P}$ = 40.8 Hz, 2 x CIV-PPh_2), 114.5 (s, 2 x CH-Ar), 111.2 (s, CIV-p-cymene), 97.5 (s, CIV-p-cymene), 89.3 (m, 2 x CH-Ar p-cymene), 88.8 (m, 2 x CH-Ar p-cymene), 30.9 (s, CH-iPr), 22.2 (s, CH_3), 22.1 (s, CH_3), 18.1 (s, CH_3). ESI-MS (CH_2Cl_2/MeOH, positive mode) exact mass for $C_{59}H_{52}Cl_2N_7O_1P_1Ru_2$ ($[M]^{2+}$, theoretical *m/z* 589.57208): found *m/z* 589.57389 (err. 4.559 ppm). UV-Vis (DMSO): λ_{max} (nm) (ε, mol^{-1} cm^{-1}) 429 (6230). IR (golden gate diamant & FIR): ῡ (cm^{-1}) 3410 (ν_{NH} amide), 3092 (ν_{CH} Ar), 1680 ($\nu_{C=N}$), 1601 ($\nu_{C=C}$ Ar), 1465 (ν_{C-N}), 211 (νRuCl).

2C: In a Schlenk tube under argon were introduced 49 mg (0.042 mmol, 1 eq.) of Ru(bipy)$_2$(dipy)PPh_2 (2) and 13 mg (0.021 mmol, 0.5 eq.) of [(Cp*)$RhCl_2$]2. Degassed benzene (3 mL) was added, and the reaction mixture was stirred 4 hours in the dark at room temperature. The desired coordination product precipitated; it was filtered and dried under vacuum to obtain 2C as a red powder; yield 63 mg (0.042 mmol, 99%). ^1H NMR (500.13 MHz, CD_2Cl_2): δ = 8.75-8.18 (m, 10 H, 10 x CH-bipy), 8.11-8.04 (m, 4 H, 2 x CH (3 and 3') + 2 x CH-bipy), 7.85-7.68 (m, 7 H, CH (4') + 6 x CH-bipy), 7.67-7.62 (m, 2 H, 2 x CH (2 and 2')), 7.59-7.47 (m, 14 H, 10 x CH-PPh_2 + 4 x CH-Ar), 7.26-7.09 (m, 2 H, 2 x CH (1 and 1')), 6.20 (broad d, 1 H, $^3J_{H-H}$ = 7.2 Hz, CH (4)), 1.72 (s, 15 H, 5 x CH_3-Cp*). $^{31}P\{^1H\}$ NMR (202.46 MHz, CD_2Cl_2): δ = 30.8 (d, 1JP-Rh = 144.6 Hz, PPh_2), -144.6 (hept, $^1J_{P-F}$ = 711 Hz, PF_6). $^{13}C\{^1H\}$ NMR (125.76 MHz, CD_2Cl_2): δ = 168.3 (s, CIV-CON), 157.9-157.3 (m, 4 x CIV), 153.5-151.3 (m, 4 x CH-bipy + CIV), 150.6 (s, 2 x CH (1 and 1')), 139.5 (m,

CIV + CH (4')), 138.7 (broad s, 3 x CH (2', 3 and 3')), 135.3 (s, 2 x CH-bipy), 135.0 (s, 2 x CH-bipy), 135.0 (broad s, 2 x CH-PPh_2 ortho), 134.5 (m, 4 x CH-PPh_2 ortho + para), 133.9 (s, CIV-C_6H_4CO), 132.5 (m, CIV-$C_6H_4PPh_2$), 131.5 (s, 2 x CH-bipy), 131.3 (s, 2 x CH-bipy), 128.7 (m, 4 x CH-PPh_2 meta + 2 x CH-Ar), 128.4 (broad s, 4 x CH-bipy), 127.3-127.1 (m, CH (2) + CH (4) + 2 x CIV-PPh_2), 100.0 (s, 2 x CH-Ar), 46.4 (s, 5 x CIV-Cp*), 10.1 (s, CH_3), 9.1 (s, 2 x CH_3), 8.8 (s, 2 x CH_3). ESI-MS (CH_2Cl_2/MeOH, positive mode) exact mass for $C_{59}H_{53}Cl_2N_7O_1P_1Rh_1Ru_1$ ($[M]^{2+}$, theoretical *m/z* 590.57619): found *m/z* 590.57844 (err. 4.654 ppm). UV-Vis (DMSO): λ_{max} (nm) (ε, mol^{-1} cm^{-1}) 418 (6240). IR (golden gate diamant & FIR): ῡ (cm^{-1}) 3361 (ν_{NH} amide), 1680 ($\nu_{C=N}$), 1601 ($\nu_{C=C}$ Ar), 1371 (ν_{C-N}), 374 (νRhCl).

2D: In a Schlenk tube under argon were introduced 129 mg (0.101 mmol, 1 eq.) of $Ru(bipy)_2$(dipyAuCl) (2A), dissolved in distilled acetone (5 mL). The reaction mixture was cooled down to 0°C and stirred 5 minutes. In another Schlenk tube under argon were introduced 37 mg (0.101 mmol, 1 eq.) of 1-thio-β-D-glucose tetraacetate, dissolved in distilled acetone (5 mL). 101 µL (0.101 mmol, 1 eq.) of 1 M NaOH were added, and the reaction mixture was stirred 10 minutes at room temperature in the dark. This solution was slowly added to the previous one at 0 °C, and the resulting reaction mixture was stirred 3 hours at room temperature. The solvent was evaporated, and distilled dichloromethane (5 mL) was added. The salts were removed by filtration under argon; the filtrate was evaporated and dried to obtain the desired product as a bright red powder; yield 103 mg (0.072 mmol, 71%). ^{1}H NMR (500.13 MHz, CD_2Cl_2): δ = 8.56 (broad d, 2 H, $^3J_{H-H}$ = 5.5 Hz, 2 x CH-bipy), 8.49 (broad d, 2 H, $^3J_{H-H}$ = 8.3 Hz, 2 x CH-bipy), 8.39 (broad d, 2 H, $^3J_{H-H}$ = 8.1 Hz, 2 x CH-bipy), 8.18 (td, 2 H, $^3J_{H-H}$ = 7.9 Hz and $^4J_{H-H}$ = 1.4 Hz, 2 x CH (3 and 3')), 8.08 (broad t, 1 H, $^3J_{H-H}$ = 7.9 Hz, CH (4')), 7.99 (td, 2 H, $^3J_{H-H}$ = 7.9 Hz and $^4J_{H-H}$ = 1.4 Hz 2 x CH (2 and 2')), 7.74-7.22 (m, 22 H, 4 x CH-Ar + 8 x CH-bipy + 10 x CH-PPh_2), 7.12 (dd, 2 H, $^3J_{H-H}$ = 6.1 Hz and $^4J_{H-H}$ = 1.4 Hz, 2 x CH (1 and 1')), 6.75 (m, 2 H, 2 x CH-bipy), 6.43 (broad d, 1 H, $^3J_{H-H}$ = 7.4 Hz, CH(4)), 5.20-5.03 (m, 4 H, 4 x CH-glucose), 4.16-4.15 (m, 2 H, CH_2), 3.80 (broad s, 1 H, $CHCH_2OAc$), 2.11-1.97 (m, 12 H, 4 x CH_3). $^{31}P\{^1H\}$ NMR (121.49 MHz, $CDCl_3$): δ = 38.5 (broad s, PPh_2), -144.6 (hept, $^1J_{P-F}$ = 712.2 Hz, PF_6). $^{13}C\{^1H\}$ NMR (125.76 MHz, $CDCl_3$): δ = 209.8 (s, CIV-CON), 169.8 (s, CIV-$COCH_3$), 157.3 (s, CIV-$COCH_3$), 157.1 (s, CIV-$COCH_3$), 157.0 (s, CIV-$COCH_3$), 156.1 (d, $^1J_{C-P}$ = 47.6 Hz, CIV-Ar), 153.5 (s, 2 x CIV-dipy), 152.4 (s, 2 x CIV-bipy), 151.4 (s, 2 x CIV-bipy), 149.1 (s, 2 x CH (4 and 4')), 139.2 (s, 2 x CH-bipy), 138.5 (d, $^1J_{C-P}$ = 53.2 Hz, 2 x CIV-PPh_2), 138.4 (s, CH(1')), 138.1 (s, 2 x CH (2 and 2')), 137.6 (s, 2 x CH (3 and 3')), 134.8 (d, $^1J_{C-P}$ = 52.4 Hz, CIV-$C_6H_4PPh_2$), 134.4-134.2 (m, 4 x CH-PPh_2 ortho + 2 x CH-Ar), 132.2 (broad s, 2 x CH-PPh_2 para), 129.4-129.3 (m, 4 x CH-PPh_2 meta + 2 x CH-Ar), 128.2 (s, CH (1)), 127.7 (s, 2 x CH-bipy), 127.6 (s, 2 x CH-bipy), 124.3 (s, 4 x CH-bipy), 124.2 (s, 2 x CH-bipy), 119.7 (s, 2 x CH-bipy), 115.8 (s, 2 x CH-bipy), 83.0 (s, CHOAc), 78.6 (s, $CHCH_2OAc$), 73.4 (s, CHOAc), 71.2 (s, CHOAc), 69.0 (s, CHS), 62.0 (s, CH_2), 20.9 (s, CH_3), 20.5 (s, 2 x CH_3), 20.4 (s, CH_3). ESI-MS (H2O/ACN, positive mode) exact mass for $C_{63}H_{57}Au_1N_7O_{10}P_1Ru_1S_1$ ($[M]^{2+}$, theoretical *m/z* 716.61701): found *m/z* 716.61616 (err. -0.006 ppm). UV-Vis (DMSO): λ_{max} (nm) (ε, mol^{-1} cm^{-1}) 436 (9540). IR (golden gate diamant & FIR): ῡ (cm^{-1}) 3438 (ν_{NH} amide), 3087 (ν_{CH} Ar), 2963 (ν_{CH} alcane), 1740 ($\nu_{C=O}$ ester), 1630 ($\nu_{C=N}$), 1221 (νC-O ester), 372 (νAuS).

4: In a round bottom flask protected from light were introduced under argon 1.06 g (5.314 mmol, 1 eq.) of (4'-methyl-[2,2'-bipyridin]-4-yl)methanamine (3), 1.41 g (5.314 mmol, 1 eq.) of 4-iodobenzoyl chloride and 733 mg (5.314 mmol, 1 eq.) of potassium carbonate (K2CO3) in 25 mL of distilled acetonitrile. The mixture was refluxed at 85°C under argon overnight in the dark. After cooling at room temperature, the solvent was removed under vacuum. The resulting pink powder was dissolved in a mixture of dichloromethane and distilled water. The aqueous phase was extracted with dichloromethane; the organic layers were washed with distilled water, and dried over Na2SO4. The solvent was removed by rotary evaporation to obtain 4-iodo-N-((4'-methyl-[2,2'-bipyridin]-4-yl)methyl)benzamide (4) as a pale pink powder; yield 2.088 g (4.87 mmol), 92%). ^{1}H NMR (300.13 MHz, $CDCl_3$): δ = 8.65 (dd, 1 H, $^3J_{H-H}$ = 4.8 Hz and $^5J_{H-H}$ = 0.6 Hz, CH (6')), 8.53 (d, 1 H, $^3J_{H-H}$ = 5.1 Hz, CH (6)), 8.45 (pseudo-q, 1 H, $^4J_{H-H}$ = 0.9 Hz, CH (3')), 8.28 (pseudo-t, 1 H, $^4J_{H-H}$ = 0.9 Hz, CH (3)), 7.81 (dt, 2 H, $^3J_{H-H}$ = 8.7 Hz and $^4J_{H-H}$ = 2.1 Hz, 2 x CH-Ar), 7.61 (dt, 2 H, $^3J_{H-H}$ = 8.7 Hz and $^4J_{H-H}$ = 1.8 Hz, 2 x CH-Ar), 7.32 (dd, 1 H, $^3J_{H-H}$ = 5.1 Hz and $^4J_{H-H}$ = 1.5 Hz, CH (5)), 7.21 (dq, 1 H, $^3J_{H-H}$ = 5.1 Hz and $^4J_{H-H}$ = 0.8 Hz, CH (5')), 6.86 (pseudo-t, 1 H, NH), 4.74 (d, 2 H, $^3J_{H-H}$ = 6.0 Hz, CH_2), 2.48 (s, 3 H, CH_3). $^{13}C\{^1H\}$ NMR (75.47 MHz, $CDCl_3$): δ = 166.8 (s, CIV-CONH), 156.8 (s, CIV), 155.6 (s, CIV), 149.6 (s, CH (6')), 148.9 (s, CH (6)), 148.4 (s, CIV), 148.0 (s, CIV), 137.9 (s, 2 x CH-Ar), 133.3 (s, CIV-Ar), 128.6 (s, 2 x CH-Ar), 125.0 (s, CH (5')), 122.5 (s, CH (5)), 122.2 (s, CH (3)), 119.7 (s, CH (3')), 98.9 (s, CIV-CI), 43.2 (s, CH_2), 21.2 (s, CH_3). ESI-MS (CH_2Cl2/MeOH, positive mode) exact mass for $C_{19}H_{17}N_3O1I_1$ ($[M + H]^+$, theoretical *m/z* 430.04108): found *m/z* 430.04138 (err. 0.694 ppm). Elemental analysis for $C_{19}H_{16}N_3IO$ (429.03): C: 53.16, H: 3.76, N: 9.79; found: C: 53.72, H: 2.90, N: 10.95. IR (golden gate diamant): ῡ (cm^{-1}) 3307 (ν_{NH} amide), 3055 (ν_{CH} Ar), 1637 (ν_{CO} amide).

5: In a round-bottom flask under argon and equipped with a cooling system, were introduced 150 mg (0.350 mmol, 1 eq.) of 4-iodo-N-((4'-methyl-[2,2'-bipyridin]-4-yl)methyl)benzamide (4) and 169 mg (0.350 mmol, 1 eq.) of cis-dichlorobis(2,2'-bipyridine)ruthenium (II) dihydrate. A degassed 1:1 mixture of ethanol and chloroform (10 mL) was added, and the reaction was stirred under argon at gentle reflux during 48 hours in the dark. The mixture was let to return to room temperature. The solvent was then evaporated. To get the derivative with the hexafluorophosphate counter-ion (5-PF_6) (in spite of the chloride one (5-Cl)), the residue was then dissolved in a minimum amount of acetonitrile, and the desired crude product obtained by precipitation after addition of a NH_4PF_6 saturated aqueous

solution. In both cases, the residue was finally purified by silica gel chromatography (eluent: 100 acetonitrile/10 distilled water/1 KNO3 aq. saturated); yield 368 mg (or 297 mg) (0.325 mmol, 93%). ^{1}H NMR (300.13 MHz, CD_2Cl_2): δ = 9.31 (m, 4 H, 4 x CH-bipyridine), 8.32 (broad s, 1 H, CH (3)), 8.11-8.03 (m, 4 H, 4 x CH-bipyridine), 7.86 (td, 2 H, $^{3}J_{H-H}$ = 8.6 Hz and $^{4}J_{H-H}$ = 1.9 Hz, 2 x CH-Ar), 7.79-7.70 (m, 4 H, 4 x CH-bipyridine), 7.66 (td, 2 H, $^{3}J_{H-H}$ = 8.6 Hz and $^{4}J_{H-H}$ = 1.9 Hz, 2 x CH-Ar), 7.56-7.42 (m, 8 H, 8 x CH-bipyridine), 7.25 (m, 1 H, CH (3')), 4.81 (d, 2 H, $^{3}J_{H-H}$ = 6.0 Hz, CH_2), 2.60 (s, 3 H, CH_3). (^{31}P{^{1}H} NMR (121.49 MHz, CD_2Cl_2): δ = -144.5 (hept, $^{1}J_{P-F}$ = 715.3 Hz, PF_6)). (19F{^{1}H} NMR (470.6 MHz, CD_2Cl_2): δ = -72.6 (d, $^{1}J_{P-F}$ = 711.2 Hz, PF_6)). ^{13}C{^{1}H} NMR (125.76 MHz, CD_2Cl_2): δ = 166.8 (s, CO), 157.0 (s, CIV-bipyridine), 156.8 (s, CIV-bipyridine), 156.7 (s, 2 x CIV-bipyridine), 156.6 (s, CIV-bipyridine), 156.2 (s, CIV-bipyridine), 151.5 (s, CH-bipyridine), 151.4 (s, CIV (4'), 151.3 (s, CH-bipyridine), 151.2 (s, 2 x CH-bipyridine), 151.1 (s, 2 x CH-bipyridine), 151.0 (s, CIV (4')), 137.9 (s, 2 x CH-bipyridine), 137.8 (s, 2 x CH-bipyridine), 137.7 (s, 2 x CH-Ar), 132.9 (s, CIV-CCONH), 128.9 (m, 2 x CH-Ar + CH-bipyridine), 128.2 (s, CH-bipyridine), 128.1 (s, CH-bipyridine), 128.0 (s, CH-bipyridine), 127.8 (s, CH-bipyridine), 127.0 (s, CH-bipyridine), 125.3 (s, CH-bipyridine), 124.2 (s, CH-bipyridine), 124.1 (s, CH-bipyridine), 124.0 (s, CH-bipyridine), 123.9 (s, CH-bipyridine), 123.3 (s, CH-bipyridine), 98.8 (s, CIV-CI), 42.6 (s, CH_2), 21.1 (s, CH_3). ESI-MS (CH_2Cl_2/MeOH, positive mode) exact mass for C39H32N7O1I1Ru1 ($[M]^{2+}$, theoretical *m/z* 421.53780): found *m/z* 421.53722 (err. -0.136 ppm). IR (golden gate diamant): ῡ (cm^{-1}) 3321 (ν_{NH} amide), 3077 (ν_{CH} Ar), 1654 ($\nu_{C=O}$ amide), 1620 ($\nu_{C=N}$).

6: In a round bottom flask under argon, protected from light and equipped with a cooling system, were introduced 1.053 g (3.960 mmol, 1 eq.) of 4-iodobenzoyl chloride, 677 mg (3.960 mmol, 1 eq.) of di(pyridin-2-yl)amine and 546 mg (3.960 mmol, 1 eq.) of potassium carbonate (K2CO3). Distilled acetonitrile (50 mL) was added, and the reaction mixture was stirred at 85°C overnight. The resulting mixture was filtered while hot to remove the salts. During the cooling, colorless crystals grown up in the filtrate, which was evaporated under reduced pressure to obtain 4-iodo-N,N-di(pyridin-2-yl)benzamide (6) as a white powder; yield 1.460 g (3.641 mmol, 92%). ^{1}H NMR (300.13 MHz, $CDCl_3$): δ = 8.41 (ddd, 2 H, $^{3}J_{H-H}$ = 4.9 Hz, $^{4}J_{H-H}$ = 1.9 Hz and $^{5}J_{H-H}$ = 0.78 Hz, 2 x CH (1 and 1')), 7.72 (td, 2 H, $^{3}J_{H-H}$ = 7.8 Hz and $^{4}J_{H-H}$ = 2.0 Hz, 2 x CH (2 and 2')), 7.60 (dd, 2 H, $^{3}J_{H-H}$ = 8.6 Hz and $^{4}J_{H-H}$ = 2.2 Hz, 2 x CH-Ar), 7.31 (dt, 2 H, $^{3}J_{H-H}$ = 8.1 Hz and $^{4}J_{H-H}$ = 0.87 Hz, 2 x CH (3 and 3')), 7.23 (dt, 2 H, $^{3}J_{H-H}$ = 8.6 Hz and $^{4}J_{H-H}$ = 2.1 Hz, 2 x CH-Ar), 7.18 (ddd, 2 H, $^{3}J_{H-H}$ = 7.4 Hz, $^{4}J_{H-H}$ = 4.8 Hz and $^{5}J_{H-H}$ = 0.96 Hz, 2 x CH (4 and 4')). ^{13}C{^{1}H} NMR (125.76 MHz, $CDCl_3$): δ = 170.3 (s, CIV-CO), 155.1 (s, 2 x CIV-pyridine), 148.9 (s, 2 x CH (1 and 1')), 138.2 (s, 2 x CH (2 and 2')), 137.5 (s, 2 x CH-Ar), 135.3 (s, CIV-C_6H_4CO), 130.6 (s, 2 x CH-Ar), 122.1 (s, 2 x CH (3 and 3')), 121.7 (s, 2 x CH (4 and 4')), 97.9 (s, CI). ESI-MS (CH_2Cl_2/MeOH, positive mode) exact mass for $C_{17}H_{13}N_3O_1I_1$ ($[M+H]^{+}$, theoretical *m/z* 402.00978): found *m/z* 402.01004 (err. 0.643 ppm). Elemental analysis for $C_{17}H_{12}N_3OI$ (401.03): C: 50.89, H: 3.01, N: 10.47; found: C: 50.78, H: 3.01, N: 10.63. IR (golden gate diamant): ῡ (cm^{-1}) 3418 (ν_{NH} amide), 3001 (ν_{CH} Ar), 1659 ($\nu_{C=O}$ amide).

7: In a round-bottom flask under argon and equipped with a cooling system, were introduced 1.079 g (2.691 mmol, 1 eq.) of 4-iodo-N,N-di(pyridin-2-yl)benzamide (6) and 1.304 g (2.691 mmol, 1 eq.) of cis-dichlorobis(2,2'-bipyridine) ruthenium (II) dihydrate. A degassed 1:1 mixture of methanol and distilled water (40 mL) was added, and the reaction was stirred under argon at gentle reflux overnight in the dark. The mixture was let to return to room temperature. The desired crude product was obtained by precipitation after addition of a KPF_6 saturated aqueous solution and the residue was finally purified by silica gel chromatography (eluent: 100 acetonitrile/10 distilled water/1 KNO3 aq. saturated); yield 2.619 g (2.370 mmol, 88%). ^{1}H NMR (300.13 MHz, CD_2Cl_2): δ = 8.68 (d, 2 H, $^{3}J_{H-H}$ = 8.2 Hz, 2 x CH-bipyridine), 8.57 (m, 4 H, 4 x CH-bipyridine), 8.17 (td, 2 H, $^{3}J_{H-H}$ = 8.0 Hz and $^{4}J_{H-H}$ = 1.3 Hz, 2 x CH (2 and 2')), 8.09 (td, 1 H, $^{3}J_{H-H}$ = 8.0 Hz and $^{4}J_{H-H}$ = 1.3 Hz, 2 x CH (1')), 8.00 (td, 2 H, $^{3}J_{H-H}$ = 8.0 Hz and $^{4}J_{H-H}$ = 1.3 Hz, 2 x CH (3 and 3')), 7.82 (broad d, 2 H, $^{3}J_{H-H}$ = 8.5 Hz, 2 x CH-Ar), 7.67-7.61 (m, 6 H, 6 x CH-bipyridine), 7.44 (broad d, 2 H, $^{3}J_{H-H}$ = 8.6 Hz, 2 x CH-Ar), 7.36 (m, 2 H, 2 x CH-bipyridine), 7.07 (dd, 2 H, $^{3}J_{H-H}$ = 6.3 Hz and $^{4}J_{H-H}$ = 1.5 Hz, 2 x CH (4 and 4')), 6.66 (m, 2 H, 2 x CH-bipyridine), 6.08 (broad d, 1 H, $^{3}J_{H-H}$ = 8.5 Hz, CH (1)). ^{31}P{^{1}H} NMR (151.33 MHz, CD_2Cl_2): δ = -144.6 (hept, $^{1}J_{P-F}$ = 715.2 Hz, PF_6). ^{13}C{^{1}H} NMR (75.47 MHz, CD_2Cl_2): δ = 168.3 (s, CIV-CO), 157.5 (s, CIV-dipyridyl), 157.4 (s, 2 x CIV-bipyridine), 157.3 (s, 2 x CIV-bipyridine), 154.0 (s, CIV-dipyridyl), 152.1 (s, 2 x CH-bipyridine), 151.2 (s, 2 x CH-bipyridine), 148.8 (s, 2 x CH (4 and 4')), 138.7 (s, 2 x CH-bipyridine), 138.5 (s, 2 x CH (2 and 2')), 138.3 (s, CH (1')), 138.0 (s, 2 x CH (3 and 3')), 137.6 (s, 2 x CH-Ar), 132.0 (s, CIV-CCON), 129.1 (s, CH (1)), 127.6 (s, 2 x CH-bipyridine), 127.3 (s, 2 x CH-bipyridine), 124.7 (s, 2 x CH-bipyridine), 124.6 (s, 2 x CH-bipyridine), 118.9 (s, 2 x CH-bipyridine), 116.3 (s, 2 x CH-Ar), 99.1 (s, CIV-CI). ESI-MS (CH_2Cl_2 / MeOH, positive mode) exact mass for C37H28N7O1I1Ru1 ($[M]^{2+}$, theoretical *m/z* 407.52182 Da): found *m/z* 407.52212 Da (err. 0.473 ppm). IR (golden gate diamant): ῡ (cm^{-1}) 3355 (ν_{NH} amide), 2935 (ν_{CH} Ar), 1722 ($\nu_{C=O}$ amide), 1328 ($\nu_{C=N}$).

Electrochemistry: Cyclic voltammograms were recorded using a PalmsSens EmStat3+ potentiostat. Samples (~ 2 mmol) were dissolved in DMSO containing 0.1 M tetrabutylammonium perchlorate (TBAP) as supporting electrolyte and 1 mM ferrocene (Fc) as an internal reference. Voltammograms were recorded in a single compartment electrochemical cell (0.5 mL volume) containing a glassy carbon disk working electrode (3 mm diameter), an Ag/AgCl reference electrode and a Pt wire counter electrode. All measurements were recorded under nitrogen at room temperature.

Antiproliferative assays: The human embryonic kidney (HEK293), human lung cancer (A549), and human ovarian cancer sensitive and resistant to cisplatin (A2780/A2780cisR) cell lines, obtained from the European Centre of Cell Cultures ECACC, Salisbury, UK, were cultured in DMEM (HEK293, A549) and RPMI (A2780, A2780cisR) both containing GlutaMax-I supplemented with 10% FBS and 1% penicillin/streptomycin (all from Invitrogen), at 37 °C in a humidified atmosphere of 95% of air and 5% CO_2 (Heraeus, Germany). For evaluation of growth inhibition, cells were seeded in 96-well plates (Costar, Integra Biosciences, Cambridge, MA) at a concentration of 15.000 cells/well and grown for 24 h in complete medium. Solutions of the compounds were prepared by diluting a freshly prepared stock solution (10 2 M in DMSO) of the corresponding compound in aqueous media (RPMI or DMEM depending on the cell lines). The percentage of DMSO in the culture medium never exceeded 0.2%: at this concentration DMSO has no effect on the cell viability. Cisplatin (Sigma-Aldrich) stock solutions were prepared in MilliQ water. Afterwards, the intermediate dilutions of the compounds were added to the wells (200 μL) to obtain a final concentration ranging from 0.01 to 200 μM, and the cells were incubated for 72 h. Following 72 h drug exposure, 3 (4,5-dimethylthiazol-2-yl)-2,5-diphenyltetrazolium bromide (MTT) was added to the cells at a final concentration of 500 μg.mL−1 incubated for 3-4 h, then the culture medium was removed and the violet formazan dissolved in DMSO. The optical density of each well (96-well plates) was quantified in quadruplicate at 540 nm using a multi-well plate reader (iEMS Read-er MF, Labsystems, Bioconcept) and the percentage of surviving cells was calculated from the ratio of absorbance between treated and untreated cells. The IC_{50} value was calculated as the concentration reducing the proliferation of the cells by 50% and is presented as a mean (± SE) of at least three independent experiments.

Fluorescence microscopy: Sterile 8-well chambers mounted on a slide with cover (Thermo Scientific) were coated with 10 mg/mL solution of poly-L-lysine hydrobromide (Sigma-Aldrich) in sterile water (400 μL per well). After 24 h the wells were washed with PBS and coated plates were used to culture the cells, A2780 and A549, at a density of 5x104 cells per well, with the respective complete medium (RPMI for A2780, DMEM for A549). After 24h, the culture medium was removed and replaced with fresh medium, without FCS, containing 10, 50 or 100 μM of complex 1D, 2A or 2D for 3 hours either in 37 °C or 4 °C. At the end of incubation time, cells were rapidly washed with cold PBS and fixed with 2% paraformaldehyde (Klinipath) for 30 minutes at 4 °C. Nuclei were stained using DAPI solution of 10 μg/mL ([4',6-diamidino-2-phenylindole, dihydrochloride], Invitrogen) in PBS and incubated for 15 minutes at room temperature, in the dark. Following incubation, cells were permeabilized with 0.2% Triton X-100 for 20 min at 4° C and treated with 1μg/μl of propidium iodide for 10 min at room temperature. Cells were washed twice with PBS and then prepared for visualization by removal of the wells were and drying of the glass slide. Slides were then mounted with a glass slipcover with 20% PBS-glycerol (Sigma) and analyzed under a fluorescence microscope (DM 4000 B, Leica). PI was excited at 547 nm (emission wavelength 572 nm) and the compounds at 358 nm (emission wavelength 461 nm, DAPI filter). The acquired images were obtained using individual filters and a combined image, overlaying the fluorescence acquired with the two filters, was obtained using the Leica microscope software.

Electrophoresis with plasmid DNA: Aliquots of pUC19 plasmid DNA (10 μL, 20 μg/mL) in buffer (5 mM Tris/HCl, 50 mM NaClO4, pH 7.4) were incubated with different concentrations of the compounds (in the range 0.1 and 1 metal complex/DNAbp) at 37° C overnight. After the incubation period, the samples were loaded in 1% agarose gel. Samples were separated by electrophoresis for ca. 1 h at 80 V in Tris-acetate/EDTA buffer (TAE). Afterwards, the gel was stained for 30 min in EtBr.

GluT-1 inhibition assay: A2780 and A549 cells were grown on a coated glass slide for 24 h with the respective complete medium, at a density of 5x104 cells per well. After 24 h, the medium was removed and the cells were pre-incubated for 30 min at 37ºC with GluT-1 inhibitor WZB117 (EMD Chemicals) at a concentration of 50 μM. Following the pre-incubation, the solution of inhibitor was removed and the cells were incubated with the various solutions of compounds, freshly prepared in medium without FCS (RPMI for A2780, DMEM for A549), for 3 h at 37ºC. At the end of incubation time, cells were rapidly washed with cold PBS and fixed with 2% paraformaldehyde (Klinipath) for 30 minutes. Nuclei were stained using DAPI solution of 10 μg/mL ([4',6-diamidino-2-phenylindole, dihydrochloride], Invitrogen) in PBS and incubated for 15 minutes at room temperature, in the dark. Following incubation, wells were washed once with PBS and prepared for visualization by removal of the wells were and drying of the glass slide. Slides were then mounted with a glass slipcover with 20% PBS-glycerol (Sigma) and analyzed under a fluorescence microscope (DM 4000 B, Leica). PI was excited at 547 nm (emission wavelength 572 nm) and the compounds at 358 nm (emission wavelength 461 nm, DAPI filter). The acquired images were obtained using individual filters and a combined image, overlaying the fluorescence acquired with the two filters, was obtained using the Leica microscope software.

2.4. References

[1] M.S. Robillard, J. Reedijk, Platinum-based Anticancer Drugs, in: R.B. King (Ed.) Encyclopedia of Inorganic Chemistry, Vol. VII, John Wiley & Sons, 2005, pp. 4488-4498.
[2] K.R. Barnes, S.J. Lippard, Metal Ions in Biolgical Systems, Vol 42: Metal Complexes in Tumor Diagnosis and as Anticancer Agents, 2004.

[3] M.A. Jakupec, M. Galanski, V.B. Arion, C.G. Hartinger, B.K. Keppler, Dalton Trans, (2008) 183-194.
[4] S. Nobili, E. Mini, I. Landini, C. Gabbiani, A. Casini, L. Messori, Medicinal Research Reviews, 30 (2010) 550-580.
[5] G. Sava, A. Bergamo, P.J. Dyson, Dalton Trans, 40 (2011) 9069-9075.
[6] C. Billecke, S. Finniss, L. Tahash, C. Miller, T. Mikkelsen, N.P. Farrell, O. Bögler, Neuro-Oncology, 8 (2006) 215-226.
[7] C.G. Hartinger, A.D. Phillips, A.A. Nazarov, Curr Top Med Chem, 11 (2011) 2688-2702.
[8] S. Tian, F.-M. Siu, S.C.F. Kui, C.-N. Lok, C.-M. Che, Chem Comm, 47 (2011) 9318-9320.
[9] M. Serratrice, F. Edafe, F. Mendes, R. Scopelliti, S.M. Zakeeruddin, M. Gratzel, I. Santos, M.A. Cinellu, A. Casini, Dalton Trans, 41 (2012) 3287-3293.
[10] R.M. Snyder, C.K. Mirabelli, R.K. Johnson, C.-M. Sung, L.F. Faucette, F.L. McCabe, J.P. Zimmerman, M. Whitman, J.C. Hempel, S.T. Crooke, Cancer Res, 46 (1986) 5054-5060.
[11] C.K. Mirabelli, D.T. Hill, L.F. Faucette, F.L. McCabe, G.R. Girard, D.B. Bryan, B.M. Sutton, J.O.L. Barus, S.T. Crooke, R.K. Johnson, J Med Chem, 30 (1987) 2181-2190.
[12] J.F. González-Pantoja, M. Stern, A.A. Jarzecki, E. Royo, E. Robles-Escajeda, A. Varela-Ramírez, R.J. Aguilera, M. Contel, Inorg. Chem, 50 (2011) 11099-11110.
[13] J. Fernandez-Gallardo, B.T. Elie, T. Sadhukha, S. Prabha, M. Sanau, S.A. Rotenberg, J.W. Ramos, M. Contel, Chem Sci, 6 (2015) 5269-5283.
[14] B. Bertrand, A. Citta, I. Franken, M. Picquet, A. Folda, V. Scalcon, M. Rigobello, P. Le Gendre, A. Casini, E. Bodio, J Biol Inorg Chem, 20 (2015) 1005-1020.
[15] F. Pelletier, V. Comte, A. Massard, M. Wenzel, S. Toulot, P. Richard, M. Picquet, P. Le Gendre, O. Zava, F. Edafe, A. Casini, P.J. Dyson, J Med Chem, 53 (2010) 6923-6933.
[16] M. Wenzel, B. Bertrand, M.-J. Eymin, V. Comte, J.A. Harvey, P. Richard, M. Groessl, O. Zava, H. Amrouche, P.D. Harvey, P. Le Gendre, M. Picquet, A. Casini, Inorg Chem, 50 (2011) 9472-9480.
[17] M. Wenzel, E. Bigaeva, P. Richard, P. Le Gendre, M. Picquet, A. Casini, E. Bodio, J Inorg Biochem, 141 (2014) 10-16.
[18] J. Fernández-Gallardo, B.T. Elie, F.J. Sulzmaier, M. Sanaú, J.W. Ramos, M. Contel, Organometallics, 33 (2014) 6669-6681.
[19] L. Massai, J. Fernandez-Gallardo, A. Guerri, A. Arcangeli, S. Pillozzi, M. Contel, L. Messori, Dalton Trans, 44 (2015) 11067-11076.
[20] J. Schulz, J. Tauchman, I. Císařová, T. Riedel, P.J. Dyson, P. Štěpnička, Journal of Organometallic Chemistry, 751 (2014) 604-609.
[21] E. Viry, E. Battaglia, V. Deborde, T. Müller, R. Réau, E. Davioud-Charvet, D. Bagrel, ChemMedChem, 3 (2008) 1667-1670.
[22] H. Goitia, Y. Nieto, M.D. Villacampa, C. Kasper, A. Laguna, M.C. Gimeno, Organometallics, 32 (2013) 6069-6078.
[23] E. Bodio, P. Le Gendre, F. Denat, C. Goze, Advances in Inorganic Chemistry - Insights from Imaging in Bioinorganic Chemistry, in: V.E.a. Hubbard (Ed.) Advances in Inorganic Chemistry - Insights from Imaging in Bioinorganic Chemistry, 2016.
[24] K.Y. Zhang, K.K.-W. Lo, Metal Complexes for Cell and Organism Imaging, in: Inorganic Chemical Biology, John Wiley & Sons, Ltd, 2014, pp. 99-147.
[25] M.P. Coogan, V. Fernandez-Moreira, Chem Comm, 50 (2014) 384-399.
[26] R. Kumar, W.S. Shin, K. Sunwoo, W.Y. Kim, S. Koo, S. Bhuniya, J.S. Kim, Chemical Society Reviews, 44 (2015) 6670-6683.
[27] J.F. Zhang, C.S. Lim, B.R. Cho, J.S. Kim, Talanta, 83 (2010) 658-662.
[28] E.E. Langdon-Jones, S.J.A. Pope, Chem Comm, 50 (2014) 10343-10354.
[29] S. Banerjee, A.R. Chakravarty, Accounts of Chemical Research, 48 (2015) 2075-2083.
[30] P. Jaividhya, M. Ganeshpandian, R. Dhivya, M.A. Akbarsha, M. Palaniandavar, Dalton Trans, 44 (2015) 11997-12010.
[31] T. Zhu, Chen, R., Yu, H., Feng, Y., Chen, J., Lu, Q., Xie, J., Ding, W., Ma, T., Mol Med Rep, 10 (2014) 2477-2482.
[32] W.-K. Tsui, L.-H. Chung, M.M.-K. Wong, W.-H. Tsang, H.-S. Lo, Y. Liu, C.-H. Leung, D.-L. Ma, S.-K. Chiu, C.-Y. Wong, Scientific Reports, 5 (2015) 9070.
[33] S. Tasan, C. Licona, P.-E. Doulain, C. Michelin, C. Gros, P. Le Gendre, P. Harvey, C. Paul, C. Gaiddon, E. Bodio, J Biol Inorg Chem, 20 (2015) 143-154.
[34] P.D. Harvey, S. Tasan, C.P. Gros, C.H. Devillers, P. Richard, P.L. Gendre, E. Bodio, Organometallics, 34 (2015) 1218-1227.
[35] P.-E. Doulain, R. Decreau, C. Racoeur, V. Goncalves, L. Dubrez, A. Bettaieb, P. Le Gendre, F. Denat, C. Paul, C. Goze, E. Bodio, Dalton Trans, 44 (2015) 4874-4883.
[36] S. Tasan, O. Zava, B. Bertrand, C. Bernhard, C. Goze, M. Picquet, P. Le Gendre, P. Harvey, F. Denat, A. Casini, E. Bodio, Dalton Trans, 42 (2013) 6102-6109.
[37] A. Citta, E. Schuh, F. Mohr, A. Folda, M.L. Massimino, A. Bindoli, A. Casini, M.P. Rigobello, Metallomics, 5 (2013) 1006-1015.
[38] B. Bertrand, A. de Almeida, E.P.M. van der Burgt, M. Picquet, A. Citta, A. Folda, M.P. Rigobello, P. Le Gendre, E. Bodio, A. Casini, European J Inorg Chem, 2014 (2014) 4532-4536.
[39] M. Ali, L. Dondaine, A. Adolle, C. Sampaio, F. Chotard, P. Richard, F. Denat, A. Bettaieb, P. Le Gendre, V. Laurens, C. Goze, C. Paul, E. Bodio, J Med Chem, 58 (2015) 4521-4528.
[40] C. Roder, M. Thomson, Drugs R D, 15 (2015) 13-20.
[41] E. Vergara, E. Cerrada, C. Clavel, A. Casini, M. Laguna, Dalton Trans, 40 (2011) 10927-10935.
[42] C. Busche, P. Comba, A. Mayboroda, H. Wadepohl, European J Inorg Chem, 2010 (2010) 1295-1302.
[43] M. Li, J. Liu, C. Zhao, L. Sun, Journal of Organometallic Chemistry, 691 (2006) 4189-4195.
[44] D. Thompson, Gold Bull, 33 (2000) 37-37.
[45] K. Nakamaru, Bulletin of the Chemical Society of Japan, 55 (1982) 1639-1640.
[46] K. Suzuki, A. Kobayashi, S. Kaneko, K. Takehira, T. Yoshihara, H. Ishida, Y. Shiina, S. Oishi, S. Tobita, Phys Chem Chem Phys, 11 (2009) 9850-9860.
[47] M. Goral, T. McCormac, E. Dempsey, D.-L. Long, L. Cronin, A.M. Bond, Dalton Trans, (2009) 6727-6735.
[48] G. Gritzner, J. Kůta, Electrochimica Acta, 29 (1984) 869-873.
[49] N.G. Connelly, W.E. Geiger, Chem Rev, 96 (1996) 877-910.
[50] A.B.P. Lever, Inorg Chem, 29 (1990) 1271-1285.
[51] C.-J. Yao, L.-Z. Sui, H.-Y. Xie, W.-J. Xiao, Y.-W. Zhong, J. Yao, Inorg Chem, 49 (2010) 8347-8350.

[52] M. Pažický, A. Loos, M.J. Ferreira, D. Serra, N. Vinokurov, F. Rominger, C. Jäkel, A.S.K. Hashmi, M. Limbach, Organometallics, 29 (2010) 4448-4458.
[53] A. Casini, C. Gabbiani, F. Sorrentino, M.P. Rigobello, A. Bindoli, T.J. Geldbach, A. Marrone, N. Re, C.G. Hartinger, P.J. Dyson, L. Messori, J Med Chem, 51 (2008) 6773-6781.
[54] A. Casini, C. Hartinger, A. Nazarov, P. Dyson, Organometallic Antitumour Agents with Alternative Modes of Action, in: G. Jaouen, N. Metzler-Nolte (Eds.) Medicinal Organometallic Chemistry, Springer Berlin Heidelberg, 2010, pp. 57-80.
[55] O. Zava, S.M. Zakeeruddin, C. Danelon, H. Vogel, M. Grätzel, P.J. Dyson, ChemBioChem, 10 (2009) 1796-1800.
[56] M. Gottschaldt, U.S. Schubert , S. Rau, S. Yano, J.G. Vos, T. Kroll, J. Clement, I. Hilger, ChemBioChem, 11 (2010) 649-652.
[57] M.A. Bennett, T.N. Huang, T.W. Matheson, A.K. Smith, S. Ittel, W. Nickerson, 16. (η6-Hexamethylbenzene)Ruthenium Complexes, in: Inorganic Syntheses, John Wiley & Sons, Inc., 2007, pp. 74-78.
[58] R. Uson, A. Laguna, M. Laguna, D.A. Briggs, H.H. Murray, J.P. Fackler, (Tetrahydrothiophene)Gold(I) or Gold(III) Complexes, in: Inorganic Syntheses, John Wiley & Sons, Inc., 2007, pp. 85-91.

Discussion and Future Perspectives

The work presented in this thesis focuses on metal-based compounds and their role in medicine and chemical biology. Metallodrugs have currently several different applications in medicine, such as anticancer, antiartritic or treatment for parasitic diseases. Despite their broad range of applications, the mechanism of action of several of these drugs is poorly understood and their biological targets still remain uncertain. Within this scope, the work presented in this thesis is divided in two separate, yet complementary parts: A and B.

PART A

In **Part A**, the work focuses on the study of aquaporins and related metal-based inhibitors. As described in the previous chapters, aquaporins (AQPs) are involved in several physiological processes and their essential roles of water and glycerol channels in different cells and tissues make them attractive drug targets in a variety of diseases related to their malfunction. Nonetheless, the development of aquaporin inhibitors and modulators for therapeutic purposes is a challenging task [1].

Thus, in part A we aim at elucidating the mechanism of AQPs' inhibition by metal-based compounds, as well as the physiological pH gating mechanisms of aquaglyceroporins. The latter is of interest since new approaches to inhibiting AQPs function may be derived. The main findings of our investigations are summarized below.

Initial Structure-Activity Relationships on gold compounds as possible AQPs inhibitors

Our group has recently identified a gold(III) compound, Auphen, as a selective inhibitor of the human aquaglyceroporin isoform AQP3 which does not inhibit the orthodox water channel AQP1 [2]. After these initial promising results, as described in **Chapter A.1**, we expanded the library of gold(III) compounds as aquaporin inhibitors. Thus, we described the inhibitory effects of a new series of gold(III) compounds with N-donor ligands (Figure 1) on hAQP3, using human red blood cell (hRBC) as model. Initially, in order to achieve structure-activity relationship information, a series of Auphen-related compounds was studied, namely Aubipy and its derivatives, as well as Auterpy (Figure 1). Even though all compounds were effective as hAQP3 inhibitors (IC_{50} in the low micromolar range) only two of them (AubipyMe and Auterpy) showed a similar potency to Auphen at about 1 μM, while Aubipy and $AubipyNH_2$ were significantly less effective. Subsequently a second series of gold(III) compounds was investigated as hAQP3 inhibitors, comprising one organometallic Au(III) complex (py^b-H)$AuCl_2$, and three other Au(III) compounds with N-donor ligands, including Audipyam, AuPbImH and AuPbImMe (Figure 1).

The inhibition potency followed the trend: AuPbImMe > AuPbImH ≥ Audipyam > (py^b-H) $AuCl_2$. Interestingly, AuPbImMe showed to be even more potent than Auphen on hAQP3 permeability, with an IC_{50} of 0.57 ± 0.13 μM. The least active compound is the organometallic complex, which is known to be more stable in solution than the others due to the direct Au-C bond, and whose organometallic scaffold influences its reactivity also in terms of redox properties and nucleophilicity. Importantly, none of the tested compounds affected water permeability via hAQP1 showing the necessary degree of selectivity to study aquaglyceroporin-3 and aquaporin-1 isoforms in situation where both of them are expressed in the same cell.

To investigate the molecular mechanism of inhibition, and based on previous knowledge on aquaporin inhibition by $HgCl_2$ [3] and our previous studies on Auphen [2], we studied the effects of

a reducing agent, such as 2-mercaptoethanol (EtSH) (which may also be a possible sulphur donor to metal ions) on the potency of the compounds. In fact, EtSH-washing after 30 min of incubation with the gold-based drugs, allowed an almost complete recovery of glycerol permeability in the hRBC model. Thus, we suggest that the AQP3 inhibition by gold complexes involves direct binding to cysteine residues (namely, Cys40 in hAQP3). Indirect evidence in support of this hypothesis was achieved by site-directed mutagenesis studies published later on by our group [4], as well as by molecular modelling studies [2, 5].

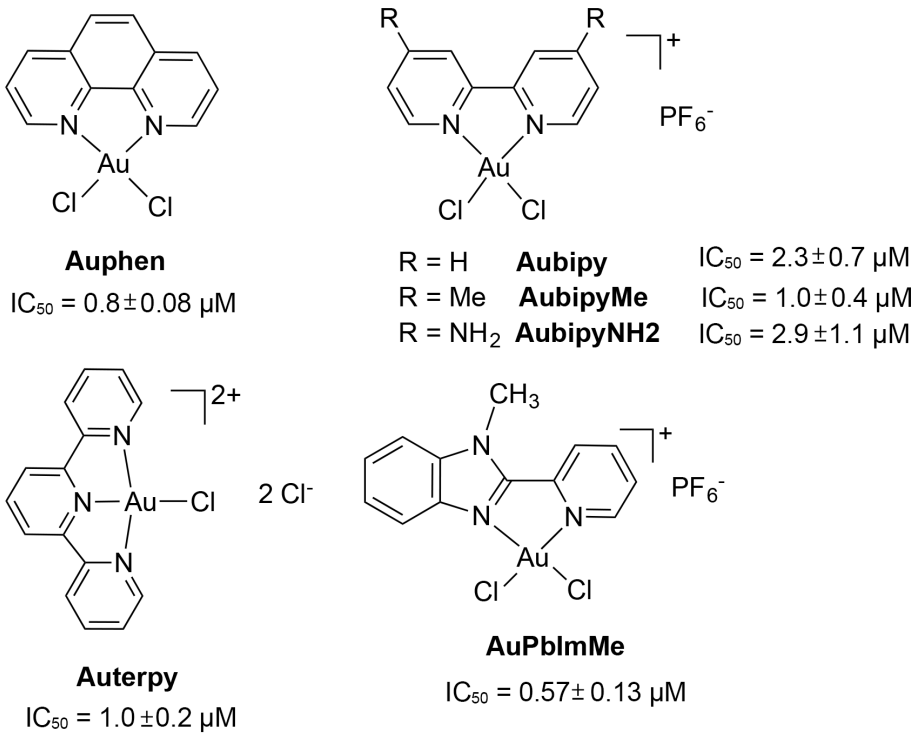

Figure 1. Gold(III) compounds investigated as AQP3 inhibitors and related potency.

As described in **Chapter A.1**, the differences between AuPbImMe and AuPbImH are limited to the addition of a CH_3 group to one of the N atoms in the imidazole ring, conferring a positive charge to AuPbImMe and most likely affecting the reactivity of the gold(III) center (e.g. redox properties). How these small differences may affect the potency of this compound so drastically still remains to be identified. Future *in silico* studies, as well as non-covalent docking or potent DFT and QM/MM calculations may help disclosing the mechanistic details behind the inhibition of hAQP3 by AuPbImMe.

Moreover, as for the first series of gold-based drugs, the reversibility of AuPbImMe inhibition was investigated. This time, in addition to direct binding of the gold centre to Cys40, oxidation of cysteines was considered as another possible mechanism of inhibition of AQP3, as this oxidation could affect the permeability of the channel. Thus, the reversibility of inhibition was tested by washing cells with EtSH (sulphur donor and reducing agent), as well as with 1 mM of L-cysteine (sulphur donor). In both cases, restored AQP3 activity was observed, which leads us to conclude that the mechanism of inhibition does not involve oxidation of cysteine residues.

Future work in the development of AQP3 gold-based inhibitors involves expanding the library of compounds to deepen the knowledge on structure-activity relationships and improve drug design. As an example, our group is currently studying a series of dinuclear gold(III) complexes

with N-donor ligands, where the gold centres are bridged by oxygen atoms (Figure 2).

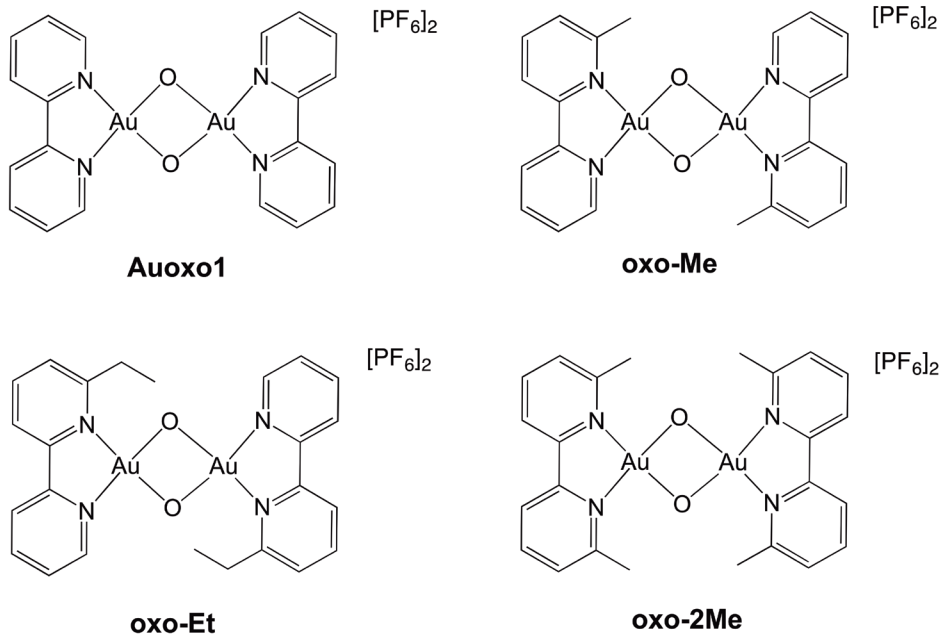

Figure 2. Series of dinuclear gold(III) compounds, currently being investigated as AQP3 inhibitors.

In terms of structure-activity relationships derived so far for the design of gold compounds as AQPs inhibitors, the following conclusions can be drawn:

- The gold centre is essential for inhibition;
- Gold(III) ions should be present in the molecule, while gold(I) complexes are not active;
- The presence of an aromatic ligand is crucial for enhancement of inhibition potency;
- The presence of two chlorido ligands bound to gold, capable of undergoing substitution reactions, favour inhibition most likely due to enhanced protein binding properties of the resulting metal complex.

Selectivity of inhibition towards aquaglyceroporins isoforms

Inhibitors of aquaglyceroporins can be used as probes to assess their function in several models, as discussed further, and without the need for RNA silencing or knockout models, which have additional limitations and drawbacks, such as adaptive changes in phenotypes. However, when developing a new inhibitor, possible selectivity issues among different aquaglyceroporin isoforms (in humans AQP3, AQP7, AQP9, AQP10 and AQP11) should be considered. Thus, we started studying the effects of the lead gold compound Auphen (Figure 1) on the hAQP7 isoform [6], (see **Chapter A.2**).

The glycerol channel isoform AQP7, which is expressed in adipocytes and liver among other organs, plays a role in lipidogenesis and insulin secretion, and has an interplay with another glycerol channel isoform, AQP9. For the functional studies, a murine adipocyte model was chosen, overexpressing human AQP7, and the permeability analysed by fluorescence microscopy. Our results show the potent inhibition of water and glycerol permeability by Auphen via hAQP7, with an IC_{50} of 6.5 ± 3.7 μM.

With our previous knowledge on the possible mechanism of gold binding to hAQP3, we investigated the possible mechanism of inhibition of hAQP7 by Auphen, using *in silico* approaches, such as molecular modelling and non-covalent docking. Interestingly, despite their overall similar structural features, aquaporins have different aminoacid composition. Thus, whereas certain regions are highly conserved, such as the asparagine-proline-alanine (NPA) and the aromatic/arginine (ar/R) selectivity filters, the channel lining may vary substantially. At variance with AQP3, AQP7 does not have a cysteine in the position of Cys40. Instead, using our new AQP7 homology model, the mapping of the channel evidenced the presence of thiol groups of methionine residues, in particular Met47, which are likely candidates for binding to the gold(III) complex. While the Cys40 of AQP3 was located in the extracellular opening of the channel, the methionine residues of AQP7 are located in the NPA region, bellow the ar/R selectivity filter. Moreover, the investigation of non-covalent binding of Auphen by docking approaches revealed its preferential binding to AQP7 in the NPA filter region, which is accessible only from the intracellular side (Figure 3). Therefore, the exact mechanism of inhibition of gold compounds in the two isoforms may differ substantially. In the case of AQP7, most likely the compound needs to enter the cell before being able to exert its inhibition. This may explain why the potency of inhibition of this isoform is lower than AQP3.

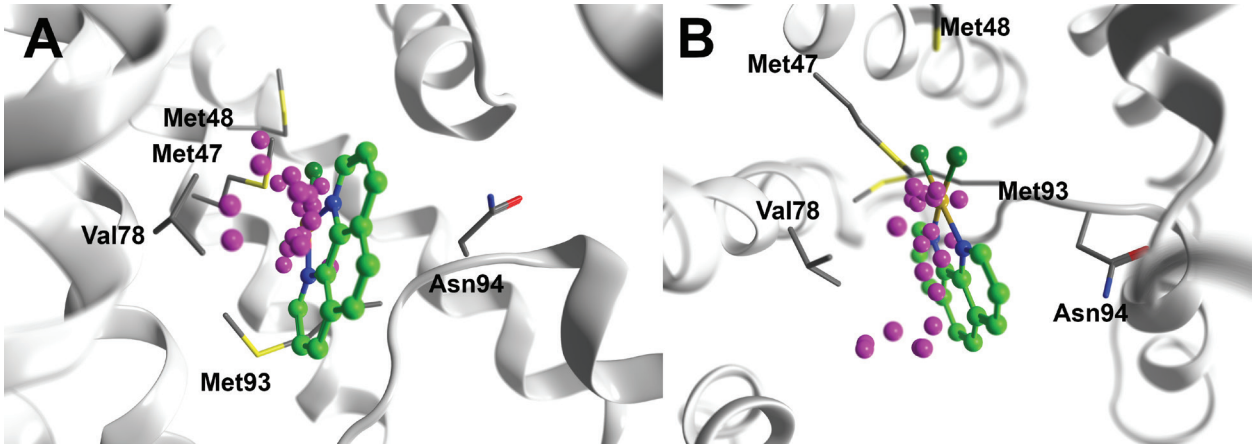

Figure 3. Molecular docking of gold(III) complex Auphen (in green ball-and-stick representation) in a lateral (A) and top view (B, from extracellular side) of NPA pocket of hAQP7 (grey cartoon ribbon representation). Chlorides are shown in dark green. Gold atom in the selected position is shown in yellow-gold colour, while the other positions for this atom are shown as magenta spheres. The atoms in the protein are coloured by element.

Alternatively, other mechanisms of binding to amino acids outside the protein channel may be possible, which then induce loop movements and pore closure.

Currently, despite all the structural knowledge on human and non-human aquaporin isoforms, the knowledge on aquaglyceroporin structure is still very limited. Up to now, only two glycerol channels have been structurally characterized: the bacterial glycerol facilitator (bGlpF) and the *P. falciparum* aquaglyceroporin (PfAQP) [7, 8]. Even though the current sequence analysis methods allow prediction of secondary structure of proteins, such as helices, the exact position of certain aminoacid side-chains will still remain unknown without structural information. Thus, homology modelling reveals to be a powerful *in silico* tool that allows the understanding of important aquaporin features and the composition of the channel lining. Indeed, as shown for AQP3 and AQP7, the detailed modelling information allowed us predicting the possible binding modes of our compounds in the two isoforms, as well as possible pH gating mechanisms.

Thus, based on these promising results, our next research question has been:

- *Can Auphen and other gold-based compounds inhibit hAQP9?*

By analysing the different sequences and pore lining in the homology models, we can predict two binding sites for gold compounds in this isoform. In Figure 4 we can observe that, while AQP9 does not share any of the predicted sites with AQP7, it has a cysteine corresponding to Cys40 in AQP3. Moreover, another cysteine residue, Cys213, is lining the channel, close to the NPA region and, if the orientation of the side-chain is favourable, this amino acid can be suitable for gold binding. Therefore, we believe that AQP9 may also be inhibited by gold-based drugs and may share the inhibition mechanism and binding site with AQP3. Thus, an important addition to our current knowledge on aquaglyceroporin inhibition would be testing our library of gold-based drugs in a system expressing AQP9.

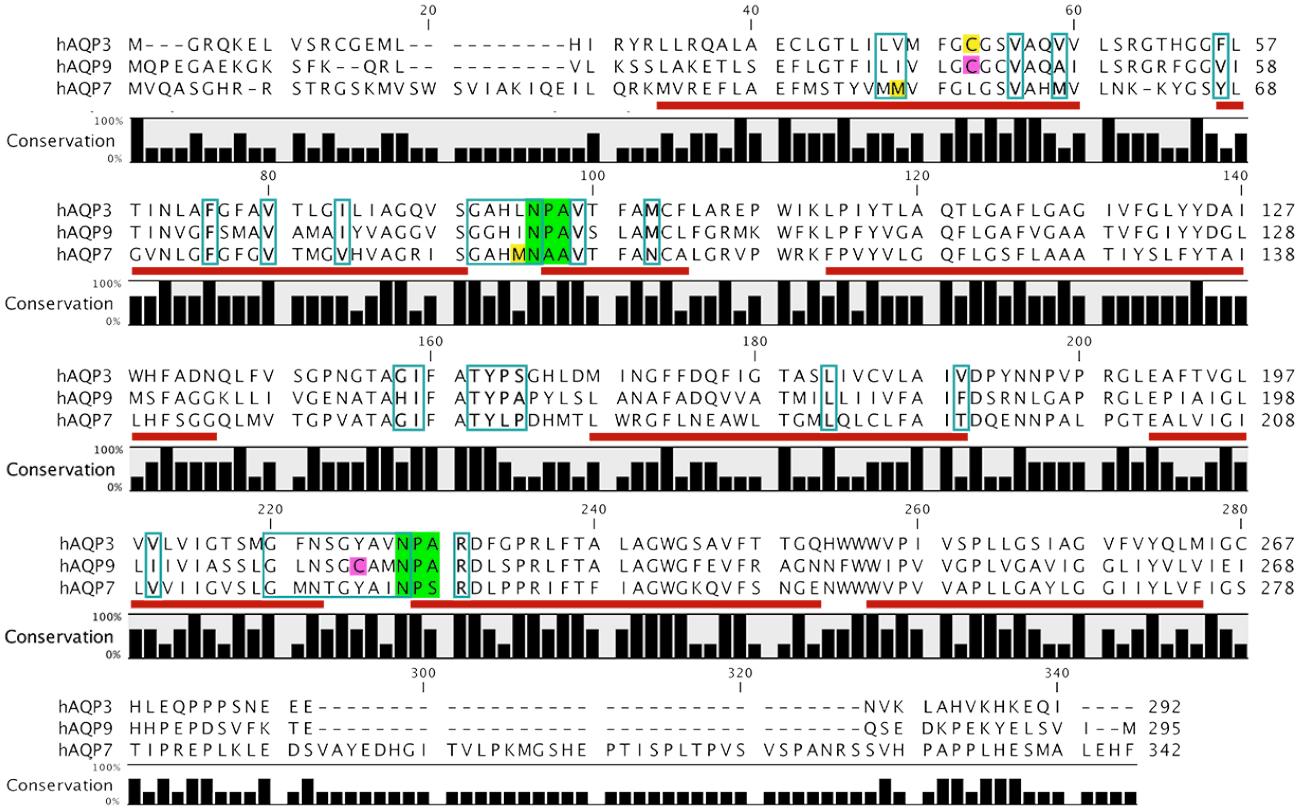

Figure 4. Sequence alignment of the sequences of human aquaporin 3, 7 and 9. Red bars represent helical regions, predicted by homology modelling, while blue boxes highlight residues lining the pore. The NPA regions are highlighted in green and predicted binding sites for gold compounds in human AQP3 and AQP7 are represented in yellow. The predicted binding sites for gold-based drugs in AQP9 are highlighted in magenta.

Mechanisms of AQP inhibition by mercury

Gold-based drugs are not the only inorganic inhibitors of aquaporins. In fact, mercurial compounds, such as $HgCl_2$, have been shown to inhibit water and glycerol permeation through aquaporins and are widely used as a standard for aquaporin inhibition in functional studies [1, 9]. Up to now, studies on the molecular mechanism of mercury inhibition were focused mainly on orthodox aquaporins, namely AQP1.

Overall, the mechanism of aquaporin inhibition by mercury supports two main mechanisms of inhibition: i) simple pore occlusion by mercury atoms/ions, in the proximity of cysteine residues; ii) conformational changes at the ar/R SF, induced by mercury binding to cysteines [10-12].

These hypotheses are based on results from X-ray crystallography and molecular dynamics (MD) simulations.

Since knowledge on the exact mechanism of mercury inhibition could help the understanding of the mechanism of other metal-based compounds such as our gold complexes, we investigated the mechanism of inhibition of AQP3 by mercury, using MD simulations, described in **Chapter A3**. Even though a few MD studies have already reported on the glycerol permeation in GlpF (a bacterial glycerol facilitator) some bias was always included, as glycerol permeation is a rare event in molecular dynamics simulations, due to its concentration during simulation [13-17]. Before our MD work, no other similar studies were published reporting on glycerol permeation of human aquaglyceroporins. In fact, the only known MD study of human aquaglyceroporin AQP9 transport only focuses on water permeation [18].

In our study, we performed MD simulations of human tetrameric AQP3, for 200 ns in the absence and presence of Hg^{2+} ions. Interestingly, in the absence of Hg^{2+}, we were able to simulate, for the first time, the unbiased passage of a glycerol molecule through the pore. Interestingly, the glycerol molecule was predicted to adopt different molecular geometries, but the favourable ones correspond to the observed glycerol positions in the crystal structures of GlpF and PfAQP [8, 19]. Glycerol forms several hydrogen bonds with residues in the channel lining, which guides the molecule towards the intracellular side. Moreover, the MD modelling showed the phenomenon of the flipping of water molecules in the NPA region, as previously observed by other authors [20]. This information is important for future inhibitor design, since disruption of the hydrogen bond network, crucial for the permeation of both water and glycerol, may be a part of the mode of action of novel AQP inhibitors.

Furthermore, in order to study the mechanism of inhibition, Hg^{2+} was simulated to bind to deprotonated Cys40 in each monomer. Overall, the following effects could be observed:

- Binding of Hg^{2+} leads to a decrease in the diameter of the channel, which leads to a higher degree of selectivity and hinders the passage of bulkier molecules, as glycerol.
- Each monomer showed a different behaviour upon metal binding: while three channels were completely closed to both water and glycerol, one was only partially closed and maintained low water permeability.
- We have identified two main mechanisms of channel closure, both involving residues in the ar/R SF region:

  i) Rotation of the aromatic ring of Phe63, leading to blockage of the pore;

  ii) Displacement of Arg218, leading to collapse of ar/R SF and consequent blockage of permeation.
- Upon metal binding, a movement of flexible extracellular loops was modelled, which may occlude the pore and prevent the passage of substrates.

The observation of movement of the flexible extracellular loops, previously observed in spinach aquaporin SoPIP2 [21], and resulting (fully or partial) channel blockage, is a main step forward in our current knowledge of aquaporin permeation and closure, as we described in detail in **Chapter A.4**.

Future work on solving the structure of human aquaglyceroporin adducts with metal

compounds, is crucial for our understanding of the mechanisms of inhibition by metals. Nevertheless, MD simulations and other in silico approaches have proven to be reliable tools to study aquaporin permeation and inhibition.

Unravelling the mechanisms of pH gating in AQPs

In a biological context, the regulation of the activity of aquaporins is probably not achieved by inhibitors. In fact, it has been shown that eukaryotic orthodox aquaporins may be subjected to physiological regulation by several processes, including pH changes [22, 23]. Previous studies show that rat AQP3 permeation is regulated by pH [24-26]. In **Chapter A.4** we report on the pH gating of two human aquaglyceroporins AQP3 and AQP7 in different cellular models, as well as on their mechanisms of closure upon pH changes.

Interestingly, although both isoforms show gating by pH, their mechanisms of pore closure appear to be different:

- AQP3 shows approximately the same pK_a for water and glycerol, but different Hill slopes, while AQP7 has the same pK_a and Hill slope for both solutes.
- AQP3 and AQP7 have less than 40% of sequence identity (see Table 1 in the introductory chapter and Figure 4 in this chapter), even though both are human glycerol channels, which may lead to different mechanisms of regulation.
- Several similarities are observed between the homology model structure and the sequence of AQP3 and AQP7 isoforms. However, the two isoforms do not share all the residues found to be responsible for pH sensitivity.

Homology modelling is again a very advantageous asset to study protein function, and specifically in the case of pH gating, the use of tetrameric homology models allows identification of pH-sensitive residues located at the monomer-monomer interface, which would remain otherwise impossible to predict.

The homology models can also be used to study important features of the pores, such as their hydrophilicity. In fact, the hydrophilicity of the intra- and extracellular entrances may differ among aquaporins (Figure 15 in **Chapter A.4**) which may account not only for the pH sensitivity and for different mechanisms of pore closure, but also for the orientation of the solutes when they approach the AQPs before entering the channel. In fact, both the shape/dimension and hydrophilicity of the entrances differ among isoforms and a relatively small structural change can have diverse outcomes in pore closure and permeability. Thus, we hypothesize that:

- For both isoforms, protonation of the sensitive amino acid residues is achieved sequentially, with pH changes, rather than all at the same pH.
- The same amino acid residues may have different pK_a values, according to where they are located in the protein and to what their chemical neighbourhood is.
- Gradual structural changes, induced by protonation/deprotonation of aminoacid side-chains may close the channel for glycerol permeation, while keeping the channel open for water passage, in the case of AQP3 (see mechanism described in **Chapter A3**).
- Protonation or deprotonation of the pH-sensitive residues in AQP3 may lead to disruption/formation of hydrogen bonds, which may change the overall channel structure, as well as the important monomer-monomer interactions.

Our group is currently performing mutagenesis studies to confirm the importance of the identified residues in AQP7 pH sensitivity.

As we have observed that not only hAQP3 but also hAQP7 is gated by pH, it is interesting to investigate the possible gating of other aquaglyceroporin isoforms. As an initial study, we performed sequence alignments of the human aquaglyceroporins, hAQP3, 7, 9 and 10, in order to investigate if the pH-sensitive residues are present in any other isoforms (Figure 5). Interestingly, hAQP9 has none of the pH-sensitive histidines of hAQP3. While the location and pK_a of the sidechains of histidines in AQP3 and AQP7 makes them very susceptible for pH changes, the residues in AQP9 may not be interacting with each other in the same way as in AQP3. In addition, the high pK_a (>9) of the sidechains of both residues in AQP9 makes them less likely to be involved in a mechanism of gating of this isoform, in a range of pH 5-8. Moreover, AQP9 has an alanine in the same position of Ser152 in hAQP3. However, this residue itself may not be crucial for the gating of aquaglyceroporins, because AQP7 also has a substitution of serine by a proline and still holds the features of pH gating. Nonetheless, the residue corresponding to Tyr135 is conserved in AQP7 and

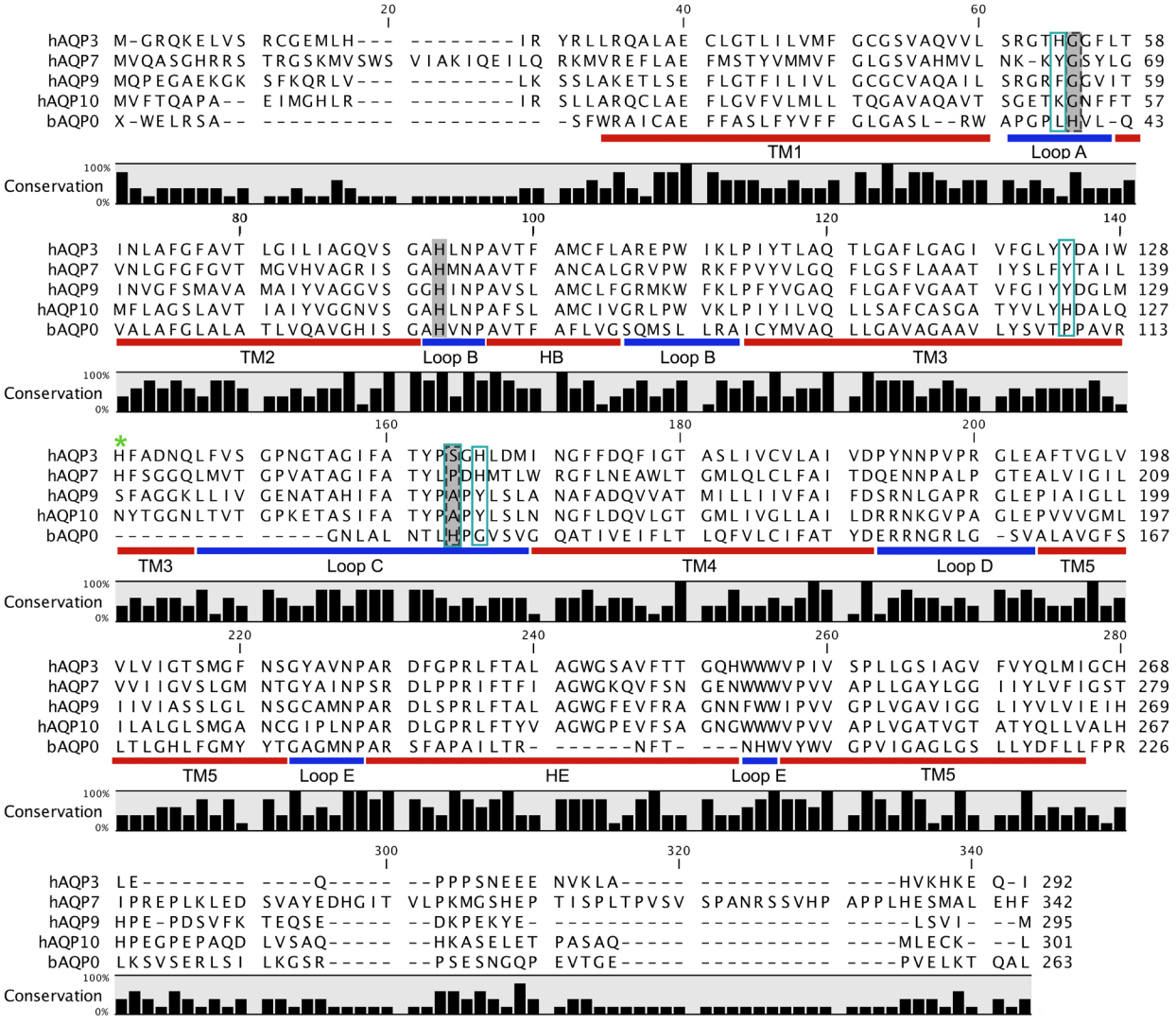

Figure 5. Sequence alignment of the sequences of human aquaporin 3, 7, 9, 10 and bovine AQP0. Red bars represent helical regions, predicted by homology modelling, while dark blue bars represent loops. The pH-sensitive residues identified in hAQP3 are highlighted by blue boxes, while the grey dashed box represents the pH-sensitive residue in bAQP0. The grey box highlights the pH-sensitive residue of AQP6 and AQP4 (not represented in this alignment), which is a conserved histidine. The green (*) represents the histidine residues in both AQP3 and AQP7, predicted to interact with His154 and His165, respectively. The sequence alignement is based on a structural alignement between the homology model of hAQP3 described in Part A and the X-Ray structure of bAQP0 (pdb 2B6P).

also AQP9. Since we could not disclose a possible role for this tyrosine neither in AQP3 or AQP7, it is questionable if this residue is involved in gating *per se*.

AQP10, like AQP9, does not share the sensitive residues of AQP3, not even Tyr135, as this is substituted by a histidine. Possibly, this histidine may be involved in pH gating of hAQP10 but, given the location of this residue in the protein, this is unlikely. Again, similar to AQP9, His 154 and His 129 are replaced by a tyrosine and asparagine. Moreover, as these residues have very high pK_a, it is not very likely that these sidechains would be interacting as we observed for AQP3 and less likely to be influenced by pH.

As can be observed in Figure 5 (and in the full sequence alignment in the introductory chapter), the His residue responsible for pH sensitivity in AQP6 and AQP4 [27] is conserved in all the isoforms, even in those with no pH sensitivity, as AQP1 [24]. It is difficult to imagine that this residue alone may be responsible for gating in one isoform, but not in others, even though it is present in all isoforms. Therefore, the role of this histidine could be related to its location and neighbouring residues, as the composition of the channel lining and the size of the pore varies among isoforms. On the other hand, a few of the pH-sensitive residues in hAQP3 are the pH sensitive residues of bovine AQP0 (hAQP), or are in similar positions (Figure 5) [28]. The mechanism of pore closure upon pH changes in bAQP0 has been described as the movement of extracellular loops [28], as we describe in Chapter A4, for both hAQP3 and hAQP7 and also as observed in molecular dynamics of hAQP3, after Hg^{2+} binding [29].

Taking into account this analysis, we can conclude that it is unlikely that AQP9 and AQP10 are gated by pH in the same range of pH as AQP3 and AQP7. The fact that most residues are not conserved may not mean that these isoforms are not gated at all, but only that they do not share the same gating mechanism. It is therefore, interesting to investigate the gating of both AQP9 and AQP10, using a similar methodology as the one applied for AQP7.

The investigation of the detailed mechanism of pH gating of aquaporins and in particular aquaglyceroporins, is very important to understand how structural changes may affect the permeability of the channels. Such knowledge can allow us to identify new pathways to achieve AQPs inhibition, for example targeting the inter-monomer interactions, and provide us with new clues to the design of isoform selective inhibitors.

On-going work on the relation between aquaglyceroporins and cancer development

As previously mentioned, aquaporins have an important role in physiological and pathophysiological states and this is why they are such important drug targets [1, 30]. AQP3, in particular, has been proven to be involved in skin elasticity, hydration and wound healing, as well as in cell proliferation, diabetes and cancer [1, 31]. Moreover, AQP3 was shown to be expressed in several lung cancer types, with higher prevalence in lung adenocarcinomas, as well as in healthy lung tissue [32].

In cancer disease, the hypothesis concerning the roles of aquaglyceroporins, such as AQP3, mainly concerns tumour cell migration and formation of metastasis [33, 34]. Aquaporins have also been implicated in cancer progression and their expression levels in tumours show a positive correlation with cancer stage. Specifically, the roles of aquaglyceroporins in cell physiology have been correlated with synthesis of triglycerides and with the maintenance of optimal glycerol levels for ATP production, both of importance in cancer tissues [1]. In addition the concentration of

glycerol in cancer cells has been associated with p53 activity and induction of apoptosis, suggesting a role of AQP in cell proliferation [35].

Within this frame, our gold inhibitors could be used to clarify the function of AQP3 in cancer development. As a matter of fact our group has already demonstrated that Auphen inhibits cell proliferation in cells with high expression levels of AQP3. Furthermore, the role of the gold binding site, Cys40 in AQP3, was confirmed by analysing the effects of Auphen in wild type AQP3-expressing cells. The obtained result showed that mutated AQP3 cells are less sensitive to Auphen's antiproliferative effects [4].

In spite of these initial evidences of AQP3 relation to cancer cells proliferation, the situation is much more complicated than it appears. In fact, different factors have been implicated in the upregulation of AQP3 in cell lines, tissues and *in vivo* models, as well as in the development of certain diseases, such as diabetes mellitus [36].Even other proteins, such as transferrin [37], have been shown to affect AQP3 expression. Additionally, drug treatments with the nucleoside analogues gemcitabine and 5'deoxy-5-fluoridine (5'DFUR) (commonly used as anticancer drugs) [38-40], the anti-inflammatory glucocorticoid dexamethasone (administered to treat acute lung inflammation) and the mucolytic agent ambroxol (used to treat chronic bronchitis and neonatal respiratory distress syndrome (used to treat chronic bronchitis and neonatal respiratory distress syndrome) also show to upregulate AQP3 *in vitro* (Figure 6), [41, 42].

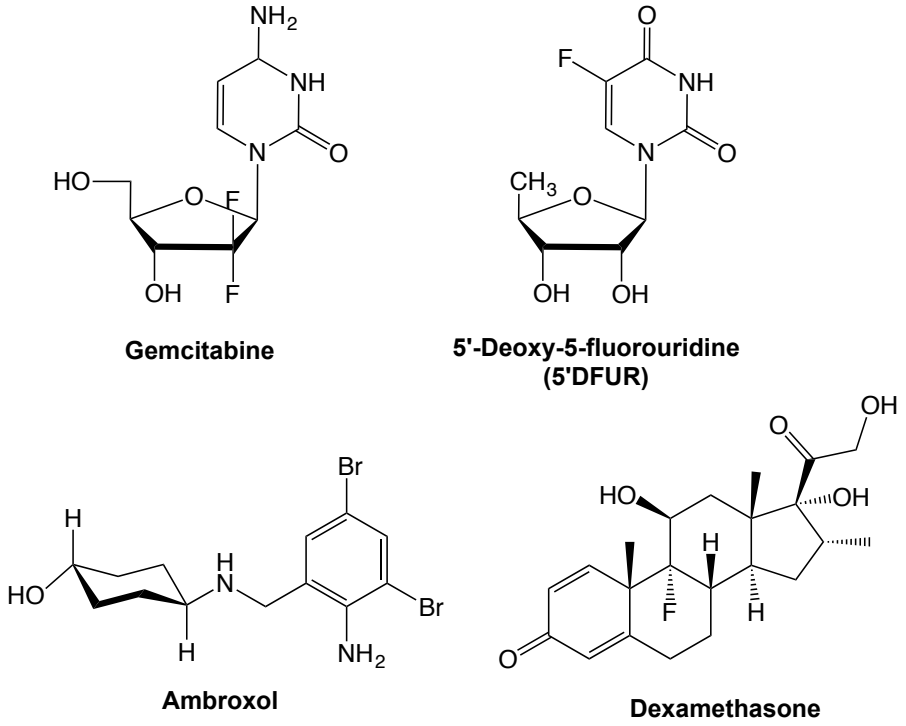

Figure 6. Anticancer drugs gemcitabine and 5'DFUR, mucolytic agent ambroxol and glucocorticoid dexamethasone, shown to upregulate AQP3 *in vitro*.

Based on these considerations and in order to continue our investigation in this area and to further apply gold complexes as chemical probes to study AQP3 function, two main questions need to be addressed:

- Do our gold compounds influence AQP3 expression in biological systems?
- Is increased AQP3 expression in response to drug treatment responsible for cancer progression and cell proliferation or vice-versa?

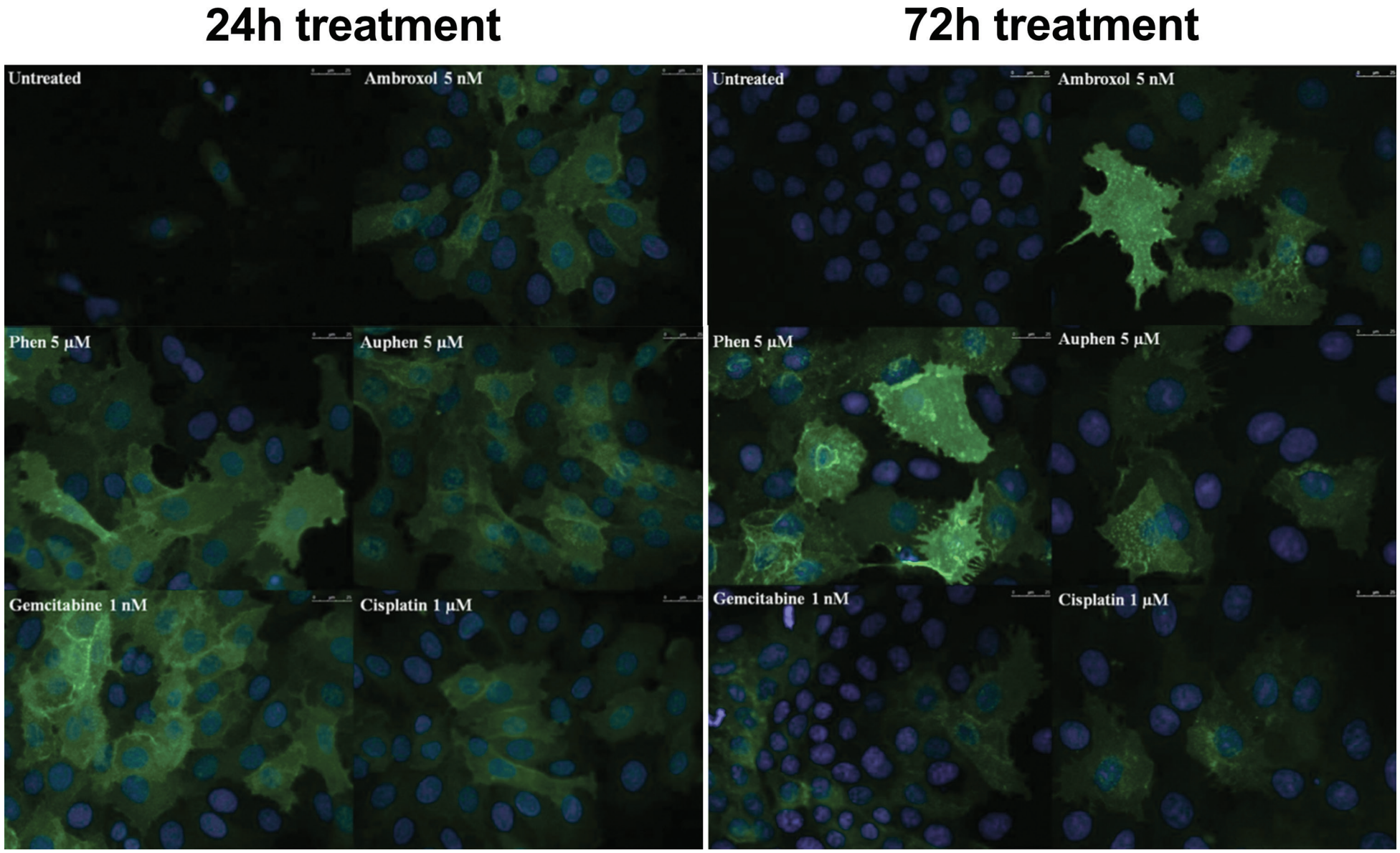

Figure 7. Subcellular localization of AQP3 after 24 and 72 hours of treatment. AQP3 immunoreactivity is shown in green, DAPI staining for nucleus is shown in blue. Bars represent 25 µm.

In vitro work

Knowing that several drugs, used for the treatment of various diseases, including lung diseases, can upregulate AQP3 expression, we investigated the influence of different compounds *in vitro*, in the lung adenocarcinoma cell line A549, known for expressing AQP3 [40, 42](Figure 6). We tested our gold compound Auphen, its ligand Phen and the anticancer drug cisplatin for their possible effects on AQP3 expression with gemcitabine and ambroxol as positive controls. Cells were treated for 24 or 72 h with the compounds at concentrations below their IC_{50}, (the concentration that induces cell death in 50% of the cells) in order to avoid toxicity. Preliminary results show that after 24 h drug treatment we observed an increase in AQP3 expression compared to control cells, but no differences between the different treatments. With this exposure time, expression of AQP3 is localized in the cytoplasm and cell membrane (Figure 7). After 72 h treatment, the differences among different drug treatments are marked: even though all compounds appear to upregulate AQP3, the highest expression was found for ambroxol and Phen, while gemcitabine, cisplatin and Auphen showed a similar lower effect. The subcellular localization is slightly altered in the 72 h treatment, as AQP3 appears to be expressed also at the nuclear membrane, which is best visible after Phen treatment (Figure 7). Moreover, with longer incubation time the cells appear to swell to double the size, in particular when treated with Phen, Auphen and ambroxol. This may be a direct effect of the upregulation of AQP3 and increased water permeation due to drug-induced stress. Additionally, in Figure 7 it is observed that not all cells upregulate AQP3 in response to treatment. In fact, flow cytometry data show that most untreated cells have basal levels of AQP3 and, though the number of AQP3-positive cells decrease, there is an increase in fluorescence intensity after treatment (data not shown). Thus only few cells show upregulation of AQP3, while others keep their basal protein level or even downregulate the AQP3 expression. This phenomenon needs further investigation. Interestingly AQP3 was shown to be linked to the process of gemcitabine-induced cell cycle arrest [43] and other aquaporins, such as AQP1 and AQP2 were found to be involved in cell-cycle control [44-47].

In vivo work

In order to better characterize the expression patterns of AQP3 in lung cancer tissues with respect to normal tissues, we decided to address the *in vivo* situation. Thus, in collaboration with Prof. W. Timens of the Pathology Department of the Groningen University Medical Centre (UMCG), we are currently studying the expression profile and immunolocalization of AQP3 in healthy lung sections as well as in primary and secondary lung cancer tissues.

Figure 8 shows that AQP3 is expressed in epithelia of lower and upper respiratory tract, in cell types linked to proliferation and migration, suggesting a role in processes in healthy and tumour cells. Further studies need to be carried out, in order to confirm the cell types in which AQP3 expression is observed.

In lung cancer, it is important to separate the two types of cancer: primary, which is originated from lung cells, such as adenocarcinoma, and secondary lung cancer, metastasized from several other cell types and organs. In primary lung cancer, it is known that AQP3 expression is predominantly higher in adenocarcinoma, when compared to healthy lung [32, 48]. Our data, from three different primary lung cancer subtypes - adenocarcinoma, little and mixed adenocarcinoma and papillary adenocarcinoma - show that AQP3 expression is observed in the same cell types as in

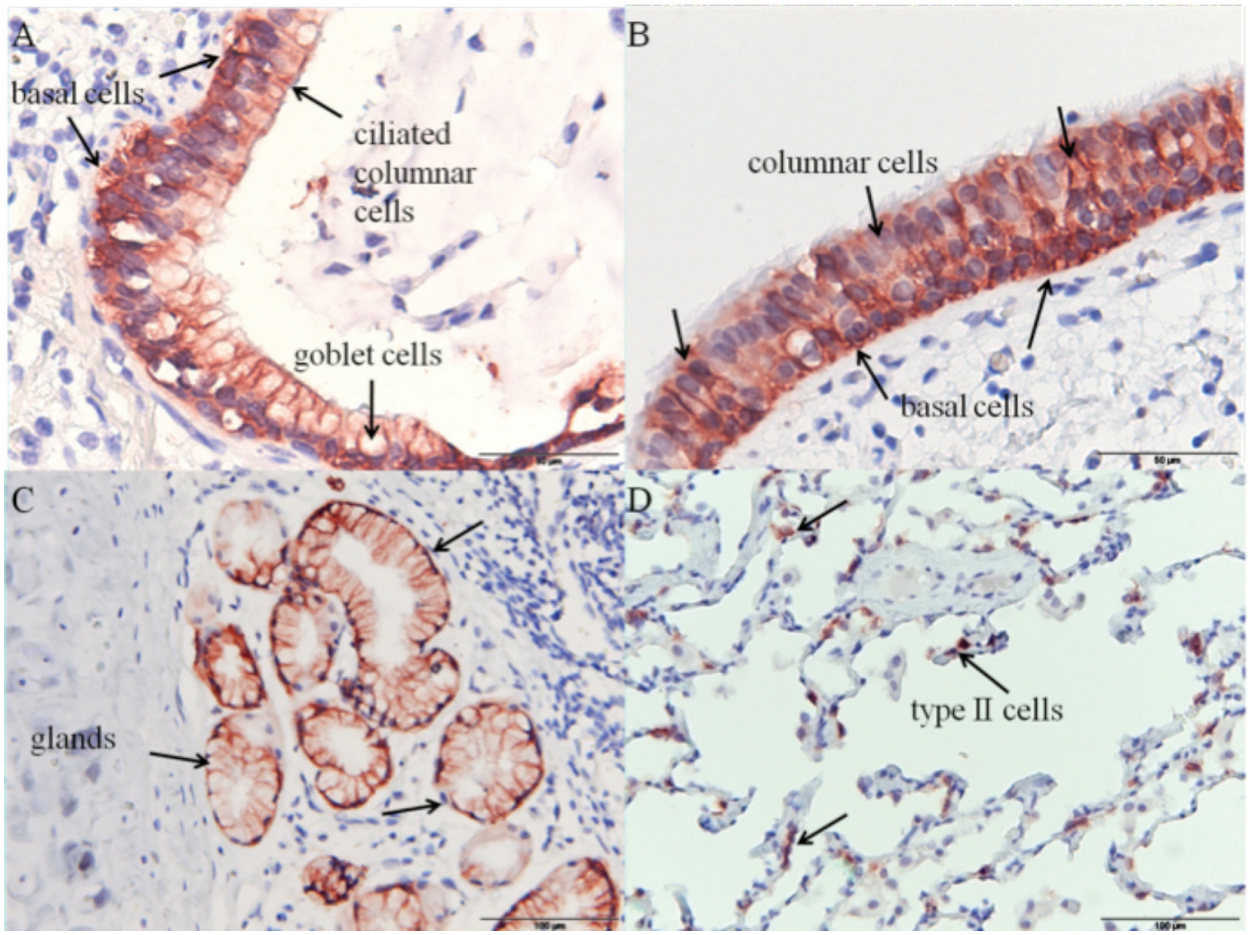

Figure 8. AQP3 in healthy lung tissue. (A) AQP3 expression is observed in the basal cells of the bronchus, (B) bronchiolar cells, (C) bronchial gland cells, (D) and type II alveolar cells. The bars correspond to 50 μm in the top panels and 100 μm in the lower panels. The red staining indicates AQP3, blue staining the cell nucleus.

healthy lung (Figure 9). However, in the primary lung tissue, AQP3 expression was generally lower than observed for healthy lung and different in the various subtypes. This observation is in line with literature and appears to be related to lung cancer stage, as it has been shown that higher AQP3 expression is observed in earlier cancer stages [32]. As for secondary lung cancer, several metastatic cancer subtypes from different origins were analysed: rectum and mucinous rectum carcinomas, intestinal carcinoma and adenocarcinoma, endometrium adenocarcinoma and renal carcinoma. Not much is known about expression of AQP3 in secondary lung cancer and our preliminary studies show that the expression levels highly differ among subtypes, in particular in bronchial cells (Figure 9). To further investigate the role of AQP3 in the development of cancer in the lung, it is important to add specific markers to distinguish between primary and secondary lung cancer cells.

An important addition to this research topic would be to correlate the type of anticancer treatment these patients were subjected to, if any, with their lung cancer type and with the AQP3 expression levels and cellular/subcellular distribution.

Relationship between aquaglyceroporins and other diseases

Interestingly, aquaporins have been also correlated with cholestasis and fibrosis, processes related with high proliferation of certain liver cell types. In the liver, aquaglyceroporins are present in most cell types and AQP7 and AQP9 are thought to play an important role in uptake of glycerol in the liver, for *de novo* synthesis of glucose and triglycerides [49], essential for several metabolic processes and for cell proliferation.

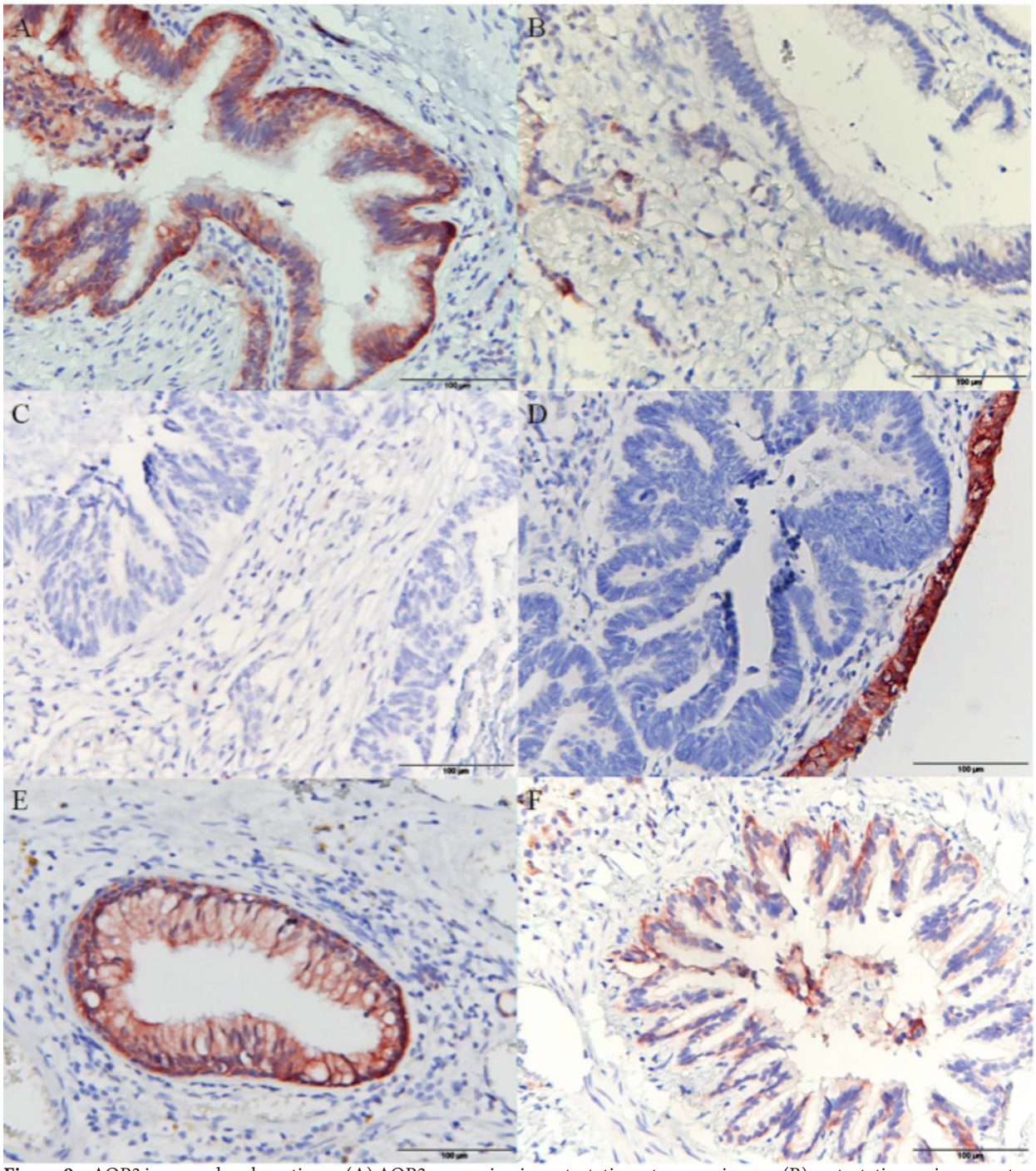

Figure 9. AQP3 in secondary lung tissue. (A) AQP3 expression in metastatic rectum carcinoma, (B) metastatic mucinous rectum carcinoma, (C) metastatic intestinal adenocarcinoma, (D) metastatic intestinal carcinoma, (E) metastatic renal carcinoma, (F) metastatic endometrium adenocarcinoma. The bars correspond to100 µm. The red staining indicates AQP3, blue staining the cell nucleus.

In cholestasis, three aquaporins were found to be upregulated: AQP7, AQP8 and AQP9. While AQP7 is expressed in hepatocytes, AQP9 is expressed in cholangiocytes and, as glycerol channels, both may have an important role in cell proliferation. It would be very interesting to study the effect of inhibition of the aquaglyceroporins in the liver, either in healthy or cholestatic/fibrotic tissue. Several inhibitors are available for influx and efflux transporters in the liver and our identified gold-based inhibitors would be an added asset to study the interplay between aquaporins and other membrane transporters involved in liver disease. Furthermore, the *ex vivo* model used in our lab, precision-cut tissue slices [50], could be a very good model to test this type of interplay

and to disclose the role of aquaporins in the liver. With this model, it is possible to use fresh tissue, either from animal models or human tissue, usually from transplants or biopsies, and culture the tissue for several days. These slices contain all the liver cell types in their natural matrix and thus mimic a whole liver model, while cell cultures are often limited to the use of cells lines, which only represent one particular cell type, and often lost their differentiation. It has been shown by our group that these slices maintain the metabolic functions of a liver and that it is possible to assess drug metabolism, transport and toxicity [50-52]. Therefore, this *ex vivo* model offers many more advantages than the *in vitro* models, and even allows us to overcome species differences, by using human tissue.

PART B

Part B of this thesis is focused on investigating the biological activity and possible biological targets for gold-based compounds others than aquaporins.

Several metal-based drugs are currently on the market as anticancer agents. Among them the platinum-based complex, cisplatin, is widely used in different chemotherapic regimes alone or in combination therapy [53]. However, severe side effects, such as kidney toxicity, reveal the need to develop new anticancer drugs, more selective and targeted. Therefore, several non-platinum drugs are currently investigated for their antitumor properties [54]. Gold compounds, in particular organometallic gold complexes, appear as promising anticancer agents [55]. These complexes present several advantages when compared to coordination compounds, such as an easier way to fine-tune their reactivity.

In **Chapter B1**, we describe the the antiproliferative effects of gold(I) N-heterocyclic carbenes (NHC) with fluorescent coumarin moiety, synthesized and characterized by Dr. B. Bertrand, in several cancerous and non-cancerous cell lines. The antiproliferative effects of three gold(I) complexes were evaluated in three cancer cell lines and a non-cancerous cell line (HEK-293T, human embryonic kidney cells), after 72 h of drug exposure. The uptake and cellular distribution of the most promising complex, compound 3 (Figure 10) was also evaluated by fluorescence microscopy. Furthermore, all three compounds were tested as inhibitors of the seleno-enzymes thioredoxin reductase (TrxR) and glutathione peroxidase (Grpx), as well as the enzyme glutathione reductase (GR), responsible for the maintenance of the levels of reduced glutathione. The enzyme inhibition studies were performed in collaboration with the group of Prof. Maria Pia Rigobello (University of Padova, Italy). Overall, we could observe the following:

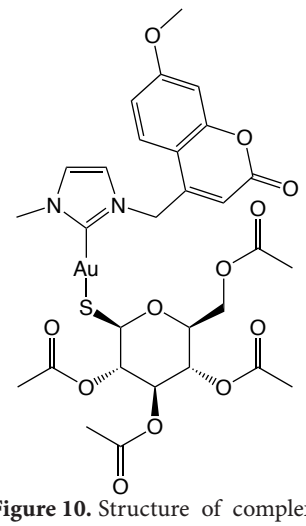

Figure 10. Structure of complex 3, a gold(I) complex bearing coumarin and acetylated thioglucose as ligands.

- Complex **3** (Figure 10) is the most potent of the series and shows toxicity in all cancer cell lines and also in the non-cancerous cell line HEK-293T. However, the complex is still less toxic than cisplatin, in most cell lines tested (with the exception of MCF-7).

- Complexes **1** (ligand) and **2** (gold-coumarin) are only moderately toxic against all cell lines, while complex 4 (gold-coumarin with thioglucose moiety) shows no toxicity against most of the cell lines, and is only moderately toxic in MCF-7 cells.

- Complexes **2-4** have inhibitory activity for TrxR, targeting the selenocysteine residue. Interestingly, complex 4, non-active in the tested cell lines, is the most effective TrxR inhibitor. None of the complexes inhibited GR or Gpx.
- Complex **3** is taken up in A2780 cells and localizes in the nuclei.

Interestingly, the complex that showed the highest inhibition of TrxR is the most ineffective compound *in vitro*. Despite being the most toxic compound, complex **3** appears to have other targets in the cells. However, complex **4**, despite the low IC_{50} as TrxR inhibitor, is not toxic in the tested cell lines, which may be due to poor uptake of this compound.

The use of sugar-like moieties is aimed at improving the cellular uptake of the drugs. In **Chapter B2** we followed a similar approach, Dr. Margot Wenzel (University of Burgundy), prepared several fluorescent complexes, with and without acetylated thioglucose. In contrast to the complexes described in **Chapter B1**, these new complexes bear two metal centres: one ruthenium metal centre with a fluorescent moiety, and a gold centre, which is the therapeutic moiety. Additionally, the complexes were also synthesized with different metals in the therapeutic moiety (osmium, rhenium and ruthenium). The fluorescent moiety was aimed at tracing the uptake and cellular distribution of the complexes *in vitro*, functioning as a "diagnostics" moiety. They were synthesized with organic linkers of two different sizes, binding the therapeutic and diagnostic moieties together. The complexes were evaluated for their antiproliferative effects against four different cell lines (A2780 and A280cisR, ovarian carcinoma sensitive and resistant to cisplatin, respectively; A549, lung adenocarcinoma; HEK-293T, human embryonic kidney cells), after 72 h of drug exposure, using a classical MTT assay.

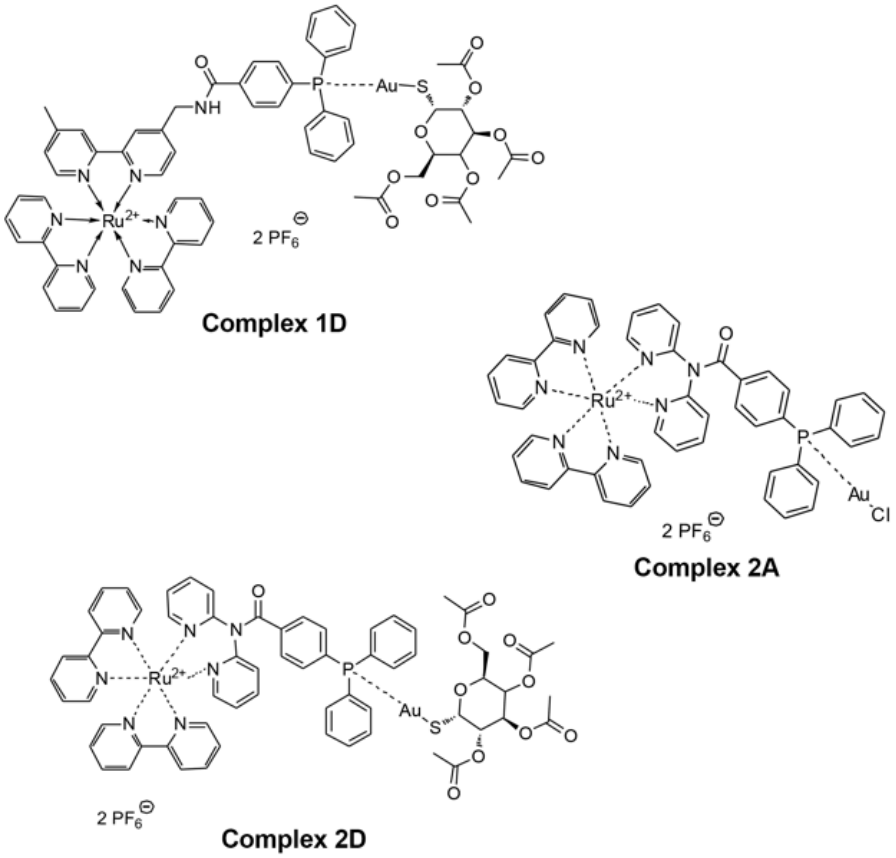

Figure 11. Structures of complexes 1D, 2A and 2D, the most potent compounds from the fluorescent polynuclear metal complex series.

Overall, several factors appear to be contributing to the toxicity of the complexes:

- The complexes containing Ru, Rh or Os instead of gold in the therapeutic moiety, are non-toxic or have low toxicity in the tested cell lines.
- Only the heteronuclear Ru-Au complexes have antiproliferative effects against the tested cells.
- The linker itself appears to change the toxic properties of the complexes, as complexes **2D** and **1D** have different cytotoxic properties: the complex with the "long linker" (**1D**) is non-toxic, while the complex with the "short linker" (**2D**) shows moderate toxicity.
- Complexes **2A**, **2D** and **1D** (Figure 11) were the most effective compounds against the tested cell lines and showed higher toxicity than cisplatin against the cisplatin resistant cell line, A2780cisR.

Moreover, the complexes bearing the acetylated thioglucose show higher cytotoxicity against the tested cell lines than the complexes without this targeting moiety. In order to assess the involvement of glucose transporters in the uptake of the complexes, in particular GluT-1, highly expressed in cancer cells, we tested the influence of a GluT-1 inhibitor on the toxicity of the drugs. Interestingly, the presence of the GluT-1 inhibitor did not influence the toxicity of the complexes bearing the targeting moiety, which makes the involvement of GluT-1 in the uptake of the complexes unlikely, even though we cannot infer about the influence of other glucose transporters in the cells.

The use of complexes bearing two types of moieties and centres, therapeutic and fluorescent, is very appealing, as we can trace the intracellular fate of the complexes while testing their toxic properties. Knowing the intracellular localization of the tested drugs takes us one step closer to target identification, as it is possible to infer if the complexes are targeting nucleic acids or proteins, and if it acts in the cytoplasm or in a particular organelle. These complexes could be further developed for use in the clinic, where several metallodrugs are already being tested as imaging/ therapeutic agents [56].

Additionally, the presence of two (or more) metal centres can also improve the cytotoxic properties of the complexes. In fact, our group reported on the toxic Fe-Au and Fe-Pd complexes

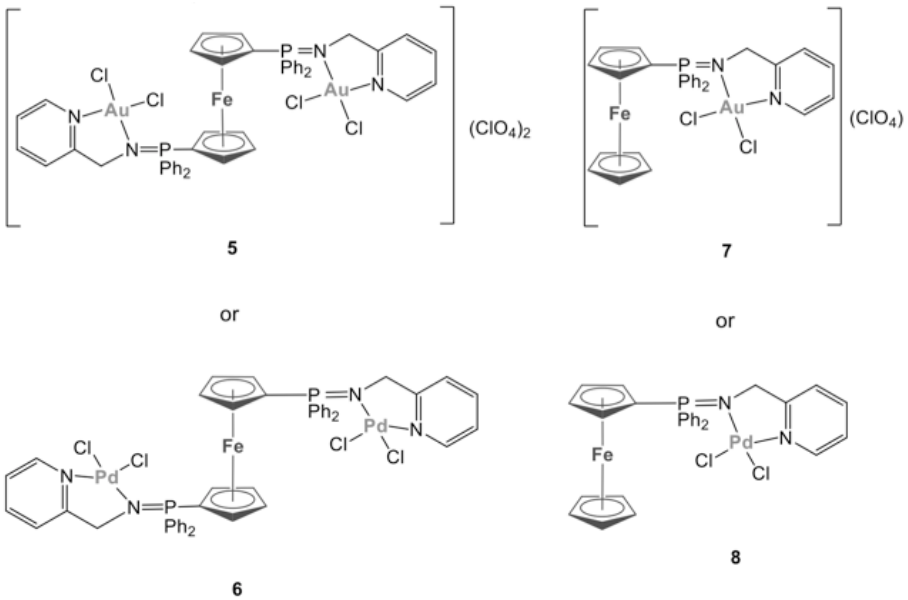

Figure 12. Structure of the tri and bimetallic iminophosphorane Fe-Au and Fe-Pd complexes.

[57]. In this study, several complexes were synthesized, based on Fe-iminophosphorane complexes, with one or two gold or palladium centres, in addition to the Fe centre (Figure 12). Interestingly, the trimetallic derivatives show antiproliferative effects against several cell lines (A2780/A2780cisR, MCF-7 and HEK-293T) and are more potent than their correspondent monometallic complexes, which indicates that there might be a synergistic effect of the metal centres. The complexes also showed a high toxic effect in the cisplatin resistant cell line (A2780cisR), suggesting a different mechanism of toxicity than cisplatin. Indeed, Pd and Au complexes appear to have different targets: while the palladium derivatives showed high affinity towards nucleic acids, the Au complexes had very low affinity to nucleic acids but showed to be good inhibitors of the zinc-finger protein PARP-1.

Due to the attractive properties of fluorescent moieties, described in this **Part B**, we later reported on a similar series to the iminophosphorane Fe-Au and Fe-Pd, described above, of luminescent iminophosphorane complexes of gold(III), palladium(II) and platinum(II), derived from 8-aminoquinoline (Figure 13) [58]. The antiproliferative effects of the complexes were evaluated in three cell lines (A2780, A549 and HEK-293T). All complexes showed good antiproliferative effects against A2780 cells, but only 5 and 7, both containing platinum, were also active on the A549 cell line. Despite showing good antiproliferative effects, similar to those of cisplatin, in A549 cells, the platinum complexes also have high toxicity in our non-cancerous cell model, HEK-293T, which makes them less promising lead drugs. The gold(III) complex 2, as well as the palladium complexes

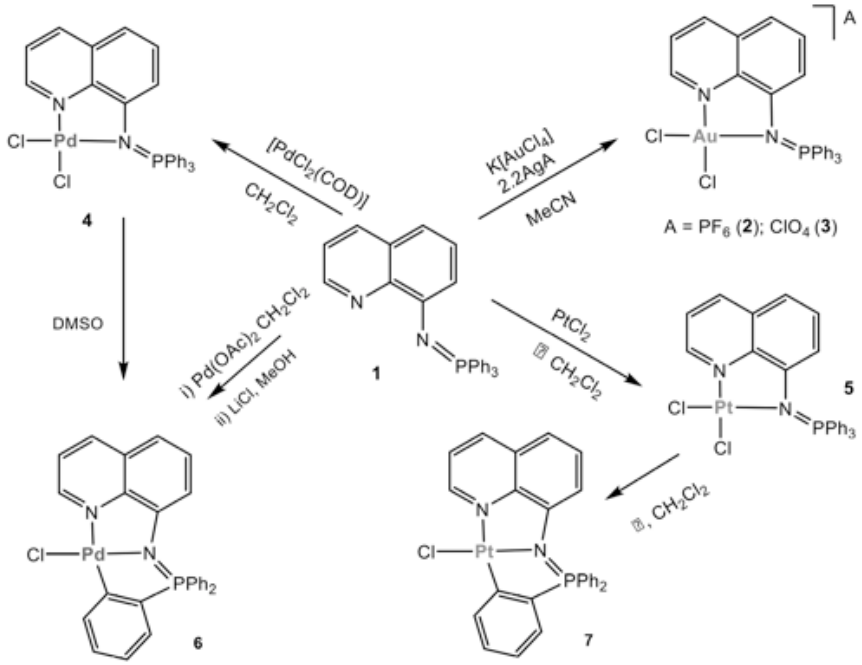

Figure 13. Structure of the Au, Pd and platinum luminescent complexes.

4 and 6 showed also good effects in growth inhibition of A2780 cells, but higher activity in A549 cells. These three complexes have a higher IC_{50} in the non-tumorigenic HEK-293T. Therefore, they are more promising, as we wish to have a higher selectivity for cancer cells, compared to healthy tissues.

Futhermore, the complexes were also tested for possible targets and, contrary to the iminophosphorane Fe-Pd complexes, none of the derivatives showed DNA interaction, which suggests a different mechanism of action than cisplatin, and also than the previous palladium

complexes. Unfortunately, the luminescence of the compounds was not sufficient to allow intracellular monitoring of uptake and intracellular distribution. Nonetheless, these are good starting materials for the design of more selective and potent complexes, with improved luminescent properties.

Silver compounds are also used in clinical practice as anti-bacterial agents [59]. We have recently reported on the anticancer properties of silver complexes with norharmane (9H-Pyrido[3,4-b] indole, abbreviated as Hnor;) ligand. Three complexes were synthesized, containing a silver(I) center, as well as the ligand Hnor, with the general formula $[Ag(Hnor)_2](anion)$, with three different anions (NO_3^-, ClO_4^-, BF_4^-). A fourth complex with PF_6^- anion was obtained, with a weak acetonitrile coordinated as a co-ligand ($[Ag(CH_3CN)(Hnor)_2](PF_6)$). The antiproliferative activities of the complexes were tested in two cancer cell lines (A2780 and A549) and all complexes showed toxicity in both cell lines. Unfortunately, these complexes are not promising as anticancer agents: the most active compound $[Ag(Hnor)_2](ClO_4)$ has similar antiproliferative effects as cisplatin, but its effect can be attributed to the presence of the perchlorate anion, since this is the only difference between this and the other complexes.

Interestingly, the Hnor ligand is not toxic in any of the tested cell lines; therefore, it is interesting to develop other metallodrugs based on this ligand. In recent work (Rais & de Almeida, et al., unpublished results), we described the synthesis of first transition-row metal (Cu(II), Co(II)) complexes, with Hnor and polypiridine co-ligands (2,2'-bipyridyl, bpy; 1,10-phenantroline, phen) (Figure 14).

The use of endogenous metals is attractive, since generally they may have less side effects than elements of the second or third row transition series (Figure 14). The complexes were tested in two cancer cell lines (A2780 and A549), and their antiproliferative effects were evaluated after 24 h and 72 h. The most cytotoxic compounds are the copper complexes **1** and **2** (Cu(Hnor)phen and Cu(Hnor)bpy), with a similar effect as cisplatin after 72 h, but already highly toxic after 24 h. On the other hand, the cobalt complexes **3** and **4** (Co(Hnor)phen and Co(Hnor)bpy) are both not toxic after 24 h of drug exposure, but complex 3 has a potent antiproliferative effect after 72 h incubation. In order to evaluate if copper transporters were involved in the uptake of the complexes, we performed competition experiments, by using $CuCl_2$ as a competitor for drug uptake. Surprisingly, not only $CuCl_2$ did not inhibit uptake of the complexes, it even potentiated the antiproliferative effects of all derivatives, with a marked effect on the cobalt complexes, that showed to be toxic at 24 h drug exposure when co-incubated with the copper salt. In fact, despite being endogenous and

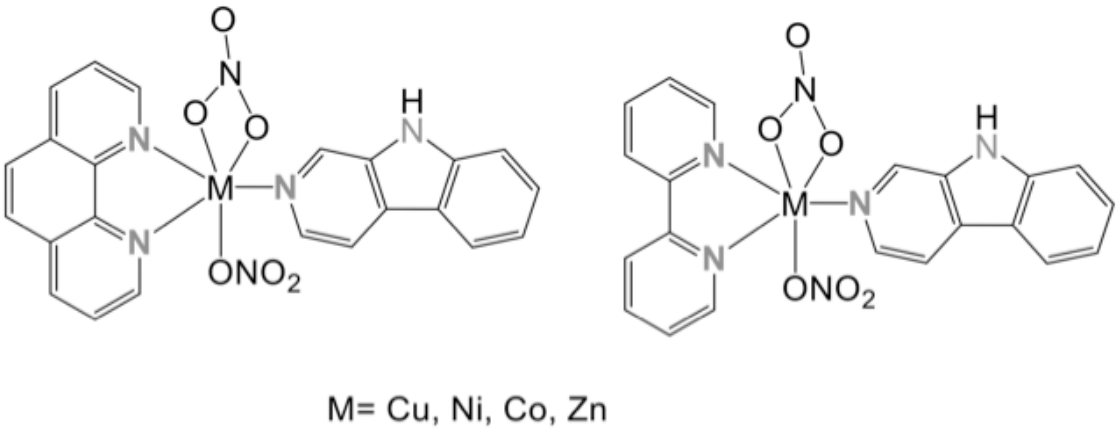

Figure 14. Schematic description the metal complexes with Hnor and phen/bpy ligands.

potentially less toxic, coordination complexes with endogenous metals as Cu and Co are prone to fast ligand exchange reactions in biological environment. We wanted to investigate if the addition of the copper salt leads to formation of complex **1** when co-incubated with complex **3**. Using absorption spectroscopy, we were able to observe the formation of a copper complex, when $CuCl_2$ is added to complex **3**, which may explain the increase in toxicity, as this new complex would be similar to complex **1**. It is important to note that, while Hnor is a non-toxic ligand, phen and bpy show high toxicity in both cell lines. Therefore, we cannot exclude that a part of the toxicity of these complexes may be due to the ligand.

Recently, we also evaluated the anticancer properties of a series of first row-transition metal (Cu(II), Ni(II) and Zn(II)) complexes, with phen ligand, as well as a with flumequine (Hflmq) ligand [60]. Flumequine is currently used as treatment for urinary tract infections and is effective against Gram positive and Gram negative bacteria [61]. Like Hnor, the ligand Hflmq *per se* is also non-toxic in the tested cell lines (A2780 and A549). The most effective compound of the series was, like in the previous series, the copper complex, with higher toxicity than cisplatin. The Ni complex shows only moderate toxicity in A2780 and no toxicity in A549. These two complexes show a higher IC_{50} in the lung adenocarcinoma cells, different from the Zn complex, which has a similar potency in both cell lines. Since the only difference between the copper and the zinc complexes is the metal itself, it appears that the difference in toxicity in the two cell lines may be due to different uptake or toxicity mechanisms/pathways for the different metals.

Regarding metallodrugs, with this work we have shown that the antiproliferative effects of these drugs do not depend only on the metal, but on several other factors:

- Type and number of metal centres;
- Type of counter ion present in each charged complex;
- Overall reactivity of the complexes and ability to ligand exchange in biological media;
- Ligands used may be also toxic *per se*;
- Different metal complexes may have different uptake routes, as well as cytoplasmic targets, which lead to different toxic effects and selectivity. The fate of the metal complexes in the cell, including the formation of metabolites of the ligands and possible toxification and detoxification and the involvement of uptake and excretion transported is a largely unexplored area, but needs to be addressed, preferably in human tissues *ex vivo*.

Overall, when synthesizing metal-based drugs, it is necessary to take into account all these elements. Most importantly, in addition to *in vitro* studies, the possibility to use tissue cultures to assess metallodrugs efficacy and toxicity should also be developed in this field, profiting of techniques such as the so-called Precision Cut Tissue Slices (PCTS) developed in our department.

We now believe that we have moved a few steps further in understanding the mechanisms of glycerol permeation, and consequently the role of aquaglyceroporins in health and disease. The use of selective inhibitors to assess aquaporin function *in vitro* and *ex vivo*, will be a major asset in the development of new therapies for aquaporin-related diseases.

Metals have been around us for millennia and humanity has always used metals for therapeutic

purposes. But not only the metals makes the drug. We have showed with our work, that there are several factors that may influence the mechanism of action, reactivity and toxicity of a metal-based drug and, therefore, not only the choice of the metal centre is important, but the overall drug scaffold.

References

[1] A.S. Verkman, M.O. Anderson, M.C. Papadopoulos, Nat Rev Drug Disc, 13 (2014) 259-277.
[2] A.P. Martins, A. Marrone, A. Ciancetta, A. Galán Cobo, M. Echevarría, T.F. Moura, N. Re, A. Casini, G. Soveral, PloS one, 7 (2012) e37435.
[3] C.M. Niemietz, S.D. Tyerman, FEBS letters, 531 (2002) 443-447.
[4] A. Serna, A. Galan-Cobo, C. Rodrigues, I. Sanchez-Gomar, J.J. Toledo-Aral, T.F. Moura, A. Casini, G. Soveral, M. Echevarria, J Cell Physiol, 229 (2014) 1787-1801.
[5] A.P. Martins, A. Ciancetta, A. de Almeida, A. Marrone, N. Re, G. Soveral, A. Casini, ChemMedChem, 8 (2013) 1086-1092.
[6] A. Madeira, A. de Almeida, C. de Graaf, M. Camps, A. Zorzano, T.F. Moura, A. Casini, G. Soveral, Chembiochem, 15 (2014) 1487-1494.
[7] E. Tajkhorshid, P. Nollert, M.O. Jensen, L.J. Miercke, J. O'Connell, R.M. Stroud, K. Schulten, Science, 296 (2002) 525-530.
[8] Z.E.R. Newby, J. O'Connell Iii, Y. Robles-Colmenares, S. Khademi, L.J. Miercke, R.M. Stroud, Nat Struct Mol Biol, 15 (2008) 619-625.
[9] R.I. Macey, R.E. Farmer, Biochim Biophys Acta, 211 (1970) 104-106.
[10] R. Zhang, A.N. van Hoek, J. Biwersi, A.S. Verkman, Biochemistry, 32 (1993) 2938-2941.
[11] G.M. Preston, J.S. Jung, W.B. Guggino, P. Agre, J Biol Chem, 268 (1993) 17-20.
[12] D.F. Savage, R.M. Stroud, J Mol Biol, 368 (2007) 607-617.
[13] Y. Wang, K. Schulten, E. Tajkhorshid, Structure, 13 (2005) 1107-1118.
[14] M.O. Jensen, S. Park, E. Tajkhorshid, K. Schulten, P Natl Acad Sci USA, 99 (2002) 6731-6736.
[15] P. Grayson, E. Tajkhorshid, K. Schulten, Biophys J, 85 (2003) 36-48.
[16] D. Lu, P. Grayson, K. Schulten, Biophys J, 85 (2003) 2977-2987.
[17] J. Henin, E. Tajkhorshid, K. Schulten, C. Chipot, Biophys J, 94 (2008) 832-839.
[18] S.J. Wacker, C. Aponte-Santamaría, P. Kjellbom, S. Nielsen, B.L. de Groot, M. Rützler, Mol Memb Biol, (2013) 1-15.
[19] D. Fu, A. Libson, L.J.W. Miercke, C. Weitzman, P. Nollert, J. Krucinski, R.M. Stroud, Science, 290 (2000) 481-486.
[20] N. Smolin, B. Li, D.A. Beck, V. Daggett, Biophys J, 95 (2008) 1089-1098.
[21] S. Törnroth-Horsefield, Y. Wang, K. Hedfalk, U. Johanson, M. Karlsson, E. Tajkhorshid, R. Neutze, P. Kjellbom, Nature, 439 (2006) 688-694.
[22] C. Tournaire-Roux, M. Sutka, H. Javot, E. Gout, P. Gerbeau, D.-T. Luu, R. Bligny, C. Maurel, Nature, 425 (2003) 393-397.
[23] L. Leitão, C. Prista, T.F. Moura, M.C. Loureiro-Dias, G. Soveral, PloS one, 7 (2012) e33219.
[24] T. Zeuthen, D.a. Klaerke, J Biol Chem, 274 (1999) 21631-21636.
[25] M. Zelenina, A.a. Bondar, S. Zelenin, A. Aperia, J Biol Chem, 278 (2003) 30037-30043.
[26] M. Zelenina, S. Tritto, A.a. Bondar, S. Zelenin, A. Aperia, J Biol Chem, 279 (2004) 51939-51943.
[27] S. Kaptan, M. Assentoft, H.P. Schneider, R.A. Fenton, J.W. Deitmer, N. MacAulay, B.L. de Groot, Structure, 23 (2015) 2309-2318.
[28] K.L. Németh-Cahalan, K. Kalman, J.E. Hall, J Gen Physiol, 123 (2004) 573-580.
[29] A. Spinello, A. de Almeida, A. Casini, G. Barone, J Inorg Biochem, (2015).
[30] Aquaporins in health and disease: new molecular targets for drug discovery, CRC Press
Taylor & Francis Group, 2016.
[31] A.S. Verkman, Annual Review of Medicine, 63 (2012) 303-316.
[32] Y.L. Liu, T. Matsuzaki, T. Nakazawa, S.-I. Murata, N. Nakamura, T. Kondo, M. Iwashina, K. Mochizuki, T. Yamane, K. Takata, R. Katoh, Human Pathol, 38 (2007) 171-178.
[33] D. Ribatti, G. Ranieri, T. Annese, B. Nico, Biochim Biophys Acta (BBA) - General Subjects, 1840 (2014) 1550-1553.
[34] A.S. Verkman, M. Hara-Chikuma, M.C. Papadopoulos, J Mol Med, 86 (2008) 523-529.
[35] K. Yuki, A. Takahashi, I. Ota, K. Ohnishi, J. Yasumoto, K. Yane, H. Kanata, N. Okamoto, H. Hosoi, T. Ohnishi, Apoptosis, 9 (2004) 853-859.
[36] L.N. Nejsum, T.H. Kwon, D. Marples, A. Flyvbjerg, M.A. Knepper, J. Frokiaer, S. Nielsen, Am J Physiol, Renal Physiol, 280 (2001) F715-726.
[37] J.C.K.L. Sydney Tang, Christopher W.K. Lam, Fernand Mac-Moune Lai, Tak Mao Chan, Kar Neng Lai, Am J Kidney Dis, 38 (2001) 317 - 330.
[38] H. Hernandez-Vargas, S.M. Rodriguez-Pinilla, M. Julian-Tendero, P. Sanchez-Rovira, C. Cuevas, A. Anton, M.J. Rios, J. Palacios, G. Moreno-Bueno, Breast cancer Res Tr, 102 (2007) 157-172.
[39] P. Cano-Soldado, M. Molina-Arcas, B. Alguero, I. Larrayoz, M.P. Lostao, A. Grandas, F.J. Casado, M. Pastor-Anglada, Biochem Pharmacol, 75 (2008) 639-648.
[40] L. Trigueros-Motos, S. Perez-Torras, F.J. Casado, M. Molina-Arcas, M. Pastor-Anglada, BMC Cancer, 12 (2012) 434.
[41] M. Tanaka, N. Inase, K. Fushimi, K. Ishibashi, M. Ichioka, S. Sasaki, F. Marumo, Am J Physiol, 273 (1997) L1090-1095.
[42] Y. Ben, J. Chen, R. Zhu, L. Gao, C. Bai, Resp Physiol Neurobiol, 161 (2008) 111-118.
[43] S. Pérez-Torras, F.J. Casado, M. Pastor-Anglada, BMC Cancer, 12 (2012) 434-434.
[44] T. Ma, A.S. Verkman, J Physiol, 517 (1999) 317-326.
[45] G. Di Giusto, P. Flamenco, V. Rivarola, J. Fernandez, L. Melamud, P. Ford, C. Capurro, J Cell Biochem, 113 (2012) 3721-3729.
[46] C. Moon, J.B. Williams, G.M. Preston, N.G. Copeland, D.J. Gilbert, D. Nathans, N.A. Jenkins, P. Agre, Genomics, 30 (1995)

354-357.
[47] C. Moon, J.C. Soria, S.J. Jang, J. Lee, M. Obaidul Hoque, M. Sibony, B. Trink, Y.S. Chang, D. Sidransky, L. Mao, Oncogene, 22 (2003) 6699-6703.
[48] D. Niu, T. Kondo, T. Nakazawa, T. Yamane, K. Mochizuki, T. Kawasaki, T. Matsuzaki, K. Takata, R. Katoh, Histopathology, 61 (2012) 543-551.
[49] J. Lebeck, J Mol Endocrinol, 52 (2014) R165-178.
[50] I.a.M. de Graaf, P. Olinga, M.H. de Jager, M.T. Merema, R. de Kanter, E.G. van de Kerkhof, G.M.M. Groothuis, Nature protocols, 5 (2010) 1540-1551.
[51] M. Hadi, I.M. Westra, V. Starokozhko, S. Dragovic, M.T. Merema, G.M. Groothuis, Chem Res Toxicol, 26 (2013) 710-720.
[52] M. Li, I.A. de Graaf, M.H. de Jager, G.M. Groothuis, Toxicol in vitro, 29 (2015) 1070-1078.
[53] S.V. Hato, A. Khong, I.J. de Vries, W.J. Lesterhuis, Clin Cancer Res, 20 (2014) 2831-2837.
[54] S. Komeda, A. Casini, Curr Top Med Chem, 12 (2012) 219-235.
[55] B. Bertrand, A. Casini, Dalton Trans, 43 (2014) 4209-4219.
[56] K.D. Mjos, C. Orvig, Chem Rev, 114 (2014) 4540-4563.
[57] N. Lease, V. Vasilevski, M. Carreira, A. de Almeida, M. Sanaú, P. Hirva, A. Casini, M. Contel, J Med Chem, 56 (2013) 5806-5818.
[58] M. Frik, J. Jiménez, V. Vasilevski, M. Carreira, A. de Almeida, E. Gascón, F. Benoit, M. Sanaú, A. Casini, M. Contel, Inorg Chem Front, 1 (2014) 231.
[59] A.D. Politano, K.T. Campbell, L.H. Rosenberger, R.G. Sawyer, Surg Infect, 14 (2013) 8-20.
[60] I. Tsitsa, A. Tarushi, P. Doukoume, F. Perdih, A. de Almeida, A. Papadopoulos, S. Kalogiannis, A. Casini, I. Turel, G.L. Psomas, RSC Advances, (2016).
[61] C.R. Steer, C.L. Huby, A.P. Ball, R.J. Dickinson, S. Pickens, E.T. Wallace, A.M. Wilson, J.A. Gray, J Antimicrob Chemot, 7 (1981) 643-648.

Samenvatting

Op metaal gebaseerde medicijnen worden al duizenden jaren gebruikt in de geneeskunde, en sommigen van hen worden nog steeds gebruikt in de hedendaagse geneeskunde. Bijvoorbeeld bij de behandeling van ziektes zoals kanker (Cisplatine) of reumatoïde artritis (Auranofine), maar ook door gebruik als antibiotica (zilversulfadiazine) of radiofarmaceutica. Ondanks dit brede scala aan toepassingen is het mechanisme van verschillende metallomedicijnen nog niet goed begrepen, met nog verscheidene onbekende biologische doelwitten.

In het geval van op goud gebaseerde stoffen, het onderwerp van dit proefschrift, zijn interacties met nucleïnezuren over het algemeen niet relevant met betrekking tot hun biologische mechanisme. Daarom is ons werk gericht op het bestuderen van op goud gebaseerde stoffen als selectieve eiwitremmers, welke gebruikt zouden kunnen worden om eiwitfunctie te onderzoeken, of gebruikt kunnen worden voor therapeutische doeleinden. Verder, de mogelijke antikankereigenschappen en mechanismes van twee nieuwe series op goud gebaseerde stoffen met fluorescerende eigenschappen werden bestudeerd *in vitro*. Daarom is het hier beschreven werk verdeeld in twee delen, aangeduid als A en B.

DEEL A

Hier bestuderen we de aquaporines (AQPs), hun functie en mechanisme van remming door op metaal gebaseerde stoffen, en ook hun pH-regulatie.

Het bepalen van de functie van een AQP is een zeer uitdagende taak [1] en de mogelijkheid om een remmer te gebruiken om dit te ontdekken is zeer aanlokkelijk om licht te schijnen op de rol van deze eiwitten in gezondheid en ziekte. In Hoofdstukken A1 en A2 wordt de remming van twee aquaglyceroporine-isovormen (AQP3 en AQP7) door op goud gebaseerde stoffen beschreven. Na het eerste rapport over de remming van AQP3 door een goud(III)-complex met N-donor-liganden (Auphen) door onze groep [2], hebben we een nieuwe serie op goudcomplexen van dezelfde serie ontworpen, en hebben we hun potentieel als AQP3-modulatoren onderzocht door gebruik te maken van humane rode bloedcellen (hRBC). Dit model maakte het ons mogelijk om onderscheid te maken tussen de remming van het doorlaten van water of glycerol door de desbetreffende stoffen. In dit geval observeerden we dat de op goud gebaseerde stoffen selectief waren als remmers van glycerol-doorlating via de aquaglyceroporine-isovorm AQP3. Verder, in Hoofdstuk A1, hebben we de serie goudcomplexen uitgebreid met drie N-donor-ligand-complexen en een organometalen stof met een direct-metaal-koolstof-verbinding die de stabiliteit in fysiologische omstandigheden verbetert. Interessant is dat een van de nieuwe stoffen met een N-donor-ligand zelfs potenter bleek te zijn dan Auphen.

In silico-methodes zijn ook gebruikt om het moleculaire mechanisme van remming door goudcomplexen. Moleculair modeleren en non-covalente-docking-studies zorgden ervoor dat Cys40 werd geïdentificeerd als de bindingsplaats van goud op hAQP3, gelokaliseerd in de extracellulaire opening. Indirect bewijs uit metagenese-studies hebben later bevestigd dat deze cysteïne cruciaal is voor de remming van hAQP3 door Auphen [3].

Om de selectiviteit van op goud gebaseerde stoffen voor bepeaalde AQPs te onderzoeken hebben we onze studies uitgebreid naar een andere aquaglyceroporine-isovorm, namelijk AQP7 (hAQP7). In dit geval werd een gistcelmodel dat hAQP7 tot expressie brengt gebruikt om de remmende capaciteiten van op goud gebaseerde stoffen te bepalen, zoals beschreven in Hoofdstuk A2. Auphen remt deze isovorm ook, maar in mindere mate dan AQP3. De afgenomen potentie is

in dit geval toegeschreven aan de verschillende bindplaatsen van de goudionen in AQP7. (Met-residuen), terwijl dit bij AQP3 is toegeschreven aan Cys40, zoals aangetoond door moleculaire-modeleringsstudies.

Gezamenlijk, van deze studies kunnen de volgende conclusies worden getrokken:

- Goud(III)-complexen met N-donor-liganden zijn potente remmers van hAQP3;
- De goud-kern is essentieel voor remming
- *In silico*-tools hebben geholpen bij het identificeren van de zwavelbevattende aminozuurresiduen als bindingsplaatsen voor de goud(III)-complexen in zowel hAQP3 als hAQP7;
- Isovorm-selectiviteit van de op goud gebaseerde stoffen moet geoptimaliseerd worden.

In de literatuur is $HgCL_2$ gebruikt als een niet-selectieve benchmarkremmer voor aquaporine-remming. Door de overeenkomsten tussen Hg en Au op het gebied van binding aan zwaveldonoraminozuurresiduen, zou het interessant zijn om te bepalen of de mechanismes van remming gelijk is voor de twee klasses van op metaal gebaseerde stoffen. Een aantal studies zijn verschenen over het mechanisme van AQP-remming door kwik [4,5], maar er zijn nog geen definitieve conclusies te trekken. Daarom hebben we in **Hoofdstuk A3** het moleculaire mechanisme van remming van AQP3 door $HgCL_2$ onderzocht. We begonnen met het bouwen van een homologie-model van tetrameer-AQP3 en onderzochten, door gebruik van moleculaire dynamica-simulaties, de structurele veranderingen in het eiwit na binding van Hg^{2+} aan Cys40. Gezamenlijk zijn de volgende eigenschappen geobserveerd:

- Binding door Hg^{2+} leidt tot een afname in poriediameter, wat waarschijnlijk de porieselectiviteit voor het doorlaten van vloeistoffen laat toenemen;
- Elke monomeer liet verschillend gedrag zien en, terwijl drie kanalen volledig gesloten waren voor vloeistofdoorlating, bleef één gedeeltelijk open met een lage doorlatingscapaciteit voor water;
- Twee verschillende mechanismes voor poriesluiting werden geïdentificeerd, waarbij beide te maken hebben met het instorten van de aromatische/arginine-selectiviteitsfilter in het kanaal;
- Na Hg^{2+}-binding komt herpositionering van extracellulaire eiwit-loops voor, wat bij kan dragen aan het verstoppen van de poriën.

Belangwekkend is dat de beweging van extracellulaire loops eerder was geobserveerd bij andere AQPs [6,7], waarbij al werd gesuggereerd dat dit porieverstopping teweegbrengt. In Hoofdstuk A4 was het mogelijk om te observeren door moleculaire modellering dat een soortgelijk mechanisme van loop-herpositionering betrokken kan zijn bij het zogenaamde pH-gating van zowel humaan AQP3 als AQP7. In dit hoofdstuk hebben we de permeabiliteit voor water en glycerol van rat en humaan AQP3 gekarakteriseerd bij pH-wijzigingen, door gebruik te maken van respectievelijk een gistcel- als hRBC-model. Op dezelfde manier is ook pH-gating onderzocht bij AQP7 in hetzelfde gistcelmodel. De rat- en humane isovormen vertonen, zoals verwacht, gelijkwaardig gedrag bij pH-veranderingen, met dezelfde pK_a-waarden en permeabiliteitsveranderingen. Zowel AQP3-isovormen als humaan AQP7 vertoonden pH-gating op dezelfde wijze, met poriesluiting bij zure

pH en maximale permeabiliteit bij een pH hoger dan 6,5. Belangwekkend is dat de Hill-helling voor water en glycerol en tweevoudig verschil laat zien in beide AQP3-isovormen, wat niet gebeurt bij hAQP7. Onze rekenkundige studies geven de volgende conclusies:

- Alle eerder geïdentificeerde pH-gevoelige residuen [8] van hAQP3 zijn aanwezig in de rat-isovorm, wat het gelijksoortige gedrag kan verklaren;
- AQP7 heeft sommige van deze residuen, waaronder histidine en tyrosine op dezelfde posities;
- De beweging van loops A en C in elke monomeer na protonering van de pH-gevoelige residuen kunnen voor significante structurele veranderingen zorgen, wat kan leiden tot poriesluiting;
- De structurele veranderingen bij het variëren van de pH kan geleidelijk verlopen, wat verklaard kan worden door het verschil in Hill-hellingen die zijn gevonden bij AQP3 voor water- en glycerol-doorlating;
- Lokale aminozuurverschillen kunnen de pK_a sterk beïnvloeden, net als de geobserveerde structurele veranderingen.

Mutagenesestudies zouden behulpzaam zijn om de verschillen in pH-gating-mechanismes van hAQP3 en hAQP7 beter te begrijpen, en worden momenteel uitgevoerd in onze groep.

DEEL B

In **Deel B** presteren we de studie van verschillende families van op goud gebaseerde stoffen als antikankermiddelen. Specifiek, een eerste serie van bifunctionele fluorescerende stoffen (goud(I)-ruthenium(II)) demonstreerde een veelbelovend antikankereffect *in vitro* en kon bestudeerd worden via fluorescentiemicroscopie. In deze op metaal gebaseerde stoffen is de gouden kern het therapeutische gedeelte, terwijl de ruthenium-bevattende groep gebruikt kan worden om het intracellulaire lot van de stof te volgen. Deze complexen zijn ook ontworpen om de opname via actieve transport te verbeteren, via de glucose-transporters (GluT-1) die tot overexpressie worden gebracht in kankercellen. Een aantal goudcomplexen hebben daarom een thioglucose-deel, die de opname van het gehele complex zou kunnen verbeteren en verder laten de complexen met het thioglucosedeel een sterkere cytotoxiciteit zien. De complexen zijn ook geprepareerd met twee verschillende organische "linkers" om de fluorescerende eigenschappen te verbeteren. Ook lijkt de grootte van deze linker een effect te hebben op de cytotoxische activiteit van de stoffen, met de kortere linker zorgend voor een toename in de cytotoxische effecten van de stoffen. We hebben ook de mogelijke rol van de GluT-1-transporter onderzocht in de cellulaire opname van de complexen door gebruik te maken van een remmer van deze transporter. Helaas lijkt GluT-1 niet betrokken te zijn bij de opname van onze stoffen en is er mogelijk een ander mechanisme betrokken, iets dat verder onderzocht moet worden. Wat betreft de opeenstapeling van de stoffen in cellen hebben we gevonden dat de complexen meestal nuclei en mogelijk kleine organellen in het cytoplasma als doelwit hebben.

Een tweede nieuwe serie stoffen die zijn getest op antikankereffecten zijn vervaardigd op basis van organometalen goud(I)-N-heterocyclische-carbenen met een fluorescerende coumarine-deel. De stoffen demonstreerden een veelbelovend antikankereffect, waarschijnlijk door de remming van het seleno-enzym thioredoxinereductase (TrxR). Wederom zat bij de meeste effectieve stoffen

diegenen met een thioglucose-deel. We geloven dat, net als bij de vorige serie, dit komt door de verbeterde hydrofiele/lipofiele eigenschappen die worden veroorzaakt door dit ligand. De opname van de meeste effectieve stof 3 is ook onderzocht door fluorescentiemicroscopie en er werd geobserveerd dat het voornamelijk in de nuclei voorkwam. Belangwekkend is het minst actieve complex van de serie, stof 4, de meest potente remmer van TrxR is, en de matige cytotoxiciteit veroorzaakt kan worden door matige opname. Aan de andere kant, complex 3 was geen potente remmer van dit enzym, wat mogelijk aangeeft dat de cellulaire doelwitten verschillen en dat de complexen verschillende actiemechanismes hebben.

Van de gerapporteerde studies kunnen we volgende overwegingen noteren:

- Een belangrijke eigenschap van cytotoxische goud(I)-stoffen is hun intracellulaire opname, welke verbeterd kan worden door de aanwezigheid van bepaalde liganden (bijvoorbeeld thioglucose-delen), die de goudkern stabiliseren.
- Op goud gebaseerde organometalen complexen zijn het waard om te verkennen als antikankermiddelen als er voor wordt gezocht dat ze voldoende oplosbaar zijn in waterige mediums.
- Andere doelwitten dan TrxR moeten overwogen worden (bijvoorbeeld nucleïnezuren voor stof 3, welke zich ophoopt in de cellulaire nuclei).

Tezamen genomen laten onze resultaten zien dat op goud gebaseerde stoffen als mogelijke eiwit/enzym-remmers grote potentie hebben voor toepassingen in chemische biologie en geneeskunde en dat zij het waard zijn om verder te onderzoeken. Onderzoek naar de mogelijke toxiciteit in gezonde cellen/weefsels zou ook uitgevoerd moeten worden, parallel aan het ontwerpen van gerichte stoffen die geen bijwerkingen hebben.

Referenties

[1] A.S. Verkman, M.O. Anderson, M.C. Papadopoulos, Nat Rev Drug Disc 13 (2014) 259-277.
[2] A.P. Martins, A. Marrone, A. Ciancetta, A. Galán Cobo, M. Echevarría, T.F. Moura, N. Re, A. Casini, G. Soveral, PloS one, 7 (2012) e37435.
[3] A. Serna, A. Galan-Cobo, C. Rodrigues, I. Sanchez-Gomar, J.J. Toledo-Aral, T.F. Moura, A. Casini, G. Soveral, M. Echevarria, J Cell Physiol, 229 (2014) 1787-1801.
[4] D.F. Savage, R.M. Stroud, J Mol Biol, 368 (2007) 607-617.
[5] Y. Zhang, Y. Cui, L.Y. Chen, Biophys Chem, 160 (2012) 69-74.
[6] S. Törnroth-Horsefield, Y. Wang, K. Hedfalk, U. Johanson, M. Karlsson, E. Tajkhorshid, R. Neutze, P. Kjellbom, Nature, 439 (2006) 688-694.
[7] K.L. Nemeth-Cahalan, J.E. Hall, J Biol Chem, 275 (2000) 6777-6782.
[8] M. Zelenina, A.a. Bondar, S. Zelenin, A. Aperia, J Biol Chem, 278 (2003) 30037-30043.

Resumo

Há milénios que compostos com metais na sua composição têm sido utilizados em medicina. Alguns destes continuam ainda uso nos dias de hoje, no tratamento de doenças como cancro (Cisplatina) ou artrite reumatoide (Auranofina), assim como agentes antimicrobianos (sulfadiazina de prata) ou ainda como radiofármacos. Apesar do seu largo espectro aplicacional, o mecanismo de acção de muitos destes metalo-compostos é pouco conhecido, com pouca informação sobre os seus possíveis alvos celulares.

No caso de compostos com ouro, tema desta tese, a interação com ácidos nucleicos não é relevante para o seu mecanismo de ação. Deste modo, o trabalho desenvolvido nesta tese foca-se no estudo de compostos de ouro como inibidores selectivos de proteínas, podendo ser utilizados como forma de investigar a sua função ou com objectivos terapêuticos. Ademais, as eventuais propriedades anticancerígenas e mecanismos de acção de duas novas séries de compostos de ouro, com características fluorescentes, foram estudados *in vitro*. Assim, o trabalho aqui descrito encontra-se dividido em duas partes complementares, A e B.

PARTE A

A parte A desta tese é dedicada ao estudo de aquaporinas (AQP), a sua função e mecanismos de inibição por metalo-compostos, assim como a sua regulação por pH.

Sendo a investigação da função de aquaporinas um tópico bastante desafiante [1], a possibilidade de utilização de um inibidor para este fim é bastante interessante do ponto de vista fisiológico e pode ser útil para apurar o papel destas proteínas em fisiologia e em determinadas patologias. Nos capítulos A1 e A2 encontra-se descrita a inibição de duas aquaglyceroporinas (AQP3 e AQP7) por compostos de ouro. Após os primeiros resultados de inibição da AQP3 por um composto de Au(III) com ligandos do tipo N-doadores (Auphen), descritos pelo nosso grupo [2], foi projectada uma nova série de compostos de ouro da mesma família, e as suas propriedades como moduladores da AQP3 foram avaliadas, usando eritrócitos humanos (hRBC). Este modelo celular permite-nos distinguir entre a inibição da passagem de água ou de glicerol. Observou-se que os compostos de ouro são inibidores selectivos da passagem de glicerol através da AQP3.

Como descrito no capítulo A1, os estudos foram expandidos para incluir uma nova série de compostos: três compostos de ouro com ligandos N-doadores e um organometálico, com uma ligação covalente directa entre o carbono e o metal, o que aumenta a sua estabilidade em condições fisiológicas. Curiosamente, um dos novos compostos desta série revelou-se ainda mais potente que o Auphen, como inibidor da AQP3. Métodos *in silico* foram utilizados para investigar o mecanismo molecular de inibição da AQP3 por compostos de ouro. Modelação molecular e docking não-covalente permitiram a identificação do *binding site* para o ouro, na AQP3: Cys40, localizada na abertura extracelular do canal. Através de estudos de mutagénese e de forma indirecta, este *binding site* foi mais tarde validado como crucial para inibição da AQP3 por Auphen [3].

De forma a avaliar a selectividade dos compostos de ouro, foi estudada a interacção destes compostos com outra isoforma humana, AQP7 (hAQP7). Neste caso foi utilizado um modelo celular de levedura, *S. Cerevisiae*, com sobre-expressão de hAQP7, como descrito no capítulo A2. Foi demonstrado que Auphen também inibe esta isoforma, embora com menos potência que AQP3, o que pode ser explicado pelo facto de ter diferentes *binding sites* para este composto: modelaçãoo molecular revelou que o *binding site* da hAQP7 é composto por duas metioninas , localizadas junto da entrada intracelular do canal, em contraste com a Cys40 da hAQP3, localizada

no lado extracelular

Em geral, deste estudo, podem retirar-se as seguintes conclusões:

- Compostos de Au(III) com ligandos N-doadores são potentes inibidores da hAQP3;
- O centro metálico composto por Au(III) é essencial para a inibição;
- Ferramentas *in silico* foram essenciais para a identificação dos aminoácidos no *binding site*, cruciais para inibição da hAQP3 e hAQP7 por complexos de Au(III);
- É necessária a optimização da selectividade destes compostos para diferentes isoformas.

Na literatura, $HgCl_2$ é utilizado como um inibidor padrão (não selectivo) para estudar a inibição de aquaporinas. Devido às semelhanças entre Hg e Au, no que diz respeito às suas interacções com aminoácidos que contenham enxofre, é interessante investigar as possíveis semelhanças entre os mecanismos de inibição de aquaporinas pelas duas classes de compostos metálicos. Alguns estudos reportaram o mecanismo de inibição de AQP por mercúrio [4, 5], mas a informação disponível não é conclusiva. Deste modo, no capítulo A3 encontra-se descrito o estudo do mecanismo molecular de inibição da hAQP3 por $HgCl_2$. O primeiro passo deste estudo foi a construção de um modelo de homologia da hAQP3, mas na sua forma tetramérica, e este utilizado posteriormente em simulações de dinâmica molecular. Os nossos estudos demonstraram que, após ligação covalente de Hg^{2+} à Cys40 da hAQP3, a proteína sofre alterações conformacionais. Neste estudo, foi possível observar o seguinte:

- Ligação de Hg^{2+} leva a uma diminuição do diâmetro do poro e, consequentemente, a um aumento da selectividade por tamanho de solutos;
- Foi observado um comportamento diferente em cada monómero; enquanto três dos monómeros se encontravam totalmente fechados no final da simulação, um dos monómeros manteve-se parcialmente aberto, com uma baixa permeabilidade a água;
- Foram observados dois mecanismos diferentes de fecho do canal, ambos envolvendo colapso do filtro de selectividade aromático/argnina.
- Após ligação de Hg^{2+}, os *loops* extracelulares sofrem um rearranjo e reposicionamento, o que pode contribuir para a oclusão do canal.

Curiosamente, o movimento de *loops* extracelulares foi observado anteriormente em outras AQPs [6] [7], e este comportamento foi associado ao fecho do poro. No capítulo A4, usando modelação molecular, observámos um semelhante movimento de *loops* extracelulares, que pode estar também envolvido no mecanismo de *gating* por pH, tanto no caso da hAQP3 como da hAQP7. Neste capítulo está descrita a caracterização completa, após alterações de pH, da permeabilidade a água e a glicerol da AQP3 murina e humana, usando um modelo celular de levedura e hRBC, respectivamente. O *gating* por pH foi estudado de forma semelhante para a isoforma humana AQP7, no mesmo modelo celular de levedura. As isoformas de rato e humana de AQP3, como esperado, têm um comportamento semelhante após alterações de pH, com valores de pK_a e alterações de permeabilidade semelhantes. Ambas as isoformas, e também AQP7 , demonstraram *gating* por pH na mesma gama, com fecho do poro a pH acídico e com máximo de permeabilidade a pH acima

de 6,5. Curiosamente, as Hill slope para água e glicerol têm uma diferença de duas vezes entre si, em ambas as isoformas de AQP3. No entanto, o mesmo comportamento não é observado para a hAQP7, que possui Hill slopes semelhantes para água e glicerol. Os nossos estudos computacionais permitiram retirar as seguintes conclusões:

- Todos os resíduos responsáveis pela sensibilidade da hAQP3 ao pH [8] estão presentes na isoforma de rato, o que pode explicar as semelhanças de comportamento;
- A hAQP7 partilha alguns destes resíduos, incluindo uma histidina e tyrosina nas mesmas posições;
- Movimento dos *loops* A e C em cada monómero, após protonação dos resíduos responsáveis pela sensibilidade ao pH, pode causar alterações conformacionais significativas, que poderão levar ao fecho do poro;
- As alterações conformacionais devido às variações de pH podem ser graduais, o que pode explicar as diferenças nas Hill *slopes* observadas para águas e glicerol;
- As diferenças entre as isoformas em composição em aminoácidos em determinados locais da proteína, nomeadamente próximo dos resíduos cruciais para o *gating* por pH, podem influenciar de forma significativa o pK_a e as alterações conformacionais observadas.

Estudos de mutagénese podem ser bastante úteis para melhor compreender as diferenças entre os mecanismos de *gating* da hAQP3 e hAQP7 e estão actualmente a ser executados no nosso grupo.

PARTE B

Na parte B encontram-se descritos estudos relativos a diferentes famílias de compostos de ouro como agentes anticancerígenos. Mais especificamente, uma primeira série de compostos fluorescentes e bifuncionais (Au(I)-Ru(II)), mostraram efeitos anticancerígenos promissores *in vitro*, e foi possível o seu estudo através de microscopia de fluorescência. Nestes compostos metálicos o ouro é o centro "terapêutico", enquanto que a parte que contém ruténio e que possui propriedades fluorescentes, pode ser usada para "seguir" o destino intracelular destes compostos. Estes compostos foram também desenhados de forma a terem um uptake mais eficiente, possivelmente através dos transportadores de glucose (GluT-1), sobre-expressos em células cancerígenas. Deste modo, alguns destes compostos possuem uma parte que contém uma thioglucose, que pode ajudar a promover o uptake de todo o complexo. De facto, uma forma geral, os compostos que contém tioglucose demonstraram maior citotoxicidade. Os compostos foram também preparados com dois tamanhos de *linkers* orgânicos, de forma a aumentar as propriedades de fluorescência. De qualquer forma, o tamanho destes *linkers* aparenta influenciar a citotoxicidade dos compostos, com os *linkers* de menor tamanho a terem um maior efeito. Também foi investigado o possível papel do transportador GluT-1 no *uptake* dos compostos, usando um inibidor do GluT-1. Infelizmente, GluT-1 não parece estar envolvido no mecanismo de *uptake* celular destes compostos, mas futura investigação deve aprofundar este facto e investigar outros possíveis mecanismos envolvidos. No que se refere à acumulação destes compostos em células, observou-se que o principal alvo aparenta ser o núcleo, ou ácidos nucleicos, ou pequenos organelos no citoplasma.

Uma outra série de compostos foi testada quanto aos seus possíveis efeitos anticancerígenos,

e é formada por carbenos N-heterocíclicos organometálicos de ouro(I), com uma coumarina fluorescente na sua constituição. Estes compostos demonstraram efeitos anticancerígenos promissores, possivelmente devido à inibição da seleno-enzima reductase de tioredoxina (TrxR). Uma vez mais, entre os compostos mais eficientes encontram-se aqueles que possuem uma parte com tiolgucose. Acreditamos que, tal como a primeira série de compostos, o aumento de toxicidade se deve a um aumento no *uptake* dos compostos, devido a um aumento das suas propriedades hidrofóbicas/lipofílicas induzidas por este ligando.

O *uptake* do composto mais effeciente, composto 3, foi também estudado por microscopia de fluorescência e observou-se que se encontra localizado no núcleo. Curiosamente, o composto menos activo, composto 4, é o mais potente inibidor da enzima TrxR e a sua baixa toxicidade pode dever-se a baixo *uptake*. Em contrapartida, o composto 3 não é um bom inibidor desta enzima, o que pode indicar que tem outros alvos celulares e os compostos podem ter diferentes modos de acção.

Destes estudos, foi possível retirar algumas conclusões:

- Uma característica importante dos compostos de Au(I) é o seu *uptake*, que pode ser melhorado graças à adição de determinados ligandos, como tioglucose, que podem estabilizar o centro metálico;
- Os compostos de ouro organometálicos podem ser interessantes como agentes no tratamento de cancro, se a sua estabilidade em solução aquosa for garantida;
- Outros alvos celulares, para além da TrxR, devem ser considerados (e.g. ácidos nucleicos para o composto 3, que aparentam acumular no núcleo).

Em geral, os nossos resultados demonstram que compostos de ouro são possíveis inibidores de proteínas/enzimas, com grande potencial para aplicação em bioquímica e medicina. Certamente, o seu estudo em células/tecidos saudáveis deverá ser realizada em paralelo, de forma a desenhar melhores compostos, com maior selectividade e menos efeitos secundários.

Referências

[1] A.S. Verkman, M.O. Anderson, M.C. Papadopoulos, Nat Rev Drug Disc 13 (2014) 259-277.
[2] A.P. Martins, A. Marrone, A. Ciancetta, A. Galán Cobo, M. Echevarría, T.F. Moura, N. Re, A. Casini, G. Soveral, PloS one, 7 (2012) e37435.
[3] A. Serna, A. Galan-Cobo, C. Rodrigues, I. Sanchez-Gomar, J.J. Toledo-Aral, T.F. Moura, A. Casini, G. Soveral, M. Echevarria, J Cell Physiol, 229 (2014) 1787-1801.
[4] D.F. Savage, R.M. Stroud, J Mol Biol, 368 (2007) 607-617.
[5] Y. Zhang, Y. Cui, L.Y. Chen, Biophys Chem, 160 (2012) 69-74.
[6] S. Törnroth-Horsefield, Y. Wang, K. Hedfalk, U. Johanson, M. Karlsson, E. Tajkhorshid, R. Neutze, P. Kjellbom, Nature, 439 (2006) 688-694.
[7] K.L. Nemeth-Cahalan, J.E. Hall, J Biol Chem, 275 (2000) 6777-6782.
[8] M. Zelenina, A.a. Bondar, S. Zelenin, A. Aperia, J Biol Chem, 278 (2003) 30037-30043.

Aknowledgements

At first, as a small child, I remember telling everyone that I wanted to become a teacher and be as good as my primary school teacher. Later in life I started thinking about becoming a medical doctor but blood, wounds, emergency rooms and so, were never that appealing to me. At a point in time it also occurred to me to have a more artistic career but, now that I look back, I feel that I managed to combine all of the options together. After all, what is science if not an art.

I would like to start by thanking the Rijksuniversiteit Groningen for funding this PhD project, in the scope of the Rosalind Franklin Funds, attributed to women in science and given to my supervisor, Prof. Angela Casini, during her stay in Groningen. Furthermore, I would like to thank the European COST network for providing the opportunities to join brilliant scientists in international meetings, with great outcomes in terms of collaborative work. In particular, I would like to acknowledge the COST Actions CM1105 and CM1106 for funding for two Short-Term Scientific missions (STSM) abroad.

I will start by thanking my promotor and supervisor, Prof. Geny Groothuis and Prof. Angela Casini.

Geny, thank you for taking me into your group. Working in such different fields was a lot to take in, for both of us, and took a bit of adaptation to incorporate the different areas into the projects. In the end, I feel like I gained so much with the interaction with you and the rest of the group and I really think the way we managed to mix the projects together and bring different expertise into the discussions, was very fruitful. Even though we did not interact as much as if you were my only supervisor, you were always very supportive and I always felt that I could ask you anything and get any help from you. Thank you also for being very supportive of new ideas: as a PhD student, is really great to have a supervisor that is excited and supportive of your new ideas. You are a great scientist and great person. Also, congratulations on having your new lab named after you!

Angela, it is difficult to express how lucky I feel to have you as my supervisor during my PhD. You are definitely a role model for women in science. Your social skills and energy, besides being highly contagious, are surely a part of your success. In these past four years I had the chance to meet most of your scientific network and I feel very lucky to have met such brilliant minds, but mostly, such beautiful people. I would like to congratulate you on your new, very well deserved position as full professor. I know you will always have a highly successful career and I hope I will be, at least, a little bit like you "when I grow up". Thank you for everything.

I would like to thank the assessment committee that reviewed this thesis: **Prof. Wim Quax, Prof. Hidde Haisma** and **Prof. Rudolf Allemann**; as well as the rest of the committee members: **Prof. Klaas Poelstra, Prof. Barbro Melgert, Prof. Graça Soveral** and **Dr. Armagan Kocer.** Thank you for taking the time to read this work and I hope you found it worthily.

During my PhD, I met brilliant minds that also happen to be great human beings. This work was also possible due to the many good collaborations we have. So, to all our collaborators a big thanks for the great work you did and that, hopefully, we will continue doing together in the future.

The Pharmacokinetics, Toxicology and Targeting group is amazing. Geny and Klaas, you have built a great working group and I feel very lucky to have worked here with all of you. I would like to thank **Prof. Klaas Poelstra, Prof. Barbro Melgert, Dr. Hans Proost, Dr. Anna Salvati, Dr. Inge**

de Graaf and **Dr. Leonie Beljaars** for all the fruitful discussions during our weekly group meetings. All of your comments helped me improve a lot during my time here. Barbro, thank you for the nice collaborative work we did together. You and Angela developed great projects together and I hope we will continue our nice collaborations.

The technicians in this group are an essential pillar for all the work that is done every day. Jan, thank you so much for all the organizational and bureaucratic work you do for all of us. You always have nice words and smile to give to people every day. I hope you enjoy your retirement and keep spreading happiness wherever you go. Marjolijn and Marina, we never worked closely, as I never worked with slices, but you were always there to help if I needed something. Thank you so much for your help. Marjolijn, keep me updated about your adventures with your "boss"! Eduard and Catharina, thank you so much for all the help with the cells and for putting up with me and my students always coming to you to ask questions. Eduard, keep being "The great minion" of our group.

Many thanks to all my other colleagues: Gillian, Henk, Bert, Sylvia, Kaisa, Ming, Suresh, Amirah, Christina, Fransien, Adhy, Laura, Roberta, Daphne and Kenni. Gillian, you are great person (a bit dirty minded, but who isn't?). You do a lot of great work and you are a great friend. Sylvia, our "white standard" for being a good person, thank you for the great time. You are a really nice colleague and friend and I hope that you will have a bright future. Ming, don't worry, I didn't open the present you left me yet, and I promise I will send you pictures of my future babies with Tiago. I hope you find a good job in China and I am sure you will have a brilliant career. I wish you lots of happiness for your family. Suresh, you will defend your PhD just before me so, I wish lots of luck. I hope you will find a good job here in The Netherlands. Don't forget to keep us posted every now and then. To all my fellow PhD colleagues, I wish you good luck with the rest of your PhD and lots of success in your careers.

To my dear paranimfen, Carian and Viktoriia: Carian, my dear Dutchie, you were one of the first people I got along with here in the group. You introduced me to the salsa scene in Groningen, took me to my first Queen's day, we had lots of fun together and became known as "The tall one and the short one". Thank you for the friendship, love and support you gave me during these years. I really hope we will never lose contact and that we keep visiting each other throughout the years (I want to see your very tall future babies with Siegard!!!). Good luck with your new job. You are a great scientist and an amazing person, so I know you will do very well in every aspect of your life. Vika, my dear Ukrainian, I remember that you were still a master student when I started; such a little scientific baby. Your friendship means a lot to me and I hope we will never be too far from each other (you know we can't keep Bauke and Tiago apart; they have to keep the bromance going on). (Bauke, I know you don't want any acknowledgments, so I won't write anything for you). Thank you for everything, from talks in the office, to "bridesmading" together (or for me!) and taking care of my plants (and flower vases) when I am away. You are a smart, beautiful woman and I am sure your career will be brilliant. I love you my dear girls.

During this time in Groningen, I also gained a scientific family (mostly sisters): Benoit, Sarah, Natalia, Andrea, Sophie, Eva, Ozden, Andreia, Jiaying and, more recently, Margot. Benoit, my only brother! I know I gave you a hard time, but I also know we are really good friends and that I can count on you for everything I need. We had so much fun together, either dancing in the lab, light saber fighting with pipette tips, or drinking a few beers at "De drie gezusters". You will always be

my little annoying brother. Sarah, Andrea and Sophie, my cute Germans, thank you for being such great sisters. Loved the time here with you (not so much with Jägermeister) and can't wait to work together with you again soon. Natalia, "the dark one", who will bring me cookies and chocolates now? I know the only reason you ever gave me some was just so you would have an excuse to pass by my office and chat! But I will miss that. Andreia, my other Portuguese half, it is great working with you. We make a great team and I am sure we will continue to produce really nice aquaporin "things" together. Eva, Ozden and Jiaying, good luck for the rest of your PhD and your future careers. Margot, see you soon sista!

I would also like to thank my students, who did such great work during these years: Emilia, Evelien, Mirja and Sjoukje. Girls, you all did a really nice job and it was a pleasure to have you as my students. I am happy that I am still in contact with all of you and I will want to witness your successes in life.

The list of acknowledgments is getting a bit long, but I still have a few people to thank. For example, there are people that pass by your life during your PhD that will never leave. Mackenzie, you are a force of nature. I am sure that I will never meet someone quite like you during my whole life. Take care, don't be too adult and don't eat too many rainbows, you will get fat. Magda and Daan, thank you for you friendship. You are such a great couple and I whish you two the best and lots of happiness for your beautiful family. Xiaoyu, my little chinese: I saw such big changes in you and in your life in these past few years, all of them positive. You grew as a woman, as a person and now have such a beautiful family together with Hein and little June. Wherever I will be, you will always be in my heart and I want to see my niece very often!! Hein, you are a great father and husband, but also a brilliant scientist. We worked really well together and I am really happy that the university didn't make the mistake of letting you leave.

I could not be here ending my PhD without thanking Prof. Graça Soveral and Prof. Teresa Moura, my supervisors during my bachelor and master thesis. We fortunately continue to collaborate and this is something I value a lot. Thank you so much for the great supervision you always gave me and for the work you continue doing with us.

Finally, life is not all about science. I made really good friends in Groningen and I will like to thank you all for helping me having such a fulfilled, happy social life (I will not mention any names here, but I am sure they can identify themselves in this paragraph).

I cannot finish without thanking my family for their support, specially my mother and husband. Mãe, obrigada por tudo. Sei que não deve ser fácil ver um filho sair de casa para tão longe, mas sei que estás muito orgulhosa de mim. Tiago, you left everything behind and moved to a completely different country just to be with me. You were always the most supportive person on Earth to all of my choices and the best husband I could ask for. Words cannot express how grateful I am to have you in my life. Thank you for everything. Tiago and Mom, I love you both lots and lots.

To all of you that managed to read through this huge section until here (or not),

Thank you.

Publication List and Curriculum Vitae

Publications (published)

**authors contributed equally to the work*

• de Almeida, A.*, Martins, A.P*, Mósca, A. Wijma, H.J., Prista, C., Soveral, G., Casini, A. (submitted) Exploring the gating mechanisms of aquaporin-3: new clues for inhibitor's design? **(2016)** *Mol. Biosyst.* DOI: 10.1039/C6MB00013D **(In this thesis)**

• Tsitsa, I., Tarushi, A., Kalogiannis, S., Perdih, F., de Almeida, A., Papadopoulos, A., Casini, A., Turel, I., Psomas, G. (**2016**) Structure and biological perspectives of metal complexes of flumequine. *RSC Advances* 6: 19555-19570, DOI: 10.1039/C5RA25776J

• Wenzel, M.*, de Almeida, A.*, Bigaeva, E., Bertrand, B., Le Gendre, P., Bodio, E., Picquet, M., Casini, A. (**2016**) Fluorescent polynuclear metal complexes with anticancer properties: towards new theranostics. *Inorg. Chem.,* DOI: 10.1021/acs.inorgchem.5b02910 **(In this thesis)**

• Spinello, A., de Almeida, A., Casini, A. and Barone, G. (**2015**) The inhibition of glycerol permeation through aquaglyceroporin-3 induced by mercury(II): a molecular dynamics study. *J.Inorg. Biochem.* DOI:10.1016/j.jinorgbio.2015.11.027 **(In this thesis)**

• Casini, A. and de Almeida, A. (**2015**) Aquaporins in health and disease: New molecular targets for drug discovery. Chapter: Inorganic compounds as aquaporin substrates or as potent inhibitiors: a coordination chemistry point of view. *CRC Press/Taylor & Francis Group* **(In this thesis)**

• de Almeida, A., Soveral, G., Casini, A. (**2014**) Gold compounds as aquaporin inhibitors: new opportunities for therapy and imaging. *Med. Chem. Comm.* 5: 1444-1453 DOI: 10.1039/c4md00265b **(In this thesis)**

• Khan, R.A, Al-Farhan, K., de Almeida, A., Alsalme, A., Casini, A., Ghazzali, M., Reedijk, J. (**2014**) Light-stable bis(norharmane)silver(I) compounds: synthesis, characterization and antiproliferative effects in cancer cells. *J. Inorg. Biochem.* 140:1-5. DOI: 10.1016/j.jinorgbio.2014.06.019

• Madeira, A.*, de Almeida, *A.**, de Graaf, C., Camps, M., Zorzano, A., Moura, T. F., Casini, A. and Soveral, G. (**2014**), A Gold Coordination Compound as a Chemical Probe to Unravel Aquaporin-7 Function. *Chem. Bio. Chem.*, 15: 1487–1494. DOI: 10.1002/cbic.201402103 **(In this thesis)**

• Bertrand, B.*, de Almeida, A.*, van der Burgt, E. P. M., Picquet, M., Citta, A., Folda, A., Rigobello, M. P., Le Gendre, P., Bodio, E. and Casini, A. (**2014**), New Gold(I) Organometallic Compounds with Biological Activity in Cancer Cells. *Eur. J. Inorg. Chem.* DOI: 10.1002/ejic.201402248 **(Front cover pitcure) (In this thesis)**

• Rubbiani, R., Salassa, L., de Almeida, A., Casini, A. and Ott, I. (**2014**), Cytotoxic Gold(I) N-heterocyclic Carbene Complexes with Phosphane Ligands as Potent Enzyme Inhibitors. *Chem. Med. Chem*, 9: 1205–1210. DOI: 10.1002/cmdc.201400056 **(VIP paper, Front cover pitcure)**

• Frik, M., Jiménez, J., Vasilevski, V., Carreira, M., de Almeida, A., Gascón, E., Benoit, F., Sanaú, M., Casini, A. and Contel, M. (**2014**). Luminescent iminophosphorane gold, palladium and platinum complexes as potential anticancer agents. Inorg. Chem. Front. 1, 231-241 DOI: 10.1039/C4QI00003J **(Front cover pitcure)**

• Lease, N., Vasilevski, V., Carreira, M., de Almeida, A., Sanaú, M., Hirva, P., Contel, M. (**2013**). Potential anticancer heterometallic Fe-Au and Fe-Pd agents: initial mechanistic insights. *J. Med. Chem.*, 56 (14), pp 5806–5818 DOI: 10.1021/jm4007615

• Martins, A. P., Ciancetta, A., de Almeida, A., Marrone, A., Re, N., Soveral, G. and Casini, A. (**2013**), Aquaporin Inhibition by Gold(III) Compounds: New Insights. *Chem. Med. Chem.*, 8: 1086–1092. doi: 10.1002/cmdc.201300107 **(In this thesis)**

• de Almeida, A., Oliveira, B. L., Correia, J. D. G., Soveral, G., & Casini, A. (**2013**). Emerging protein targets for metal-based pharmaceutical agents: An update. *Coordination Chemistry Reviews*, 1–16. DOI:10.1016/j.ccr.2013.01.031 **(In this thesis)**

Publications (submitted)

**authors contributed equally to the work*

• de Almeida, A., Mósca, A., Soveral G., Casini, A. (submitted) Insights in the mechanism of aquaporin inhibition by gold compounds with N-donor ligands **(In this thesis)**

• Martins, A.P*, de Almeida, A.*, Mósca, A.*, Wijma, H.J., Madeira, A., Loureiro-Dias, M.C., Casini, A., Moura, T.F., Prista, C., Soveral, G., (submitted) Human aquaporin-7 expressed in yeast reveals pH gating **(In this thesis)**

• Boorsma, C.E., Putri, K.S.S., de Almeida, A., Maud, Thais, Brandsma, C., van den Berge, M., Olinga, P., Timens, W., Casini, A., Melgert, B.N. (submitted) The Role of Tartrate Resistant Acid Phosphatase in Alveolar Macrophages in the Context of Obstructive Pulmonary Diseases

• Khan, R.A.*, de Almeida, A.*, Al-Farhan, K., Alsalme, A., Casini, A., Ghazzali, M., Reedijk, J. (submitted) First-row transition-metal norharmane compounds as possible cytotoxic agents: new insights based on a coordination chemistry perspective

Publications (in preparation)

• de Almeida, A., Veelthuis, S., Schulze, M., Timens, W., Melgert, B.N., Casini, A. (*in preparation*) Role of aquaporins in diseases: aquaglyceroporin-3 in lung tissue and lung carcinoma

• de Almeida, A., Veelthuis, S., Schulze, M., Casini, A. (*in preparation*) Effects of anticancer treatment in aquaglyceroporin-3 expression

• de Almeida, A., Martins, A.P, Soveral, G., Casini, A. (*in preparation*) Dinuclear organogold(III) compounds as aquaglyceroporin-3 inhibitors

Curriculum Vitae

Andreia de Almeida

Citizenship: Portuguese **Birth Date:** 13 May 1986

Email: A.F.Batista.de.Almeida@rug.nl

For updated contact information and publication list, use the following QR-codes to access ResearchGate and LinkendIn profiles:

Work Exerience

01.April.2012 – 08.April.2016

PhD in the field of Medicinal Inorganic Chemistry

Metallodrugs as Protein Modulators

Pharmacokinetics, Toxicology and Targeting Group, Research Institute of Pharmacy, Rijksuniversiteit Groningen

Additional Scientific Training

05.Jan.2016 – 15.Jan.2016

Research Stay at Biological Transport Group

Prof. Graça Soveral, Faculty of Pharmacy, Universidade de Lisboa, Lisboa, Portugal

Study of the inhibition propertie of gold(III) complexes with N-donor ligands, as AQP3 inhibitors

01.Mar.2014 – 14.Mar.2014

Short-Term Scientific Mission at Mind the Byte, SL

Dr. Alfons Nonell Canals, Barcelona, Spain

Short-Term Scientific Mission (STSM) in the AScope of COST Action CM1106

Molecular modelling approaches to identify novel AQP inhibitors

01.Aug.2013 – 31.Aug.2013

Short-Term Scientific Mission at Biological Transport Group

Prof. Graça Soveral, Faculty of Pharmacy, Universidade de Lisboa, Lisboa, Portugal

Short-Term Scientific Mission (STSM) in the Scope of COST Action CM0902

Screening of copper complexes as AQP inhibitors

04.Feb.2013 – 15.Feb.2013

Research Stay at Medicinal Chemistry Group

Dr. Chris de Graaf, Faculty of Sciences, Vrije Universiteit Amsterdam, Amsterdam, The Netherlands

Computational Design and Synthesis of Drugs

01.Sep.2009 – 31.Jul.2010

Training at Biological Transport & Microbial Bioenergetics Group

Prof. Teresa Moura & Dr. Joana Matos, REQUIMTE (FCT-UNL), Caparica, Portugal

Prof. Mª Conceição Loureiro Dias & Dr. Catarina Prista, CBAA (ISA-UTL), Lisboa, Portugal

Investigation of transport and metabolism of glucose in S. cerevisiae

01.Mar.2008 – 31.Mar.2009

Training at Bio-Prot Group

Dr. Sofia Pauleta, REQUIMTE (FCT-UNL), Caparica, Portugal

Cloning of the periplasmic sensor domain of a histidine protein kinase, involved in the copper resistance regulation

Education

15.Dec.2011

Master in Structural and Functional Biochemistry (MSc, 120 ECTS)

Faculty of Science and Technology, Universidade Nova de Lisboa, Caparica, Portugal

Title of MSc thesis (1 year): *Mathematical modelling of kinetic and metabolic behaviour of S. cerevisiae: pH variations after a glucose pulse*

23.Jul.2009

Licenciatura in Biochemistry (BSc, 188 ECTS)

Faculty of Science and Technology, Universidade Nova de Lisboa, Caparica, Portugal

Title of BSc thesis (6 months): *Mathematical modelling of kinetic and metabolic behaviour of S. cerevisiae: pH variations after a maltose pulse*

Extra Scientific Activities

Dec.2015

Organization and Volunteer Staff at CEMM 2015

International Symposium on Clinical and Experimental Metallodrugs in Medicine: Cancer Chemotherapy (CEMM)

Workshop in "Translational Research)

Sullivan Center, Univerisity of Hawaii Cancer Center, Honolulu, USA

Aug.2014

Volunteer Staff at MCB Symposium

Symposium organized by the Division of Medicinal Chemistry and Bioanalysis (MCB) of the Groningen University Institute for Drug Exploration (GUIDE) and the Department of Analytical Biochemistry

Groningen Institute of Pharmacy, Groningen, The Netherlands

Feb.2013

Organization and Volunteer Staff of COST Action Meeting

WG1 + WG5 Joint Meeting of the COST Action CM1105

Groningen Institute of Pharmacy, Groningen, The Netherlands

Jun.2010

Volunteer Staff at XVIII Yeast Biology Meeting

National meeting "Prof. Nicolau van Uden", organized by the Portuguese Microbiology Society

Instituto Superior de Agronomia, Universidade Técnica de Lisboa, Lisboa, Portugal

May.2009

Organization, Planning and Volunteer Staff at Biochemistry JORTEC

Meeting organized by students, with invited lectures, open to the academic community.

Faculty of Science and Tecnology, Universidade Nova de Lisboa, Caparica, Portugal

April.2009 &
April 2009

Volunteer Staff at EXPO-FCT

Annual open-day at Faculty of Science and Tecnology, Universidade Nova de Lisboa, Caparica, Portugal

Sep.2008
Sep.2009

Tutoring

Tutoring of seven junior students in Biochemistry.

Faculty of Science and Tecnology, Universidade Nova de Lisboa, Caparica, Portugal